Assessment of the factors controlling sea ice algal and bacterial production in Dease Strait of the Northwest Passage

by

Karley Campbell

A thesis submitted to the Faculty of Graduate Studies of

The University of Manitoba

in partial fulfillment of the degree of

Doctor of Philosophy

Department of Environment and Geography

University of Manitoba

Winnipeg, Manitoba, Canada

Copyright © 2017, Karley Campbell

ABSTRACT

Algae and heterotrophic bacteria inhabiting the bottom of sea ice contribute to carbon cycling and food web dynamics in the Arctic marine system. The extent of their influence is dependent on cellular productivity, which is affected by environmental conditions that vary seasonally, between study areas, and with ongoing climate change. In this research, estimates of ice algal and bacterial production are presented for the first time in Dease Strait of the Canadian Arctic Archipelago, and the physical or biological processes affecting production are evaluated.

A new incubation method that uses oxygen optodes instead of radioisotopes is developed to quantify gross primary production and net production of the bottom-ice community. It also permits assessment of ice algal photophysiological state through the calculation of photosynthesis-irradiance parameters, which are comparable to commonly reported ^{14}C-based measurements. Production estimates acquired from oxygen optodes, along with separate bacterial production incubations, show that sea ice in Dease Strait is only moderately productive relative to other regions of the Arctic. Algal composition (carbon, nitrogen, chlorophyll *a*) and photophysiology further indicate that low primary production in the region is due to co-limitation by both light and nitrogen. In comparison, bacterial production is largely affected by the supply of organic carbon substrate from sea ice brines and the smallest size fraction of ice algae (< 0.2 μm).

Light, nutrient, as well as salinity conditions influence the taxonomic composition of the ice algal community that is present, where low nitrogen and salinity in Dease Strait appear to favor a community of centric over pennate diatoms when sufficient light is available. Collectively these factors drive biomass accumulation, and determine whether

the bottom-ice will be autotrophic (net consume CO_2) or heterotrophic (net release CO_2). We note the potential for heterotrophic conditions to occur well into the spring season, which challenges the common assumption that the spring bloom is consistently autotrophic as a result of algal photosynthesis. The findings from this research improve our ability to effectively monitor ice algal and community production, and contribute to our understanding of sea ice microbial response to environmental changes.

ACKNOWLEDGEMENTS

I would like to thank my supervisors Drs. C.J. Mundy and Søren Rysgaard for their leadership and encouragement.

I would like to thank my committee members Drs. Brenda Hann, Christine Michel and Andrew McMinn for their guidance and assessments of this research project.

I would like to thank the community of Cambridge Bay, Nunavut, for the opportunity to study the smallest members of their backyard.

Financial support for this research was provided by Natural Sciences and Engineering Research Council of Canada (NSERC), ArcticNet of the Network of Centres of Excellence, the Canada Foundation for Innovation (CFI), the Canada Excellence Research Chair (CERC) unit at the University of Manitoba's Centre for Earth Observation and Science (CEOS), the Canadian High Arctic Research Station (CHARS), and the Marine Environmental Observation Prediction and Response (MEOPAR) Network. I have personally received support from the V.E. Barber Memorial Fellowship in Arctic Research, the Faculty of Graduate Studies Travel Award, the C.H. Riddell Endowment Fund, the Northern Scientific Training Program grant, the Alexander Graham Bell Canadian Graduate Scholarship from NSERC, the Canadian Meteorological and Oceanographic Society (CMOS) Scholarship Supplement, and the Manitoba Graduate Scholarship.

This work represents a contribution to the research programs of ArcticNet, the Arctic Science Partnership (ASP) and Dr. Rysgaard's CERC.

To my colleagues and friends, including:

Dr. Tim Papakyriakou, Dr. John Iacozza, Kerri Warner, Meredith Pind;

my family:

Mom, Dad, Kristyn, Nathan;

and Jack.

Thank you for your patience and support; I could not have done this without you.

CONTENTS

ABSTRACT ii
ACKNOWLEDGEMENTS iv
CONTENTS 1
LIST OF TABLES 6
LIST OF FIGURES 11
LIST OF ABBREVIATIONS AND NOTATIONS 17
USE OF COPYRIGHTED MATERIAL 18
CHAPTER ONE: INTRODUCTION 20
1.1 Motivation 20
1.2 Thesis Objectives 21
1.3 Thesis Structure 22
References 24
CHAPTER TWO: BACKGROUND 25
2.1 Arctic sea ice algae and bacteria 26
2.1.1 Regional definition of the Arctic 26
2.1.2 Definitions of sea ice in the Arctic 28
2.1.3 Physical characteristics of sea ice 29
Physical characteristics of first-year sea ice 30
Physical characteristics of old sea ice 32
2.1.4 Algal and bacterial communities in sea ice 33
Algal colonization and abundance 34
Bacterial colonization and abundance 36
2.1.5 Comparison of Arctic and Antarctic sea ice ecosystems 37
2.2 Production 40
2.2.1 The processes of photosynthesis and respiration 40
Photosynthesis 40
Respiration 42
Gross and net primary production 43
Algal photosynthesis-irradiance curves 44
2.2.2 Reported estimates of Arctic ice algal and bacterial production 46
Regional estimates of algal production 46
Regional estimates of photosynthesis-irradiance response 52
Regional estimates of bacterial production 54
2.3 Local factors controlling algal and bacterial production in sea ice 55
2.3.1 Factors affecting algal production 55
Temperature 56
Salinity 56
Light 57
Nutrients 62
2.3.2 Factors affecting bacterial production 65
Temperature 66
Salinity 66

Light 67
Nutrients 67
Oxygen 68
Substrate availability 69
2.3.3 Physical losses of algae and bacteria from sea ice 70
Predation 71
Viral infection 72
Mechanisms of bloom termination 72
2.4 Regional and pan-Arctic variability of production in sea ice 73
2.4.1 Light availability 73
2.4.2 Nutrient availability 76
Arctic inflows and surface water circulation 76
Turbulence 78
Stratification 80
2.4.3 Processes of dissolved organic matter transport 81
2.4.4 Summary of the processes controlling regional production in sea ice 83
2.5 Potential influence of current and future climate changes 85
2.5.1 Reduction in sea ice extent and thickness 86
Observed and predicted changes 86
Potential response of production in sea ice 87
2.5.2 Changes in snow cover 89
Observed and predicted changes 89
Potential response of production in sea ice 91
2.5.3 Increase in freshwater inputs 92
Observed and predicted changes 92
Potential response of production in sea ice 92
2.5.4 Summary 93
2.6 Conclusions 95
References 97

CHAPTER THREE: RATIONALE FOR METHODS OF PROCESSING SEA ICE 114
3.1 Introduction 114
3.2 Sampling Methods 114
3.3 Collecting the bottom 5 cm of sea ice 116
3.4 Melt procedures 118
3.5 Conclusion 126
References 127

CHAPTER FOUR: COMMUNITY DYNAMICS OF BOTTOM-ICE ALGAE IN DEASE STRAIT OF THE CANADIAN ARCTIC 129
Abstract 129
4.1 Introduction 130
4.2 Materials and methods 133
4.2.1 Field site 133
4.2.2 Field sampling 134
4.2.3 Laboratory analysis 136
Environmental variables 136
Bacteria production using ^{3}H-Leucine 136
Optode experimental set-up 137
Primary production using optodes 139
4.2.4 Fitting photosynthesis-irradiance relationships 142
4.2.5 Statistical analysis 142
4.3 Results 143

4.3.1 Physical characteristics of the field site 143
4.3.2 Chlorophyll *a*, carbon and nitrogen 147
4.3.3 Bacterial production 150
4.3.4 Photosynthesis-irradiance parameter response 150
4.4 Discussion 153
4.4.1 Seasonality of nutrients in sea ice 153
4.4.2 Nitrogen limitation in Dease Strait 154
4.4.3 Light versus nutrient limitation 155
4.4.4 Measuring photosynthetic-irradiance response using optodes 158
4.4.5 Photosynthesis-irradiance parameters under thin and thick snow cover 160
4.4.6 Seasonal response of photosynthesis-irradiance to local environmental controls 161
Maximum photosynthetic rate 161
Photosynthetic efficiency 163
Parameter of photoacclimation 165
Minimum light for photosynthesis and production in darkness 165
4.5 Conclusions 166
Acknowledgements 167
References 168
Chapter Four Supplementary Material 175
4.S.1 Tables 175
4.S.2 Description of ^{14}C measurement of gross primary production 176

CHAPTER FIVE: SEASONAL DYNAMICS OF ALGAL AND BACTERIAL COMMUNITIES IN ARCTIC SEA ICE UNDER VARIABLE SNOW COVER 178
Abstract 178
5.1 Introduction 179
5.2 Materials and Methods 182
5.2.1 Sample collection 182
5.2.2 Measurements of photosynthetically active radiation and brine volume 183
5.2.3 Biological parameters 184
5.2.4 Bacterial and primary production 185
5.2.5 Flow cytometry 185
5.2.6 Light microscopy 186
5.2.7 Estimates of relative abundance 187
5.2.8 Statistical Analysis 187
5.3 Results 188
5.3.1 Study site 188
5.3.2 Environmental conditions 189
5.3.3 Composition of the bottom-ice community 192
Heterotrophic bacterial abundance and production 192
Abundance of cyanobacteria and eukaryotes in sea ice 194
Abundance of picoeukaryotes 195
Abundance of nanoeukaryotes 198
Abundance of microeukaryotes 199
Ice algal total cell abundance and production 200
5.3.4 Taxonomic composition of the ice algal community 200
5.3.5 Controls of community composition, biomass and production 204
Controls of bacterial abundance and production 204
Controls on ice algal community composition 206
Ice algal biomass and production 211

5.4 Discussion **212**
5.4.1 Influences of heterotrophic bacterial abundance and production 212
5.4.2 Using flow cytometry and light microscopy to estimate nanoeukaryote abundance 214
5.4.3 Seasonal controls of algal community composition, biomass and production 216
Size classification of the algal community 216
Taxonomic composition of the algal community 219
5.5 Conclusions **221**
Acknowledgements **223**
References **224**
Chapter Five Appendices **231**
Chapter Five Supplementary Material **241**

CHAPTER SIX: NET COMMUNITY PRODUCTION IN THE BOTTOM OF ARCTIC SEA ICE OVER THE SPRING BLOOM **244**
Abstract **244**
6.1 Introduction **245**
6.2 Data collection and processing **247**
6.3 The ice algal community **248**
6.4 Optode-derived measurements of net community production **251**
6.5 Seasonal changes in net community production **253**
6.6 Early spring biomass accumulation under net heterotrophic conditions **256**
6.7 Conclusions **259**
Acknowledgements **260**
References **261**
Chapter Six Supplementary Material **266**
6.S.1 Ice core collection and processing 266
6.S.2 Oxygen optode incubations 266
6.S.3 Measurements of light intensity 267

CHAPTER SEVEN: SUMMARY AND CONCLUSIONS **269**
7.1 Summary of major contributions **269**
7.1.1 Contribution 1 269
7.1.2 Contribution 2 270
7.1.3 Contribution 3 272
7.2 Future recommendations **273**
7.2.1 Modifications to the oxygen optode incubation method 274
7.2.2 Standardized approaches for processing sea ice biological samples 277
7.2.3 Laboratory studies for assessing the controls of algal and bacterial production 278
7.2.4 Documenting *in situ* light conditions 279
7.2.5 Statistical assessments of time series data 279
7.3 Closing Comments **280**
References **282**

APPENDIX A: CONTRIBUTIONS OF COLLABORATING AUTHORS **285**
Chapter Three **285**
Chapter Four **285**
Chapter Five **286**
Chapter Six **286**
Chapter Seven **286**

APPENDIX B: ADDITIONAL CONTRIBUTIONS TO THE PEER-REVIEWED LITERATURE 287
Published manuscripts 287
Manuscripts in preparation or review 290
Other Contributions 291

LIST OF TABLES

Table 2.1. Summary of the physical and biological properties of Antarctic and Arctic marine systems, with differences highlighted. This includes differences in firstyear (FYI) and multiyear (MYI) sea ice coverage and the concentration of chlorophyll a (chl *a*) [Horner et al., 1985; Tucker et al., 1987; Lange et al., 1989; Spindler et al., 1990, Dieckmann et al., 1991; Gloerson et al., 1992; Hiel & Anderson, 1999; McMinn et al., 1999; Wadhams, 2000; Pavlov & Pavlova, 2007; Comiso et al., 2010; Thomas & Dieckmann, 2010; NSIDC, 2017].....38

Table 2.2. Summary of oxygen-derived production measurements in Arctic sea ice, including the type of sample collected (e.g. DBL, O_2 flux across the sub-ice diffuse boundary layer), the type of production measured (NCP, net community production; GPP, gross primary production; CR, community respiration), range or average (± standard deviation) of production estimates, as well as comments detailing the sampling procedure. 41

Table 2.3. Supplementary information for algal studies presented in Figure. 2.6 including: type of sample collected (brine, bottom centimeters, scraped or suctioned skeletal layer), type of ice (F, first-year; M, multiyear; P, pack ice of unspecified age; +, combination), incubation method (*in situ*, modeled, laboratory incubator at set irradiance). Dominant control on production (*see* Section 2.3) is also indicated when possible for each study (grey) including light (from self-shading, sediments present, extremely thick snow), nutrients (N, nitrogen; P, phosphorus; Si, silica; bloom, occurred during peak biomass), or other (I, ice type or structure; T, temperature, G, grazing; S, salinity; PI, photoinhibition; bloom, occurred during peak biomass). Additional information: (-), no data; blue shading, study included in Table 2.4; bold, hourly production values multiplied by 24 to obtain daily estimates. 48

Table 2.4. Supplementary information for algal studies presented in Figure 2.7 including: type of sample collected (bottom centimeters or suctioned skeletal layer), ice type (F, first-year; M, multiyear; P, pack ice of unspecified age), incubation method (*in situ*, modeled, laboratory incubator at set irradiance). Dominant control on production (*see* Section 2.3 for explanations) is also indicated when possible for each study (grey) including light (from self-shading; pre-bloom, early in the spring), nutrients (stratification; bloom, occurred during peak biomass), or other (I, ice type or structure). Additional information: (-), no data; blue shading, study included in Table 2.3; bold, hourly production values multiplied by 24 to obtain daily estimates. 51

Table 2.5. Summary of ^{14}C-derived photosynthesis-irradiance parameters reported for the Arctic during the spring, with ranges or mean values indicated and standard deviations (±) in parentheses. The type of sample collected (S, skeletal

layer; I, interface ice slurry; In, interface with no ice; B, depth of bottom ice thickness in cm), ice thickness (cm) and snow depth (H_s, cm) prior to collection is specified for each reference, in addition to the number of observations contributing to each summary (*n*). Photosynthetic parameters include the maximum photosynthetic rate under the influence of photoinhibition P^B_m (mg C mg chl *a* $^{-1}$ h^{-1}) or in its absence $\underline{P^B_S}$ (mg C mg chl *a* $^{-1}$ h^{-1}), the photosynthetic efficiency, α^B (mg C mg chl *a*$^{-1}$ h^{-1} (µmol photons m^{-2} s^{-1})$^{-1}$), the photoinhibition index β^B (mg C mg chl *a* $^{-1}$ h^{-1} (µmol photons m^{-2} s^{-1})$^{-1}$) x 10^{-2}, the photoacclimation index E_s (µmol photons m^{-2} s^{-1}), the optimal light intensity $\underline{E_m}$ (µmol photons m^{-2} s^{-1}), and the compensation light intensity E_c (µmol photons m^{-2} s^{-1}). 52

Table 2.6. Supplementary information for bacterial production studies presented in Figure 2.6, 2.7, including: type of sample collected (brine, bottom centimeters), incubation method (T, ^{3}H-Thymidine; L, ^{3}H-Leucine). Dominant control on production (*see* Section 2.3) is also indicated when possible for each study (grey) including: substrate availability (I, associated with ice algae), grazing pressure or other (V, viral infection; S, salinity; M, losses from ice melt; B, brine drainage). Additional information: (-), no data. 54

Table 3.1. Summary of supplementary data presented in this chapter (highlighted) from the 2014 ICE-CAMPS field campaign. Data include salinity, chlorophyll *a* (chl *a*), ^{14}C derived gross primary production (^{14}C GPP), dissolved inorganic carbon (DIC), inorganic nutrients (nutrients) and cell viability assessed using light microscopy (microscopy). The number of sample cycles for each variable is also listed, where 15 indicates data collection between 7 March to 9 June, 5 between 17 May to 5 June, and 1 on 30 May. 116

Table 3.2. Average estimates of photosynthesis-irradiance parameters (*see* text for definitions) with standard deviations (brackets) for samples melted in filtered sea water added at a ratio of three parts water to one part ice ($FSW_{3:1}$), melted without filtered seawater added (FSW_{zero}) and 1 cm scrapes ($FSW_{8:1}$). Results from Student's paired t-tests between these melt treatments is also presented, including the test statistic (top) and significance (bottom). Parameters that are significantly different between melt treatments ($p < 0.05$) are in bold. 123

Table 4.1. Pearson correlation coefficients (top) and *p*-value (bottom) of particulate organic carbon (POC) to chlorophyll *a* (chl *a*) and POC to particulate organic nitrogen (PON) ratios with environmental variables chl *a*, ice thickness (H_I), snow depth (H_s) and transmittance of photosynthetically active radiation (T_{PAR}), for thin and thick snow cover separately and grouped together. Missing data is excluded pairwise and significance ($p < 0.05$) is indicated in bold. The number of observations for each parameter is 12, except for T_{PAR} where the outliers from 5 and 9 June are omitted ($n = 8$). 149

Table 4.2. Pearson correlation coefficients (top) and significance (middle) of photosynthesis-irradiance (see text for definitions) and environmental parameters including chlorophyll *a* (chl *a*), snow depth (H_s) and transmittance of photosynthetically active radiation (T_{PAR}), for samples of thin and thick snow covered ice collectively, except for correlations between I_s and P^B_s or α^B due to co-linearity. Missing data is excluded pairwise and relationships of significance ($p < 0.05$) are highlighted with bold text. The number of observations for each correlation is also indicated (bottom). 152

Table 4.S.1. Pearson correlation coefficients (top) of T_{PAR} data inclusive of 5 and 9 June, with particulate organic carbon (POC) to chlorophyll *a* (chl *a*) ratios, POC to particulate organic nitrogen (PON) ratios and photosynthesis-irradiance (*see* text for definitions). Correlations are for samples collected under thin, thick or thin and thick snow covers collectively based on their statistical similarity. Significance (middle) and the number of observations for every correlation (bottom) are also indicated. 175

Table 4.S.2. Maximum photosynthetic rates (P^B_s) (mg C mg chl a^{-1} h^{-1}) and photosynthetic efficiencies α^B (mg C mg chl a^{-1} h^{-1} (µmol photons m^{-2} $s^{-1})^{-1}$) modeled from 10 or 4 points following incubation of thin or thick snow covered samples with the ^{14}C radioisotope. 175

Table 5.3. Pearson correlation coefficients (top)—including *p*-values (middle) and sample size (bottom) of correlations—of picoeukaryote and nanoeukaryote abundance measured using flow cytometry ($Pico_{FC}$, $Nano_{FC}$) or estimated from light microscopy ($Pico_{LM}$, $Nano_{LM}$), average nanoeukaryote abundance of measurements from flow cytomtery and light microscopy ($Nano_{AVG}$) and abundance of microeukaryotes estimated from light microscopy ($Micro_{LM}$), with environmental parameters (*see* text for definitions) under thin snow cover. Missing data has been excluded pairwise and correlations of significance ($p<0.05$) are in bold 206

Table 5.4. Pearson correlation coefficients (top)—including *p*-values (middle) and sample size (bottom) of correlations—of picoeukaryote and nanoeukaryote abundance measured using flow cytometry ($Pico_{FC}$, $Nano_{FC}$) or estimated from light microscopy ($Pico_{LM}$, $Nano_{LM}$), average nanoeukaryote abundance of measurements from flow cytomtery and light microscopy ($Nano_{AVG}$) and abundance of microeukaryotes estimated from light microscopy ($Micro_{LM}$), with environmental parameters (*see* text for definitions) under thick snow cover. Missing data has been excluded pairwise and correlations of significance ($p<0.05$) are in bold 208

Table 5.5. Pearson correlation coefficients (top)—including *p*-values (middle) and sample size (bottom) of correlations—of centric diatom, pennate diatom and flagellate cell counts and their percent abundance of total cells enumerated using light microscopy, with environmental parameters (*see* text for

definitions) under thin snow cover. Missing data has been excluded pairwise and correlations of significance (p<0.05) are in bold.....209

Table 5.6. Pearson correlation coefficients (top)—including p-values (middle) and sample size (bottom) of correlations—of centric diatom, pennate diatom and flagellate cell counts and their percent abundance of total cells enumerated using light microscopy, with environmental parameters (*see* text for definitions) under thick snow cover. Missing data has been excluded pairwise and correlations of significance (p<0.05) are in bold.....210

Table 5.1 Detailed list of species abundance (cells ml^{-1}) in the bottom 0-5 cm of sea ice under thin snow cover following analysis by light microscopy. Taxonomic orders are highlighted in bold and are underlined, suborders are underlined. Algae included in the estimates of nanoeukaryotes are designated by (n) and microeukaryotes by (m).....231

Table 5.2 Detailed list of species abundance (cells ml^{-1}) in the bottom 0-5 cm of sea ice under thick snow cover following analysis by light microscopy. Taxonomic orders are highlighted in bold and are underlined, suborders are underlined. Algae included in the estimates of nanoeukaryotes are designated by (n) and microeukaryotes by (m).....236

Table 5.S.1. Results from linear regression analyses of average nanoeukaryote abundance with environmental parameters (*see* text for definitions) under thin and thick snow covers. The coefficient of determination (r^2) is presented in unstandardized and standardized (brackets) forms, along with the significance of each regression (p) and the associated regression equation when $p < 0.05$. 241

Table 5.S.2. Results from linear regression analyses of average microeukaryote abundance with environmental parameters (*see* text for definitions) under thin and thick snow covers. The coefficient of determination (r^2) is presented in unstandardized and standardized (brackets) forms, along with the significance of each regression (p) and the associated regression equation when $p < 0.05$. 242

Table 5.S.3. Results from linear regression analyses of chlorophyll *a* (chl *a*), particulate organic carbon (POC) or primary production relative to chlorophyll *a* (PP_{chla}) with average nanoeukaryote ($Nano_{AVG}$) and/or microeukaryote ($Micro_{LM}$) abundance under thin and thick snow covers. The standardized coefficient for multiple regressions (β), the coefficient of determination (r^2) in unstandardized and standardized (brackets) forms and the associated regression equation when $p < 0.05$ are shown. The significance (p) of each standardized coefficient and regression equation are also presented. 243

Table 6.S.1. Test statistic (t) and significance (p) of student independent t-tests (df = 10) performed on variables including: daily average $\bar{E}_0$ ($\bar{E}_{0(daily)}$) and $\hat{E}_0$ ($\hat{E}_{0(daily)}$), the community compensation point (C_{IC}), chlorophyll *a* (chl *a*), particulate organic carbon (POC), numerical abundance of centric (C_N) and pennate (P_N) diatoms, and percent abundance of centric (C_P) and pennate (P_P) diatoms, salinity of the ice-ocean interface, nitrate + nitrite (NO_x) in the bottom ice, bottom-ice temperature, hourly net community production in darkness (NCP_{dark}), at 10 µmol m^2 s^{-1} (NCP_{10}), 21 µmol m^{-2} s^{-1} (NCP_{21}) and 55 µmol m^{-2} s^{-1} (NCP_{55}), daily integrated net community production calculated from $\bar{E}_{0(daily)}$ ($NCP_{\bar{E}0}$) and $\hat{E}_{0(daily)}$ ($NCP_{\hat{E}0}$), and bacterial production (BP). Data were grouped based on collection date (≤ 8 May, >8 May), where the mean and standard deviation (brackets) for each time period are presented. Bolded values indicate $p > 0.05$ 268

Table 7.1. Summary of advantages and disadvantages of the oxygen optode method developed in this research, as well recommendations for its future application. 274

LIST OF FIGURES

Figure 2.1. Overview of the water bodies and bathymetry of the Arctic marine system discussed in this chapter. This includes water bodies ≤ 60°N (purple), Arctic basins (white), continental shelves (grey), mixed deep water and shelf regions (black), and the fjords associated with Greenland (orange). Russian seas and the Bering sea (brown) are also labeled but are not included in the defined Arctic marine system. Modified from Jakobson et al. [2012]. Used with permission from John Wiley & Sons.....27

Figure 2.2. Winter extent of first-year ice (blue) and multiyear ice (red) in February 2006. Modified from Comiso et al. [2012]. Used with permission from the American Meteorological Society.....29

Figure 2.3. Summary of the physical characteristics for Arctic first-year and old sea ice over spring-summer melt [Light et al., 2003; Petrich & Eiken 2010], and the sympagic algal communities that may be present in each [Horner, 1985; Quillfedt et al., 2009; Lee et al., 2011]. Seasonal changes in upper atmosphere photosynthetically active radiation (PAR) [Leu et al., 2015] and timing of the bottom-ice algal bloom in the European shelf seas [Leu et al., 2011] are also presented for the latitudes 75°N (green), 80°N (blue) and 85°N (yellow).....30

Figure 2.4. Modeled averages of bottom-ice (3 cm) chlorophyll (chl) biomass with latitude and month of year, in first-year and old sea ice collectively, 1992. Modified from Deal et al. [2011]. Used with permission from John Wiley & Sons. 36

Figure 2.5. Photosynthesis-irradiance curve depicting algal production in darkness (P_0) and net photosynthesis under illumination. The irradiance at which respiration is equivalent to production is represented by the variable I_c. *See* text for a description of other parameters. Adapted from Falkowski and Raven [2007].....45

Figure 2.6. Regional summary of minimum (light blue), maximum (red) and average (dark blue or green) values of daily primary production (PP, circles) and bacterial production (BP, squares) in sea ice: first-year (unlabeled or F), multiyear (M), pack ice of unspecified age (P), a combination types (eg. F+P). Arrows indicate the main inputs from the Pacific (blue) and Atlantic (red) Oceans, general movement of surface waters [Stein & MacDonald, 2004] and nutrient fluxes (kmol s^{-1}) into (positive) and out of (negative) the Arctic as defined by Torres-Valdes et al. [2013]. Regions are colored by definitions in Section 2.1 with chlorophyll *a* concentration (boxes) specified (*see* Table 2.3 and Arrigo et al. [2010b] for references). See Table 2.3 for algal and Table 2.6 for bacterial sampling information and references.....47

Figure 2.7. Regional summary of minimum (light blue), maximum (red) and average (dark blue) values of for assimilation rates (circles) and bacterial production (BP, squares) in sea ice: first-year (unlabeled or F), multiyear (M), pack ice of unspecified age (P), a combination types (eg. F+P). Arrows indicate the main inputs from the Pacific (blue) and Atlantic (red) Oceans, general movement of surface waters [Stein & MacDonald, 2004], and nutrient fluxes (kmol s^{-1}) into (positive) and out of (negative) the Arctic as defined by Torres-Valdes et al. [2013]. Regions are colored by definitions in Section 2.1 with bacterial cell counts (boxes; cells l^{-1}) specified (references are marked by * in *References*). See Table 2.4 for algal and Table 2.6 for bacterial sampling information and references. 50

Figure 2.8. Percent transmission (isobars) of downwelling surface irradiance through first-year sea ice as a function of snow and ice thickness. From Maykut and Grenfell [1975]. Used with permission from John Wiley & Sons. 58

Figure 2.9. Seasonal increase in spectral transmitted irradiance (mW m^{-2} nm^{-1}) through (a) first-year ice transitioning into second-year ice and (b) multiyear sea ice. Changes in snow cover and ice thickness are also indicated. Modified from (a) Wang et al. [2014] and (b) Nicolaus & Gerland [2010] drift studies >80°N and >85°N, respectively. Used with permission from the authors and John Wiley & Sons. 61

Figure 2.10. Historical averages (1979-2007) of freeze onset in the Arctic. Scale shows day of year. From Markus et al. [2009]. Used with permission from John Wiley & Sons. 74

Figure 2.11. Snow depth on first-year sea ice (colored) estimated from the Earth Observing System (EOS) for March 21, 2006. Depths of snow are colored (cm), and do not include multiyear ice (grey). From Cavalieri et al. [2012]. Used with permission from the authors 75

Figure 2.12. Nitrate, phosphate and silicate concentrations entering the Arctic Ocean from the Atlantic (through the Barents Sea Opening) and Pacific Ocean (through the Bering Strait). Modified from Torres-Valdes et al. [2013]. Used with permission from John Wiley & Sons. 76

Figure 2.13. Modeled 14-day averages of tidal current speed (cm s^{-1}) in the Arctic Ocean during the ice-free period. The 500m isobath is also included. Velocities do not account for reductions as a result of ice coverage. From Padman & Erofeeva [2004]. Used with permission from John Wiley & Sons. 79

Figure 3.1. Concentration of chlorophyll *a* (chl *a*) in the bottom 0-5 cm (black) and 5-10 cm (grey) of sea ice under a) thin (< 10 cm) or b) thick (15-25 cm) snow covers. 118

Figure 3.2. Concentration of chlorophyll *a* (chl *a*) in sample treatments including i) $FSW_{3:1}$, bottom 5 cm of ice cores melted in filtered sea water at a ratio of approximately three parts filtered seawater to one part ice, ii) FSW_{zero}, bottom 5 cm of ice melted without the addition of filtered seawater, and iii) $FSW_{8:1}$, bottom ~1 cm of ice cores scraped into FSW at a ratio of about 8 parts filtered seawater to one part ice. The $FSW_{8:1}$ sample divided by 5 cm (8:1 (0-5 cm)) is also shown for comparison with $FSW_{3:1}$ samples. Estimates with filtered seawater have been corrected for dilution. 120

Figure. 3.3. Images of ruptured *Pleurosigma* / *Gyrosigma* spp. (left) and *Attheya* spp. (right) cells of thin snow covered samples collected on 30 May that were melted without the addition of filtered seawater (FSW_{zero}) 121

Figure 3.4. ^{14}C-derived photosynthesis-irradiance curves of gross primary production determined for bottom-ice algae under thin (< 10 cm) snow covered sea ice from 17 May to 5 June. Melt treatments of algal samples include a) $FSW_{8:1}$, bottom ~1 cm of ice scraped into filtered seawater at a ratio of about 8 parts filtered seawater to one part ice melt, b) $FSW_{3:1}$, bottom 5 cm ice melted in filtered sea water at a ratio of approximately three parts filtered seawater to one part ice melt, and c) FSW_{zero}, bottom 5 cm of ice melted without filtered seawater. 122

Figure 4.1. Map of study location near Cambridge Bay, Nunavut. Inset includes approximate locations of the main rivers in the area..... 134

Figure 4.2. Illustration of an optode chamber set-up, showing incubation bottle positions 1 (closest to light) through 4-black (furthest from light) and directionality of water flow (dashed arrows)..... 138

Figure 4.3. Examples of community production estimates for thin (a, c) and thick (b, d) snow covers from 22 May. Net change in oxygen per liter during optode incubations is plotted over the 70 h incubation time period for each bottle (a, b). Optode based gross primary production are also plotted as a function of incubation light intensity, relative to chlorophyll *a*, with their corresponding exponential models (c, d)..... 141

Figure 4.4. Site characteristics over the spring sampling period, including snow and ice thickness (a, b), transmittance of photosynthetically active radiation (PAR) directly measured (Raw) or averaged ± 2 days of core collection (Average) (c, d), and bottom-ice nutrient concentrations (c, d) under thin (a, c, e) and thick (b, d, f) snow covers. Albedo measured over thin (c) and thick (d) snow is also shown. 144

Figure 4.5. Concentration of phosphate (PO_4)(black), nitrate + nitrite (NO_3 + NO_2)(grey) and silicate ($Si(OH)_4$)(white) at the ice-ocean interface over the sampling period. 146

Figure 4.6. Bulk salinity and brine volume over the spring sampling period in the bottom 5 cm of sea ice (a) and brine volume profile from the ocean-ice interface (0 cm) to air-ice interface on 17 May, 25 April and 5 June. Values are from ice under thin snow cover. 147

Figure 4.7. Seasonal changes in (a) bottom-ice chlorophyll *a* (chl *a*), (b) ratios of particulate organic carbon (POC) to chl *a*, and (c) POC to particulate organic nitrogen (PON), under thin (black) and thick (grey) snow covers. Significant (solid line) ($p < 0.05$) seasonal trends are also indicated, with associated correlation coefficients. 148

Figure 4.8. Photosynthetic parameters P^B_s (a), α^B (b), P_0 (c), E_s (d) and E_c (e) of ice algae under thin (black) and thick (grey) snow covers (*see* text for definitions). Significant (solid line) ($p < 0.05$) seasonal trends are also indicated, with associated correlation coefficients. 151

Figure 4.9. Estimates of daily-integrated production of sea ice algae under thin (black) and thick (grey) snow covers. Linear trend lines for production over the sampling period are also indicated. 158

Figure 5.1. (a) Location of sample collection in the Canadian Arctic, with (b) average snow (black) and ice (grey) thickness over the study period shown for sites designated as thin and thick. 183

Figure 5.2. Seasonal change in (a) downwelling of photosynthetically active radiation (PAR) averaged daily at the snow-ice surface (E_0(PAR)) (dashed) and measured at the ice-ocean interface (E_z(PAR)) (solid), (b) bottom-ice chlorophyll *a* (chl *a*) with standard deviation (bars) from Campbell et al. [2016] and (c) bottom-ice particulate organic carbon (POC) concentrations. With the exception of downwelling PAR at the surface, estimates were made on ice covered by thin (black) and thick (grey) snow covers. 190

Figure 5.3. (a) Abundance of heterotrophic bacteria (cells x 10^6 ml^{-1}) measured with flow cytometry (bars) under thin (dark grey) and thick (light grey) snow covers. Bacterial production (dots) with the standard deviation between replicates over the sampling period is also shown for cells under thin (solid) and thick (open) snow covers. (b) Daily bacterial production normalized by bacterial abundance in sea ice under thin (solid) and thick (open) snow covers. 193

Figure 5.4. Flow cytometry measurements of picoeukaryote (light grey), nanoeukaryote (dark grey) and cyanobacteria (black) abundance under thin (a) and thick (b) snow covers. 195

Figure 5.5. Percent abundance of picoeukaryote (< 2 um, light grey), average nanoeukaryote (2-20 um, dark grey) and microeukaryote (21-200 um, black)

cells in the bottom-ice at the beginning (7 March), middle (8 May) and end (9 June) of the spring. The average size composition of the sea ice algal community for the entire sampling period is also presented.....197

Figure 5.6. Cell abundance time series of nanoeukaryotes (2-20 μm, light grey) and microeukaryotes (21-200 μm, dark grey) under thin (a) and thick (b) snow covers, enumerated over the spring using inverted light microscopy. Seasonal change in estimated daily production from Campbell et al. [2016] is also shown (line).....199

Figure 5.7 Percent composition of the main algal taxonomic groups in the bottom-ice under thin (a) and thick (b) snow covers. Seasonal changes in pennate (open circle) and centric (solid circle) diatom abundance are also highlighted. Dashed lines indicate the average pennate and centric diatom abundance in sea ice of the Canadian Arctic [*see* Poulin et al., 2011]. 202

Figure 5.8. Linear regressions between heterotrophic bacterial abundance or bacterial production, with prokaryotic algal cell abundance (a, b) independent of an outlier on 21 April (circle) and brine volume in the bottom 0-5 cm of sea ice (c, d). Samples were collected from under thin (black) or thick (grey) snow covers although, brine volume was calculated for thin snow cover only. Significant ($p < 0.05$) linear models of the data are also shown. 205

Figure 5.9. Abundance of estimated nanoeukaryotic cells using light microscopy, versus nanoeukaryotic cell counts from flow cytomwtry analysis of samples under thin (black) and thick (grey) snow covers. Power functions (solid) and a 1:1 line (dashed) are also presented. 215

Figure 6.1. (a) ($\bar{E}_0$) (grey) and $\hat{E}_0$ (black) for days of ice core collection, (b) seasonal concentration of bottom ice particulate organic carbon (POC) and chlorophyll *a* (chl *a*) with linear trend lines and daily net production rates (P_{net}) (mg m^{-2} d^{-1}) before and after 8 May, and (c) abundance of pennate and centric diatoms in the ice algal community over the spring during Phases I (grey) and II (white). The dashed line on (c) highlights the approximate division between pennate and centric diatom dominance in the bottom ice community, where the specific percent abundance of each taxonomic group relative to the entire bottom ice community is reported for each phase. 249

Figure 6.2. (a) Net community production of bottom-ice samples (5 cm) incubated at light intensities of approximately 0, 10, 21 and 55 μmol m^{-2} s^{-1} during Phases I (grey) and II (white) and (b) an exponential model of net community production on 29 April to highlight the community light compensation point (C_{EC}) parameter. In (a), values of C_{EC} (μmol m^{-2} s^{-1}) calculated for all incubations are listed above the respective production estimates, expect for 13 May where it was not defined (ND).....252

Figure 6.3. Net community production in the bottom-ice samples (5 cm) modeled over 24 hours on core collection days, using $\bar{E}_0$ (dark grey) or $\hat{E}_0$ (light grey) during Phases I (grey) and II (white). Circles indicate daily-integrated estimates of net community production modeled from $\bar{E}_0$ (black) and $\hat{E}_0$ (hollow), respectively. 254

Figure 7.1. Minimum incubation time required for optode incubations based on 30% deviation of gross primary production from the original 70 h incubation, versus chlorophyll *a* (chl *a*) concentration (uncorrected for dilution). Samples include gross primary production for all illuminated bottles over all sample cycles, collected from thin and thick snow covers. Exponential relationship (RMSE = 12 h) with ±1 SD, and grouping of data points 1-3 discussed in the text are highlighted for reference. 277

LIST OF ABBREVIATIONS AND NOTATIONS

(List only includes those used regularly in this thesis)

Biological parameters

Chl *a*	Chlorophyll *a*
DOC	Dissolved organic carbon
POC	Particulate organic carbon
PON	Particulate organic nitrogen
$FSW_{17:1}$	Solution of one part sea ice and 17 parts filtered seawater
$FSW_{3:1}$	Solution of one part sea ice and three parts filtered seawater
FSW_{zero}	Solution of sea ice without the addition of filtered seawater
NO_x	Nitrate (NO_3^-) + nitrite (NO_2^-)
PO_4	Phosphate
$Si(OH)_4$	Silicic Acid

Photosynthesis-irradiance parameters

P^B_s	Maximum photosynthetic rate in the absence of photoinhibition
α^B	Photosynthetic efficiency
β^B	Photoinhibition index
E_s	Photoacclimation index
E_c	Cellular compensation light intensity
C_{EC}	Community compensation light intensity
P_0	Production at zero irradiance

Light

PAR	Photosynthetically active radiation
E_z(PAR)	Downwelling photosynthetically active radiation at the ocean-ice interface (Specific to study period between 7 March and 30 May)
E_z(June)	Downwelling photosynthetically active radiation at the ocean-ice interface (Specific to study period between 7 March and 9 June)
E_0(PAR)	Downwelling photosynthetically active radiation at the snow surface
$\bar{E}_0$	Scalar photosynthetically active radiation averaged for the ice algal layer
$\hat{E}_0$	Scalar photosynthetically active radiation averaged for the ice algal layer volume
T_{PAR}	Transmittance of photosynthetically active radiation

USE OF COPYRIGHTED MATERIAL

Figure 2.1. Jakobsson, M., et al. (2012), The International Bathymetric Chart of the Arctic Ocean (IBCAO) Version 3.0, *Geophys. Res. Lett.,* doi: 10.1029/2012GL052219. Copyright (2012), John Wiley & Sons.

Figure 2.2. Comiso, J.C. (2012), Large decadal decline of the Arctic Multiyear ice cover, *J. Climate* 25, 1176-1193, doi: 10.1175/JCLI-D-11-00113.1. Copyright (2012), American Meteorological Society.

Figure 2.4. Deal, C., Jin, M., Elliot, S., Hunke, E., Maltrud, M., and N, Jeffery (2011), Large-scale modeling of primary production and ice algal biomass within arctic sea ice 1992, *J. Geophys. Res.* 116, C07004, doi: 10.1029/2010JC006409. Copyright (2011), John Wiley & Sons.

Figure 2.8. Maykut, G.A., and T.C. Grenfell (1975), The spectral distribution of light beneath first-year sea ice in the Arctic Ocean, *Limnol. Oceanogr.* 20, 554–563. Copyright (1975), John Wiley & Sons.

Figure 2.9. Modified from Wang , S., Bailey, D., Lindsay, K., Moore, J.K., and M. Holland (2014), Impact of sea ice on the marine iron cycle and phytoplankton productivity, *Biogeosc.* 11, 4713-4731, doi:10.5194/bg-11-4713-2014. Copyright (2014) Authors. Nicolaus, M., Gerland, S., Hudson, S.R., Hanson, S., Haapala, J., and D.K. Perovich (2010), Seasonality of spectral albedo and transmittance as observed in the Arctic Transpolar Drift in 2007, *J. Geophys. Res.* 115, C11011, doi: 10.1029/2009JC006074. Copyright (2007), John Wiley & Sons.

Figure 2.10. Markus, T., Stroeve, J.C., and J. Miller (2009), Recent changes in Arctic sea ice melt onset, freeze-up, and melt season length, *J. Geophys. Res.* 114, C12024, doi: 10.1029/2009JC005436. Copyright (2009), John Wiley & Sons.

Figure 2.11. Cavalieri, D.J., and C.L. Parkinson, C.L. (2012), Arctic sea ice variability and trends, 1979-2010, *Cryosph.* 6, 881–889, doi: 10.5194/tc-6-881-2012. Copyright (2012), Authors.

Figure 2.12. Torres-Valdes, S., Tsubouchi, T., Bacon, S., Naveira-Garabato, A.C., Sanders, R., McLaughlin, F.A., Petrie, B., Kattner, G., Azetsu-Scott, K., and T.E. Whitledge (2013), Export of nutrients from the Arctic Ocean, *J. Geophys. Res. Oceans* 118, 1625–1644, doi: 10.1002/jgrc.20063. Copyright (2013), John Wiley & Sons.

Figure 2.13. Padman, L., and S. Erofeeva (2004), A barotropic inverse tidal model for the Arctic Ocean, *Geophys. Res. Lett.* 31, L02303, doi: 10.1029/2003GL019003. Copyright (2004), John Wiley & Sons.

Chapter Four of this thesis is reproduced with minor modifications from Campbell et al. (2016), Community dynamics of bottom-ice algae in Dease Strait of the Canadian Arctic, *Prog. Oceanogr.* 149, 27-39, doi: 10.1016/j.pocean.2016.10.005, with permission from Elsevier.

Chapter Five of this thesis is reproduced with minor modifications from Campbell et al. (2017a), Seasonal dynamics of algal and bacterial communities in Arctic sea ice under variable snow cover, submitted to *Polar Biol.*

Chapter Six of this thesis is reproduced with minor modifications from Campbell et al. (2017b), Net community production in the bottom of Arctic sea ice over the spring bloom, submitted to *Geophys. Res. Lett.*

CHAPTER ONE: INTRODUCTION

1.1 Motivation

Sea ice in the Arctic is undergoing remarkable changes in volume, seasonality and coverage due to warming of the global climate [Vihma, 2014]. The implications of these changes are far-reaching, and will include habitat disruption for the algae and bacteria living in sea ice. This is important because together ice algal and bacterial production contribute to the base of the Arctic marine ecosystem and to carbon cycling within the Arctic Ocean [Legendre et al., 1992; Deming, 2010]. Ice algae are of particular significance to the polar marine ecosystem because their pulse of production in spring represents a concentrated food resource with high poly-unsaturated fatty acid (PUFA) content that supplies higher trophic levels with nutrition [Leu et al., 2011].

Physical processes in the sea ice environment and greater pelagic system control the rate at which ice algae and bacteria produce carbon biomass. Understanding these processes is required to explain current variability in production estimates around the Arctic, and predict the potential response of sea ice algal and bacterial production to climate change. An integral part of this is efficiently measuring algal and bacterial contributions to production while assessing their responses to environmental change. However, despite variability in water masses, mixing dynamics and types of ice across the Canadian Arctic [Michel et al., 2006], production measurements in sea ice are largely restricted to the vicinity of Barrow Strait [Leu et al., 2015]. It is therefore important to not only conduct additional process studies on sea ice productivity, but to complete them in previously under-sampled regions.

Incubations with the ^{14}C radioisotope are the most common approach to measuring sea ice primary production. However, when ^{14}C is used the influence of respiration and the accuracy of measurements at low light levels are uncertain [Williams, 1993; Mara, 2009]. Furthermore, use of radioisotopes in remote field locations in the Arctic can be challenging. Developing alterative methods is therefore an important step towards improving accuracy and coverage of primary production estimates in the Arctic. Comparability of new methods with ^{14}C estimates is also crucial, as results must be placed in the context of the current literature.

1.2 Thesis Objectives

The goal of this thesis is to document algal and bacterial production in sea ice and assess controls of their variability. This is achieved by developing an oxygen optode based method of measuring gross primary and net community production, and by measuring bacterial production using ^{3}H-Leucine radioisotopes. These methods are applied to a case study on the sea ice near Cambridge Bay, Nunavut during the spring of 2014, in combination with the measurement of environmental parameters. Overall the goal of this original research is divided into two objectives:

1. Assess experimental methods of measuring sea ice productivity
    i) Identify the effects of ice melting procedure on ice algal productivity
    ii) Develop a radioisotope independent method of measuring primary production, community production, and photophysiological parameters
2. Evaluate dominant controls of ice algal and bacterial production during spring

1.3 Thesis Structure

This thesis is comprised of six chapters in addition to the introduction. Chapter Two provides context for the thesis topic by outlining properties of the sea ice environment during spring, outlining the communities present in sea ice and defining the concept of production. Current estimates of algal and bacterial production across the Arctic are also summarized in this chapter, and the documented causes of local to regional scale variability are assessed. Chapter Three outlines the rationale for sample collection and pre-processing that is used throughout this research. This chapter includes an investigation of how three different ice melt procedures may impact ^{14}C-derived primary productivity, which addresses objective 1-i listed in Section 1.2. Chapters Four and Five are original full-length manuscripts that are published or are in review with peer-reviewed journals, respectively. Chapter Six is an original research letter that is also under review in a peer-reviewed journal. Conclusions from this research are summarized and suggestions for future research are presented in Chapter Seven.

Chapter Four addresses thesis objectives 1-i and 2 by describing an oxygen optode based method for determining gross primary production and photosynthesis-irradiance parameters. The response of photosynthesis-irradiance parameters to seasonally variable environmental conditions is also investigated. This work has been peer-reviewed and published in the journal *Progress in Oceanography*:

Campbell, K., C.J. Mundy, J.C. Landy, A. Delaforge, C. Michel and S. Rysgaard (2016), Community dynamics of bottom-ice algae in Dease Strait of the Canadian Arctic, *Prog. Oceanogr.* 149, 27-39, doi: 10.1016/j.pocean.2016.10.005.

Chapter Five addresses thesis objective 2. It documents a unique seasonal succession in composition of the ice algal and bacterial community, dependent on environmental

conditions, and relates compositional changes to variability in chlorophyll *a* (chl *a*), particulate organic carbon (POC), and optode-derived gross primary production. This work is currently under review in the journal *Polar Biology*:

Campbell, K., Mundy, C.J., Belzile, C., Delaforge, A. and S. Rysgaard, Seasonal dynamics of algal and bacterial communities in Arctic sea ice under variable snow cover, *Polar Biol*. (in review).

Chapter Six addresses thesis objectives 1-i and 2. Net community production is documented over the spring using the oxygen optode set-up developed in Chapter Four. The dependency of the resulting productive state (i.e. autotrophic or heterotrophic) on environmental and biological conditions of the bloom are investigated. This work is currently under review in the journal *Geophysical Research Letters*:

Campbell, K., Mundy, C.J., Gosselin M., Landy, J.C., Delaforge, A. and S. Rysgaard, Net community production in the bottom of Arctic sea ice over the spring bloom, *Geophys. Res. Lett*. (in review).

References

Deming, J.W. (2010), Sea ice bacteria and viruses, In: Thomas D.N., Dieckmann G.S. (eds.), *Sea Ice 2nd Ed*., Wiley Blackwell Publishing, Malaysia, 248-282.

Legendre, L., Ackley, S.F., Dieckmann, G.S., Gullicksen, B., Horner, R., Hoshiai, T., Melnikov, I.A., Reeburgh, W.S., Spindler, M., and C.W. Sullivan (1992), Ecology of sea ice biota: Part 2, *Polar Biol*. 12(3), 429–444, doi:10.1007/BF00243113.

Leu, E., Mundy, C.J., Assmy, A., Campbell, K., Gabrielsen, T.M., Gosselin, M., Juul-Pedersen, T., and R. Gradinger (2015), Arctic spring awakening – Steering principles behind the phenology of vernal ice algae blooms, *Prog*. *Oceanogr*. 139, 151-170, doi:10.1016/j.pocean.2015.07.012.

Leu, E., Søreide, J.E., Hessen, D.O., Falk-Petersen, S., and J. Berge (2011), Consequences of changing sea ice cover for primary and secondary producers in European Arctic shelf seas: timing, quantity and quality. *Prog*. *Oceanog*. 90(1-4), 18–32, doi: 10.1016/j.pocean.2011.02.004.

Marra, J. (2009), Net and gross productivity: weighing in with ^{14}C. *Aquat*. *Microbiol*. *Ecol*. 1-9, doi: 10.3354/ame01306.

Michel, C., Legendre, L., Ingram, R.G., Gosselin, M., and M. Levasseur (1996), Carbon budget of sea-ice algae in spring: Evidence of significant transfer to zooplankton grazers. *J*. *Geophys*. *Res*. 101(C8), 18345-18360, doi: 10.1029/96JC00045.

Vihma, T. (2014), Effects of Arctic sea ice decline on weather and climate: A review. *Surv*. *Geophys*. 35, 1175-1214, doi: 10.1007/s10712-014-9284-0**.**

Williams, P.J. leB., 1993. Chemical and tracer methods of measuring plankton production. *–ICES Mar*. *Sci*. *Symp*. 197, 20-36.

CHAPTER TWO: BACKGROUND

In this chapter, the processes controlling Arctic sea ice algal and bacterial production across local, regional and pan-Arctic scales are reviewed. To focus on the spatial variability of production in sea ice across the Arctic, discussion is limited primarily to processes controlling production to the most biologically active and dynamic period of the year: the spring bloom. This time period is also the focus of research in the remaining chapters.

Begining in Section 2.1, the regions of interest in the Arctic and the types of sea ice habitats and communities found within them are characterized, and a brief summary of the geophysical characteristics of Arctic sea ice is provided. In Section 2.2, the processes of photosynthesis and respiration that produce algal and bacterial biomass, respectively, are introduced before measurements of algal and bacterial production reported in the literature for the Arctic are summarized (Section 2.3). In Section 2.4, the processes controlling production at the local scale are evaluated, before their role at the regional and pan-Arctic scales is assessed in Section 2.5. The controls of algal and bacterial production discussed in previous sections are then applied to evaluate current and predicted changes of production in sea ice with climate warming in Section 2.6. Finally, conclusions are provided in Section 2.7.

This chapter is largely comprised of material from the author's Ph.D. Candidacy Exam that was completed in October, 2015. It was written to address the following question:

"Describe the pertinent processes controlling sea ice bacterial and algal production in the Arctic. Please elaborate with respect to a) geographic differences in the pan-Arctic distribution of these processes, and b) their potential response to ongoing climate change."

2.1 Arctic sea ice algae and bacteria

The Arctic marine system is characterized by seasonal extremes in light and temperature that drive changes in the physical characteristics of sea ice, and its coverage on the Arctic Ocean. In turn, these changes affect the quality of environment and quantity of habitat that sea ice algae and bacteria may inhabit.

2.1.1 Regional definition of the Arctic

The Arctic marine system identifies a collection of Arctic water bodies characterized by the International Hydrographic Organization [1953]. The International Hydrographic Organization's water bodies are grouped into regions (Figure 2.1) by their approximate latitudinal limits (≤60°N or >60°N), water depth (i.e. Arctic basins, >500 m depth; continental shelf, 0-500 m depth; or a combination of deep water and shelf [Stein & MacDonald, 2004; Tang et al., 2004; Drange et al., 2005]. Greenland Fjords are also included as they represent systems that are unique to the other regional groups [e.g. Rysgaard & Glud, 2007].

The regions are defined as follows:

- **≤ 60°N**: Baltic Sea, Hudson Bay, Labrador Sea
- **Arctic basins**: central Arctic Ocean
- **Continental shelves**: Barents Sea, Beaufort Sea, Canadian Archipelago, Chukchi Sea
- **Deep water and shelf**: Baffin Bay, Davis Strait, Frobisher Bay, Greenland Sea
- **Greenland fjords**

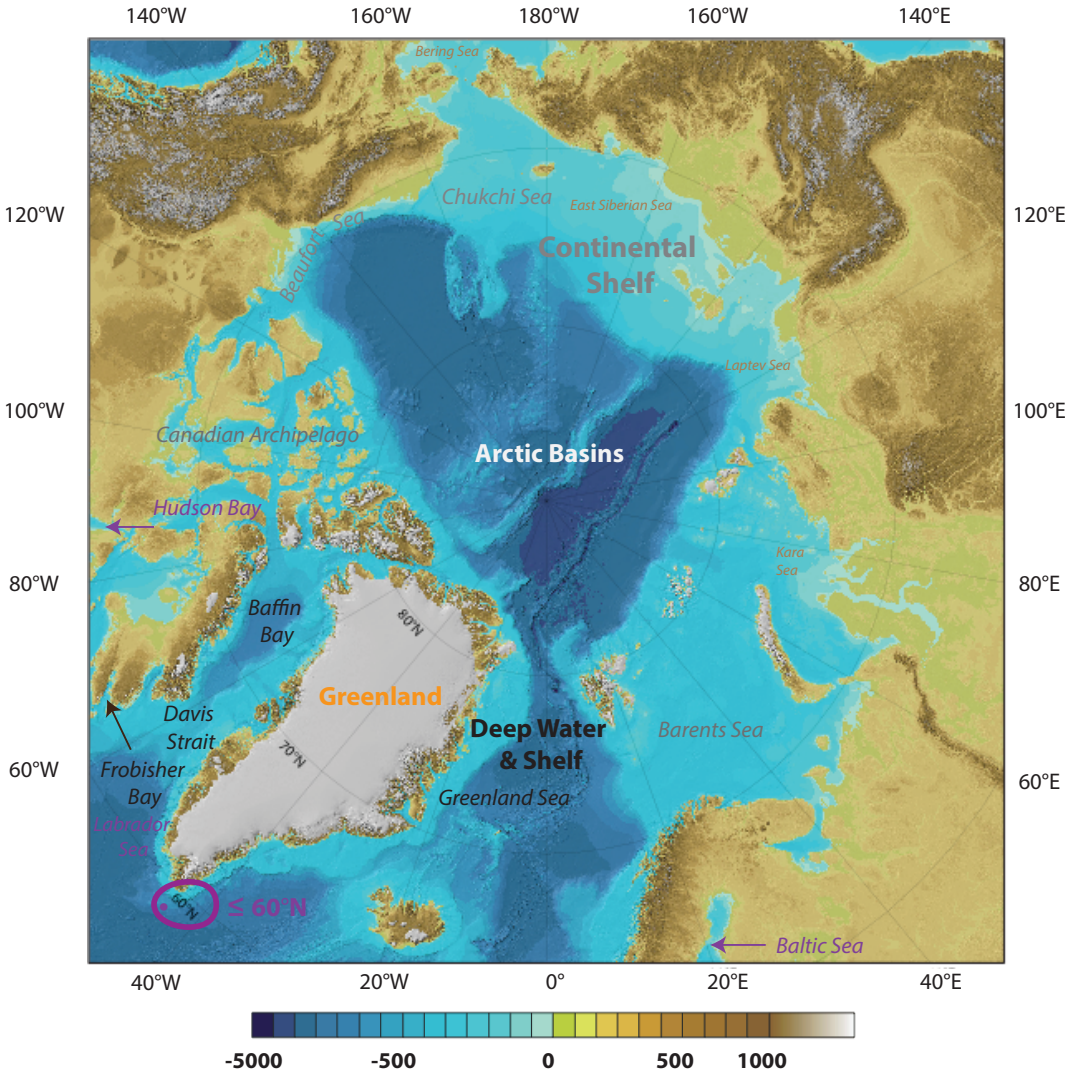

Figure 2.1. Overview of the water bodies and bathymetry of the Arctic marine system discussed in this chapter. This includes water bodies ≤ 60°N (purple), Arctic basins (white), continental shelves (grey), mixed deep water and shelf regions (black), and the fjords associated with Greenland (orange). Russian seas and the Bering sea (brown) are also labeled but are not included in the defined Arctic marine system. Modified from Jakobson et al. [2012]. Used with permission from John Wiley & Sons.

Here, the Russian Seas (Kara, Laptev, Eastern Siberian Seas) and the Bering Sea are not included because production data for these regions is not available or it could not be accessed.

2.1.2 Definitions of sea ice in the Arctic

The Canadian Ice Service [2016] defines five broad categories of floating sea ice based on age in its Manual of Ice (MANICE): (1) New ice of recently formed frazil crystals that may be loosely frozen together, but have a definite form, (2) nilas of ice up to 0.1 m thick that form a malleable crust, (3) young ice of 0.1-0.3 m commencing thermodynamic growth, (4) first-year ice greater than 0.3 m thickness with one winter's growth or less, and (5) old ice that has survived one (second-year ice) or more (multiyear ice) summers. First-year and old ice can be further classified based on their attachment to surrounding landmasses, as fixed along the coast (land-fast ice) or freely drifting (pack ice) [World Meteorological Organization 2010].

The formation of new ice, nilas and young ice in the fall/winter, and subsequent growth into first-year ice occurs mainly on the shelf seas. In comparison, old ice is mainly restricted to the central basins at latitudes ≥75°N unless ocean currents transport select ice floes elsewhere [Comiso et al., 2012]. The resultant winter coverage of first-year and old ice types in the Arctic marine system is illustrated in Figure 2.2. The majority of sea ice in the Arctic for most of the year is first-year ice, while multiyear ice currently accounts for less than 20% [Stroeve et al., 2014].

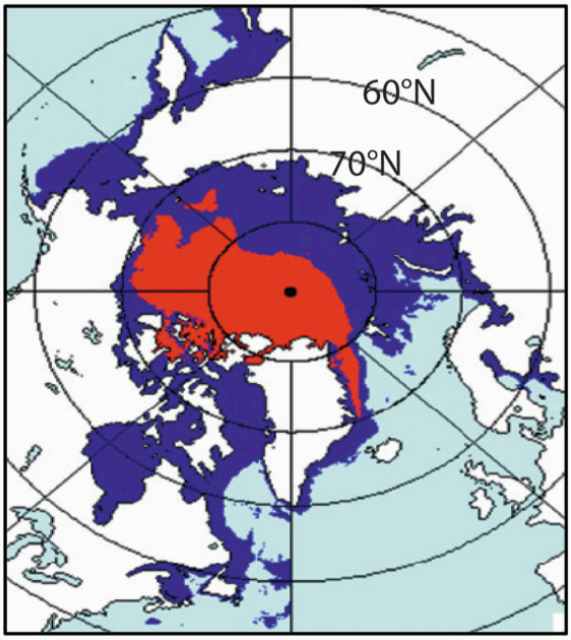

Figure 2.2. Winter extent of first-year ice (blue) and multiyear ice (red) in February 2006. Modified from Comiso et al. [2012]. Used with permission from the American Meteorological Society.

2.1.3 Physical characteristics of sea ice

The remainder of the chapter will focus on first-year ice and old ice (see Figure 2.3), as they comprise the majority of Arctic sea ice during the spring-summer when biological activity in the ice is greatest.

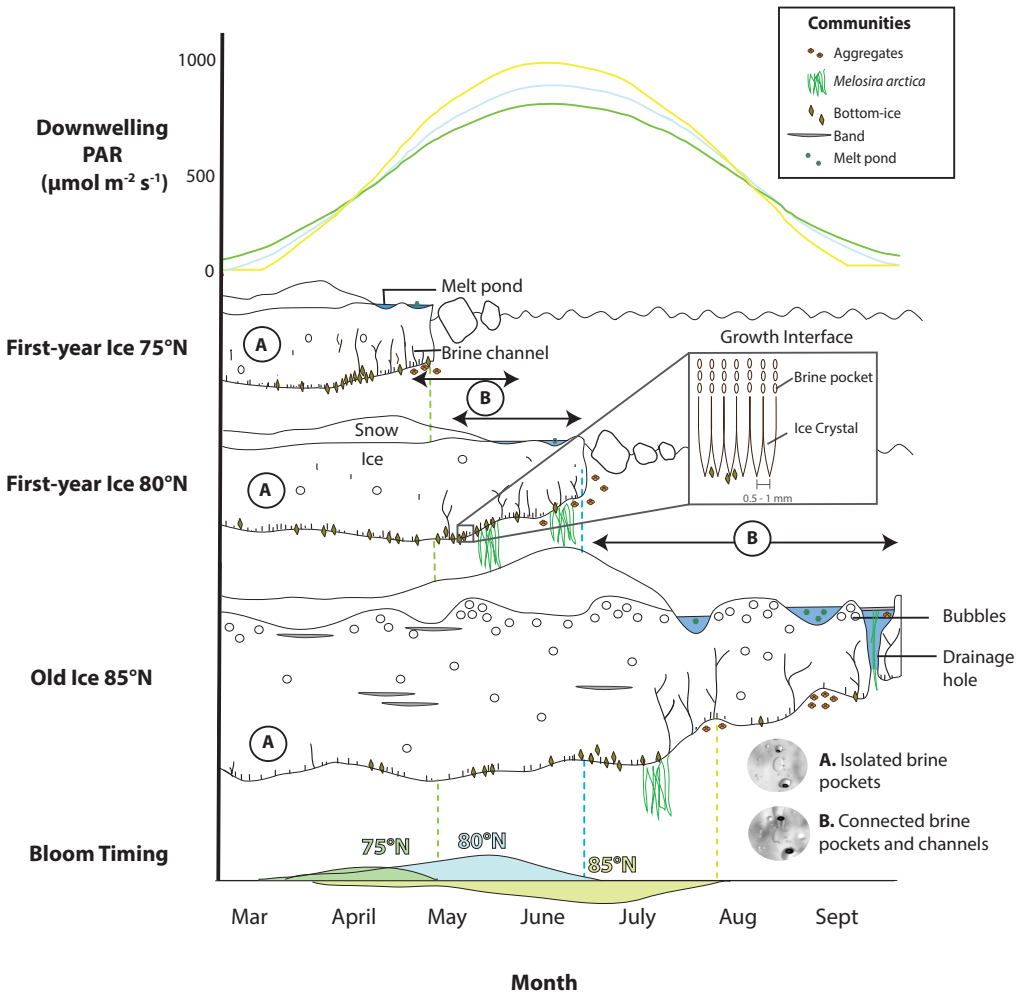

Figure 2.3. Summary of the physical characteristics for Arctic first-year and old sea ice over spring-summer melt [Light et al., 2003; Petrich & Eiken 2010], and the sympagic algal communities that may be present in each [Horner, 1985; Quillfedt et al., 2009; Lee et al., 2011]. Seasonal changes in upper atmosphere photosynthetically active radiation (PAR) [Leu et al., 2015] and timing of the bottom-ice algal bloom in the European shelf seas [Leu et al., 2011] are also presented for the latitudes 75°N (green), 80°N (blue) and 85°N (yellow).

Physical characteristics of first-year sea ice

Atmospheric cooling in the fall/winter causes the surface layer of seawater (salinity ranging from approximately 30 to 35 in the Arctic [Brandon et al., 2010] to become super cooled, forming frazil crystals that eventually consolidate at the surface to form young ice. The sea ice continues to grow thermodynamically through the winter and into the spring, as heat is removed from the ice-ocean growth interface towards the comparatively

cold atmosphere. As a result of this growth, temperatures decrease through the ice profile from the growth interface at freezing temperature, towards the atmosphere. Shortly after consolidation, snow accumulates on the ice cover and is redistributed by surface winds into drifts [Sturm & Massom, 2010]. Typically, the earlier first-year ice forms, the more snow will accumulate on its surface [Webster et al., 2014]. Snow insulates the sea ice from atmospheric temperatures, which hinders thermodynamic growth when atmospheric temperatures are low, but delays ice melt when atmospheric temperatures increase [Sturm & Massom, 2010].

During the process of ice growth, salts are concentrated into a brine solution that can become trapped between elongated ice crystals at the ice-ocean interface and incorporated into the ice cover, along with dissolved gases. The result is a growth interface with relatively high surface area that is referred to as the skeletal layer, and a multi-phase matrix of solid ice, gaseous bubbles and brine pockets (Figure 2.3). The proportion of brine trapped in the ice is a portion of total brine created during ice growth, with 60-90% of ions rejected from growing ice to the ocean below [Petrich & Eiken, 2010].

During spring in the Arctic, there is a transition from total darkness and subzero (°C) temperatures to 24 h daylight and temperatures above 0°C [Leu et al., 2015]. This causes one of the strongest seasonal shifts of light and temperature on the planet, and drives warming of the ice and eventual surface melt from snow-covered, to bare ice, and eventual coverage by melt water ponds that can deepen to form thaw holes. The transition is summarized in Figure 2.3, which includes the seasonal change in downwelling of wavelengths used in algal photosynthesis, or photosynthetically active radiation (PAR, 400-700 nm).

As sea ice melts, the volume of brine increases as bulk ice salinity decreases. At -5°C the relationship between these parameters in sea ice is well documented as the '*Rule of Fives'*, where brine volume is approximately 5% and bulk ice salinity is 5 [Petrich & Eicken, 2010]. It follows that internal ice temperatures above -5°C are an important step in the melt process, as isolated air and brine pockets created during formation connect into a network of channels that permit gravity drainage of brine, with replacement by fresher melt water as the ice undergoes advanced stages of melt [Golden et al., 1998; Eicken et al., 2002]. The drainage of brine coupled with snow and ice melt changes the overall salinity of first-year ice from cold and salty in winter and early spring (eg. bulk ice salinity of 7), to comparatively warm and fresh in late spring and summer (e.g. bulk ice salinity of 4) (*see* Figure 4.6b). Drainage of freshwater created from snow and ice melt through the brine network and via drainage holes also creates a freshwater layer immediately beneath the ice that 'floats' above the comparatively salty ocean water [Petrich & Eiken, 2010].

The timing of melt, and subsequent break up of first-year ice, ranges from May to July in the Arctic because the length of the polar day varies with latitude. It follows that first-year ice melts and disappears completely, earlier, with decreasing latitude (Figure 2.3).

Physical characteristics of old sea ice

Growth of old ice in the fall occurs from a developed layer of ice that has survived the summer. Although the mechanisms of ice growth are shared with first-year ice, the rate and total amount of annual ice growth is less because the thickness of perennial ice

buffers thermodynamic growth. As a result, the amount of brine formed and rejected from the ice is likely to be lower.

Similar to first-year ice, seasonal warming drives surface melt of old ice from snow covered, to bare ice, and melt pond coverage with thaw holes (Figure 2.3). However, the structure and composition of old ice is unique from first-year ice due to a history of annual growth and melt seasons, and collisions with other sea ice floes on the ocean. Old ice is structurally deformed, mostly drained of brine, and may contain lenses of refrozen melt water and surface melt ponds within the ice cover [Melnikov, 1997; Quillfedt et al., 2009]. As a result, old ice is fresher (e.g. 0-2) than first-year ice, with a higher density of air pockets, particularly at the surface [Horner, 1985; Petrich & Eiken, 2010]. Persistence of old ice through the summer intensifies melt features, which create a rough surface and sub-surface topography (Figure 2.3).

Finally, snow accumulation is greater on old ice than first-year ice because the ice platform is present through all seasons to catch precipitation [Iacozza & Barber, 1999]. Snow accumulation is particularly evident in the surface depressions formed by previous year's melt ponds (Figure 2.3) [Lange et al., 2015].

2.1.4 Algal and bacterial communities in sea ice

There are four microbial habitats associated with Arctic sea ice: surface, interior, bottom and sub-ice (Figure 2.3). Surface communities are largely restricted to advanced melt when algae and bacteria colonize melt ponds except when surface flooding creates infiltration assemblages (e.g. Buck et al. 1998), while algae and bacteria may inhabit the melt water and brine network of ice (interior), the growth interface (bottom) and water

directly below sea ice (sub-ice) for much of the year. Although algae and bacteria can occupy all four habitats, the majority of studies focus on the bottom-ice community because it consistently contains the greatest abundance of algae and bacteria in the Arctic [Horner, 1985].

Exceptions have been documented in the Arctic: the centric diatom *Melosira arctica* that attaches to the ice bottom and forms long strands below the ice [Gutt et al. 1995; Gosselin et al. 1997], the occasional dense interior communities of algae and bacteria in old ice [Gradinger & Zhang, 1997; Lange et al., 2015], and mucous bound accumulations of cells (aggregates) originating from *Melosira arctica* [Melnikov et al., 2002], surface communities [Lee et al., 2011] or bottom-ice algae (Figure 2.3) [Glud et al., 2014]. Documented occurrences of these communities are infrequent, likely due to a combination of limited spatial sampling and patchy spatial coverage.

Due to this uncertainty and the focus of literature on the bottom-ice algal community, discussion is limited for the remainder of this chapter to the bottom-ice community unless otherwise specified. Reference to ice algae hereafter refers to algae inhabiting the bottom-ice. Furthermore, due to sampling bias in the literature towards bottom-ice communities, assessments of sea ice bacteria are largely restricted to this region as well but may also include cells within the sea ice brine network.

Algal colonization and abundance

Algae may colonize the bottom of sea ice from the water column (1) in the fall during ice formation followed by downward movement with ice growth, or (2) repeatedly, following cell death with downward ice growth [Rózanska et al., 2008]. They are concentrated in

the bottom 0-10 cm in first-year ice [e.g Smith et al., 1990] and 0-40 cm in old ice [Quillfedt et al., 2009] as a result of favorable growth conditions that include: high surface area between ice crystals for colonization, shelter from grazers (Section 2.3.3) [Arrigo et al., 2010b], and close proximity or direct contact with ocean water (Section 2.3.1) [eg. Gradinger et al., 2002; Lund-Hansen et al., 2016].

With the transition to polar day, light is available for photosynthesis and the abundance of ice algae rapidly increases, or 'blooms' (Figure 2.3). This seasonal increase in ice algal biomass is represented in Figure 2.4 by a peak in the photosynthetic pigment chlorophyll (*see* Section 2.2.1) from February to March near 50°N, and May to June >70°N [Deal et al., 2011]. The differences in bloom duration with latitude are partially due to latitudinal variations of downwelling PAR, where the length of growing season roughly increases with latitude as a result of sustained light availability and ice stability (Figure 2.3). Figure 2.4 also highlights the latitudinal dependence of sea ice coverage, and therefore algal presence in sea ice, where >70°N chlorophyll is above 0 mg m^{-2} because old ice coverage dominates. Although, following the spring bloom chlorophyll in old ice is very low [Deal et al., 2011].

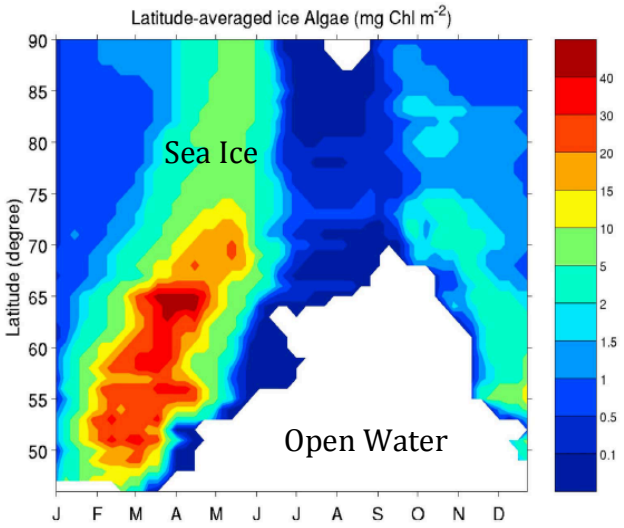

Figure 2.4. Modeled averages of bottom-ice (3 cm) chlorophyll (chl) biomass with latitude and month of year, in first-year and old sea ice collectively, 1992. Modified from Deal et al. [2011]. Used with permission from John Wiley & Sons.

With continued algal growth during the bloom, environmental conditions (i.e. nutrient availability) become limiting (Section 2.3.1) and processes associated with late spring-summer ice melt result in bloom termination (Section 2.3.3). Diatoms typically dominate over other algal groups because they can rapidly increase in biomass in response to favorable light conditions [Miller & Wheeler, 2012]. The pennate species *Nitzschia frigida* is often cited as the most abundant [Leu et al., 2015], while species of flagellates and dinoflagellates are often present in lower numbers [Mendle & Priddle, 1990].

Bacterial colonization and abundance

Bacteria are scavenged from the water column and colonize sea ice brines during ice formation, but decrease in abundance through the winter by 25-50% [Krembs et al., 2002; Collins et al., 2008], in part due to conditions of extremely high salinity (>200) and cold temperatures (< -30°C) [Kaartokallio et al., 2013; Ewert & Deming 2014]. Growth in the spring increases cell abundance again, to >5 times water column concentrations at

approximately 1.5 x 10^3 to 5 x 10^{11} cells l^{-1} [Smith et al., 1989; Maranger et al., 1994]. The spatial and temporal distribution of bacteria in the spring largely follows ice algae, peaking in the bottom-ice and during the spring bloom [e.g. Rysgaard & Glud, 2004; Comeau et al., 2013].

The majority of sea ice bacteria are heterotrophic and require external sources of organic carbon for metabolism. For this reason they are the focus of this chapter and thesis although, photosynthetic cyanobacteria can be present in low abundance (*see* Chapter Five) [Bowman et al., 2012]. Bacteria are primarily free-living, while those living in association with ice algae (epiphytic) account for less than 37% of the population [Smith et al., 1989].

2.1.5 Comparison of Arctic and Antarctic sea ice ecosystems

Physical and biological processes inherent to sea ice are largely universal, making discussion presented in this chapter applicable to the sea ice communities of both the Arctic and Antarctic. However, there are a number of physical and ice-related biological properties that are unique to each of these polar marine systems. These differences are summarized in Table 2.1, while discussion in the remainder of this document will focus on the Arctic as it is the region of interest in this thesis research.

Table 2.1. Summary of the physical and biological properties of Antarctic and Arctic marine systems, with differences highlighted. This includes differences in firstyear (FYI) and multiyear (MYI) sea ice coverage and the concentration of chlorophyll *a* (chl *a*) [Horner et al., 1985; Tucker et al., 1987; Lange et al., 1989; Spindler et al., 1990, Dieckmann et al., 1991; Gloerson et al., 1992; Hiel & Anderson, 1999; McMinn et al., 1999; Wadhams, 2000; Pavlov & Pavlova, 2007; Comiso et al., 2010; Thomas & Dieckmann, 2010; NSIDC, 2017].

Category		Antarctic	Arctic	Difference(s)
Physical Properties	**Geography**	Southern Ocean surrounds the island continent of Antarctica	Arctic Ocean is surrounded by landmasses	Unrestrained (Antarctic) versus contained (Arctic) water bodies
	Precipitation	Open water surrounding the Southern Ocean makes moisture readily available for evaporation	Surrounding landmasses and ice cover through the summer (MYI) limit moisture available for evaporation	Differing levels of evaporation causes greater precipitation in the Southern Ocean (except adjacent to to the Antarctic continent where precipitation is very low) Depth of snow cover on the majority of Antarctic sea ice is greater (except on the landfast ice), which can depress the freeboard and causes surface flooding
	Oceanography	Convergence of cold Southern Ocean water and warmer water from northern regions facilitates upwelling Divergence of water along the Antarctic continent	Inflowing water masses (Pacific and Atlantic water) are stratified below polar surface waters There is regional-based mixing on the continental shelves and at localized features such as sills	Nutrient concentrations are greater in the Southern Ocean than in the Arctic Ocean
	Sea Ice	MYI covers approximately 3.5×10^6 km^2	MYI covers approximately 9×10^6 km^2	Ice is thicker in the Arctic (FYI = 1.3 m) versus the Antarctic (FYI = 0.5-0.6 m) due to: Reduced ice movement Greater presence of MYI in the Arctic Lower salinity surface water in the Arctic facilitates greater ice growth
		FYI covers approximately 15.5×10^6 km^2 (>80% total sea ice coverage) Landfast ice is restricted to the continental boundaries	FYI covers approximately 7×10^6 km^2 (<50% total sea ice coverage)	
		Ice movement is unrestricted in the Southern Ocean (drift velocities >20 km d^{-1}), increasing the potential for sea ice to leave the region	Ice movement is constrained in the Arctic Ocean (drift velocities <10 km d^{-1}), staying in cold Arctic waters for a greater proportion of the year	
		Sea ice is restricted to 'lower' latitudes as the Antarctic continent covers the highest latitudes and South pole	Sea ice covers the most northern latitudes of this hemisphere, and extends to the North Pole	Ice at higher latitudes in the Arctic receives less light because downwelling solar radiation is at a lower angle of incidence
		20-50% of vertical ice profiles can be comprised of frazil ice	Ice growth is predominantly controlled by thermodynamic growth of congelation ice, while only the top few centimeters (<20%) has a frazil structure	Ice profiles in the Antarctic have a greater proportion of granular ice (frazil origin) congelation crystals

		Freshwater flowing out from ice shelves facilitates growth of platelet ice crystals (only forms in proximity to them)	Limited formation of platelet ice	Platelet ice is only formed in the Antarctic
		Ice melt is driven at the ocean-ice interface	Ice melt is driven at the air-ice interface	Low potential for meltpond formation in the Southern Ocean, while melt pond coverage is significant during spring-summer melt in the Arctic
	Freshwater Inputs	Melt: Antarctic ice sheet, sea ice Precipitation	Melt: Greenland ice sheet, sea ice Precipitation Pacific Ocean (~32) inflow through the Bering Strait and river discharge	Surface waters in the Arctic Ocean (~32) are fresher than the Southern Ocean (~35) Surface waters of the Southern Ocean have been freshening in recent history
Biological Properties	**Chl *a***	Median Chl *a* 47 mg m^{-2} 170 mg m^{-3} (max >5000 mg m^{-3})	Median Chl *a* 31 mg m^{-2} 25 mg m^{-3} (max <1000 mg m^{-3})	Chl *a* is (two) orders of magnitude greater in Antarctic sea ice
	Community Location	Bottom-ice, internal assemblages (significant), infiltration communitties (surface) and sub-ice Sub-ice communities include cells in platelet ice (where present) and strands of *Berkleya* spp.	Bottom-ice, internal assemblages (limited), surface ponds and sub-ice Biomass is largely restricted to the bottom-ice communities Sub-ice communities include strands of *Melosira arctica*	Greater concentrations of algae are found throughout the vertical ice profile in the Antarctic Majority of algal biomass is located in the bottom centimeters of ice in both regions (excluding potentially dense platelet ice communities in the Antarctic)
	Community Composition	Common genera: *Amphiphora, Pinnularia, Pleurosigma, Synedra, Tropidoneis*	Common genera: *Cylindrotheca, Achnathes*	Pennate diatoms typically dominate sea ice communities in both polar regions (e.g. species of *Nitzschia, Fragilariopsis and Navicula*)
		Virtually nonexistent presence of cyanobacteria	Cyanobacteria are occassionally documented	Cyanobacteria are thought to have freshwater terrestrial origins in the Arctic, suggesting greater abundance in the Arctic may be a result of riverine inflow
	Nutrient Availability	The Southern Ocean is nutrient-rich, instead iron (Fe) is often a limiting element of growth Development of platelet ice results in stratification and can cause nutrient limitation for bottom ice algae where present	Nutrient limitation of algal photosynthesis is often documented, especially nitrogen Nutrient limitation is particularly pronounced towards the termination point of ice algal blooms	Overall nutrient availability is greater in the Southern Ocean

2.2 Production

Production refers to the energetic processes of microorganisms used to synthesize biomass. Here these processes are defined and methods of how they are measured are outlined (Section 2.2.1). Estimates of sea ice production in the Arctic are also summarized by region (Section 2.2.2). Processes affecting algal and bacterial production may be listed, but discussion on them is reserved until Section 2.3.

2.2.1 The processes of photosynthesis and respiration

Photosynthesis

Photosynthesis in the marine system is summarized from left to right by the equation of Sarmiento & Gruber [2006], with average stoichiometry:

$$106\ CO_2 + 16NO_3 + PO_4 + 19H + 78H_2O \overset{energy}{\longleftrightarrow} C_{106}H_{175}O_{42}N_{16}P + 150\ O_2 \qquad (2.1)$$

where carbon dioxide (CO_2), nutrients (NO_3, PO_4), water and energy in the form of light are used to synthesize organic matter. The term primary production refers to the rate of organic material production by photosynthesis [Sarmiento & Gruber, 2006]. Primary production is most often measured by monitoring the amount of radioactive carbon (^{14}C) incorporated into cellular material per unit area or volume over time [Miller & Wheeler, 2012]. Alternative techniques include: stable isotope tracers [e.g. Gradinger et al., 2009], pulse-amplitide-modulated fluorometers [e.g. Glud et al., 2002] and monitoring oxygen release using O^{18} [e.g. Kana et al., 1990], winkler titration [e.g. Søgaard et al., 2010], or microsensors (electrodes or optodes) [Rysgaard et al., 2001]. To limit variability associated with methodology and focus on environmental controls, only literature measurements of primary production quantified using the ^{14}C method are reported in this

chapter (Section 2.2.2). However, a summary of production estimates using oxygen-based methods of sampling is provided in Table 2.2.

Table 2.2. Summary of oxygen-derived production measurements in Arctic sea ice, including the type of sample collected (e.g. DBL, O_2 flux across the sub-ice diffuse boundary layer), the type of production measured (NCP, net community production; GPP, gross primary production; CR, community respiration), range or average (± standard deviation) of production estimates, as well as comments detailing the sampling procedure.

Reference	Location (Ice Type)	Timing	Method	Sample Collected	Production		Comments
					Type	Estimate	
Kuhl et al. 2001 & Rysgaard et al. 2001	Young Sound, Greenland 74°18'N 20°15'W (Landfast FYI)	June-July	Electrode probe	*In situ* (DBL)	-	-	Production estimates could not be derived as a result of unknown influences of physico-chemical properties of the sea ice System deployed using divers 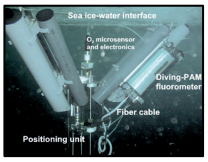
McMinn & Hegseth 2007	Barents Sea 77°10'N 29°18'W (Ice floe)	May	Electrode probe	*In situ* (DBL)	NCP	+0.071 to +1.1 mg C m^{-2} h^{-1}	System deployed using a mechanical arm
Rysgaard et al. 2008	Franklin Bay 70°02'N 126°18'W (FYI)	April	Winkler titration	Bottom 10 cm	NCP	-1 to -3 µmol O_2 L^{-1} d^{-1}	Melted ice samples were incubated at in situ light intensities from zero to 12 days
Søgaard et al. 2010	Malene Bight, Greenland 64°82'N 51°42'W (Landfast FYI)	Feb-March	Winkler titration	Top and bottom 50% of the ice profile (≤65 cm total depth)	NCP	Top 50%: +0.5 ± 3 µmol O_2 L^{-1} d^{-1} Bottom 50%: 1.3 ± 5 µmol O_2 L^{-1} d^{-1}	Samples incubated within the ice, and collected at 1-2 week intervals over the sampling period for analysis
		March-April				Top 50%: +0.8 ± 3.5 µmol O_2 L^{-1} d^{-1} Bottom 50%: 6.3 ± 2.3 µmol O_2 L^{-1} d^{-1}	
Nguyen & Maranger 2011	Amundsen Gulf 69° to 70°N 120° to 126°W (Drift or Landfast FYI)	March-July	Optode probe	Bottom 4.5 cm	CR	-9.7 to -75.5 µg C L^{-1} d^{-1}	Spot sensors on glass flasks incubated in darkness, for 5-10 days at 2-4°C Ice melted in filtered seawater at a ratio between 3 and 4 parts water to one part ice
Zhou et al. 2013	Barrow 71°22'N 156°32'W	Feb – June	O^{18}/Argon	Permeable and impermeable	NCP	Permeable ice: +3.8 to 122 µmol	Dissolved and gaseous O_2 measured as ice was crushed (no incubation)

	(Landfast FYI)			ice of the vertical profile		O_2 L^{-1} d^{-1} Impermeable ice: -6.6 to +3.6 µmol O_2 L^{-1} d^{-1}	Use of Argon corrects for the physical processes (temperature, salinity, bubble effects)
Glud et al. 2014	Fram Strait 81°N 5°E (Ice floe)	June-July	Electrode (lab incubation)	Sub-ice Aggregates	GPP	+0.49 mmol C m^{-2} d^{-1}	Point measurements on subsamples from aggregates incubated in gas-tight syringes 
			Electrode + ^{14}C (lab incubation)	Sub-ice Aggregates + bottom ice algae (10 cm)	NPP	-0.32 mmol O_2 m^{-2} d^{-1}	

Light for photosynthesis is largely collected by algae using the chlorophyll *a* (chl *a*) pigment, which preferentially absorbs light in the blue spectrum at 440 and red at 665-675 nm [Bricaud et al., 2004]. Accessory pigments also present in ice algae can be photosynthetic, expanding the algal absorption spectra (e.g. fucoxanthin) or photoprotective (e.g. diadinoxanthin), absorbing and quenching excess light energy that would otherwise damage the cell (i.e. photoinhibition). Sea ice algae in particular contain high concentrations of the photosynthetic accessory pigment fucoxanthin, which absorbs from 450-550 nm, and gives the algae their brown appearance [SooHoo et al., 1987].

Respiration

Following equation 2.1 from right to the left summarizes the process that effectively competes with photosynthesis in ice, respiration. Here, oxygen is used to break down organic molecules to form inorganic CO_2 and water. Respiration is required of all organisms, whether the original organic material is produced by photosynthesis, as in algae (i.e. algal respiration), or is sourced from the consumption of organic matter, as in heterotrophic bacteria (i.e. bacterial respiration) [Campbell et al., 2005]. Heterotrophic

respiration can also take place in the absence of oxygen (anaerobic), but documentation of its contribution to sea ice production is limited [see Rysgaard & Glud, 2004].

Bacterial production differs from bacterial respiration, as it represents the rate of organic carbon actually converted to cellular biomass through the process of respiration, rather than simply the rate of organic to inorganic carbon conversion [del Giorgio and Cole, 1998]. Bacterial production and respiration have a positive relationship that can vary significantly in strength, but bacterial production is consistently an order of magnitude lower than bacterial respiration due to energetic losses [Kirchmann, 2008]. Bacterial production is most often quantified by monitoring tritiated (^{3}H) leucine or thymidine incorporation into cellular protein or DNA, respectively [Kemp et al., 1993].

Gross and net primary production

Primary production can be further defined as gross or net production. Gross primary production is the rate of total organic matter fixed by photosynthesis or, alternatively, the total conversion of light into metabolic energy by photosynthetic organisms [Williams, 1993]. In comparison, subtracting the influence of algal respiration from gross primary production yields net primary production, which represents the assimilation of photosynthetic products by algae after respiratory losses. It follows that at low levels of algal respiration net primary production will approach gross primary production [Geider & Osborne, 1992]. Net community production may also be defined when the influence of all respiring organisms in a sample are removed from total gross primary production [Ulfsbo et al., 2014].

The influence of algal respiration varies with species composition [Williams, 1993] and light intensity, and may be as high as 35% of gross primary production [Kana, 1990; Suzuki et al., 1997]. However, respiration rates of natural algae populations are largely unknown and reported production is often not specified as gross or net primary production. Instead, the length of ^{14}C incubations may indicate whether gross primary production (1-3 h) or net primary production (≥ 8-12 h) was measured, because the influence of respiration increases with time [Geider & Osborne, 1992; Williams et al., 1993]. For the remainder of this chapter, the encompassing term of primary production will be used without and specifying gross or net, with the exception of the discussion on photosynthesis-irradiance curves below. Where estimates of production obtained from the literature are specified, information on the incubation time and sampling method are provided.

Algal photosynthesis-irradiance curves

A relationship fitted to gross primary production (P; mg C l^{-1} h^{-1}) plotted over a range of light intensities (E; μmol m^{-2} s^{-1}) represents a photosynthesis-irradiance curve (Figure 2.5). An ideal photosynthesis-irradiance curve can be modeled from empirical photosynthesis and irradiance data, using functions to determine parameters that describe algal physiological state and photosynthetic potential. The commonly used function is exponential:

$$P = P_{\mathrm{m}}\left(1 - e^{\frac{\alpha \mathrm{E}}{\mathrm{Pm}}}\right) e^{\frac{-\beta \mathrm{E}}{\mathrm{Pm}}} - P_0 \qquad (2.2)$$

where P_m is the maximum photosynthetic rate in the presence of photoinhibition (mg C l^{-1} h^{-1}), α is the photosynthetic efficiency (mg C l^{-1} h^{-1} (μmol photons m^2 s^{-1})$^{-1}$), β is an index

of photoinhibition (mg C l^{-1} h^{-1} (μmol photons m^2 $s^{-1})^{-1}$), and P_0 is the production at zero irradiance (mg C l^{-1} h^{-1}) [Platt, 1980; Arrigo et al., 2010a]. A decrease in P_m beyond the optimal saturating light intensity (E_m; μmol m^{-2} s^{-1}) indicates the presence of photoinhibition however, it is not always observed and ($e^{\frac{-\beta E}{Pm}}$) of equation 2.2 may be removed as a result. In the absence of photoinhibition the parameter P_m is referred to as P_s. These parameters are used to calculate the minimum irradiance required for photosynthesis (E_c; μmol m^{-2} s^{-1}):

$$E_c = P_0 / \alpha \quad (2.3)$$

and the light intensity at which photosynthesis stops linearly increasing with light intensity, referred to as the light acclimation index (E_s; μmol m^{-2} s^{-1})):

$$E_s = P_m / \alpha \quad (2.4).$$

The parameter E_s can also be defined as E_k.

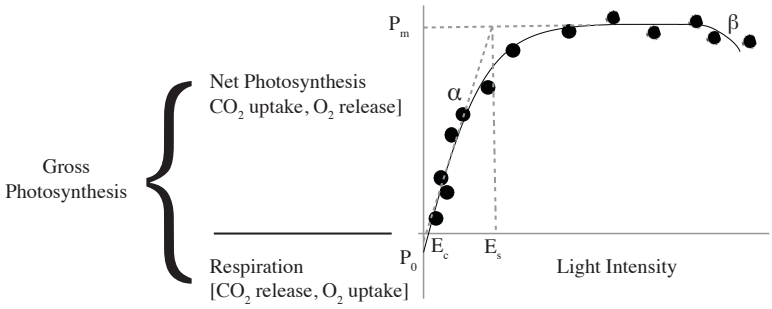

Figure 2.5. Photosynthesis-irradiance curve depicting algal production in darkness (P_0) and net photosynthesis under illumination. The irradiance at which respiration is equivalent to production is represented by the variable I_c. *See* text for a description of other parameters. Adapted from Falkowski and Raven [2007].

The parameters P_m (or P_s) and α are often reported relative to chl *a* biomass, indicated by superscript B (P^B_m, P^B_s, α^B), to aid comparisons between studies with different biomass

concentrations [Falkowski & Raven, 2007]. Photosynthetic rates at *in situ* light intensities can also be reported relative to chl *a* for this reason, and are referred to as assimilation rates.

2.2.2 Reported estimates of Arctic ice algal and bacterial production

Regional estimates of algal production

Figure 2.6 summarizes regional ice algal chl *a* (<1-340 mg m^{-2}) and daily production estimates (0.01-576 mg C m^{-2} d^{-1}) in the Arctic at under-ice light intensities (Table 2.3). The median value for Arctic-wide chl *a* concentration suggested by Arrigo [2010b] of 31 mg m^{-2}, with the distribution of daily production estimates (excluding *Melosira arctica*), is used to approximately define areas of high and low sea ice primary production. This is possible because there is a strong relationship between biomass accumulation and total production (Section 2.3). Note that the number of studies in each area varies likely due to accessibility and interest in highly productive areas (*see* Table 2.3), potentially introducing bias into these definitions.

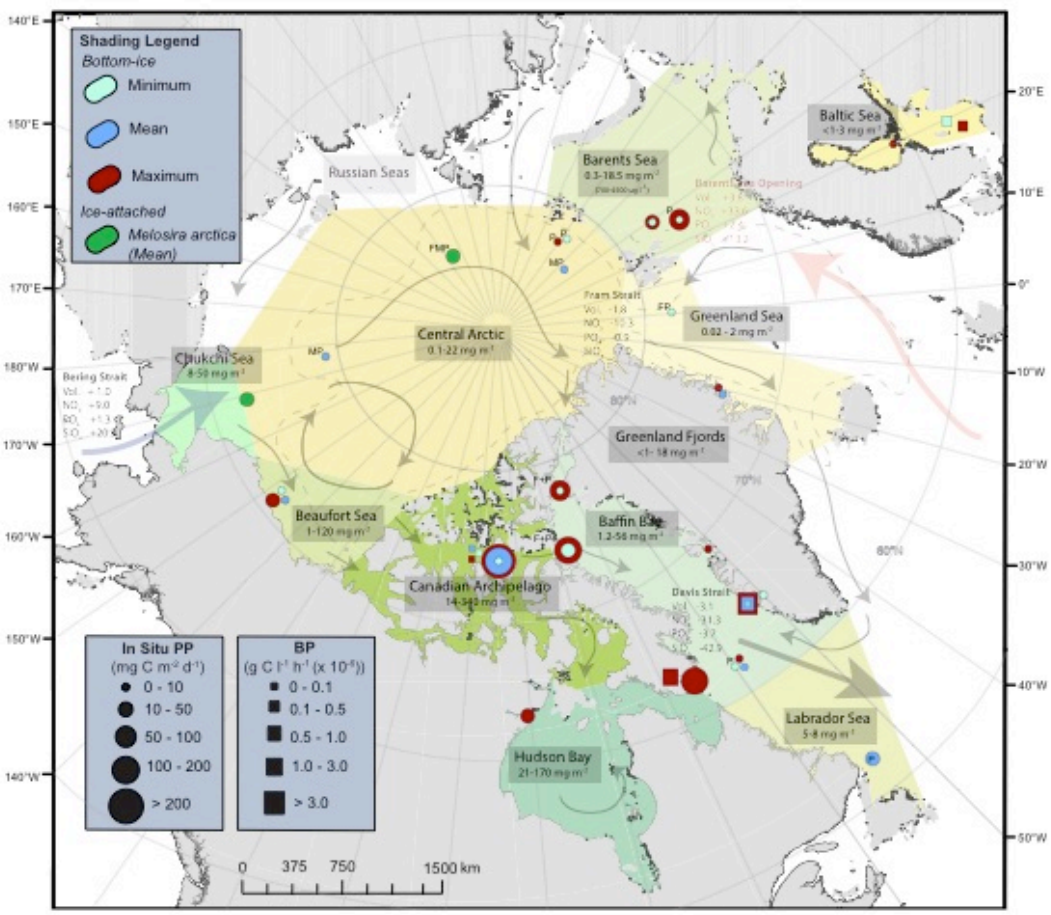

Figure 2.6. Regional summary of minimum (light blue), maximum (red) and average (dark blue or green) values of daily primary production (PP, circles) and bacterial production (BP, squares) in sea ice: first-year (unlabeled or F), multiyear (M), pack ice of unspecified age (P), a combination types (eg. F+P). Arrows indicate the main inputs from the Pacific (blue) and Atlantic (red) Oceans, general movement of surface waters [Stein & MacDonald, 2004] and nutrient fluxes (kmol s^{-1}) into (positive) and out of (negative) the Arctic as defined by Torres-Valdes et al. [2013]. Regions are colored by definitions in Section 2.1 with chlorophyll *a* concentration (boxes) specified (*see* Table 2.3 and Arrigo et al. [2010b] for references). See Table 2.3 for algal and Table 2.6 for bacterial sampling information and references.

Table 2.3. Supplementary information for algal studies presented in Figure. 2.6 including: type of sample collected (brine, bottom centimeters, scraped or suctioned skeletal layer), type of ice (F, first-year; M, multiyear; P, pack ice of unspecified age; +, combination), incubation method (*in situ*, modeled, laboratory incubator at set irradiance). Dominant control on production (*see* Section 2.3) is also indicated when possible for each study (grey) including light (from self-shading, sediments present, extremely thick snow), nutrients (N, nitrogen; P, phosphorus; Si, silica; bloom, occurred during peak biomass), or other (I, ice type or structure; T, temperature, G, grazing; S, salinity; PI, photoinhibition; bloom, occurred during peak biomass). Additional information: (-), no data; blue shading, study included in Table 2.4; bold, hourly production values multiplied by 24 to obtain daily estimates.

Region	Location	Reference	Production Controls			Incubation Summary				
			Low light	Nutrients	Other	Timing	Sample collected	Ice Type	Time (hr)	14C Method
≤60N	Baltic Sea	Haeky and Anderson 1999	(pre bloom)	P (bloom)		Jan - April	brine	F	3-4	in situ
		Kaartokallio et al. 2007		P (stratification)	S, I (structure)	March	0-5 cm	F	4	incubator at 80 lE cm–2 s–1
	Hudson Bay	Bergmann et al. 1991				March - May	scrapes	F	-	model
	Labrador Sea	Irwin 1990	-	-	-	March	-	P	-	-
Deep Basin	Central Arctic	Gosselin et al. 1997		N	I (FYI vs. MYI)	July - Aug	0-2, 0-4 cm	MFP	4-12	in situ
Continental Shelf	Barents	Hegseth et al. 1998			I/T (detachment)	May-July	suction	F	6	in situ
		Johnsen and Hegseth 1991	**(self-shading)**			**May**	**suction**	**FP**	**1**	**model**
	Beaufort	Horner and Schrader 1982	(sediment)			May-June	0-2 cm	FP	3-4	in situ
		Clasby et al. 1973				May	0-4 cm	F	5-6	in situ
	Archipelago	**Smith and Herman 1992**	**(pre-bloom)**	**(bloom)**		**May-June**	**0-5 cm**	**F**	**1 or 24**	**in situ**
		Smith et al. 1988			G	March-May	0-3 cm	F	1	model
DWS	Baffin Bay	**Hsaio et al. 1988**			**T**	**spring**	**0-5**	**F**	**24**	**in situ**
	Baffin Bay	Michel et al. 2002			G, I (melt)	April-June	0-2, 0-4cm	F + P	2-4	model
	GL Sea	**Mock and Gradinger 1999**		**N**	I (FYI vs. MYI)	**May-June**	**0-5 cm**	**FP**	**8**	**in situ**
Greenland Fjords		Mikkelson et al. 2008		N, Si	I (structure)	Nov-June	0-10 cm	F	2	model
		Rysgaard et al. 2001			S	June	0-4 cm	F	2	in situ
		Sogaard et al. 2010		(bloom)		March-April	60 cm	F	5	model
		Sogaard et al. 2013		N, Si		Feb-may	0-12 cm	F	5	model
		Glud et al. 2007	(snow)		I (structure)	May-June	0-4, 0-30 cm	F	2	in situ

Regions of low production with chl *a* concentrations < 31 mg m^{-2} and comparatively low productivity (0.01-21 mg C m^{-2} d^{-1}) include the Baltic Sea, the central Arctic, Greenland Sea and the Greenland fjords. It is interesting to note the significant difference *Melosira arctica* communities can have in the otherwise marginally productive central Arctic. However, as specified in Section 2.1.4, their sporadically documented distribution, compared to the more regular coverage of bottom-ice algae, makes their total areal contribution to production uncertain.

Regions of high productivity (2.3-576 mg C m^{-2} d^{-1}) with chl *a* concentrations >31 mg m^{-2} and comparatively high primary production include the Hudson Bay, Beaufort Sea, Canadian Archipelago, Barents Sea (considering the high mg m^{-3} chl *a* estimates available) and Baffin Bay. The Labrador Sea is an exception to this high/low productivity/biomass classification due to its low chl *a* ranges but comparatively high production estimates. Estimates of primary production for bottom-ice algae in the Chukchi Sea could not be obtained; however, the region's high chl *a* suggest high productivity.

Figure 2.7 shows regional assimilation values approximated for ambient under-ice light conditions (<0.01 - 1.6 mg C mg chl a^{-1} h^{-1}) in the Arctic (*see* Table 2.4 for supplementary information). Where available, the overlap of daily primary production (Figure 2.6) and assimilation (Figure 2.7) estimates largely agree with the previous regional classifications of low and high primary productivity.

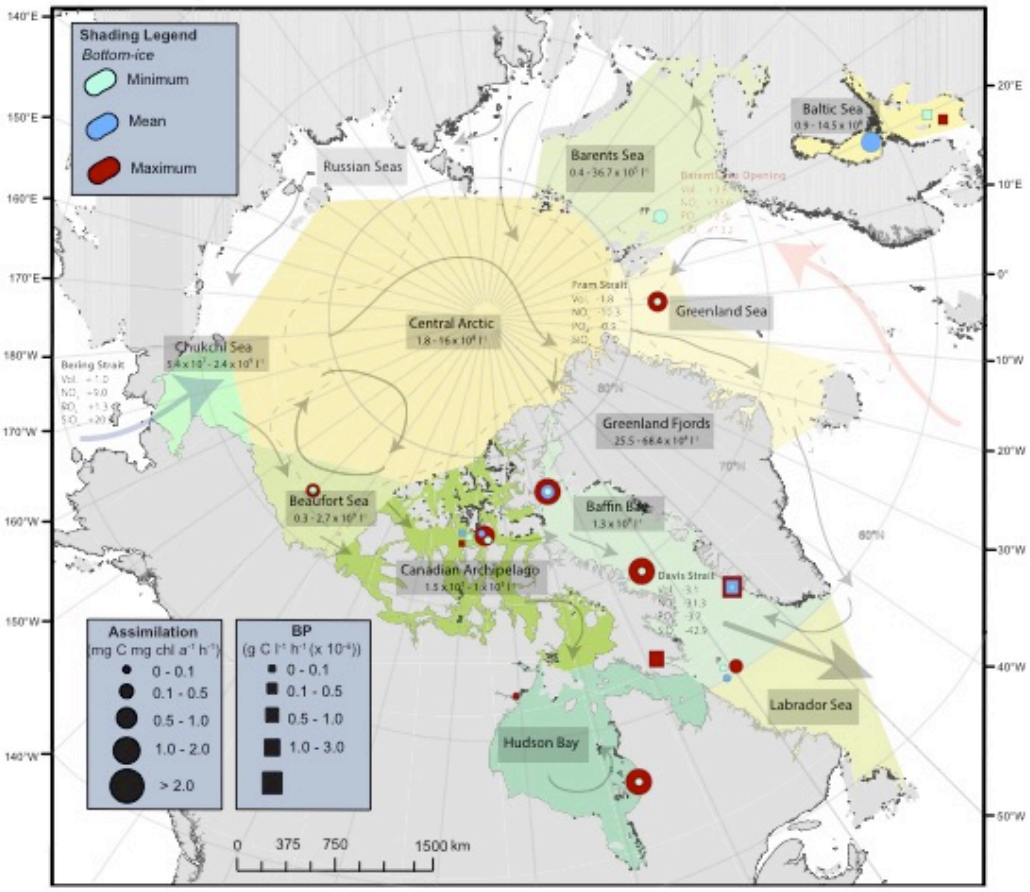

Figure 2.7. Regional summary of minimum (light blue), maximum (red) and average (dark blue) values of for assimilation rates (circles) and bacterial production (BP, squares) in sea ice: first-year (unlabeled or F), multiyear (M), pack ice of unspecified age (P), a combination types (eg. F+P). Arrows indicate the main inputs from the Pacific (blue) and Atlantic (red) Oceans, general movement of surface waters [Stein & MacDonald, 2004], and nutrient fluxes (kmol s^{-1}) into (positive) and out of (negative) the Arctic as defined by Torres-Valdes et al. [2013]. Regions are colored by definitions in Section 2.1 with bacterial cell counts (boxes; cells l^{-1}) specified (references are marked by * in *References*). See Table 2.4 for algal and Table 2.6 for bacterial sampling information and references.

Table 2.4. Supplementary information for algal studies presented in Figure 2.7 including: type of sample collected (bottom centimeters or suctioned skeletal layer), ice type (F, first-year; M, multiyear; P, pack ice of unspecified age), incubation method (*in situ*, modeled, laboratory incubator at set irradiance). Dominant control on production (*see* Section 2.3 for explanations) is also indicated when possible for each study (grey) including light (from self-shading; pre-bloom, early in the spring), nutrients (stratification; bloom, occurred during peak biomass), or other (I, ice type or structure). Additional information: (-), no data; blue shading, study included in Table 2.3; bold, hourly production values multiplied by 24 to obtain daily estimates.

Region	Location	Reference	Production Controls			Incubation Summary				
			Low light	Nutrients	Other	Timing	Sample collected	Ice Type	Time (hr)	14C Method
≤60N	Baltic Sea	Kaartakallios et al. 2007		(stratification)		March	0-5 cm	F	4	incubator
	Hudson Bay	Gosselin et al. 1985		(stratification)		April-May	0-20 cm	-	2	incubator
	Labrador Sea	Booth et al. 1984	-	-	-	April-May	0-5 cm	P	12	in situ
Deep Basin	-									
Continental Shelf	Barents Sea	Johnsen and Hegseth 1991	(self-shading)			May	suction	FP	1	incubator
	Beaufort	Cota and Smith 1991	-	-	-	Spring	-	-	? And ≤1	in situ or incubator
	Archipelago	Cota and Smith 1991 (II)	-	-	-	Spring	-	-	? And ≤1	in situ or incubator
		Herman et al. 1993				March-May	0-5 cm	F	1.5-2	in situ
		Smith and Herman 1992	(pre-bloom)	(bloom)		May-June	0-5 cm	F	1 or 24	in situ or incubator
DWS	Baffin Bay	Cota and Smith 1991	-	-	-	Spring	-	-	? And ≤1	in situ or incubator
	Eastern Canadian	Lee et al. 2001	-	-	-	April-June	0-2 cm	FP	-	incubator
	GL Sea	Mock and Gradinger 1999		N	I (FYI vs. MYI)	May-June	0-5cm	FMP	8	in situ
Greenland Fjords	-									

Regional estimates of photosynthesis-irradiance response

The photosynthetic response of ice algae can vary considerably within and between studies in response to changing environmental conditions. This is reflected by the considerable variability in Table 2.5, which summarizes photosynthesis-irradiance across the Arctic. As a result, discerning specific regional patterns of photosynthetic response is difficult.

Table 2.5. Summary of ^{14}C-derived photosynthesis-irradiance parameters reported for the Arctic during the spring, with ranges or mean values indicated and standard deviations (±) in parentheses. The type of sample collected (S, skeletal layer; I, interface ice slurry; In, interface with no ice; B, depth of bottom ice thickness in cm), ice thickness (cm) and snow depth (H_s, cm) prior to collection is specified for each reference, in addition to the number of observations contributing to each summary (*n*). Photosynthetic parameters include the maximum photosynthetic rate under the influence of photoinhibition P^B_m (mg C mg chl a^{-1} h^{-1}) or in its absence $\underline{P^B_S}$ (mg C mg chl a^{-1} h^{-1}), the photosynthetic efficiency, α^B (mg C mg chl a^{-1} h^{-1} (µmol photons m^{-2} s^{-1})$^{-1}$), the photoinhibition index β^B (mg C mg chl a^{-1} h^{-1} (µmol photons m^{-2} s^{-1})$^{-1}$) x 10^{-2}, the photoacclimation index E_s (µmol photons m^{-2} s^{-1}), the optimal light intensity $\underline{E_m}$ (µmol photons m^{-2} s^{-1}), and the compensation light intensity E_c (µmol photons m^{-2} s^{-1}).

Reference	Sample type (ice thickness)	H_s	*n*	P^B_m or $\underline{P^B_S}$	α^B	β^B	E_s or $\underline{E_m}$	E_c	Comments
Canadian Archipelago									
Bates & Cota 1986[R]	S (170)	3-4	4	0.007 – 0.011 0.011 (± 0.002)	0.01 – 0.003 0.003 (± 0.001)	0.001 – 0.002 0.002 (± 0.001)	-	-	Chl *a* ranges (0-4500 µg l^{-1})
			6	0.013 – 0.046 0.029 (± 0.015)	0.001 – 0.007 0.004 (± 0.002)	-	7.15 – 17.5 9.94 (± 3.85)	-	Salinity ranges (10-50)
Bergman et al. 1991[R]	S (150-190)	3-20	66	0.39 – 0.78 0.585 (± 0.41 - 0.45)	0.047 – 0.065 0.056 (± 0.041 – 0.043)	-	-	-	
Cota 1985[Ra]	B:2-5 (180)	0-25	4	0.03 – 0.08 0.05 (± 0.02)	0.0002 – 0.033 0.014 (± 0.012)	0.04 – 2.20 1 (± 1.1)	2 – 12 7 (± 4) 8 – 64 40 (± 24)	0.18	Corrected values as per Cota & Smith 1991
Cota & Horne 1989[R]	S (185)	0	2	0.78 - 4.8 2.79 (± 2.84)	0.036 - 0.270 0.153 (± 0.165)	-	18.1 – 21.9 20 (± 2.68)	-	
		3 - 5	12	0.068 – 1.19 0.472 (± 0.374)	0.011 - 0.2209 0.074 (± 0.063)	0.00 – 0.010[b]	3.81 – 15.6 8.36 (± 4.59) 26.1 – 112 48.9 (± 28.8)	-	Time series
		10 - 25	4	0.205 - 1.10 0.623 (± 0.011)	0.036 - 0.315 0.176 (± 0.030)	0.03 – 0.04 0.078 (± 0.018)	3.50 – 5.55 4.525 (± 0.106)	-	
Smith & Herman 1991[R]	B:1 (150-190)	10-15	24	0.082 - 0.412 0.206 (± 0.094) 0.089 – 0.4431 0.224 (±0.101)	0.006 - 0.022 0.014 (± 0.004)	0.016 - 0.108 <0.000	6 - 22.1 14.9 (± 4.7) 30.5 – 104.3 67.6 (± 23.8)	-	
Smith et al. 1988[Rc]	B:1 -	0	5	1.17 (± 0.844)	0.061 (± 0.047)	-	19.1 (± 1.7)	-	

		2 - 22	17	0.6 (± 0.130)	0.125 (± 0.030)	-	4.8 (± 0.6)	-	
Summary				**0.007 – 4.8** **0.6536**	**0.089 – 0.4431** **0.206**	**0 – 2.2** **0.360**	**2 – 22.1** **10.5** **8 – 112** **52.2**	**0.18**	**β^B does not include (-) values**
Hudson Bay									
Bergman et al. 1991	S -	3 - 45	13	0.2 – 0.48 0.34 (± 0.12 – 0.17)	0.011 – 0.030 0.021 (± 0.007 – 0.015)	-	-	-	
Gosselin et al. 1985	B:20 + I (90 – 100)	0 - 15	11	-	0.022 - 0.190 0.091 (± 0.058)	-	10.8 – 68.5 39.1 (± 19.4)	7.6	Time series
Gosselin et al. 1986	B:20 + I (60 – 90)	0 - 45	13	1.8 – 5.2 3.5 (± 0.9 – 2.1)	0.11 – 0.32 0.215 (± 0.07 – 0.13)	0.5 – 1.1 0.8 (± 0.3 – 0.4)	64 – 69 66.5 (±1.3 – 20)	-	
Johnsen & Hegseth 1991	I -	2 - 5	5	0.032 – 0.24 0.15 (± 0.088) 0.033 – 0.24 0.155 (± 0.089)	0.0025 – 0.0055 0.004 (± 0.001)	0.015 – 1.1 0.302 (± 0.455)	13 – 46 33 (±14.7) 64 – 370 215 (±140)	-	Spatial sampling
			5	0.15 – 0.18 0.16 (± 0.014)	0.003 – 0.008 0.005 (± 0.002)	-	19 – 52 35 (± 11.9) 170 – 289 238 (±50.2)	-	Diurnal time series
Michel et al. 1988a	I (90 – 100)	0 - 35	18	0.4 – 3.51 1.29 (± 0.736)	0.022 – 0.250 0.075 (± 0.055)	0 – 0.203 0.630 (± 0.763)	3.04 – 71.4 21.8 (±16.3)	-	
Michel et al. 1988b	I (90 – 100)	0 - 35	18	0.27 – 3.88 1.26 (± 0.755)	0.007 – 0.137 0.052 (± 0.028)	-	-	-	Temperature acclimation experiment [-1.5 to 10C]
Rochet et al. 1986	In -	-	11	0.512 – 8.87	0.026 – 0.461	0.100 – 1.90	10.4 – 28.7 45.5 - 104	-	Blue light
				0.514 – 9.13	0.019 – 0.246	0.036 – 0.830	7.03 – 57.2 100 - 190	-	White light
Summary				**0.032 – 9.13** **1.12** **0.033 – 0.24** **0.155**	**0.0025 – 0.461** **0.069**	**0 – 1.9** **0.577**	**7.03 – 71.4** **32.2** **45.5 – 370** **173.2**	**7.6**	
Labrador Sea									
Irwin 1990 [d]	S + I -	-	9	1.43 – 3.11 2.32 (± 0.536) 1.52 – 3.30 2.41 (± 0.566)	0.311 – 0.700 0.460 (± 0.120)	0 – 0.002 0.001 (± 0.001)	44.8 – 69.2 56.9 (± 8.99) 53.5 – 444 224 (± 159)	2.34 – 4.68 3.57 (± 0.836)	^{14}C Incubation
			7	4.24 – 9.62 6.46 (± 2.14) 4.25 – 10.3 7.05 (± 2.54)	0.431 – 2.15 0.932 (± 0.628)	0 – 0.027 0.009 (± 0.010)	33.8 – 222 104 (± 65.2) 33.4 – 264 117 (± 80.7)	-	O_2 Incubation [winkler titration]
Summary				**1.43 – 9.62** **4.39** **1.52 – 10.3** **4.73**	**0.311 – 2.15** **0.696**	**0 – 0.027** **0.005**	**44.8 – 222** **80.5** **33.4 – 444** **170.5**	**3.57**	
Baffin Bay									
Lee et al. 2001	B:2 -	-	67	0.108 – 4.67 1.23 (± 0.61 – 1.13)	0.002 – 0.078 0.020 (± 0.034 – 0.019)	-	-	-	
All Regions in the Canadian Arctic									
Summary				**0.007 – 9.62** **1.85** **0.033 – 10.3** **1.70**	**0.0002 – 2.15** **0.213**	**0 – 2.2** **0.314**	**2 – 222** **41.1** **8 – 444** **131.9**	**0.18 – 7.6** **3.78**	

[R] Indicates samples collected in the vicinity of Resolute Bay, Canada
[a] Corrected values as per Cota & Smith 1991 (III), except for Ic which is from the original paper
[b] Values from single day, n=2
[c] Values in parentheses are SE
[d] Values reported in Wm^{-2} have been converted to µmol photons m^{-2} s^{-1} assuming a wavelength of 400 nm

Regional estimates of bacterial production

Figures 2.6 and 2.7 also summarize sea ice bacterial production ($3.6 \times 10^{-8} - 3.09 \times 10^{-6}$ g C l^{-1} h^{-1}) in the Arctic for samples collected from the bottom-ice or brine network (Table 2.4). Bacterial production in the sea ice (per volume) is orders of magnitude greater than in the pelagic system, but in comparison to algal production described above, it contributes <10% of the total production in spring sea ice [Deming, 2010]. Estimates represent values from first-year ice only, as information pertaining to bacterial production in old ice is limited [Deming, 2010]. Unlike the regional variability described for ice algal production previously, bacterial production does not appear to exhibit strong regional patterns across the Arctic. For example, bacterial production is similar between the Greenland fjords and parts of the Canadian Archipelago that had very different primary production. These observations could be in part due to limited studies and the varying collection methods (Table 2.6).

Table 2.6. Supplementary information for bacterial production studies presented in Figure 2.6, 2.7, including: type of sample collected (brine, bottom centimeters), incubation method (T, ^{3}H-Thymidine; L, ^{3}H-Leucine). Dominant control on production (*see* Section 2.3) is also indicated when possible for each study (grey) including: substrate availability (I, associated with ice algae), grazing pressure or other (V, viral infection; S, salinity; M, losses from ice melt; B, brine drainage). Additional information: (-), no data.

Region	Location	Reference	Production Controls			Incubation Summary				
			Substrate	Grazing	Other	Timing	Sample collected	Time (h)	Temp (°C)	Method
≤60N	Baltic Sea	Mock et al. 1997	I			Feb-March	brine	1-1.3	-1 or 0	TL
		Haecky and Anderson 1999	I			Jan-April	brine	-	in situ	T
Deep Basin			-							
Continental Shelf	Canadian Archipelago	Maranger et al. 1994	I		V	April-May	0-4 cm	6	in situ (-1.8)	T
		Smith and Clement 1990	I		M	April-June	1-2 cm	-	in situ (-1.8)	T
DWS	Baffin Bay	Bunch and Harland 1990	I		B, G	March and May	0-5 cm	8	2	T
Greenland Fjords		Kaartokallio et al. 2013	I			March	brine and 0-4 cm	17-18	-5	T or L
		Sogaard et al. 2010	I			March-April	0-60 cm	6	-2 to +4	T
		Sogaard et al. 2013	I			Feb-May	0-12 cm	6	-2 to +4	T

Furthermore, bacterial abundance in Figure 2.6, 2.7 varies significantly between regions and does not appear to correlate with bacterial or primary production within the regions themselves. The poor association between bacterial production and abundance

within regions may represent the varying activities of individual cells, where only 2-27% of bacteria cells in a sample may be taking up ^{3}H-leucine or thymidine [Junge et al., 2002].

2.3 Local factors controlling algal and bacterial production in sea ice

The total integrated primary productivity in sea ice depends on the activity of cells and the amount of biomass present. These variables are strongly correlated as higher cell activity promotes growth and reproduction. The processes controlling sea ice algal and bacterial activity therefore affect total production directly by influencing production rates, and indirectly by promoting biomass accumulation. As a result, the shared processes affecting algal (Section 2.3.1) or bacterial (Section 2.3.2) activity and biomass are not differentiated from one another, except when the processes controlling physical cell removal from the ice are discussed (Section 2.3.3). Here the local factors affecting primary production within sea ice are discussed, whereas the regional-scale factors that affect pan-Arctic variations in production are discussed in Section 2.4.

2.3.1 Factors affecting algal production

The principal mechanisms affecting algal production in sea ice are: ice bottom temperature and salinity, light availability and nutrient accessibility. However, the final two mechanisms: light and nutrients, are particularly dominant [Michel et al., 2002]. Seasonal changes of light, temperature and salinity in the sea ice environment were described in Section 2.2. Their combined effect on algal production at the cellular level is multiplicative, but independent from one another [Arrigo & Sillivan, 1992]. As a result

each is outlined separately in this section, in addition to a review of algal nutrient requirements and accessibility.

Temperature

Rates of chemical reactions are temperature sensitive. The effect of temperature on production is illustrated by the exponential relationship between maximum algal growth rate (μ_{max}) (μg C cell^{-1} d^{-1}) and temperature (T) (°C):

$$\mu_{max} = \mu_o e^{rT} \quad (2.5)$$

where μ_o is growth at 0°C (μg C cell^{-1} d^{-1}), and *r* is a temperature-sensitivity rate constant [Eppley, 1972]. The *r* of ice algae (0.099-0.158) increases as temperatures deviate from their optimal range of carbon-fixation at 4-14°C [Kottmeirer & Sullivan, 1988; Arrigo and Sullivan, 1992].

In situ temperatures in the bottom of sea ice (typically < 0 °C) are outside of this preferred range, indicating that ice algal productivity is temperature limited. Moreover, the exponential nature of equation (2.5) indicates that small changes in temperature can greatly affect primary production, and positive relationships between α^B, P^B_m and temperature have been documented as a result [Arrigo & Sullivan, 1992].

Salinity

Osmotic stress influences physiological processes related to production, such as pigment arrangement (light absorption), up-take and storage of nutrients [Arrigo & Sullivan, 1992] and energy transport in photosynthetic pathways [Ralph et al., 2007]. Photosynthetic rates of ice algae are optimized in a range that limits these stresses, particularly at the lower

end of the optimal 30 to 50 range reported by Arrigo & Sullivan [1992] [Søgaard et al., 2011]. The lower end of this range also roughly corresponds to the average salinity of seawater at the ice-ocean interface (~30) [Anderson et al., 1989; Brandon et al., 2010], but indicate that production under the direct influence of brine or fresh water (e.g. ice melt) is likely to be reduced. Salinity tolerance, and therefore primary production, is thought to vary with species [Hsaio et al., 1988], but more research is needed to quantify the effect of species composition on primary production.

Light

Photosynthesis cannot occur in the absence of light (equation 2.1). It has been estimated that ice algae require incident solar irradiance between 0.36 and 7.6 μmol photons m^{-2} s^{-1} before photosynthesis can begin (i.e. I_c) [Gosselin et al., 1985; Mock and Gradinger 1999]. After this point, primary production increases approximately linearly over a range of sub-saturating light intensities (Figure 2.5). This indicates that seasonally intensifying irradiance (Figure 2.3) increases the potential for ice algal production as the spring progresses. However, there are a number of processes that decrease the amount of incident PAR actually reaching algae in the bottom-ice. These include: a latitudinal dependence of photoperiod intensity and duration (Section 2.1.3), cloud attenuation reducing downwelling radiation by 55-65% [Mundy et al., 2005], and attenuation of light by snow, sea ice and absorbing particulates therein [Petrich & Eiken, 2010]. This discussion is limited to the biologically relevant wavelengths of PAR once they have reached the snow-sea ice surface.

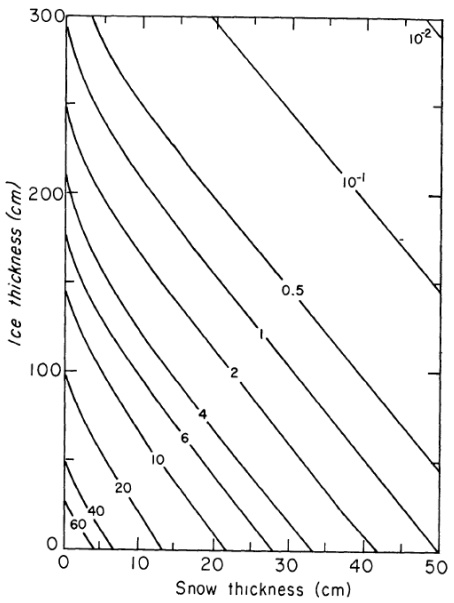

Figure 2.8. Percent transmission (isobars) of downwelling surface irradiance through first-year sea ice as a function of snow and ice thickness. From Maykut and Grenfell [1975]. Used with permission from John Wiley & Sons.

The sea ice albedo is the ratio of incident light that is reflected by the ice cover. The remaining light is either absorbed by the ice cover (low for PAR wavelengths) [Perovich, 2003] or is transmitted through the ice to algae at the ice bottom and the underlying ocean [Ehn et al., 2008]. Prior to the onset of melt in late spring-summer, the albedo of snow-covered first-year or multiyear ice is about 0.8 [Perovich & Polashenski, 2012]. The reflectance and scatter of 80% of incoming light, in addition to further scattering within the snowpack, makes snow the dominant control on light transmission in the sea ice environment [Ehn et al., 2008]. This is highlighted in Figure 2.8, which demonstrates that the percent transmission of surface downwelling decreases rapidly with increasing snow thickness [Horner, 1985].

Applying the average snow depth of 30 cm on Arctic sea ice for March-April [Sturm & Massom, 2010], Figure 2.8 shows that on average, < 6% surface downwelling radiation

is transmitted to the bottom-ice. It follows that for most of the spring, photosynthesis does not reach its maximum potential (i.e. P^B_s), and ice algal growth and production is limited by light as a function of the overlying snow thickness [Mundy et al., 2005]. The combination of low solar angle and maximum snow and ice thickness in early spring makes light limitation especially severe during this time [Campbell et al., 2015].

Actual snow depth on sea ice will vary due to the formation of snow drifts on first-year ice [Iacozza & Barber, 1999] and snow accumulation in melt depressions on multiyear ice [Lange et al., 2015]. The result is spatial variability in light transmission that translates to patchy sub-ice distributions of algae, which accumulate under thin snow cover prior to ice melt [Rysgaard et al., 2001]. However, this relationship reverses during melt as snow protects algae from excess light and insulates the ice from atmospheric warming, which prolongs algal attachment (Section 2.3.3) [Campbell et al., 2015].

Saturating light intensities required for photosynthesis to reach an asymptote (P_s) do not occur at the ice bottom until late spring to summer. At this time, light transmission increases exponentially with the onset of melt, as snow cover decays, sea ice thins and surface melt ponds begin to form [Arndt & Nicolaus, 2014]. However, the ice algal bloom is in its termination phase by this point due to mechanisms described in Section 2.3.3, so light availability is not a limiting factor. During this time, light intensities may also reach levels high enough to inhibit photosynthesis of the shade-adapted algae and cause photoinhibition (β) (Section 2.3.3).

To a lesser extent than snow, downwelling irradiance is also scattered by sea ice as it interacts with air pockets and brine inclusions. The resulting attenuation causes a decrease in light transmission that intensifies with ice thickness (Figure 2.8). In addition to ice

thickness, the scattering efficiency of sea ice is also related to its physical state, where air bubbles scatter light more than inclusions of liquid brine or melt water [Perovich, 2003]. The net result is a decline in albedo (and scatter efficiency) as the ice begins to melt (Figure 2.3), from 0.5 to 0.3 in first-year ice and 0.7 to 0.55 in multiyear ice [Horner, 1985].

The difference between first-year and multiyear ice albedo is due to the highly scattering surface layer and greater air bubble density in multiyear ice [Horner, 1985]. These characteristics in combination with a typically deeper snow cover and total thickness, indicate that light transmission through old ice is less than through first-year ice [Melnikov et al., 2002]. The difference in PAR transmission between ice types is highlighted by the high Arctic drift studies in Figure 2.9, which summarize light measured during the polar day beneath first-year ice transitioning to second-year ice (i.e. the ice did not fully melt in the summer) and under multiyear ice. Transmitted irradiance through both types of ice is very low prior to snowmelt. However, once snow begins to melt, light transmission rapidly increases under first-year ice, but does not appear to do the same under multiyear ice until zero snow thickness is reached. Furthermore, the magnitude of transmitted irradiance in the range of PAR (400-700 nm) during snowmelt under first-year ice is over 200% greater than under multiyear ice (note the difference in scales in Figure 2.9).

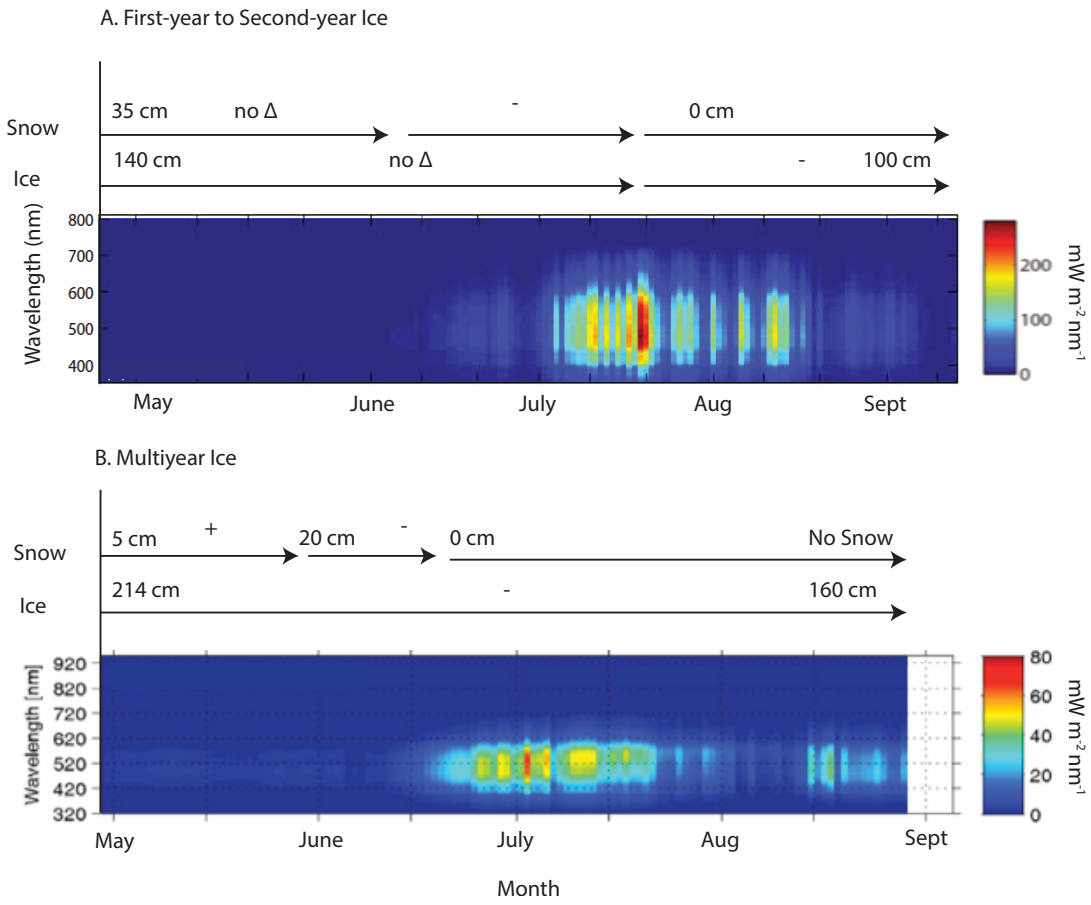

Figure 2.9. Seasonal increase in spectral transmitted irradiance (mW m^{-2} nm^{-1}) through (a) first-year ice transitioning into second-year ice and (b) multiyear sea ice. Changes in snow cover and ice thickness are also indicated. Modified from (a) Wang et al. [2014] and (b) Nicolaus & Gerland [2010] drift studies >80°N and >85°N, respectively. Used with permission from the authors and John Wiley & Sons.

Under low light conditions, ice algae can increase chl *a* and accessory pigments to maximize light absorption, while under light stress algae may produce photoprotective pigments to avoid photoinhibition. These responses have varied effects on photosynthesis-irradiance parameter response. For example, both increased chl *a* and photoprotective pigment production can decrease α^B [Arrigo et al., 2010a]. Please refer to Chapter Four for more details on the photoacclimative response of sea ice algae to changing light conditions.

Downwelling PAR transmitted through the overlying snow and sea ice will be absorbed first by cells higher in the ice column. The result is removal of wavelengths preferred by the dominant photosynthetic pigments in ice algae (*see* Section 2.2.1). This shading process of 'self-shading' can impact the spectral quality and quantity of PAR, and can be an important factor of light limitation when algal biomass is dense. For example, Johnson and Hegseth [1991] report self-shading in their study due to high chl *a* concentrations of 700-4500 $\mu g\ l^{-1}$ (Table 2.3). Other colored particulates trapped in sea ice or deposited after formation can absorb light and affect transmitted radiation [Perovich et al., 1998]. Algae that are shaded by these absorbing particulates [e.g. Horner and Schrader, 1982] may produce more pigments, and broaden their absorption spectrum by increasing abundance of accessory pigments like fucoxanthin (Section 2.2.1). Alternatively, a shift in community composition may occur towards species with affinities to low light. For example, there is evidence that pennate diatoms thrive under lower light conditions relative to centric diatoms [Mendle & Priddle, 1990; Melnikov et al., 2002; Różańska et al., 2009], but more research is need on how this may affect primary production specifically.

Nutrients

The molar composition of marine diatoms at 106:16:15:1 of C:N:Si:P (carbon, nitrogen, silica and phosphorus) highlights the principal nutrients required for ice algal metabolism [Miller & Wheeler, 2012]. Without them, algae typically reduce protein synthesis and increase lipid storage [Lee et al., 2008]. This has a varied effect on α^B but often results in a decline of primary production and P^B_s due to co-dependence of these parameters on light

harvesting as well as light-independent photosynthetic reactions (carboxylation) [Geider & Osborne, 1992]. Nitrogen, silica and phosphorus are the focus here, as they are most often cited as limiting nutrients to production (Tables 2.1, 2.2).

Nitrogen is abundant in seawater as a result of dinitrogen (N_2) gas dissolving directly from the atmosphere to the ocean. However, this form of nitrogen cannot be used by microorganisms except for a specialized group of N_2-fixing bacteria that create ammonium (NH_4) from it. It is the less abundant NH_4 and its reduced forms of nitrate (NO_3) and nitrite (NO_2) that are biologically available to algae. In comparison to nitrogen, phosphorus (as PO_4) and silica (as $Si(OH)_4$) are largely sourced from weathering of the Earth's crust [Miller & Wheeler, 2012]. The efficiency of algae to take-up these nutrients, and store nitrogen (largely as nitrate) and phosphorus, is thought to be species dependent [Glover, 1980]. This suggests that in addition to the processes discussed below, the taxonomic composition of the algal community may play a role in nutrient availability.

Nutrient concentrations in the bottom of sea ice can range considerably, for example from 0.03 to 18.8 μmol l^{-1} N (NO_3 +/or NO_2), <0.2 to 15 μmol l^{-1} PO_4 and 0.6 to 21 μmol l^{-1} $Si(OH)_4$ [Cota et al., 1990; Lee et al., 2008; Mikkelson et al., 2008; Riedel et al., 2008; Galindo et al., 2014], with maximum concentrations occurring prior to the spring bloom, and minimum concentrations occurring during peak biomass [Lee et al., 2008; Mikkelson et al., 2008]. Nutrients to support the ice algal bloom are primarily sourced from the water column rather than from sea ice brine or microbial recycling of nutrients. However, concentrations in the bottom ice are typically greater than the underlying surface water, as ice algae regenerate, or uptake nutrients and subsequently 'leak' them, particularly when under cell stress [Cota et al., 1990].

Access to nutrients from the water column is controlled at the ice-ocean interface by factors that limit or enhance water movement into the sea ice (e.g. under-ice turbulence). The nutrient flux (F_n, mmol m^{-2} d^{-1}) to the sub-ice ice environment:

$$F_n = \left(\frac{\Delta n}{\Delta z} \times K_z \right) \quad (2.6)$$

is dependent on the gradient in nutrient concentration (Δn, mmol m^{-3}) over depth (Δz, m), and the vertical eddy diffusivity (K_z, m^{-2} d^{-1}), which summarizes movement by diffusion and turbulence [Cota & Horne, 1989]. It follows that the nutrient flux to the ice will increase given a strengthening of the sub-ice nutrient gradient, and enhancement of physical (mixing) or molecular (temperature) energy.

The sub-ice gradient is strong at times of high biomass and nutrient availability, when nutrients immediately beneath the ice are used quickly but are readily replaced. However, the surface waters of the Arctic Ocean are largely nutrient depleted (oligotrophic) (Section 2.4). Nutrient supply is therefore unlikely to keep up with demand during periods of high biomass, making times (Figure 2.3) and regions of high chl *a* accumulation (Figure 2.6, 2.7) susceptible to nutrient limitation [Cota & Horne, 1989]. This is documented by a number of studies in Tables 2.1 and 2.2 (designated as bloom in the nutrient column) that specify nutrient limitation during peak biomass.

The vertical eddy diffusivity will increase as a result of: warming interface temperatures in the spring, saltwater entrainment across the pycnocline (layer of steepest density gradient in the water column), mixing of local currents [Gosselin et al., 1985], eddies from brine drainage and current speed from tidal cycles [Cota & Horne, 1989]. The influence of bi-weekly tidal cycles is demonstrated in Cota & Horne [1989], where

minimum and maximum estimates of α^B and P^B_s ranges correspond to measurements during neap (low) and spring (high) tides, respectively.

Inputs of freshwater to the ice-covered system, like sea ice melt, glacial melt or river runoff, will float above the comparatively dense seawater to form a low salinity layer at the ocean-ice interface. Although in some instances river runoff has enhanced nutrient supply to ice algae [Kaartokallio et al., 2007], the result of these significant freshwater inputs is most often a decrease in F_n. This is due to: lowered *n* immediately beneath the ice, an increase in distance (Δz) to the nutrient containing seawater below the freshwater layer, and a drop in K_z as mixing between the fresh surface and saline underlying layers are limited. When stratification is enhancing nutrient limitation, strong turbulence is required to mix the nutrient depleted surface layer with the saltwater below. Tides are an important source of turbulence in the Arctic marine system, and strong tidal activity has been linked to increased algal production in otherwise stratified conditions [Gosselin et al., 1985]. Formation of a freshwater layer beneath sea ice may also negatively affect production through salinity stress (*see Salinity* above) [Rysgaard et al., 2001] or by modifying the bottom-ice lamellar structure and affecting colonization [Poulin et al., 1983; Legendre et al. 1991]. Examples of these limitations on primary production from freshwater inputs are highlighted in Tables 2.3 and 2.4 by (S) and (I, structure) under *other* limitations, and stratification under *nutrient*s.

2.3.2 Factors affecting bacterial production

Owing to the shared environment between sea ice algae and bacteria, the mechanisms controlling algal production in sea ice (Section 2.3.1) also influence bacterial production.

In addition to these, bacteria require oxygen and organic matter to respire and produce biomass (equation 2.1). Here the mechanisms of how each factor affect bacterial productivity are reviewed.

Temperature

Sub-zero temperatures of the Arctic marine system suppress bacterial production due to the exponential relationship between basal metabolic rate (V) (μg C ml^{-1} h^{-1}) and temperature (T) (°K) described by the Boltzmann-Arrhenius model:

$$V = V_0 \times e^{(-Ea/kT)} \quad (2.7)$$

which also includes a normalization constant independent of body size and temperature (V_0) (μg C ml^{-1} h^{-1}), the Boltzmann constant (k, 8.62 x 10^{-5} eV K^{-1}) and the energy of interest at a given rate (E_a, ie. slope of BP over increasing temperature) [Maranger et al., 2016] (μg C ml^{-1} h^{-1} K^{-1}). As a result of slow metabolism, bacterial uptake of substrate for respiration is limited and high concentrations may be required to overcome it [Pomeroy et al., 1991; Kirchman, 2008]. Both equations 2.5 and 2.7 highlight the dependence of algal and bacterial production on temperature, however bacterial production is more sensitive to changes in temperature than primary production [Pomeroy et al., 1991].

Salinity

Sea ice bacteria are able to osmoregulate to a range of seasonal extremes in salinity of the brine network (Section 2.1.3) by regulating intracellular concentrations of solutes. However, decreased abundance near the air-ice interface with the onset of melt pond formation suggests some vulnerability to low salinities [Deming, 2010].

Light

The positive association between sub-saturating light intensity and primary production (Figure 2.5) has also been documented for heterotrophic bacteria [Church et al., 2004]. Despite the light independent reactions of bacterial respiration, photostimulation of ^{3}H-leucine uptake is thought to occur as a result of production from cyanobacteria or unidentified photoheterotrophs. Further research is needed to quantify the effect of light on BP estimates and currently [Kirchman, 2008], bacterial incubations seem to be done at *in situ* light intensities or darkness in an attempt to avoid this uncertainty.

Nutrients

Nutrients are sources of energy for bacterial respiration, and are required for genetic exchange and maintenance of cellular membranes. Bacteria have an especially high affinity for NH_4 and PO_4, and may compete with ice algae for them in confined space environments like sea ice [Kirchman, 2008]. Bacteria also require large quantities of iron for the process of respiration, but concentrations are not considered limiting in the Arctic [Tortell et al. 1999; Wang et al., 2014].

Nutrients in the internal brine network are sourced from ocean water that was trapped during ice formation, and resupply comes with brine movement after the percolation threshold has been reached (Section 2.1.3) [Dieckmann et al., 1991]. After initial entrapment of seawater, enrichment of nutrients in the brines can occur from microbial degradation of particulate organic matter also present in the ice, bacterial recycling of nutrients [Helmke & Wayland, 1995] and regeneration of nutrients by phagotrophic

prostists [Stoecker et al., 1993]. Riedel et al., [2007a] also documented significant rates of NH_4 enrichment in newly formed sea ice at 0.48 μmol l^{-1} d^{-1} from bacterial N_2-fixation.

However, bacteria trapped in isolated brine pockets are removed from the more readily supplied nutrients at the ice interface (Section 2.3.1) and may deplete their pool of nutrients as a result [Dieckmann et al., 1991]. For this reason, bacteria associated with oligotrophic environments have been documented in the upper portion of Arctic sea ice, whereas bacteria characteristic of nutrient-sufficient (eutrophic) habitats have been documented in the bottom [Kaartokallio et al., 2013].

Oxygen

Oxygen is trapped in sea ice during formation, but the majority is locked away in bubbles until spring warming permits merging with the brine network [Rysgaard & Glud, 2004]. Furthermore, O_2 is lost during the process of sea ice growth with brine drainage [Rysgaard et al., 2008]. Bacteria inhabiting brine inclusions could therefore be oxygen limited with concentrations of about 50 μmol l^{-1} (melted sea ice) [Rysgaard et al., 2008] and daily requirements up to 3 μmol l^{-1} [Sogaard et al., 2010], until sea ice porosity reaches 5% (Section 2.1.3) and allows significant gas exchange between the brine, atmosphere and ocean [Loose et al., 2010].

In comparison, bacteria in the bottom ice have access to oxygenated ocean water directly or via diffusion, but O_2 may still become limiting in the bottom-ice when algal photosynthesis is low. For example, Rysgaard et al. [2008] documented net heterotrophy in the bottom 50 cm of sea ice as O_2 consumption rates were > 100 times larger than O_2 release by primary production.

Substrate availability

Together the dissolved fractions (< 0.7 μm) of organic carbon (DOC), nitrogen (DON) and phosphorus (DOP) represent dissolved organic matter, with the majority in Arctic surface waters (90%) [Sarmiento & Gruber, 2006] and sea ice (approximately 9:1 parts DOC:DON) [Thomas et al., 2001] being of the carbon fraction. Dissolved organic matter is classified depending on its resistance to microbial degradation and therefore bioavailability, as: (1) labile, immediately available (2) semilabile, weeks to months for degradation (3) refractory, years to millennia for degradation [Sarmiento & Gruber, 2006]. It is the labile fraction that is readily available for uptake by bacteria and use in respiration, and is the focus here.

The concentration of DOC in sea ice is often reported as the dominant factor controlling bacterial production (Table 2.4). Dissolved organic carbon can be produced in sea ice from: algal and bacterial excretions, particularly when under stress [Gosselin et al., 1997], grazing or cell lysis from viral infection (Section 2.3.3) and the decomposition of particulate organic material [Sarmiento and Gruber, 2006; Robinson et al., 2008]. As a result of these mechanisms, 40-60% of DOC in sea ice is considered labile [Kähler et al., 1997]. The relationship between DOC and bacterial production in sea ice is attributed to the presence of ice algae, where high algal productivity produces greater abundance of DOC for bacterial respiration. This is documented in nearly all studies of Table 2.4, as noted by the designation of (I) under *substrate*. The relationship between bacterial and primary production may be in part due to algal synthesis of cryoprotective compounds called exopolymeric substances (EPS, 1 nm to micrometers in size) [Thomas et al., 2010], that can be used as a substrate in bacterial respiration. However, the role of EPS as a high

[Junge et al., 2004] or low [Pomeroy & William, 2001] quality bacterial substrate is uncertain.

The processes of DOC formation also occur elsewhere, followed by transport to the Arctic marine system (*see* Section 2.4) and sea ice interface (Section 2.3.1). These external inputs control the concentration of DOC in surface waters (although the labile fraction is typically <1%) [Kirchman, 2008], which is responsible for the amount of DOC trapped in sea ice during formation. In this process DOC becomes entrained at up to 30 times pelagic concentrations [Thomas et al., 2001], which supplies bacteria living in the internal brine network. However, without access to additional DOC fluxes from the water column, bacterial production over the winter depletes resources of DOC [Riedel et al., 2008]. In the bottom ice external sources supplement bacterial production when DOC concentrations are low, but brine exchange with seawater may also dilute DOC that accumulated during ice formation or algal production [Thomas et al., 2001].

2.3.3 Physical losses of algae and bacteria from sea ice

Sea ice algae and bacteria can be physically removed from their environment. This represents a loss of production that is independent from the decreases in cell activity that have been described in Sections 2.3.1 and 2.3.2. Physical losses may occur throughout the bloom period, although the greatest levels occur during sea ice melt and ultimately result in algal bloom termination. Here the main causes of cell loss are reviewed while the mechanisms specific to bloom termination separately are also outlined.

Predation

Over 60% of ice algae are consumed in the upper water column by pelagic protozoa [Levinson, 2000], zooplankton and under-ice amphipods once they have been removed from the ice [Michel et al., 1996; 2002]. Grazing pressure directly on algae attached to the sea ice is therefore limited in comparison [Michel et al., 2002]. Nevertheless, removal of algal biomass by consumers has been influential in regions of both high (e.g. Canadian Archipelago) [Smith et al., 1988] and low (e.g. ≤ 60°N) [Haecky & Anderson, 1999] primary production (Table 2.3). It is also an important consideration in relative terms, where grazing pressure is likely to be greater in regions of low pelagic primary production as ice algae represent one of the few available food resources [Legendre et al., 1992].

Grazing of bacteria by heterotrophic protists in sea ice during the spring has the potential to remove up to 60% of bacterial biomass per day, and can be a key factor in controlling bacterial abundance in sea ice [Riedel et al., 2007b; Deming, 2010]. Mixotrophic phytoplankton such as dinoflagellates also feed on sea ice bacteria, but their specific contributions to sea ice grazing remain largely unknown [Miller & Wheeler, 2012].

Grazing pressure on bacteria likely increases over the spring bloom as grazer abundance increases with algal and bacterial growth [Telesphore Sime-Ngando et al., 1997] and temperature [Maranger et al., 2016]. Unfortunately the net effect of grazing is often uncertain, as losses from grazer consumption are indistinguishable from the physical losses associated with brine drainage or ocean turbulence (e.g. Smith and

Clement, 1990), unless grazer abundance and/or activity is specifically quantified (eg. Riedel et al., 2007b).

Viral infection

Viral concentrations in sea ice of 10-100 times greater than the water column suggest that ice algal and bacterial death by viral infection and cell lysis is likely to occur [Maranger et al., 1994]. The net impact on biomass loss in sea ice is uncertain as bacteria can develop resistance to viruses over the bloom [Maranger et al., 1994] and infections of the diatom class are not often documented [Van Etten et al., 1991; Nagasaki et al., 2005]. However, analysis of bacterial-viral coupling in the Arctic pelagic system indicates that viral control on bacterial production may be significant through infection and subsequent cell death [Maranger et al., 2016]. Unlike grazer pressure that is thought to occur largely in the spring, losses from viral infection can occur through all seasons of ice cover [Deming, 2010].

Mechanisms of bloom termination

The greatest release of algal biomass to the water column occurs during late spring in the termination phase of the bloom. Cell loss is caused by processes associated with ice melt that include: substrate loss [Campbell et al., 2015]; absorption and subsequent melting of cells from the ice (biological melt) [Zeebe et al., 1996]; forceful drainage of meltwater through the brine network [Lavoie et al., 2005]; and brine drainage [Mundy et al., 2007]. Cells may also be physically removed as a result of strong tidal velocities, which competes with their positive influence on nutrient supply (Section 2.3.1) [Campbell et al.,

2014]. Finally, increased light transmission during late melt (Section 2.1.3) has the potential to photoinhibit cells to the extent of causing death [Rintala et al., 2006].

Bacteria living in association with ice algae will be directly affected by the mechanisms above. Bacterial abundance in sea ice also declines due to the direct impact of melt water and brine drainage or flushing, which removes cells throughout the sea ice. Cell removal by brine drainage occurs throughout the year, but losses are greatest with melt onset [Deming, 2010].

2.4 Regional and pan-Arctic variability of production in sea ice

The dominant factors regulating ice algal and bacterial production described in Section 2.3 are reviewed at regional and pan-Arctic scales in this section. This includes light availability as a result of ice type and snowfall (Section 2.4.1), nutrient access and abundance in surface waters of the Arctic Ocean (Section 2.4.2), and non-ice algal sources of dissolved organic matter (Section 2.4.3). It is important to remember that the processes affecting primary production here may also indirectly affect bacteria due to the tight coupling between primary and bacterial production in sea ice. This section concludes with a review of the processes governing productivity within the regions defined in Section 2.1.1.

2.4.1 Light availability

Snow accumulation and ice type are dominant controls on light transmission, where thick snow cover and old ice limit its availability to ice algae (Section 2.3.1). As a result, regional snowfall patterns and the distribution of old ice in the Arctic may highlight

regions of intensified light limitation. Here these controls are summarized at the regional to pan-Arctic scale.

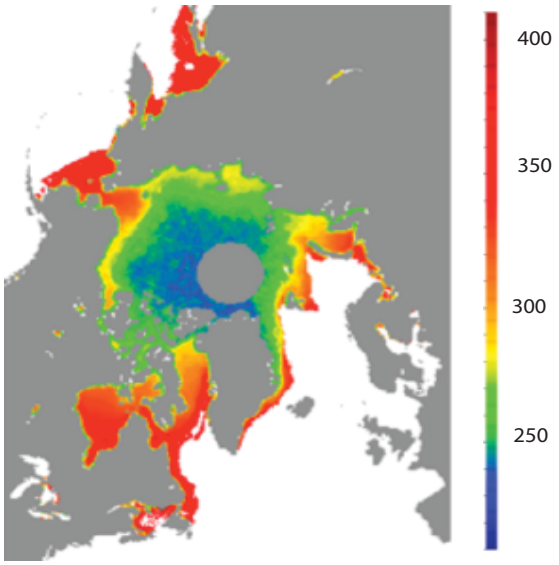

Figure 2.10. Historical averages (1979-2007) of freeze onset in the Arctic. Scale shows day of year. From Markus et al. [2009]. Used with permission from John Wiley & Sons.

Annual snowfall is greatest in the eastern Arctic, in regions that include the Barents Sea, Greenland Sea and Greenland fjords (roughly < 70°N) [Serreze & Maslanik, 1997]. However, peak snowfall in these regions occurs from October to January when ice in Barents and eastern Greenland Seas has not yet, or only recently formed (Figure 2.10) [Markus et al., 2009]. As a result, this greater snowfall largely impacts light availability in the Greenland Fjords and coastal Greenland Sea where ice is present to accumulate snowfall during this time. Location of low first-year ice primary production estimates (Figures 2.6, 2.7) in these areas with earlier freeze-up near Greenland (Figure 2.10), and reported light limitation in Greenland fjords (Table 2.3) support this hypothesis. In comparison, regions ≤60°N have late freeze-up dates similar to the Barents Sea (and therefore shorter times for snow accumulation), so studies from these areas typically do not report light as a dominant limiting factor (Table 2.3).

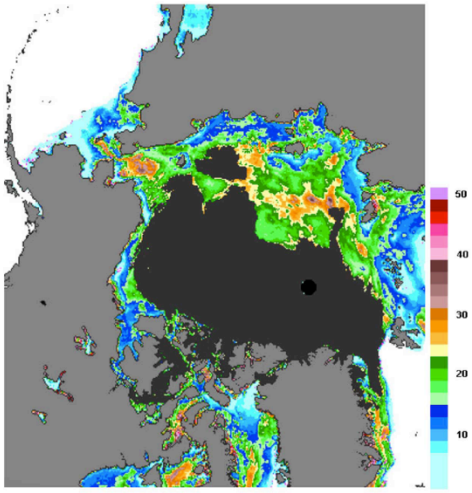

Figure 2.11. Snow depth on first-year sea ice (colored) estimated from the Earth Observing System (EOS) for March 21, 2006. Depths of snow are colored (cm), and do not include multiyear ice (grey). From Cavalieri et al. [2012]. Used with permission from the authors.

Figure 2.11 depicts that old ice is largely situated above 75°N in the central Arctic and first-year ice is mainly located on the continental shelves, which have thicknesses of approximately 2 m and 1.5 m, respectively (*see* Figure 2.9). In addition to ice type and thickness, the distribution of snow between these regions is also different. This is illustrated in Figure 2.11 where average spring snow thicknesses are >20 cm in the central Arctic but ~15 cm on the shelf seas [Cavalieri et al., 2012]. Coupled with weather patterns that concentrate snow deposits north of Canada and Greenland in the spring [Warren et al., 1998], limitation of primary production by light availability is an important factor in the central Arctic basins due to the presence of thick snow covered old ice. This conclusion is highlighted by the study of Gosselin et al. [1997], which states that the different conditions (ie. light, brine drainage etc.) inherent to multiyear and first-year ice were a dominant control on observed variability in primary production (Table 2.3).

2.4.2 Nutrient availability

Arctic inflows and surface water circulation

The nutrient content of surface water in the Arctic marine system greatly affects the nutrients trapped in brine inclusions during ice formation, and is crucial for the resupply of nutrients to bottom-ice communities (Section 2.3.1). Surface waters in the Arctic have low salinity (30.75 – 32.60 over central basins) [Andersen et al., 1989] due to freshwater input from seasonal ice melt, river runoff and precipitation, and are characterized by low nutrient content [Carmack et al., 2007]. As a result, nutrients to sustain primary production in the Arctic are mainly imported. This is particularly true for nitrogen, which is the main limiting element of primary production in the Arctic Ocean [Tremblay et al., 2016].

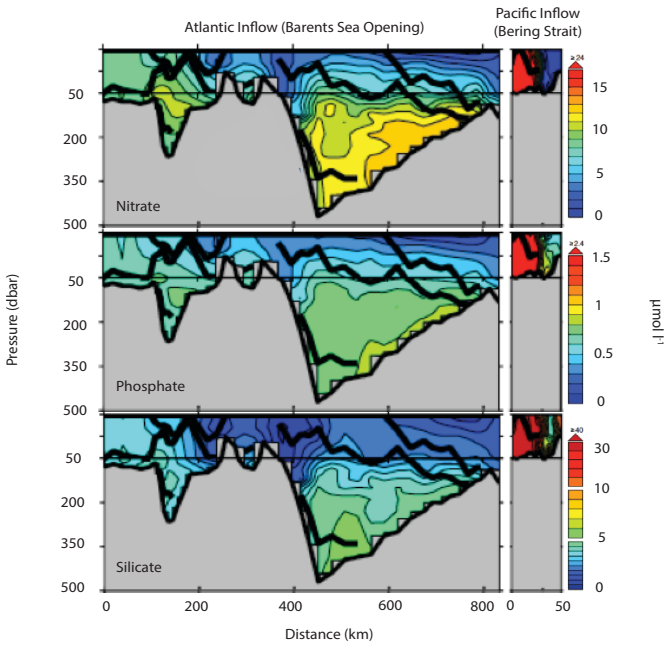

Figure 2.12. Nitrate, phosphate and silicate concentrations entering the Arctic Ocean from the Atlantic (through the Barents Sea Opening) and Pacific Ocean (through the Bering Strait). Modified from Torres-Valdes et al. [2013]. Used with permission from John Wiley & Sons.

The main import of nutrients to the Arctic, in volume and total nitrogen-phosphorus content, comes from the East as water from the Atlantic Ocean, with a salinity of approximately 35 (Figures 2.6, 2.7). This is followed by inflow from the West through the 50 m shelf of the Bering Strait (Figure 2.12) from the Pacific Ocean, which has a salinity of about 32 (*see* Figures 2.6 and 2.7 for bulk inflow concentrations) [Andersen et al. 1989; Torres-Valdes et al., 2013]. When considering both sources in the top 50 m of the ocean alone, however, nutrient inputs to the Arctic marine system are greater from the Pacific Ocean (Figure 2.12) [Tremblay et al., 2016].

Overall these water masses move in opposite directions across the Arctic, Atlantic water from East to West and Pacific water from West to East (Figures 2.6, 2.7) [Torres-Valdes et al., 2013]. Heavy salt-stratification in the Arctic marine system arranges water masses from surface downwards as Arctic surface water-Pacific water (where present)-Atlantic water. The strength of this stratification is greatest in Pacific water of the western Arctic, and weakens with Atlantic influence in the East until the upper water column becomes largely uniform in the Greenland and Barents Seas. Therefore, the most important source of nutrients in the Arctic is the water mass directly beneath the surface (Pacific water in the west, Atlantic water in the East). However, the accessibility of this water to ice algae depends on the proximity of the sea ice to inflow (e.g the Bering Strait) and physical mixing of the near-surface water [Codispoti et al., 2013]. For example, turbulence produces a stronger flux of nutrients through the upper ocean, which replenishes nutrients at the ice bottom (Section 2.3.1).

The absence of reported nutrient limitation for the Beaufort and Barents Seas in Tables 2.1 and 2.2 illustrates the importance of nutrient accessibility for regional primary

production, as these water bodies represents are directly influenced by nutrients imported by Pacific and Atlantic waters, respectively (Figures 2.6, 2.7) [Carmack, 2006]. However, in the absence of nutrient limitation, primary production in these regions can result in dense blooms that cause light limitation by self-shading (Tables 2.3, 2.4; Section 2.3.1).

Turbulence

The importance of turbulence for nutrient supply at the ocean-ice interface (Section 2.3.1) and mixing of upper ocean water masses has been discussed above. Here the regional processes that contribute to sub-ice turbulence or stratification are outlined.

Gravity governs the daily movement and seasonal strength of the global tides, but geographic differences in water depth and the profile of shorelines can create regional variations in tidal velocities. In the Arctic marine system, tidal velocities are weakest over the deep basins and greatest on the continental shelves, including parts of Baffin Bay (Figure 2.13) [Padman & Erofeeva, 2004]. Interaction between tidal currents and sea ice dampens surface velocities by 10-20% [Prinsenberg, 1986; Padman & Erofeeva 2004], but the resultant friction between ice and water further enhances the nutrient supply to the sea ice [Saucier et al., 2004].

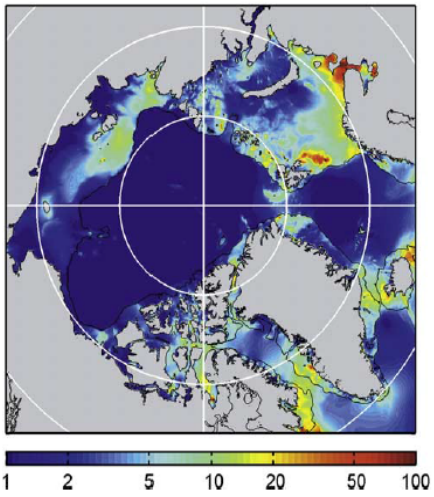

Figure 2.13. Modeled 14-day averages of tidal current speed (cm s^{-1}) in the Arctic Ocean during the ice-free period. The 500m isobath is also included. Velocities do not account for reductions as a result of ice coverage. From Padman & Erofeeva [2004]. Used with permission from John Wiley & Sons.

Continental shelves are also important regions of turbulence because of their predominantly landfast first-year ice coverage. In these regions, the expulsion of brine during seasonal ice formation creates convection as heavy brine sinks and is replaced with lower salinity seawater. This mechanism can help recharge nutrients in surface waters prior to the spring bloom [Prinsenberg & Ingram, 1991]. Indirectly, first-year ice dynamics in the shelf seas restrict nutrient availability in the central Arctic by enhancing stratification, as freshwater from sea ice melt is transported into the deep basins and forms a low salinity layer under old ice [Carmack et al., 2006].

Localized areas of turbulence occur in the Arctic marine system due to local geography. One example is the presence of sills (rises in seabed elevation) in parts of the Canadian Archipelago, which cause mixing as water masses are forced up and over them [Michel et al., 2006].

Areas of open water surrounded by ice in the Arctic marine system also experience enhanced nutrient supply from turbulence, as wind-driven mixing causes upwelling [Carmack et al., 2006]. These polynyas (non-linear opening of water surrounded by ice) and leads (linear fracture in sea ice) can be hotspots for surface mixing, as well as increased light penetration [Carmack and Kulikov, 1998; Melling et al., 2015]. Sea ice surrounding these areas, or periodically reforming in them may therefore experience greater primary production. For example, Lange et al. [2015] report high chl *a* concentrations (15 mg m^{-3}) in refrozen leads between mobile pack ice (< 4 mg m^{-3}).

One of the largest polynyas in the Arctic is the North Water located in northern Baffin Bay [Stein & MacDonald 2004]. Its formation in part by predominant winds, subsequent currents, and upwelling from the West Greenland Current contributes to the high productivity of Baffin Bay (Figures 2.6, 2.7) and lack of reported nutrient limitation in the region during the ice algal bloom (Table 2.3). However, nitrate in surface waters can become depleted in the region following uptake by phytoplankton from April to June [Tremblay et al., 2002].

Stratification

The Arctic Ocean receives 11% of global runoff, with peak flow occurring in the spring [Shiklomanov, 1997]. The impact of these freshwater inputs on stratification will vary with proximity of sea ice to river estuaries. It follows that the influence will be greatest on the continental shelves, with the Beaufort Sea receiving the greatest riverine freshwater in the boundaries of the defined Arctic marine system [Carmack et al., 2006]. Other areas highly influenced by stratification include Hudson Bay and the Baltic Sea of the ≤60°N

region [Dery et al., 2005, Thomas et al. 2010], where both studies in Table 2.4 from these regions report nutrient limitation by stratification as a result of riverine inputs. Nutrient limitation was partially alleviated by increased tidal velocities [Gosselin et al., 1985] or distance from the river mouth [Kaartakallo et al., 2007]. Nutrient limitation by stratification following snow, and potentially glacial melt, is also an important factor in the Greenland fjords [e.g. Rysgaard & Glud, 2007].

2.4.3 Processes of dissolved organic matter transport

The concentration of dissolved organic matter in Arctic surface waters controls initial brine concentrations, and could supplement bottom-ice substrate requirements when primary production is low (Section 2.3.2). Here the processes of external dissolved organic matter supply to surface waters are discussed.

Arctic surface water is considered rich in dissolved organic matter with an average of 76 ± 13.8 μmol l^{-1} DOC [Amon & Benner, 2003] that is maintained by: surface water exchanges, terrestrial inputs, under-ice primary production [e.g. Mundy et al., 2011] and open water primary production from the previous summer [Nguyen et al., 2012]. Surface water movement of Pacific and Atlantic through the Arctic marine system was described in Section 2.4.2. Similar to nutrient supply in the upper 50 m of the ocean, the import of DOC is greater from the Pacific (71 ± 20 μmol l^{-1}) [Anderson, 2002] than the Atlantic Ocean (58.2 ± 4.9 μmol l^{-1}) [Amon & Benner, 2003]. The influence of Pacific water dissolved organic matter is therefore greatest as a result of its substrate load and position below the Arctic surface water.

Terrestrial inputs of dissolved organic matter enter the Arctic directly from coastal erosion, and indirectly from rivers, wind and mobile sea ice transport [Stein & MacDonald, 2004]. Of these mechanisms the supply of DOC from rivers is highest (550-630 μmol l^{-1} DOC) [Lobbes et al., 2000; Gordeev & Rachold, 2004], indicating potentially significant substrate contributions near estuaries and on continental shelves.

Finally, 20-40% of total primary production is released as DOC, indicating that regions with high pelagic primary production in surface waters will also have greater concentrations of dissolved organic matter [Gosselin et al., 1997]. Total inputs of dissolved organic matter from phytoplankton in the Arctic Ocean are estimated at 66 Tg C y^{-1}, with the greatest production occurring on Barents and Chukchi Sea inflow shelves (320 Tg C yr^{-1}), and the lowest occurring in the central basins (21.5-32.25 Tg C yr^{-1}) [Gosselin et al. 1997]. However, the contribution of these inputs to sea ice DOC will be dependent on pelagic uptake for bacterial production.

There are not any clear regional patterns of bacterial production in Figure 2.6, 2.7, instead it appears close to uniform across the Arctic. This could be a result of too few studies measuring bacterial production to characterize spatial distributions, or variability in the type of sample collected (e.g. brine, ice thickness, melt dilution) in studies (Table 2.6). Alternatively, the uniformity in regional production may indicate that processes controlling bacterial production are close to spatially uniform in comparison to processes controlling primary production that vary considerably (*see* Section 2.4.1, 2.4.2). For example, the temperature and salinities of the bottom-ice vary with timing, but do not vary widely between areas or ice types. Also, dissolved organic matter in Arctic surface

waters is characteristically high and is unlikely to be a significant limiting factor at the regional scale.

However, the seasonal cycles of bacterial and primary production are clearly correlated, which means that algae likely drive the timing of high and low bacterial production, if not the actual quantity or rate of production at a given time. Comparison of bacterial production measured over the spring and along transects in the study by Haecky & Andersen [1989] support the temporal rather than spatial control of primary production, where variability driven by ice algal DOC over the spring was much greater than spatial variability along transects.

One area of bacterial production measurements does stand out in Figures 2.6 and 2.7: the central Canadian Archipelago, which is located near Resolute Bay, Nunavut. Here, bacterial production is considerably lower and limitations associated with cell loss (grazing, ice melt and viral lysis) are documented as (V) and (M) in Table 2.4 [Smith & Clement, 1990; Maranger et al., 1999]. This suggests that physical losses may have the potential to control bacterial production on spatial scales, an observation that is supported by the strong control of grazing pressure on sea ice [Riedel et al., 2007b] and pelagic [Maranger et al., 2016] bacterial abundance.

2.4.4 Summary of the processes controlling regional production in sea ice

Here the environmental conditions that promote or inhibit primary and/or bacterial production are summarized. Regions of the Arctic marine system most influenced by each process are also listed.

- Light and nutrient limitation of primary production is widespread in the Arctic:
    - Light is particularly limited in locations with high snow depth and/or multiyear ice (causing relatively low primary production in central Arctic basins and Greenland fjords)
    - Nutrient availability is positively associated with proximity to transient oceanic inputs (causing relatively high primary production in the Barents Sea, and parts of other continental shelves)
    - Nutrient availability is positively associated with environmental conditions that promote turbulence under sea ice (causing relatively high primary production on continental shelves, and near shelf breaks of the deep water-shelf regions)
    - Nutrient availability is negatively associated with environmental conditions that promote stratification (causing relatively low primary production in defined regions $\leq 60°N$, central Arctic basins, Greenland fjords, and estuarine zones on the continental shelves)
- The availability of dissolved organic matter regulates local bacterial production, but not pan-Arctic variability:
    - The initial concentration of dissolved organic matter in ocean surface seawater influences bacterial production within the sea ice brines, particularly in winter prior to brine movement between inclusions [e.g. Riedel et al., 2008]
    - The dominant source of dissolved organic matter in the bottom of sea ice during the spring is ice algae and, consequently, a positive relationship

between primary and bacterial production has been documented in several studies (*see* Table 2.6)

- Despite the close association between algae and bacteria, primary production and therefore dissolved organic matter availability does not appear to explain regional differences in bacterial production. As a result, regional and Pan-Arctic trends in bacterial production were not observed.
- Processes that influence spatial variability in bacterial production may include physical loss from the ice by grazing or viral lysis, and ice melt
- More research is needed to improve the number of measurements of bacterial production and their spatial coverage

2.5 Potential influence of current and future climate changes

Near surface temperatures in the Arctic are warming at twice the rate of the global average [Graversen et al., 2008]. This has profound implications for a system that has historically been covered by ice for most of the year, including the state of its sympagic habitats [Wassmann et al., 2011]. With climate warming expected to continue [Vavrus et al., 2015], it is important to identify the potential impacts of future changes on production in sea ice.

The increase in Arctic atmospheric temperature is also warming the surface of the Arctic Ocean at a rate of 0.5-1.5 °C decade^{-1} [Stroeve et al., 2014]. This increase in temperature will directly affect the metabolic activity of algae (Section 2.3.1) and bacteria (Section 2.3.2), and could increase the activity of grazers and viruses [Maranger et al., 2016]. However, the influence of temperature on cellular metabolism and resulting increase in primary and bacterial production, is at the expense of the stability of the sea

ice environment. For instance, physical loss of algal and bacterial cells from the ice that currently occur during spring melt (Section 2.3.3) would intensify. As a result, the focus in this section is on how changes to the sea ice environment, rather than metabolism, are likely to affect sea ice production.

This section is organized into several subsections, each discussing a change in the Arctic marine system that is currently affecting, or is predicted to affect sea ice algal and/or bacterial production due to Arctic climate change. These include: reductions in sea ice extent and thickness (Section 2.5.1), changes in snow cover on sea ice (Section 2.5.2), and increases in freshwater inputs (Section 2.5.3). In these sub-sections the nature of each change is first outlined, followed by the potential response of sea ice primary and bacterial production. Finally, due to the complexity of potential changes and responses, a summary of the processes that could potentially modify Arctic primary and bacterial production is given in Table 2.5 (Section 2.5.4)

2.5.1 Reduction in sea ice extent and thickness

Observed and predicted changes

Together, the increase in atmospheric and oceanic temperature is driving changes in sea ice type, seasonality, extent and thickness. These changes are summarized in this section.

Warmer temperatures limit ice growth in the fall and winter, and enhance melting in the spring and summer. One of the greatest impacts of this change is that old ice cannot sustain net mass balance or growth annually. The resulting loss in sea ice cover have been most pronounced for multiyear ice, which is decreasing in area by 1.5 million km^2 $decade^{-1}$ [Nghiem et al., 2007] and has lost ≥ 50% of its total volume between 1958 and

2000 [Kwok & Rothrock, 2009]. As a result of this decline, the central Arctic, which is currently covered by old ice in the summer (appx. 5 million km^2; NSIDC), could be ice-free within the next 20 years [Wassmann et al., 2011].

Declines in ice extent and thickness are also documented for first-year ice, particularly at the southern peripheries of the Arctic like the Barents and Labrador Seas. This is due to warmer ocean temperatures limiting ice growth, or preventing it entirely [Cavalieri & Parkinson, 2012; Vihma et al., 2014]. However, the loss of old ice and subsequent replacement by first-year ice in the fall has increased the proportion of first-year ice in winter from 30 to > 80% in the Arctic since the mid 1980s [Stroeve et al., 2014]. The seasonality of first-year ice has also changed, with earlier onset of melt in the spring by 1-9 days $decade^{-1}$ and later freeze-up in the fall [Markus et al., 2009; Vihma, 2014]. The resulting change in duration of first-year ice ice-coverage varies with region, but overall reductions have been more pronounced on the continental shelves than the central Arctic [Markus et al., 2009].

Potential response of production in sea ice

The decline of sea ice coverage over time and space represents a loss of algal and bacterial habitat. The impact of sea ice decline on ice habitat abundance may be conceptualized with reference to Figure 2.4, where colored regions represent the current presence of ice and white spaces the presence of open water. With climate change the following changes are expected:

- Loss of multiyear ice: northward (upward) extension of the open water period as the Arctic summer progressively becomes ice-free. Under future scenarios of an

ice-free Arctic, the open water would extend to all northern latitudes during the summer and form a band along the entire height of Figure 2.4.

- Reduction in first-year ice extent: lower latitudes of the y-axis become open water without ice formation in the fall
- A decrease in duration of first-year ice coverage: more open water along the months of the x-axis.

The resulting decline in ice coverage following these changes will likely cause a net decline in sea ice production over time and space, due to habitat loss. Specifically, the ice algal bloom will occur in fewer places in the Arctic marine system and for a shorter amount of time in late spring [ACIA, 2005; Wassmann et al., 2011]. The associated lengthening of the open water season and its expansion North is likely to increase pelagic production as a result, which may increase the overall productivity of the future Arctic marine system [Arrigo et al., 2008]. However, increased pelagic primary production could put a greater strain on surface water nutrient concentrations available to ice algae in the spring [Tremlay et al., 2016].

The change in timing of the bloom may have cascading effects for the ecosystem, as aquatic grazers like the zooplankton *Calanus glacialis* and *C. hyperboreus* have timed their reproductive cycles to coincide with the ice and pelagic algal blooms. Changes and variability in the timing of ice break-up can affect the reproductive success of these organisms by causing a mismatch between life-stages and high quality food resources [Leu et al., 2011]. In turn, reduced grazing pressure could also positively affect primary production during the algal bloom by diminishing physical losses. The impact of these

changes on viral activity and bacterial grazing is unknown, but the positive association between bacterial and grazer abundance, and to a lesser extent viral abundance, in the Arctic pelagic system, suggests a collective response to potential changes in their environment [Maranger et al., 2016].

Change in the type of ice also affects the quality of remaining algal and bacterial habitat. In particular, the differences in light availability and resulting primary production between old and first-year ice (Sections 2.3.1, 2.4.1) indicate that the increasing proportion of first-year ice will promote greater instantaneous ice algal production during the bloom. However, maximum growth in the 'new first-year ice' will still be limited by factors discussed previously (Sections 2.3, 2.4) including, light limitation by self-shading and nutrient availability. The latter may be particularly important for first-year ice over the central Arctic, where low turbulence and distance from terrestrial and transient nutrient supplies will still be an important control on sea ice production.

2.5.2 Changes in snow cover

Observed and predicted changes

The thickness of snow on sea ice affects the temperature of ice through all seasons, as well as light availability and the timing of the onset of ice melt during the spring (Sections 2.1.3, 2.3.3). Historical assessments of snow on sea ice show that spring snow cover is decreasing in thickness over the Arctic Ocean by about 3 cm decade^{-1} [Webster et al., 2014]. This indicates that the ice has become more susceptible to changes in atmospheric temperatures and that light transmission in the spring has increased. Thinner snow in the winter has not promoted increased growth as a result of coincident warming,

but loss of insulation in the spring contributes to the earlier spring melt [Markus et al., 2009; Vihma, 2014]. The impact on light transmission is illustrated Figure 2.8, which shows that a change in average Arctic snow depth of 3 cm decade^{-1} could represent up to a 40% decade^{-1} increase in transmission.

Studies indicate that the amount of snow falling over the Arctic will increase with climate change as a result of the positive feedback between warmer temperatures, longer open water seasons, increased evaporation and increased precipitation [Rinke & Dethloff, 2008; Hezel et al., 2012; Webster et al., 2014]. However, thinning of the snow cover on sea ice is expected to continue as a result of decreasing old-ice coverage and later freeze-up of first-year ice. The majority of snowfall occurs during the fall and winter [Bintanja & Selten, 2014] but, in this scenario, sea ice would not be present to catch the precipitation. Furthermore, predicted increases of snowfall in fall and winter would not be sufficient to make up for the deficit [Hezel et al., 2012; Webster et al., 2014]. Regional snow accumulation on sea ice therefore depends on the freeze-up trends illustrated in Figure 2.10 where regions like the Canadian Archipelago, which have comparatively earlier freeze-up dates, could temporarily experience increases in snow thickness.

Regardless of snow thickness, warmer temperatures will melt the snow cover earlier and faster in the spring. Greater precipitation in the spring also increases the likelihood that rain will fall on snow-covered sea ice (rain-on-snow events) and quicken spring melt [ACIA, 2005]. Finally, the number and severity of storms is also expected to increase with climate change [Rinke & Dethloff, 2008], which have the potential to quickly change light and melt conditions if they occur during the spring.

Potential response of production in sea ice

There is uncertainty and regional variability with observations and predictions of declining snow thickness on sea ice. However, in an effort to simplify discussion this section is focused on the potential responses to thinning snow and greater frequency of spring storm events.

The impact of thinner snow cover on sea ice algal and bacterial production is variable. Earlier melt from greater exposure to warming temperatures in the spring will trigger physical losses of algae and bacteria described in Section 2.3.3 sooner. For instance, snow removal experiments show higher algal losses from the ice, due to melt or photoinhibition, relative to snow-covered populations [Juhl & Krembs, 2010; Campbell et al., 2015]. Snow and ice melt in the spring will also be quicker under thinner snow conditions. The result may be intense sloughing events of algae from the ice rather than gradual losses, which increases the likelihood that cells will sink to the benthos instead of being consumed by grazers in the water column [Michel et al., 2006]. Rain-on-snow in the late spring also causes mass losses of algae from the ice due to enhanced snowmelt, suggesting that greater frequency of spring rainfall in the future would increase sloughing events [Fortier et al., 2002; Campbell et al., 2015]. Combined with the earlier ice break-up, these processes may shift the termination point of the bloom to earlier in the season.

In contrast to the processes described above that act to decrease net biomass and primary production over the bloom, thin snow covers in the spring will increase primary production by alleviating light limitation experienced by algae (Section 2.3.1). As a result, primary production would occur earlier in the polar day and instantaneous primary production would be greater prior to melt, or until other environmental factors (e.g.

nutrients) become limiting [Wassmann et al., 2011]. The ability of the bloom to occur earlier in the season would limit the impact of earlier termination. However, the resulting shift in timing of the bloom would still impact alignment with grazer life cycles (as described above).

2.5.3 Increase in freshwater inputs

Observed and predicted changes

Freshwater inputs to the Arctic Ocean are increasing from: 10% increase in annual river discharge (1977-2007) [Overeem & Syvitski, 2010], more precipitation directly into the ocean, greater ice melt (sea ice, glacial and ice sheet) [Holland et al., 2007] and increased inflow through the Bering Strait [Woodgate et al., 2012]. With the exception of direct precipitation into the ocean, the immediate effects of these increases are local to regional in scale and depend on the proximity of an area to the freshwater input. However, continued increases could promote a widespread freshening of Arctic Ocean surface water [Holland et al., 2007]. Together the increases in river discharge and Bering Strait inflow (~32), in addition to permafrost melt, are also driving an increase in dissolved organic matter concentrations of the Arctic surface waters [ACIA, 2005].

Potential response of production in sea ice

The freshening of Arctic surface waters could decrease production by diluting existing nutrient concentrations and enhancing stratification (Section 2.3.1). Low salinity surface water could also decrease production by affecting ice structure and colonization, and by shifting salinities outside of the preferred range for metabolism (Section 2.3.1, 2.3.2).

The timing of greatest river flow and ice melt does not affect the ice algal bloom because peak flow and ice melt occur in the summer after it has largely terminated (Figure 2.4). Nevertheless, the amount of freshwater discharge from rivers at the onset of spring melt has increased due to climate warming. For rivers draining into the Arctic Ocean, discharge in the month of May when melt begins has increased by > 60% (1977-2007) [Overeem & Syvitski, 2010]. It follows that although the negative influence of river flow on primary production will be greatest for pelagic phytoplankton, there is still likely to be a measurable impact on ice algae.

Greater nutrient limitation during the bloom may favor smaller flagellate species of algae that are better at nutrient uptake because of their high surface area to volume ratio. The impact of taxonomic changes on primary production is also unknown, but the presence of smaller species is likely to have less nutritional value to grazers and the ecosystem [Li et al., 2009; Leu et al., 2011].

In comparison to the processes described above that could decrease production, increased river discharge and inflow through the Bering Strait may enhance production by transporting more nutrients and dissolved organic matter into the Arctic marine system. The net effect of these competing influences on production in sea ice remains to be seen, but nutrient supply from increased river flow is not thought to have a significant effect on nutrient content of the overall Arctic marine system [Fouest et al., 2013].

2.5.4 Summary

A summary of climate change in the Arctic marine system and anticipated responses of primary and bacterial production is presented in Table 2.7. Inclusion of temperature refers

only to direct effect on cells, and not to related indirect changes in the environment, which are represented as separate variables.

Table 2.7. Summary of climate change and anticipated response of production. Symbols of (+) or (-) indicate how the environmental change may affect algal or bacterial production collectively.

Variable	Change	Effect on controlling processes
Temperature	↑ Ice and ocean temperature	↑ Cell metabolism (+) ↑ Heterotrophic grazer and viral activity (+/-)
Sea ice	↓ multiyear ice volume and % cover ↑ first-year ice % cover ↓ Total ice extent ↓ Time of ice coverage	↓ Summer habitat (-) ↑ Transmitted PAR (+) ↓ Winter/spring habitat (-) ↓ Bloom duration (-) ↓ Grazing pressure (?)
Snow	↓ Snow thickness ↓ Time of snow coverage ↑ Rain and storm events	↑ Transmitted PAR (+) ↑ Timing of C_0 (+) ↑ Time and speed of snow melt (-) Δ Bloom duration (?)
Freshwater	↑ Precipitation ↑ River flow ↑ Ice melt ↑ Bering Strait inflow	↑ Stratification (-) ↓ Salinity of surface water (-) ↓ Ice porosity (structure) (-) ↑ Nutrient inputs (+) ↑ DOM inputs (+)

2.6 Conclusions

In this chapter the processes controlling algal and bacterial production in Arctic sea ice were summarized. How these processes affect variability in production at the regional scale and across the Arctic was shown. Current and predicted changes to these processes as a result of climate warming was examined, and in turn, the potential impacts of these changes on sea ice algal and bacterial production was summarized.

The sea ice environment is characterized by seasonal extremes, and conditions that are governed by dynamics of sea ice growth and snow deposition (Section 2.1). Algae and bacteria inhabiting the ice use energy and carbon to sustain metabolism and growth, at rates that have been quantified by scientists in different regions of the Arctic (Section 2.2). The instantaneous rates are largely dependent on processes controlling algal access to light and nutrients, and bacterial access to dissolved organic matter produced by ice algae (Section 2.3). Processes affecting light and nutrients at the pan-Arctic scale explain regional differences in primary production; for instance, regions of reduced light limitation and nutrient accessibility are more productive (e.g. most of the Canadian Arctic Archipelago). The relationship between bacterial production and primary production is less apparent at the regional scale, and pan-Arctic bacterial production may instead be greatly influenced by physical losses (Section 2.4).

Processes controlling primary production vary between the different regions of the Arctic defined in Section 2.1.1, with some overlap. Regions ≤ 60°N have low to moderate levels of production that are influenced by a shorter season of ice cover and often, freshwater riverine inputs. The central Arctic basins have low production due to a combination of light and nutrient limitation from thick snow and ice cover, stratification and distance from nutrients imported to the Arctic. Primary production is highest in the

continental shelves because of thinner ice and snow (vs. the central Arctic) and access to nutrients. This is especially relevant for the Chukchi and Barents Seas that receive nutrient imports directly from the Pacific and Atlantic Oceans, respectively. The productivity of deep-water-shelf regions of Baffin Bay (inclusive of Davis Strait) and the Greenland Sea is variable due to the combined influence of processes characteristic of the continental shelves and central Arctic. Finally, the Greenland fjords have low production due to thick snow cover that limits light availability and freshwater inputs that limit nutrient availability and potentially affect algal attachment to the sea ice.

The future state of ice algal and bacterial production with climate change will largely depend on the extent of habitat loss over space and time, including a shorter spring growing season and limited nutrient availability in a new intensely stratified Arctic Ocean. Current predictions suggest that light availability may not be a significant factor in a new Arctic with thinner snow overlying a seasonal, thinner sea ice cover. At present the contribution of ice algae to total production in the Arctic marine system ranges from 4-25% on the continental shelves [Legendre et al., 1992] to >50% in the central Arctic [Gosselin et al., 1997]. The contribution of bacteria is lower at <1% [Haecky & Anderson, 1999]. The net effect of climate change is likely to decrease both total sea ice production and the contribution from ice algae and bacteria to overall Arctic Ocean production, as the Arctic shifts towards a pelagic dominated system.

References

ACIA (Arctic Climate Impact Assessment) (2005), Cambridge University Press, New York.

Amon, R.M.W., and R. Benner (2003), Combined neutral sugars as indicators of the diagenic state of dissolved organic matter in the Arctic Ocean, *Deep Sea Res*. 50(1), 151-169, doi: 10.1016/S0967-0637(02)00130-9.

Andersen, O.G.N. (1989), Primary production, chlorophyll, light and nutrients beneath the Arctic sea ice, In: Yvonne, H. (ed) The Arctic Seas, climatology, oceanography, geology and biology. U.S.A.

Anderson, L.G. (2002), DOC in the Arctic Ocean. In: Hansell, D.A., Carlson, C.A. (eds) Biogeochemistry of marine dissolved organic matter, Academic Press, San Diego, 665-685.

Ardnt, S., and M. Nicolaus (2014), Seasonal cycle and long-term trend of solar energy fluxes through Arctic sea ice. *The Cryosph*. 8, 2219-2233, doi:10.5194/tc-8-2219-2014.

Arrigo, K.R., Dijken, G.V., and S. Pabi (2008), Impact of a shrinking Arctic ice cover on marine primary production, *Geophys*. *Res*. *Lett*. 35, LI9603, doi: 10.1029/2008GL035028

Arrigo K.R., Mills, M.M., Kropuenske, L.R., van Dijken, G.L., Alderkamp, A.C., and D.H. Robinson (2010a), Photophysiology in two major Southern Ocean phytoplankton taxa: photosynthesis and growth of Phaeocystis antarctica and Fragilariopsis cylindrus under different irradiance levels, *Integr*. *Comp*. *Biol*. 50, 950–966, doi: 10.1093/icb/icq021.

Arrigo, K.R., Mock, T., and M. Lizotte (2010b), Primary Producers and Sea Ice, In: Thomas, D.N., Dieckmann, G.S. (eds) *Sea Ice* 2nd Ed. Wiley Blackwell Publishing, Malaysia, 283-325.

Arrigo, K.R., and C.W. Sullivan (1992), The influence of salinity and temperature covariation on the photophysiological characteristics of Antarctic sea ice microalgae, *J*. *Phycol*. 28, 746-756, doi: 10.1111/j.0022-3646.1992.00746.x.

Bergmann, M.A., Welch, H.E., Butler-Walker, J.E., and T.D. Sifred (1991), Ice algal photosynthesis at Resolute and Saqvaqjuac in the Canadian Arctic, *J*. *Mar*. *Syst*. 2, 43-52, doi:10.1016/0924-7963(91)90012-J.

Bintanja, R., and F.M. Selten (2014), Future increases in Arctic precipitation linked to local evaporation and sea-ice retreat, Nature 509, 479-482, doi: 10.1038/nature13259.

Booth, J.A. (1984), The epontic algal community of the ice edge zone and its significance to the Davis Strait Ecosystem, Arctic 37(3), 234-243.

Bowman, J.S., Rasmussen, S., Blom, N., Demine, J.W., Rysgaard, S., and T. Sicheritz-Ponten (2012), Microbial community structure of Arctic multiyear sea ice and surface seawater by 454 sequencing of the 16S RNA gene, *Int. Soc. For Microb. Ecol.* 6, 11-20, doi:10.1038/ismej.2011.76.

Brandon, M.A., Cottier, F.R., and F. Nilsen (2010), Sea ice and oceanography, In: Thomas D.N., Dieckmann G.S. (eds.), *Sea Ice* 2nd Ed., Wiley Blackwell Publishing, Malaysia, 79-112.

Bricaud, A. Claustre, H., Ras, J., and K. Oubelkheir (2004), Natural variability of phytoplanktonic absorption in oceanic waters: Influence of the size structure of algal populations, *J. Geophys. Res.* 109, C11010, doi: 10.1029/2004JC002419.

Buck, K.R., Nielsen, T.G., Hansen, B.W., Gastrup-Hansen, D., and H.A. Thomsen (1998), Infiltration phyto- and protozooplankton assemblages in the annual sea ice of Disko Island, West Greenland, spring 1996, Polar Biol. 20, 377-381, doi: 10.1007/s003000050317.

*Bunch, J.N., and R.C. Harland (1990), Bacterial production in the bottom surface of sea ice in the Canadian subarctic, *Can. J. Fish. Aquat. Sci.* 43, 1986-1995, doi: 10.1139/f90-223.

Campbell, K., Mundy, C.J., Barber, D.G., and M. Gosselin (2014), Characterizing the ice algae biomass-snow depth relationship over spring melt using transmitted irradiance, *J. Mar. Syst.* 67(3), 375-387, doi: 10.14430/arctic4409.

Campbell, K., Mundy, C.J., Barber, D.G., and M. Gosselin (2015), Characterizing the sea ice algae chl a-snow depth relationship over Arctic spring melt using transmitted irradiance, *J. Mar. Syst.* 127, 76-84, doi: 10.1016/j.jmarsys.2014.01.008.

Campbell, N.A, and J.B. Reece, J.B. (2005), *Biology* 7th Ed., Pearson Education Inc., USA.

Canadian Ice Service (CIS) (2016), Manual of Ice (MANICE), Environment Canada and Climate Change.

Carmack, E.C. (2007), The alpha/beta ocean distinction: A perspective on freshwater fluxes, convection, nutrients and productivity in high-latitude seas, *Deep-Sea Res. II* 54, 2578-2598, doi: 10.1016/j.dsr2.2007.08.018.

Carmack, E., Barber, D., Christensen, J., MacDonald, R., Rudels, B., and E. Sakshaug (2006), Climate variability and physical forcing of the food webs and the carbon

budget on panarctic shelves, *Prog. Ocean.* 71, 145-181, doi: 10.1016/j.pocean.2006.10.005.

Cavalieri, D.J., and C.L. Parkinson, C.L. (2012), Arctic sea ice variability and trends, 1979-2010, *Cryosph.* 6, 881–889, doi: 10.5194/tc-6-881-2012.

Church, M.J.H., Ducklow, W., and D.M. Karl (2004), Light dependence of [3H] leucine incorporation in the oligotrophic North Pacific ocean, *Appl. Environ. Microbiol.* 70, 4079-4087, doi: 10.1128/AEM.70.7.4079-4087.2004.

Clasby, R.C., Horner, R., and V. Alexander (1973), An in situ method for measuring primary productivity of Arctic sea ice algae, *J. Fish. Res. Board Can.* 30, 835-83.

Codispoti, L.A., Kelly, V., Thessen, A, Matrai, P., Suttles, S., Hill, V., Steele, M., and B. Light (2013), Synthesis of primary production in the Arctic Ocean: III. Nitrate and phosphate based estimates of net community production, *Prog. Oceanog.* 110, 126-150, 10.1016/j.pocean.2012.11.006.

Collins, R.E., Carpenter, S.D., and J.W. Deming (2008), Spatial heterogeneity and temporal dynamics of particles, bacteria, and pEPS in Arctic winter sea ice, *J. Mar. Syst.* 74, 902–917, 10.1016/j.jmarsys.2007.09.005.

Comeau, A.M., Philippe, B., Thaler, M., Gosselin, M., Poulin, M., and C. Lovejoy (2013), Protists in Arctic drift and land-fast sea ice, *J. Phycol.* 49, 229-240, doi: 10.1111/jpy.12026.

Comiso, J.C. (2010), Variability and trends of the global sea ice cover, In: Thomas, D.N., Dieckmann, G.S. (eds) *Sea Ice* 2nd Ed. Wiley Blackwell Publishing, Malaysia, 205-246.

Comiso, J.C. (2012), Large decadal decline of the Arctic Multiyear ice cover, *J. Climate* 25, 1176-1193, doi: 10.1175/JCLI-D-11-00113.1.

Cota, G.F. (1985), Photoadaptation of high Arctic ice algae, *Lett. Nature* 315, 219-222.

Cota, G., Anning, J., Harris, L., Harrison, W., and R.E.H. Smith (1990), Impact of ice algae on inorganic nutrients in seawater and sea ice in Barrow Strait, NWT, during spring, *Can. J. of Aquat. Sci.* 47(7), 1402-1415, doi: 10.1139/f90-159.

Cota, G., and E. Horne (1989), Physical control of arctic ice algal production, *Mar. Ecol. Prog. Ser.* 52, 111-121.

Cota, G., and R.E.H. Smith (1991), Ecology of bottom ice algae: II, Dynamics, distributions and productivity, *J. Mar. Syst.* 2, 279-295, doi: 10.1016/0924-7963(91)90037-U.

Deal, C., Jin, M., Elliot, S., Hunke, E., Maltrud, M., and N, Jeffery (2011), Large-scale modeling of primary production and ice algal biomass within arctic sea ice 1992, *J. Geophys. Res.* 116, C07004, doi: 10.1029/2010JC006409.

del Giorgio, P.A., and J.J. Cole (1998), Bacterial growth efficiency in natural aquatic systems, *Annu. Rev. Ecol. Syst.* 29, 503-541, doi: 10.1146/annurev.ecolsys.29.1.503.

Deming, J.W. (2010), Sea ice bacteria and viruses, In: Thomas D.N., Dieckmann G.S. (eds.), *Sea Ice* 2nd Ed., Wiley Blackwell Publishing, Malaysia, 248-282.

Dery, S.J., Stieglitz, M., McKenna, E.C., and E.F. Wood (2005), Characteristics and trends of river discharge into Hudson, James, and Ungava Bays, 1964–2000, *J. Climate* 18, 2540–2557, doi: 10.1175/JCLI3440.1.

Dieckmann, G.S., Lange, M.A., Ackley, S.F., and J.C. Jennings (1991), The nutrient status in sea ice of the Weddell Sea during winter: effects of sea ice texture and algae, *Polar Biol.* 11, 449–456, doi: 10.1007/BF00233080.

Drange, H., Dokken, T., Furevik, T., Gerdes, R., and W. Berger (2005), The Nordic Seas, An Integrated Perspective, *Amer. Geophys. Union*, Washington, U.S.A.

Ehn, J., Papakyriakou, T., and D. Barber (2008), Inference of optical properties from radiation profiles within melting landfast sea ice, *J. Geophys. Res.* 113, C09024, doi: 10.1029/2007JC004656.

Eicken, H., Krouse, H.R., Kadko, D., and D.K. Perovich (2002), Tracer studies of pathways and rates of meltwater transport through Arctic summer sea ice, *J. Geophys. Res.* 107, C108046, doi: 10.1029/2000JC000583.

Eppley, R.W. (1972), Temperature and phytoplankton growth in the sea, *Fish. Bull.* 70, 1063-1085.

Ewert, M., and J.W. Deming (2014), Bacterial responses to fluctuations and extremes in temperature and brine salinity at the surface of Arctic winter sea ice, *FEMS: Microbiol. Ecol.* 89, 476–489, doi: 10.1111/1574-6941.12363.

Falkowski, P.G., NS J.A Raven (2007), *Aquatic Photosynthesis* 2nd Ed., Princeton Univ. Press, Princeton, N.J.

Fortier, M., Fortier, L., Michel, C., and L. Legendre (2002), Climatic and biological forcing of the vertical flux of biogenic particles under seasonal Arctic sea ice, *Mar. Ecol. Prog. Ser.* 225, 1-16, doi: 10.3354/meps225001.

Geider, R.J., and B.A. Osborne (1992), Algal photosynthesis: The measurements of algal gas exchange, *Curr. Phycol. 2*. Springer Science.

Gloersen P., Campbell, W.J., Cavalieri, D.J., Comiso, J.C., Parkinson, C.L. and H.J. Zwally (1992), Arctic and Antarctic Sea Ice, 1978–1987: Satellite Passive Microwave Observations and Analysis. NASA, Special Publication, 511, 289 pp. National Aeronautics and Space Administration, Washington, DC.

Glover, H.E. (1980), Assimilation numbers in cultures of marine phytoplankton, *J. Plank. Res*. 2(1), 1980.

Glud, R.N., Rysgaard, S., and M. Kühl, M. (2002), A laboratory study on O2 dynamics and photosynthesis in ice algal communities: quantification by microsensors, O2 exchange rates, 14C incubations and a PAM fluorometer, *Aquat. Mic. Ecol*. 27, 301-311, 10.3354/ame027301.

Glud, R.N., Rysgaard, S., NS M. Kühl (2007), The sea ice in young sound: implications for carbon cycling, In: Rysgaard, S., Glud, R.N. (eds.), *Carbon Cycling in Arctic Marine Ecosystems: Case Study Young Sound* (58). Meddr. 1182 Grønland, Bioscience, 62–85.

Glud, R.N., Rysgaard, S., Turner, G., McGinnis, D.F., and R.J.G. Leakey (2014), Biological- and physical induced oxygen dynamics in melting sea ice of Fram Strait, *Limnol. Oceanogr*. 59(4), 1097-1111, doi: 10.4319/lo.2014.59.4.1097.

Golden, K.M., Ackley, S.F., and V.I. Lytle (1998), The percolation phase transition in sea ice, *Science* 282 (5397), 2238-2241, doi: 10.1126/science.282.5397.2238.

Gosselin, M., Legendre, L., Demers, S., and R.G. Ingram (1985), Responses of sea-ice microalgae to climatic and fortnightly tidal energy inputs (Manitounuk Sound, Hudson bay), *Can. J. Fish. Aquat. Sci*. 42, 999-1006.

Gosselin, M., Legendre, L., Therriault, J.C., Demers, S., and M. Rochet (1986) Physical control of the horizontal patchiness of sea-ice microalgae, *Mar. Ecol. Prog. Ser*. 29, 289-298.

Gosselin, M., Levasseur, M., Wheeler, P.A., Horner, R.A., and B.C. Booth (1997), New measurements of phytoplankton and ice algal production in the Arctic Ocean, *Deep-Sea Res*. II 44 (8), 1623-1644, doi: 10.1016/S0967-0645(97)00054-4.

Gradinger, R. (2002), Sea ice microorganisms, In: Bitten, G.E. (ed.) *Encyclopedia of Environmental Microbiology*, Wiley, NY, 2833-2844.

Gradinger, R. (2009), Sea-ice algae: Major contributors to primary production and algal biomass in the Chukchi and Beaufort Seas during May/June 2002, *Deep-Sea Res*. 56, 1201-1212, doi: 10.1016/j.dsr2.2008.10.016.

*Gradinger, R., and W. Zhang (1997), Vertical distribution of bacteria in Arctic sea ice from the Barents and Laptev Seas, *Polar Biol*. 17, 448-454, doi: 10.1007/s003000050139.

Graversen, R.G., Mauritsen, T., Tjernstrom, M., Kallen, E., and G. Svensson (2008), Vertical structure of recent Arctic warming, *Nature Lett*. 541, 53-57, doi: 10.1038/nature06502.

Gutt, J. (1995), The occurrence of sub-ice algal aggregations off northeast GL, *Polar Biol*. 15, 247-252, doi: 10.1007/BF00239844.

Haecky, P., and A. Anderson (1993), Primary and bacterial production in sea ice in the northern Baltic Sea, *Aquat. Microbiol. Ecol*. 20, 107-118, doi: 10.3354/ame020107.

*He, J., Inghong, C, Iaodong, J.X., Bo, C., NS Y. Yong (2005), Characterization of the summer pack ice biotic community of Canada Basin, *Acta Ocean. Sinica*. 24(6), 80-87.

Hegseth, E.N. (1998), Primary production of the northern Barents Sea, *Polar Res*. 17(2), 113-123.

Heil, P. and I. Allison (1999), The pattern and variability of Antarctic sea ice drift in the Indian Ocean and western Pacific sectors. J. Geophys. Res. 104, 789–15.

Helmke, E., and H. Weyland (1995), Bacteria in sea ice and underlying water of the eastern Weddell Sea in midwinter, *Mar. Ecol. Prog. Ser*. 117, 269–287, doi: 10.3354/meps117269.

Herman, A.W., Knox, D.F., Conrad, J., and M.R. Mitchell (1993), Instruments for measuring sub-ice algal profiles and productivity in situ, *Can. J. Fish. Aquat. Sci*. 50, 359-369, doi: 10.1139/f93-041.

Hezel, P.J., Zhang, X., Bitz, C.M., Kelly, B.P., and F. Massonnet (2012), Projected decline in spring snow depth on Arctic sea ice caused by progressively later autumn open ocean freeze-up this century, *Geophys. Res. Lett*. 39, L17505, doi: 10.1029/2012GL052794.

Holland, M.M., Finnis, J., Barrett, A.P., and M.C. Serreze (2007), Projected changes in Arctic Ocean freshwater budgets, *J. Geophys. Res*. 112, G04S55, doi: 10.1029/2006JG000354.

Horner, R.A. (1985), *Sea Ice Biota*. CRC Press, Inc., Florida, U.S.A.

Horner, R., NS G.C. Schrader (1982), Relative contributions of ice algae, phytoplankton, and benthic microalgae to primary production in nearshore regions of the Beaufort Sea, *Arctic* 35(4), 485-503.

Hsaio, S.I.C. (1988), Spatial and seasonal variations in primary production of sea ice microalgae and phytoplankton in Frobisher Bay, Arctic Canada, *Mar. Ecol. Progr. Ser.* 44, 275-285.

Iacozza, J., and D. Barber (1999), An examination of the distribution of snow on sea-ice, *Atmosph. Ocean* 1, 21-51, doi: 10.1080/07055900.1999.9649620.

IHO (International Hydrographic Organization) (1953), S-23, *Limits of oceans and seas*. Draft 3rd Edition.

Irwin, B.D. (1990), Primary production of ice algae on a seasonally-ice-covered, continental shelf, *Polar Biol.* 10, 247-254, doi: 10.1007/BF00238421.

Jakobsson, M., et al. (2012) The International Bathymetric Chart of the Arctic Ocean (IBCAO) Version 3.0, *Geophys. Res. Lett.,* doi: 10.1029/2012GL052219.

Jassby, A.D., and T. Platt (1976), Mathematical formulation of the relationship between photosynthesis and light for phytoplankton, *Limnol. Oceanogr.* 21(4), 540-547.

Johnsen, G., and E.N. Hegseth (1991), Photoadaptation of sea-ice microalgae in the Barents Sea, *Polar Biol.* 11, 179-184, doi: 10.1007/BF00240206.

Juhl, A., and C. Krembs (2010), Effects of snow removal and algal photoacclimation on growth and export of ice algae, *Polar Biol.* 33, 1057-1065, doi: 10.1007/s00300-010-0784-1.

Junge, K., Eicken, H., and J.W. Deming (2004), Bacterial activity at -2 to -20C in Arctic wintertime sea ice, *Appl. Environ. Microbiol.* 70, 550–557, doi: 10.1128/AEM.70.1.550–557.2004.

*Junge, K., Imhoff, J.F., Staley, J.T., and J.W. Deming (2002), Phylogenetic diversity of numerically important bacteria in Arctic sea ice, *Microb. Ecol.* 43, 315–328, doi: 10.1007/s00248-001-1026-4.

*Kaartokallio, H. (2004), Food web components, and physical and chemical properties of Baltic Sea ice, *Mar. Ecol. Prog. Ser.* 273, 49-63, doi:10.3354/meps273049.

Kaartokallio, H., Kuosa, H., Thomas, D.N., Granskog, M.A., and K. Kivi (2007), Biomass, composition and activity of organism assemblages along a salinity gradient in sea ice subjected to river discharge in the Baltic Sea, *Polar Biol.* 30, 183-197, doi: 10.1007/s00300-006-0172-z.

*Kaartokallio, H., Søgaard, D.H., Norman, L., Rysgaard, S., Tison, J.L-., Delille, B., and D.N. Thomas (2013), Short-term variability in bacterial abundance, cell properties, and incorporation of leucine and thymidine in subarctic sea ice, *Aquat. Microbiol. Ecol.* 71, 57-73, doi:10.3354/ame01667.

Kähler, P., Bjørnsen, P.K., Lochte, K., and A. Antia (1997), Dissolved organic matter and its utilization by bacteria during spring in the Southern Ocean, *Deep-Sea Res. II* 44(1-2), 341-353, doi: 10.1016/S0967-0645(96)00071-9.

Kana, T.M. (1990), Light-dependent oxygen cycling measured by an oxygen-18 isotope dilution technique, *Mar. Ecol. Prog. Ser.* 64, 293-300.

Kemp, P.F., Sherr, B.F., Sherr, E.B., and J.J. Cole (1993), *Handbook of methods in aquatic microbial ecology*. Lewis Publisher. U.S.A.

Kirchmann, D.L. (2008), *Microbial Ecology of the Oceans*, 2nd Ed. John Wiley and Sons Inc., N.J., U.S.A.

Kirchman, D.L., Malmstrom, R.R., and M.T. Cottrell (2005), Control of bacterial growth by temperature and organic matter in the Western Arctic, *Deep-Sea Res. II* 52, 3386-3395, doi: 10.1016/j.dsr2.2005.09.005.

Kottmeier, S.T., and C.W. Sullivan (1988), Sea ice microbial communities. IX. Effects of temperature and salinity on metabolism and growth of autotrophs and heterotrophs, *Polar Biol.* 8, 293-304.

Krembs, C.K., Eicken, H., Junge, K., and J.W. Deming (2002), High concentrations of exopolymeric substances in Arctic winter sea ice: implications for the polar ocean carbon cycle and cryoprotection of diatoms, *Deep-Sea Res. I* 49, 2163-2181, doi: 10.1016/S0967-0637(02)00122-X.

Kwok, R., and D. A. Rothrock, 2009. Decline in Arctic sea ice thickness from submarine and ICESS at records: 1958-2008, *Geophys. Res. Lett.* 36, L15501, doi: 10.1029/2009GL039035.

Lange, M.A., Ackley, S.F., Wadhams, P., Dieckmann, G.S. and H. Eicken (1989), Development of sea ice in the Weddell Sea, Antarctica. *Ann. Glaciol.*, 12, 92–96.

Lange, B.A., Michel, C., Beckers, J.F., Casey, J.A., Flores, H., Hatam, I., Meisterhans, G., Niemi, A., and C. Haas (2015), Comparing springtime ice-algal chlorophyll a and physical properties of multiyear and first-year sea ice from the Lincoln Sea, *PLOS ONE*, doi:10.1371/journal.pone.0122418.

Lavoie, D., Denman, K., and C. Michel (2005), Modeling ice algal growth and decline in a seasonally ice-covered region of the Arctic (Resolute Passage, Canadian Archipelago), *J. Geophys. Res.* 110, C11009, doi: 10.1029/2005JC002922.

Lee, S.H., McRoy, C.P., Joo, H.M., Gradinger, R., Cui, X., Yun, M.S., Chung, K.H., Kang, Kang, C.K. Choy, E.J., Son, S., Carmack, E., and T.E. Whiteledge (2011),

Holes in progressively thinning Arctic sea ice lead to new ice algae habitat, *Oceanogr*. 24(3), 302-308, doi: 10.5670/oceanog.2011.81.

Lee, S.H., Whiteledge, T.E., and S.H. Kang (2008), Spring time production of bottom ice algae in the landfast sea ice zone at Barrow Alaska, *J. Exp. Mar. Biol. Ecol*. 367, 204-212, doi: 10.1016/j.jembe.2008.09.018.

Lee, S.H., de Mora, S.J., Gosselin, M., Levasseur, M., Bouillon, R.-C., Nozais, C., and C. Michel (2001), Particulate dimethylsulfoxide in Arctic sea-ice algal communities: the cryoprotectant hypothesis revisited, *J. Phycol*. 37, 488-499, doi: 10.1046/j.1529-8817.2001.037004488.x.

Le Fouest, V., Babin M., and J.-É. Tremblay (2013), The fate of riverine nutrients on Arctic shelves, *Biogeosci*. 10, 3661-3677, doi: 10.5194/bg-10-3661-2013.

Legendre, L., Ackley, S.F., Dieckmann, G.S., Gullicksen, B., Horner, R., Hoshiai, T., Melnikov, I.A., Reeburgh, W.S., Spindler, M., and C.W. Sullivan (1992), Ecology of sea ice biota: Part 2, Global significance, *Polar Biol.,* 12, 429–444.

Legendre, L., and M. Gosselin (1991), In situ spectroradiometric estimation of microalgal biomass in first-year sea ice, *Polar Biol*. 11, 113-115, doi: 10.1007/BF00234273.

Leu, E., Mundy, C.J., Assmy, A., Campbell, K., Gabrielsen, T.M., Gosselin, M., Juul-Pedersen, T., and R. Gradinger (2015), Arctic spring awakening – Steering principles behind the phenology of vernal ice algae blooms, *Prog. Oceanogr*. 139, 151-170, doi:10.1016/j.pocean.2015.07.012.

Leu, E., Søreide, J.E., Hessen, D.O., Falk-Petersen, S., and J. Berge (2011), Consequences of changing sea ice cover for primary and secondary producers in European Arctic shelf seas: timing, quantity and quality, *Prog. Oceanog*. 90, 18–32, doi: 10.1016/j.pocean.2011.02.004.

Levinsen H., Nielsen, T.G., and B.W. Hansen (2000), Annual succession of marine pelagic protozoans in Disko Bay, West Greenland, with emphasis on winter dynamics, *Mar. Ecol. Prog. Ser*. 206, 119–134, doi: 10.3354/meps206119.

Li, W.K.W., McLaughlin, F.A., Lovejoy, C., and E.C. Carmack (2009), Smallest algae thrive as the Arctic Ocean freshens, *Science* 326, 539, doi: 10.1126/science.1179798.

Lobbes, J.M., Fitznar, H.P., NS G. Kattner (2000), Biogeochemical characteristics of dissolved and particulate organic matter in Russian Rivers entering the Arctic Ocean, *Geochim. Cosmochim. Acta* 64, 2973-2983, doi: 10.1016/S0016-7037(00)00409-9.

Loose, B., Schlosser, P., Perovich, D., Ringelberg, D., Ho, D.T., Takahashi, T., Richter-Menge, J., Reynolds, C.M., McGillis, W.R., and J.-L. Tison (2010), Gas diffusion through columnar laboratory sea ice: Implications for mixed-layer ventilation of CO_2

in the seasonal ice zone, *Tellus B*. 63, 23-39, doi: 10.1111/j.1600-0889.2010.00506.x.

Lund-Hansen, L.C., Hawes, I., Nielsen, M.H., and B.K. Sorrell (2016), Is colonization of sea ice by diatoms facilitated by increased surface roughness in growing ice crystals? *Polar Biol*., doi:10.1007/s00300-016-1981-3.

Marra, J. (2009), Net and gross productivity: weighing in with ^{14}C, *Aquat. Microbiol. Ecol*. 1-9, doi: 10.3354/ame01306.

*Maranger, R., Bird, D.F., and S.K. Juniper (1994), Viral and bacterial dynamics in Arctic sea ice during the spring algal bloom near Resolute, NWT, Canada, *Mar. Ecol. Prog. Ser*. 111, 121–127, doi: 10.3354/meps111121.

Maranger, R., Vaqué, D., Nguyen, D., Hébert, M-P., and E. Lara (2016), Pan-Arctic patterns of planktonic heterotrophic microbial abundance and processes: Controlling factors and potential impacts of warming, *Prog. Oceanog*., doi: 10.1016/j.pocean.2015.07.006.

Markus, T., Stroeve, J.C., and J. Miller (2009), Recent changes in Arctic sea ice melt onset, freeze-up, and melt season length, *J. Geophys. Res*. 114, C12024, doi: 10.1029/2009JC005436.

Maykut, G.A., and T.C. Grenfell (1975), The spectral distribution of light beneath first-year sea ice in the Arctic Ocean, *Limnol. Oceanogr*. 20, 554–563.

McMinn, A., Skerratt, J., Trull, T., Ashworth, C. and M. Lizotte (1999), Nutrient stress gradient in the bottom 5 cm of fast ice McMurdo Sound, Antarctica, *Polar Biol*. 21(4), 221-227. doi: 10.1007/s003000050356.

Melling, H., Haas, C., and E. Brossier (2015), Invisible polynyas: Modulation of fast ice thickness by ocean heat flux on the Canadian polar shelf, J. Geophys. Res. Oceans 120, 777-795, doi: 10.1002/2014JC010404.

Melnikov, I. (1997), *The Arctic Sea Ice Ecosystem*. Gordon and Breach, Amsterdam.

Mendle, L.K., and J. Priddle (1990), *Polar Marine Diatoms*. British Antarctic Survey, Cambridge, UK.

Michel, C., Ingram, R.G., and L.R. Harris (2006), Variability in oceanographic and ecological processes in the Canadian Arctic Archipelago, *Prog. Oceanog*. 71, 379-401, doi: 10.1016/j.pocean.2006.09.006.

Michel, C., Legendre, L., Ingram, R.G., Gosselin, M., and M. Levasseur (1996), Carbon budget of sea-ice algae in spring: Evidence of significant transfer to zooplankton grazers, *J. Geophys. Res*. 101(C8), 18345-18360, doi: 10.1029/96JC00045.

Michel, C., Nielsen, T.G., Nozais, C., and M. Gosselin (2002), Significance of sedimentation and grazing by ice micro- and meiofauna for carbon cycling in annual sea ice (northern Baffin Bay), *Aquat. Microbiol. Ecol.* 30, 57-68, doi: doi:10.3354/ame030057.

Mikkelson, D.M., Rysgaard, S., and R.N. Glud (2008), Microalgal composition and primary production in Arctic sea ice: a seasonal study from Kobbefjord (Kangerluarsunnguaq), west Greenland, *Mar. Ecol. Prog. Ser.* 368, 65-74, doi: 10.3354/meps07627.

Miller, C.B., and P.A Wheeler (2012), *Biological Oceanography*, Wiley Blackwell Publishing, Malaysia.

Mock, T., and R. Gradinger (1999), Determination of Arctic ice algal production with a new in situ incubation technique, *Mar. Ecol. Prog. Ser.* 177, 15-26, doi: 10.3354/meps177015.

Mock, T., Meiners, K.M., and H.C. Giesenhagen (1997), Bacteria in sea ice and underlying brackish water at 54" 26' 50" N (Baltic Sea, Kiel Bight), *Mar. Ecol. Prog. Ser.* 158, 23-40, doi:10.3354/meps158023.

Mundy, C.J., Barber, D.G., and C. Michel, C. (2005), Variability of snow and ice thermal, physical and optical properties pertinent to sea ice algae biomass during spring, *J. Mar. Syst.* 58, 107-120, doi: 10.1016/j.jmarsys.2005.07.003.

Mundy, C.J., Barber, D.G., Michel, C., and R.F. Marsden (2007), Linking ice structure and microscale variability of algal biomass in Arctic first-year sea ice using an in situ photographic technique, *Polar Biol.* 30, 1099-1114, doi: 10.1007/s00300-007-0267-1.

Mundy, C.J., Gosselin, M., Gratton, Y., Brown, K., Galindo, V., Campbell, K., Levasseur, M., Barber, D., Papakryiakou, T., and S. Bélanger (2014), Role of environmental factors on phytoplankton bloom initiation under landfast sea ice in Resolute Passage, Canada, *Mar. Ecol. Prog. Ser.* 497, 39-49, doi: 10.3354/meps10587.

NSIDC (National Snow and Ice Data Center) (2015), Arctic sea ice news. http://nsidc.org/arcticseaicenews/.

NSIDC (National Snow and Ice Data Center) (2017), Arctic vs. Antarctic. https://nsidc.org/cryosphere/seaice/characteristics/difference.html.

Nghiem, S. V., I. G. Rigor, D. K. Perovich, P. Clemente-Colon, J. W. Weatherly, and G. Neumann (2007), Rapid reduction of Arctic perennial sea ice, *Geophys. Res. Lett.* 34, L19504, doi: 10.1029/2007GL031138.

Nicolaus, M., Gerland, S., Hudson, S.R., Hanson, S., Haapala, J., and D.K. Perovich (2010), Seasonality of spectral albedo and transmittance as observed in the Arctic Transpolar Drift in 2007, J. Geophys. Res. 115, C11011, doi: 10.1029/2009JC006074.

Nyugen, D., Maranger, R., Tremblay, J.-E., and M. Gosselin (2012), Respiration and bacterial carbon dynamics in the Amundsen Gulf, western Canadian Arctic, *J. Geophys. Res.* 117, C00G16, doi: 10.1029/2011JC007343.

Overeem, I., and J.P.M. Syvitski (2010), Shifting discharge peaks in arctic Rivers, 1977-2007, *Swed. Soc. Anth. Geog.,* 285-296, doi: 10.1111/j.1468-0459.2010.00395.x.

Padman, L., and S. Erofeeva (2004), A barotropic inverse tidal model for the Arctic Ocean, *Geophys. Res. Lett.* 31, L02303, doi: 10.1029/2003GL019003.

Palmer, M.A., Arrigo, K.R., Mundy, C.J., Ehn, J.K., Gosselin, M., Barber, D.G., Martin, J., Alou, E., Roy, S., and J.-E Tremblay (2011), Spatial and temporal variation of photosynthetic parameters in natural phytoplankton assemblages in the Beaufort Sea, Canadian Arctic, *Polar Biol.* 34, 1915-1928, doi: 10.1007/s00300-011-1050-x.

Pavlov, V.K. and O.A. Pavlova (2007), Increasing sea ice drift velocities in the Arctic Ocean, 1979–2005. Geophys. Res. Abst., 9, 07124.

Perovich, D. (2003), Complex yet translucent: the optical properties of sea ice, *Physica B.* 338, 107-114, doi: 10.1016/S0921-4526(03)00470-8.

Perovich, D., and C. Polashenski (2012), Albedo evolution of seasonal Arctic sea ice, *Geophys. Res. Lett.* 39, L08501, doi: 10.1029/2012GL051432.

Perovich, D., Roesler, C., and W. Pegau (1998), Variability in Arctic sea ice optical properties, *J. Geophys. Res.* 103, 1193-1208, doi: 10.1029/97JC01614.

Petrich, C., and H. Eiken, H. (2010), Growth, structure and properties of sea ice, In: Thomas D.N., Dieckmann G.S. (eds.), *Sea Ice*, 2nd Ed. Wiley Blackwell Publishing, Malaysia, 22-77.

Pomeroy, L.R., Wiebe, W.J., Deibel, D., Thompson, R.J., Rowe, G.T., and J.D. Pakulski (1991), Bacterial responses to temperature and substrate concentration during the Newfoundland spring bloom, *Mar. Ecol. Prog. Ser.* 75, 143-159, doi: 10.3354/meps075143.

Pomeroy, L.R., and J.W. William (2001), Temperature and substrate as interactive limiting factors for marine heterotrophic bacteria, *Aquat. Microbiol. Ecol.*, 23, 187–204, doi: 10.3354/ame023187.

Prinsenberg S.J. (1986), The circulation pattern and current structure of Hudson In: Martini EP (ed.) Canadian Inland Seas, Oceanogr Ser 44, Elsevier, New York, 187–

203.

Prinsenberg, S.J., and R.G. Ingram (1991), Under-ice physical oceanographic processes, *J. Mar. Syst.* 2, 143-152.

Quillfedt, von C.H., Hegseth, E.N., Johnsen, G., Sakshaug, E., and E.E. Syvertsen (2009), Ice Algae, In: Sakshaug, E., Johnsen, G.H., Kovacs, K.M. (eds.), *Ecosystem Barents Sea*, Tapir Academic Press, Trondheim.

Ralph, P.J., Ryan, K.G., Martin, A., and G. Fenton (2007), Melting out of sea ice causes greater photosynthetic stress in algae than freezing in, *J. Phycol.* 43, 948-956, doi: 10.1111/j.1529-8817.2007.00382.x.

Riedel, A., Michel, C., Gosselin, M., and B. LeBlanc (2007a), Enrichment of nutrients, exopolymeric substances and microorganisms in newly formed sea ice on the Mackenzie shelf, *Mar. Ecol. Prog. Ser.* 342, 55-67, doi: 10.3354/meps342055.

*Riedel, A., Michel, C., Gosselin, M., and B. LeBlanc (2007b), Grazing of large-sized bacteria by sea-ice heterotrophic protists on the Mackenzie shelf during the winter-spring transition, *Aquat. Microb. Ecol.* 50, 25-38, doi: 10.3354/ame01155.

Riedel, A., Michel, C., Gosselin, G., and B. LeBlanc (2008), Winter-spring dynamics in sea-ice carbon cycling in the coastal Arctic, *J. Mar. Syst.* 74, 918-932, doi: 10.1016/j.jmarsys.2008.01.003.

Rinke, A., and K. Dethloff (2008), Simulated circum-Arctic climate changes by the end of the 21st century, *Global Planet. Change* 62, 173-186, doi: 10.1016/j.gloplacha.2008.01.004.

Rintala, J.-M., Piiparinen, J., Ehn, J., Autio, R., and H. Kuosa (2006), Changes in phytoplankton biomass and nutrient quantities in sea ice as responses to light/dark manipulations during difference phases of the Baltic winter 2003, *Hydrobiol.* 554, 11-24, doi: 10.1007/s10750-005-1002-y.

Robinson, C. (2008), Heterotrophic bacterial respiration, In: *Microbial Ecology of the Oceans* (Ed.) Kirchman, D.L., John Wiley, NewYork, 299–327.

Rózanska, M., Poulin, M., and M. Gosselin (2008), Protist entrapment in newly formed sea ice in the coastal Arctic Ocean, *J. Mar. Syst.* 74, 887-901, doi:10.1016/j.jmarsys.2007.11.009.

Rysgaard, S., and R.N. Glud (2004), Anaerobic N2 production in Arctic sea ice, *Limnol. Oceanogr.* 49, 86-94, doi: 10.4319/lo.2004.49.1.0086.

Rysgaard, S., and R.N. Glud (2007), Carbon Cycling in Arctic Marine Ecosystems: Case Study Young Sound, *Biosci.* 58.

Rysgaard, S., Glud, R.N., Sejr, M.K., Blicher, M.E., and H.J. Stahl (2008), Denitrification activity andoxygen dynamics in Arctic sea ice, *Polar Biol*. 31, 527–537, doi: 10.1007/s00300-007-0384-x.

Rysgaard, S., Kuhl, M., and J.W. Hansen (2001), Biomass, production and horizontal patchiness of sea ice microalgae in a high-Arctic fjord (Young Sound, NE Greenland), *Mar. Ecol. Prog. Ser*. 223, 15-26, doi:10.3354/meps223015.

Sarmiento, J.L., and N. Gruber (2006), *Ocean Biogeochemical Dynamics*. Princeton University Press, Princeton, N. J.

Saucier, F.J., Senneville, S., Prinsenberg, S., Roy, F., Smith, G., Gachon, P., Caya, D., and R. Larise (2004), Modelling the sea ice-ocean seasonal cycle in Hudson Bay, Foxe Basin and Hudson Strait, Canada, *Climate Dyn*. 23, 303-326.

Serreze, M.C., and J.A. Maslanik (1997), Arctic precipitation as represented in the NCEP/NCAR reanalysis, *Annals Glaciol*. 25, 429-433.

Smith, R.E.H., Anning, J., Clement, P., and G. Cota (1988), Abundance and production of ice algae in Resolute Passage, Canadian Arctic, *Mar. Ecol. Progr. Ser*. 48, 251-263.

Smith, R.E.H., and P. Clement (1990), Heterotrophic activity and bacterial productivity in assemblages in microbes from sea ice in the High Arctic, *Polar Biol*. 10, 351-357, doi: 10.1007/BF00237822.

Smith, R.E.H., Clement, P., and G.F. Cota (1989), Population dynamics of bacteria in Arctic sea ice, *Microb. Ecol*. 17, 63-76, doi: 10.1007/BF02025594.

Smith, R.E.H., Gosselin, M., and S. Taguchi (1997), The influence of major inorganic nutrients on the growth and physiology of high arctic ice algae, *J. Mar. Syst*. 11(1-2), 63-70, doi: 10.1016/S0924-7963(96)00028-0.

Smith, R.E.H., and A.W. Herman (1992), In situ patterns of intracellular photosynthate allocation by sea ice algae in the Canadian High Arctic, *Polar Biol*. 12, 545-551, doi: 10.1007/BF00236978.

Søgaard DH, Kristensen M, Rysgaard S, Glud RN, Hansen PJ, and K.M Hilligsoe (2010), Autotrophic and heterotrophic activity in Arctic first-year sea ice: seasonal study from Malene Bight, SW Greenland, *Mar. Ecol. Progr. Ser*. 419: 31-45, doi: 10.3354/meps08845.

Søgaard, D.H., Thomas, D.N., Rysgaard, S., Glud, R.N., Norman, L., Kaartokallio, H., Juul-Pedersen-Juul, T., and N.-X Gelfius (2013), The relative contributions of biological and abiotic processes to carbon dynamics in subarctic sea ice, *Polar Biol*. 36(12), 1761-1777, doi: 10.1007/s00300-013-1396-3.

SooHoo, J., Palmisano, A., Kottmeier, S., Lizotte, M., SooHoo, S., and C. Sullivan (1987), Spectral light absorption and quantum yield of photosynthesis in sea ice microalgae and a bloom of *Phaeocystis pouchetii* from McMurdo Sound, Antarctica, *Mar. Ecol. Prog, Ser.* 39, 175-189, doi: 10.3354/meps039175.

Spindler, M. (1990), A comparison of Arctic and Antarctic sea ice and the effects if different properties on sea ice biota, In: Bleil U., Theide J. (eds.) *Geological History of the Polar Oceans: Arctic versus Antarctic*, Springer, 173-186. doi: 10.1007/978-94-009-2029-3_10.

Stein, R., and R.W. MacDonald (2004), *The Organic Carbon Cycle in the Arctic Ocean*. Springer, Germany.

Stoecker, D., Buck, K.R., and M. Putt (1993), Changes in the sea-ice brine community during the spring-summer transition, McMurdo Sound, Antarctica. II. Phagotrophic protists, *Mar. Ecol. Prog. Ser.* 95, 103–113, doi: 10.3354/meps095103.

Stroeve, J.C., Markus, T., Boisvert, L., Miller, J., and A. Barrett (2014), Changes in Arctic melt season and implications for sea ice loss, *Geophys. Res. Lett.* 41, 1216-1225, doi: 10.1002/2013GL058951.

Sturm, M., and R.A. Massom (2010), Snow and sea ice, In: Thomas D.N., Dieckmann G.S. (eds.), *Sea Ice* 2nd Ed., Wiley Blackwell Publishing, Malaysia, 153-204.

Suzuki, Y., Kudoh, S., and M. Takahashi (1997), Photosynthetic and respiratory characteristics of an Arctic algal community living in low light and temperature conditions, *J. Mar. Syst.* 11, 111-121, doi: 10.1016/S0924-7963(96)00032-2.

Tang, C.C.L., Ross, C.K., Yao, T., Petrie, B., DeTracey, M., and E. Dunlap (2004), The circulation, water masses and sea-ice of Baffin Bay, *Prog. Oceanog.* 63, 183-228, doi: 10.1016/j.pocean.2004.09.005.

Telesphore, S.-N., Gosselin, M., Juniper, S.K., and M. Levasseur (1997), Changes in sea-ice phagotrophic microprotists (20-200 um) during the spring algal bloom, Canadian Arctic Archipelago, *J. Mar. Syst.* 11, 163-172, doi: 10.1016/S0924-7963(96)00036-X.

Thomas, D.N., Engbrodt, R., Giannelli, V., Kattner, G., Kennedy, H., Haas, C., and G.S. Dieckmann (2001), Dissolved organic matter in Antarctic sea ice, *Annal. Glaciol.* 33, 297–303, doi: 10.3189/172756401781818338.

Thomas, D.N., Papadimitriou, S., and C. Michel (2010), The biogeochemistry of sea ice, In: Thomas D.N., Dieckmann G.S. (eds.) *Sea ice* 2nd Ed., Wiley-Blackwell, Oxford, 425–467.

Torres-Valdes, S., Tsubouchi, T., Bacon, S., Naveira-Garabato, A.C., Sanders, R.,

McLaughlin, F.A., Petrie, B., Kattner, G., Azetsu-Scott, K., and T.E. Whitledge (2013), Export of nutrients from the Arctic Ocean, *J. Geophys. Res. Oceans* 118, 1625–1644, doi: 10.1002/jgrc.20063.

Tortell, P.D., Maldonado, M.T., Granger, J., and N.M. Price (1999), Marine bacteria and biogeochemical cycling of iron in the oceans, *FEMS Microbiol. Ecol.* 29, 1-11, doi: 10.1111/j.1574-6941.1999.tb00593.x.

Tremblay, J., Anderson, L.G., Matrai, P., Coupel, P., Bélanger, S., Michel, C., and M. Reigstad (2016), Global and regional drivers of nutrient supply, primary production and CO2 drawdown in the changing Arctic Ocean, *Prog. Oceanog.*, doi:10.1016/j.pocean.2015.08.009.

Tremblay, J.E., Gratton, Y., Carmack, E.C., Payne, C.D., and N.M. Price (2002), Impact of the large-scale Arctic circulation and the North Water Polynya on nutrient inventories in Baffin Bay, *J. Geophys. Res.*, 107(C8), 3112, doi: 10.1029/2000JC000595.

Tucker, W.B., Gow, A.J. and W.F. Weeks (1987), Physical properties of summer sea ice in the Fram Strait, *J. Geophys. Res.*, 92, 6787–6803.

Ulfsbo, A., Cassar, N., Korhonen M., van Heuvan, S., Hoppema, M., Kattner, G., and L.G. Anderson (2014), Late summer net community production in the central Arctic Ocean using multiple approaches, Global Geochem. Cycles 28, 1129-1148, doi:10.1002/2014GB004833.

Van Etten, J.L., Lane, L.C., and R.H. Meints (1981), Virus and virus-like particles of eukaryotic algae, *Microbiol. Rev.* 55, 568-620.

Vavrus S.J., Holland, M.H., Jahn, A., Bailey, D.A., and B.A. Blazey (2012), Twenty-first-century Arctic climate change in CCSM4, *Am. Met. Soc.* 25, doi: 10.1175/JCLI-D-11-00220.1.

Vihma, T. (2014), Effects of Arctic sea ice decline on weather and climate: A review, *Surv. Geophys.* 35, 1175-1214, doi: 10.1007/s10712-014-9284-0.

Wadhams, P. (2000), *Ice in the Ocean.* Gordon and Breach Science Publishers, Amsterdam.

Wang , S., Bailey, D., Lindsay, K., Moore, J.K., and M. Holland (2014), Impact of sea ice on the marine iron cycle and phytoplankton productivity, *Biogeosc.* 11, 4713-4731, doi: doi:10.5194/bg-11-4713-2014.

Warren, S.G., Rigor, I.G., and N. Untersteiner (1998), Snow depth on Arctic sea ice, *J. Climate* 12, 1814-1829, doi: 10.1175/15200442.

Wassmann, P., and M. Reigstad (2011), Future Arctic Ocean seasonal ice zones and implications for pelagic-benthic coupling, *Oceanog*. 24(3), 220–231.

Webster, M. A., Rigor, I. G., Nghiem, S.V., Kurtz, N.T., Farrell, S.L., Perovich, D. K., and M. Sturm (2014), Interdecadal changes in snow depth on Arctic sea ice, *J. Geophys. Res. Oceans*, 119, 5395– 5406, doi: 10.1002/2014JC009985.

Williams, P.J. leB. (1993), Chemical and tracer methods of measuring plankton production, *–ICES Mar. Sci. Symp*. 197, 20-36.

Williams, P.J.leB., Robinson, C., Søndergaard, M., Jesperson, A.-M., Bentley, T.L., Lefèvre, D., Richardson, K., and B. Riemann (1996), Algal 14C and total carbon metabolisms. 2. Experimental observations with the diatom Skeletonema costatum, *J. Plankt. Res*. 18(10), 1961-1974, doi: 10.1093/plankt/18.10.1961.

Woodgate, R.A., Weingartner, T.J., and R. Lindsay (2012), Observed increases in Bering Strait oceanic fluxes from the Pacific to the Arctic from 2001 to 2011 and their impacts on the Arctic Ocean water column, *Geophys. Res. Lett*. 39, L24603, doi: 10.1029/2012GL054092.

World Meteorological Organization (WMO) (2010), WMO Sea Ice Nomenclature, WMO/DMM/BMO 259-TP-125, Secretariat of the WMO, Geneva.

Zeebe, R.A., Hajo, E., Robinson, D.H., Wolf-Gladrow, D., and G.S. Dieckmann (1996), Modeling the heating and melting of sea ice through light absorption by microalgae, *J. Geophys. Res*. 101(C1), 1163-1181 doi: 10.1029/95JC02687.

CHAPTER THREE: RATIONALE FOR METHODS OF PROCESSING SEA ICE

3.1 Introduction

The research of sea ice algae in this thesis is focused on cells that inhabit the bottom 5 cm of first-year sea ice (*see* Chapters Four, Five, Six). Analysis (e.g. abundance, production) is completed on liquid samples, which are obtained by melting the ice in filtered seawater at a ratio of approximately three parts filtered seawater to one part ice. In this chapter, the rationale for collecting the bottom 5 cm portion of the vertical ice profile and subsequent melting of ice in filtered seawater is briefly explored. This is done using supplementary chlorophyll *a* (chl *a*) and ^{14}C derived gross primary production data collected during the 2014 Ice Covered Ecosystem - CAMbridge bay Process Study (ICE-CAMPS) near Cambridge Bay, Nunavut.

3.2 Sampling Methods

Sites of thin (<10 cm) and thick (15-25 cm) snow-covered sea ice were newly chosen approximately every four days in the study region, and ice samples were collected at these locations using a 9 cm *Mark II Kovacs* core barrel. The bottom 0-5 cm and 5-10 cm of six to eight cores were pooled together before transport to the laboratory for processing with different melt treatments that include:

i) the bottom 0-5 cm and 5-10 cm of ice melted separately over approximately 24 h in 0.2 μm filtered seawater (FSW), added a ratio of three parts filtered seawater to one part ice ($FSW_{3:1}$)

ii) the bottom 0-5 cm of ice melted over approximately 48 h without the addition of filtered seawater (FSW_{zero})

A third melt treatment was also collected under thin snow cover by scraping the bottom ~1 cm of six ice cores directly into 0.2 μm filtered seawater for a dilution factor of approximately 8 (assuming 1 cm of ice was collected per core; $FSW_{8:1}$). The $FSW_{8:1}$ was analyzed within 4 h of collection. The melting of all samples and melt treatments took place in darkness, within insulated cooler jugs exposed to room temperatures.

Measurements of salinity, chl *a*, ^{14}C derived gross primary production, dissolved inorganic carbon (DIC), inorganic nutrients and assessments of cell viability using light microscopy shown in this chapter are outlined in Table 3.1. Detailed protocols for each assessment can be found in in Chapters Four and Five. This includes the analyses of salinity (4.2.2), chl *a* (4.2.3), ^{14}C based gross primary production (4.S.2), DIC (4.S.2), inorganic nutrients (4.2.3) and light microscopy (5.2.6).

Table 3.1. Summary of supplementary data presented in this chapter (highlighted) from the 2014 ICE-CAMPS field campaign. Data include salinity, chlorophyll *a* (chl *a*), ^{14}C derived gross primary production (^{14}C GPP), dissolved inorganic carbon (DIC), inorganic nutrients (nutrients) and cell viability assessed using light microscopy (microscopy). The number of sample cycles for each variable is also listed, where 15 indicates data collection between 7 March to 9 June, 5 between 17 May to 5 June, and 1 on 30 May.

		Variable					
		Salinity (n = 15)	Chl *a* (n = 15)	^{14}C GPP (n = 5)	DIC (n = 5)	Nutrients (n = 5)	Microscopy (n = 1)
Thin Snow	0-5 cm $FSW_{3:1}$						
	5-10 cm $FSW_{3:1}$						
	0-5 cm FSW_{zero}						
	0-1 cm $FSW_{8:1}$	*	*	*	*		
Thick Snow	0-5 cm $FSW_{3:1}$						
	5-10 cm $FSW_{3:1}$						
FSW							

* A scrape sample could not be collected on 5 June

3.3 Collecting the bottom 5 cm of sea ice

Ice algae are typically located in the bottommost 10 cm of Arctic sea ice [Horner, 1985], and as a result, the vast majority of production studies assess samples taken from this section of the vertical ice profile (*see* Tables 2.3, 2.4). However, the distribution of algae is not homogeneous within the bottom 10 cm of sea ice, with chlorophyll *a* (chl *a*) increasing exponentially over the bottom 5 cm towards the growth interface in response to pelagic nutrient supply [Smith et al., 1990; McMinn et al., 1999]. This variability illustrates a difficulty in subsampling the bottom-ice environment; to collect as much of the algal population as possible for an accurate representation of community response (e.g. production), without diluting samples with poorly colonized ice.

The most common means of addressing this subsampling dilemma is collecting the entire bottom 5 cm region (*see* Tables 2.3, 2.4). Results from ICE-CAMPS support this

approach to sample collection, as chl *a* was significantly greater in the 0-5 cm core section than in the overlying 5-10 cm section, under both thin (< 10 cm) (t_{15} = 7.912, $p < 0.05$) and thick (15-25 cm) ($t_{15} = 5.791, p < 0.05$) snow depths (Figure. 3.1). It follows that the 0-5 cm sampling approach was adopted in this research (Chapter Four, Five, Six) because it accounts for the majority of biomass in the ice and permits a potentially more accurate comparison with existing literature estimates. Note that ice samples from both high light (thin snow) and low light (thick snow) conditions were taken in this research to account for potential spatial variability in biomass [e.g. Rysgaard et al., 2001; Campbell et al., 2014] and photoacclimative state [e.g. Alou-Font et al., 2013]. Please refer to Chapter 2.3.1 for details on the influence of snow thickness on light transmission, and therefore light availability to bottom-ice algae.

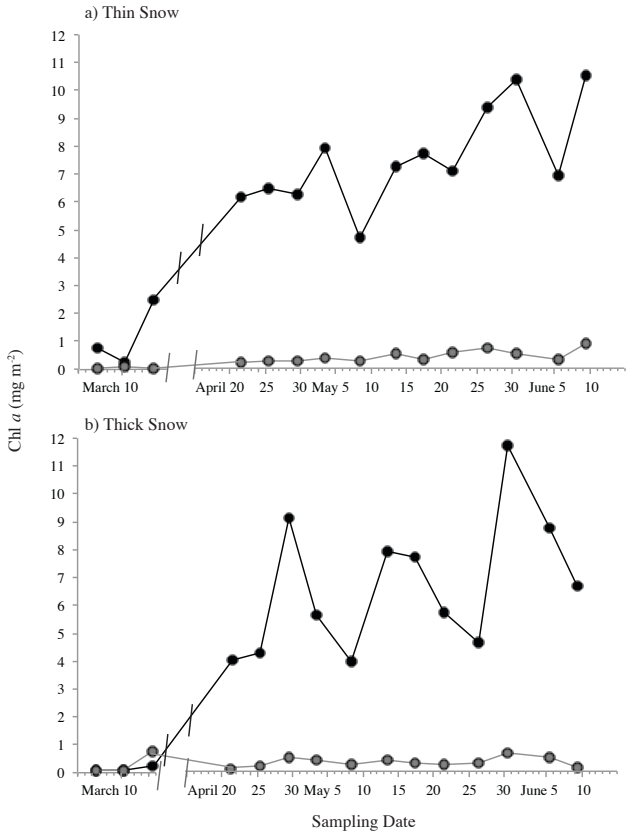

Figure 3.1. Concentration of chlorophyll *a* (chl *a*) in the bottom 0-5 cm (black) and 5-10 cm (grey) of sea ice under a) thin (< 10 cm) or b) thick (15-25 cm) snow covers.

3.4 Melt procedures

The addition of filtered seawater to limit cellular osmotic shock during the melt process has been advocated in the study of sea ice algae [Garrison & Buck 1986; Mikkelson & Witkowski 2010]. However, this sampling approach has also been criticized for its likely addition of nutrients and inorganic carbon that have the potential to falsely amplify primary production [Rintala et al., 2014]. The impact of melt procedures is briefly discussed here by assessing bottom-ice (0-5 cm) chl *a* concentrations and ^{14}C derived gross primary productivity of thin snow covered samples, which were processed using the three melt treatments described above: $FSW_{3:1}$, FSW_{zero}, $FSW_{8:1}$ (Section 3.2).

Comparison of dilution corrected chl *a* between the three melt treatments showed increasing concentrations with the proportion of filtered seawater added (Figure. 3.2). Here, chl *a* was greatest in $FSW_{8:1}$, followed by $FSW_{3:1}$ and FSW_{zero}, respectively. Significantly greater chl *a* in $FSW_{8:1}$ than $FSW_{3:1}$ ($t_{14} = 7.186$, $p < 0.05$) or FSW_{zero} ($t_{13} = 8.228$, $p < 0.05$), likely highlights the exponential increase in chl *a* concentration with proximity to the bottom-ice interface. That is, per liter of melted sea ice there is more algal pigment in the bottom 1 cm than the bottom 5 cm. Indeed, if chl *a* in the bottom 1 cm of ice ($FSW_{8:1}$) is divided by five to roughly average concentrations over the bottom 5 cm core section, we see that estimates are very similar to $FSW_{3:1}$ (Figure 3.1). This supports that the large majority of chl *a* resides in the bottom 0 to 1 cm section of ice, while only moderate concentrations of chl *a* exist in the 1 to 4 cm section. However, $FSW_{3:1}$ or FSW_{zero} samples both represent melted ice from the same 5 cm core segment, indicating that the significant difference in chl *a* between them ($t_{14} = 4.873$, $p < 0.05$) is related to the addition of filtered seawater itself.

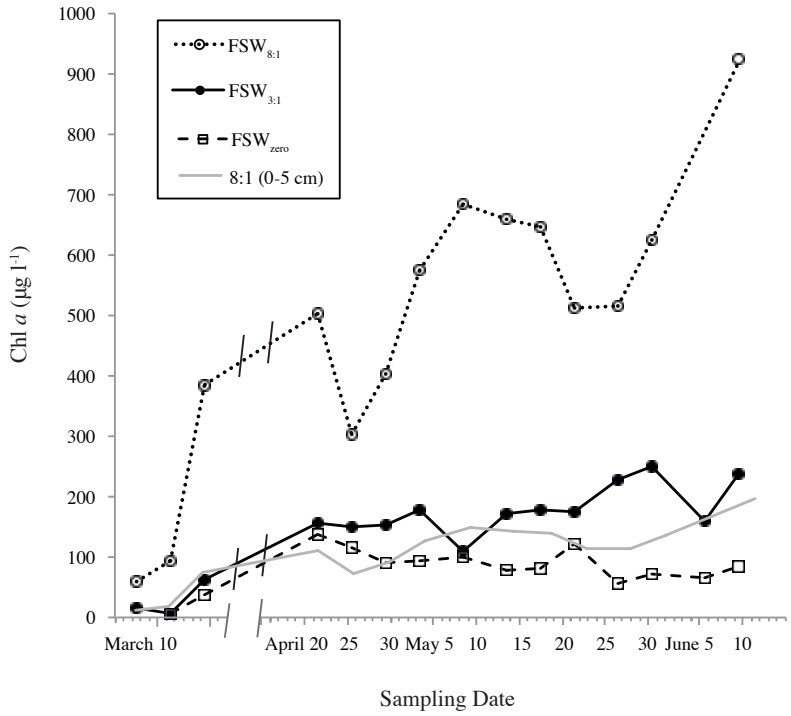

Figure 3.2. Concentration of chlorophyll *a* (chl *a*) in sample treatments including i) $FSW_{3:1}$, bottom 5 cm of ice cores melted in filtered sea water at a ratio of approximately three parts filtered seawater to one part ice, ii) FSW_{zero}, bottom 5 cm of ice melted without the addition of filtered seawater, and iii) $FSW_{8:1}$, bottom ~1 cm of ice cores scraped into FSW at a ratio of about 8 parts filtered seawater to one part ice. The $FSW_{8:1}$ sample divided by 5 cm (8:1 (0-5 cm)) is also shown for comparison with $FSW_{3:1}$ samples. Estimates with filtered seawater have been corrected for dilution.

Melting ice in filtered seawater at a ratio of three parts filtered seawater to one part ice resulted in an average salinity of 24, which is similar to the salinity of water at the ice-ocean interface (28; *see* Chapter 4). In comparison, melting ice without any filtered seawater caused salinity of the sample to decrease to an average of 9. This change in salinity of FSW_{zero} samples could have caused algal cell lysis from osmotic shock, which would decrease chl *a* captured during the filtration process [Mikkelsen & Witkowski, 2010]. Visual assessment of cells collected on 30 May with an inverted light microscope (400 x) support this suggestion, showing that 37% of cells counted in the FSW_{zero} sample were dead or ruptured, while only 17% of cells were dead in the $FSW_{3:1}$ sample (Figure. 3.3). It's noted that ruptured cells were not observed in $FSW_{3:1}$. The salinity of $FSW_{8:1}$

samples were comparable to the interface at 27, and therefore were not likely to cause osmotic stress.

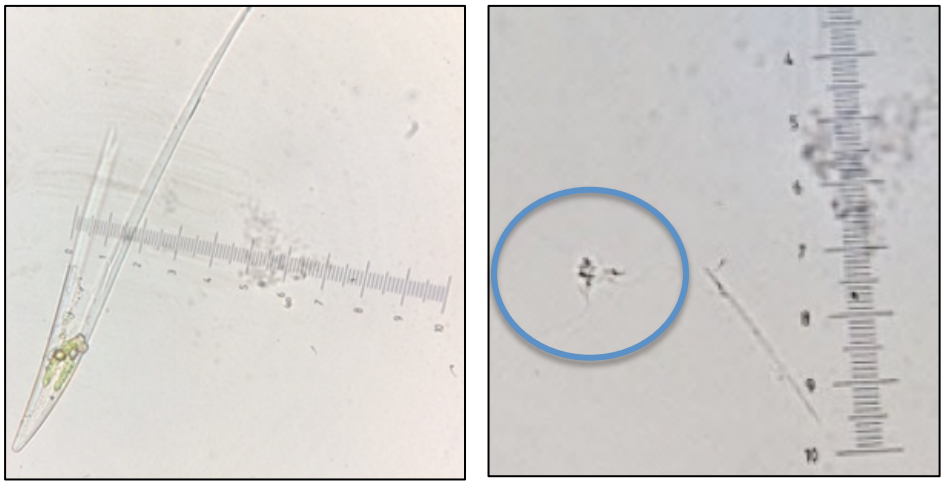

Figure. 3.3. Images of ruptured *Pleurosigma* / *Gyrosigma* spp. (left) and *Attheya* spp. (right) cells of thin snow covered samples collected on 30 May that were melted without the addition of filtered seawater (FSW_{zero})

Photosynthesis-irradiance curves of gross primary production relative to chl *a* were calculated from ^{14}C incubations of $FSW_{3:1}$, FSW_{zero} and $FSW_{8:1}$ samples (Figure 3.4). They were modeled using an exponential function in the absence of photoinhibition [Platt et al., 1980; Arrigo et al., 2010] to determine photosynthesis-irradiance parameters that include: P^B_s, maximum photosynthetic rate (mg C mg chl *a* h^{-1}), α^B, photosynthetic efficiency (mg C mg chl a^{-1} h^{-1} (µmol photons m^2 $s^{-1})^{-1}$), P_0, production at zero irradiance (mg C mg chl a^{-1} h^{-1}), E_c, the compensation point (µmol photons m^2 s^{-1}) and E_s, the photoacclimation index (µmol photons m^2 s^{-1}) (*see* Section 2.2.1) [Cota & Smith, 1991]. Please refer to Chapter Four (Sections 4.2.4 & 4.S.2) for details on modeling photosynthesis-irradiance curves.

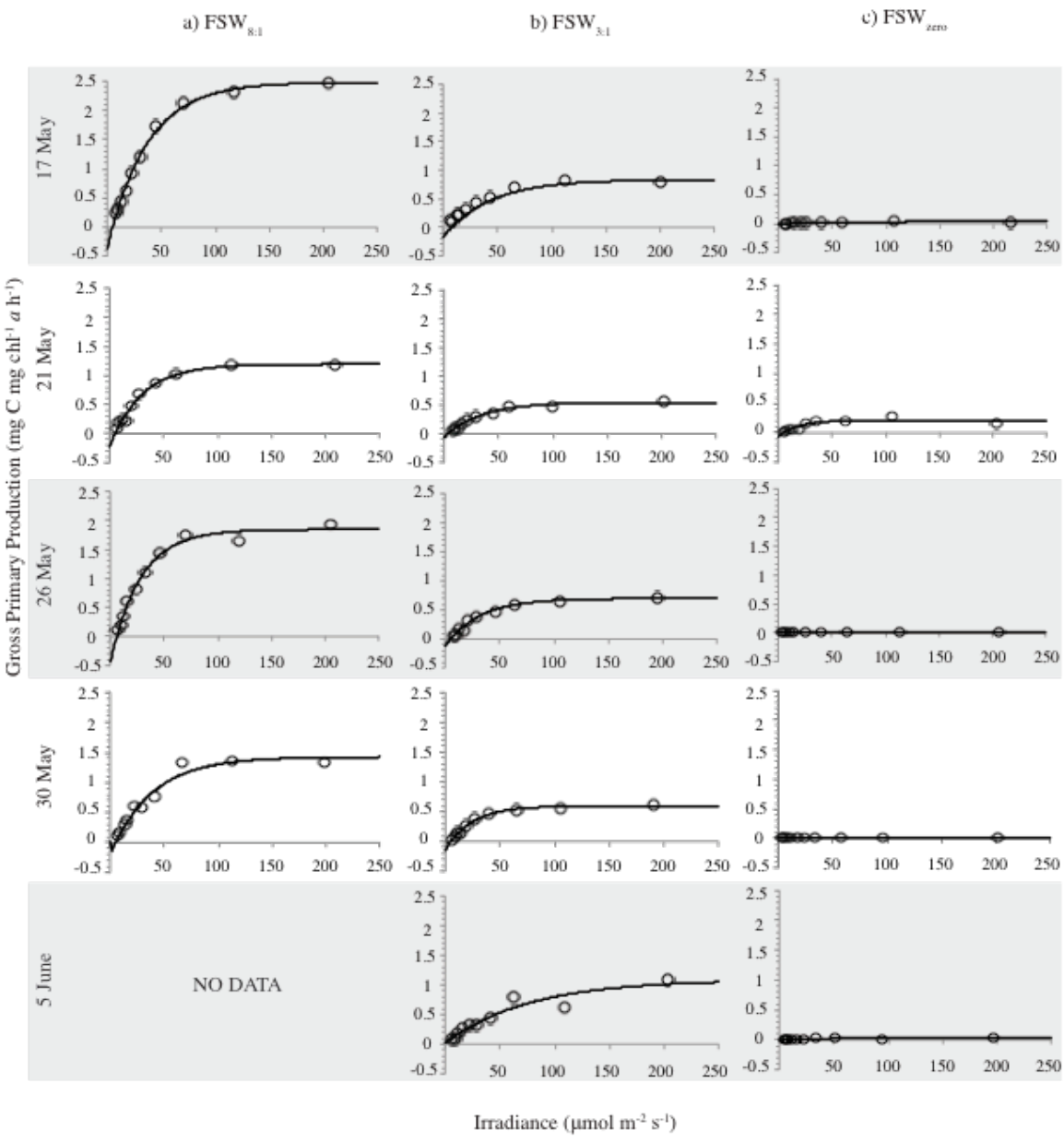

Figure 3.4. ^{14}C-derived photosynthesis-irradiance curves of gross primary production determined for bottom-ice algae under thin (< 10 cm) snow covered sea ice from 17 May to 5 June. Melt treatments of algal samples include a) $FSW_{8:1}$, bottom ~1 cm of ice scraped into filtered seawater at a ratio of about 8 parts filtered seawater to one part ice melt, b) $FSW_{3:1}$, bottom 5 cm ice melted in filtered sea water at a ratio of approximately three parts filtered seawater to one part ice melt, and c) FSW_{zero}, bottom 5 cm of ice melted without filtered seawater.

Table 3.2. Average estimates of photosynthesis-irradiance parameters (*see* text for definitions) with standard deviations (brackets) for samples melted in filtered sea water added at a ratio of three parts water to one part ice ($FSW_{3:1}$), melted without filtered seawater added (FSW_{zero}) and 1 cm scrapes ($FSW_{8:1}$). Results from Student's paired t-tests between these melt treatments is also presented, including the test statistic (top) and significance (bottom). Parameters that are significantly different between melt treatments ($p < 0.05$) are in bold.

		Average			Student's paired t-test		
		$FSW_{8:1}$	$FSW_{3:1}$	FSW_{zero}	$FSW_{8:1}$ - $FSW_{3:1}$	$FSW_{8:1}$ - FSW_{zero}	$FSW_{3:1}$ – FSW_{zero}
Photosynthesis-irradiance	P^B_s	2.031 (0.661)	0.762 (0.121)	0.077 (0.112)	**-4.606** **0.019**	**5.280** **0.013**	**6.477** **0.003**
	α^B	0.062 (0.021)	0.024 (0.005)	0.004 (0.007)	**-3.409** **0.042**	**4.713** **0.018**	**3.927** **0.017**
	P_0	0.295 (0.132)	0.097 (0.043)	0.016 (0.026)	-2.653 0.077	**3.871** **0.031**	1.771 0.151
	E_c	4.634 (0.735)	2.803 (2.555)	4.585 (1.283)	-1.075 0.361	0.113 0.917	-1.217 0.290
	E_s	33.412 (5.294)	40.817 (20.495)	32.128 (18.001)	-0.336 0.759	0.078 0.943	0.648 0.552

Average parameter response for each of the melt treatments (Table 3.2) is within ranges that have previously been reported for Arctic sea ice (*see* Chapter 4). However, the P^B_s and α^B are significantly different between the three melt treatments assessed, where estimates are greatest in $FSW_{8:1}$ sample, followed by $FSW_{3:1}$ and FSW_{zero}, respectively (Table 3.2). These observations support that primary productivity and efficiency either increase with the proportion of filtered seawater added or decrease with the duration of ice melt, potentially due to a combination of i) optimized salinity for growth and production [Arrigo & Sullivan, 1992], ii) minimized stress associated with melt time and process [Mikkelson et al., 2010; Rintala et al., 2014], iii) greater inorganic nutrient availability, iv) greater inorganic carbon availability [Rintala et al., 2014].

The optimal salinity for ice algal growth has been observed to range from 30-50 [Arrigo & Sullivan, 1992; Sogaard et al., 2011]. As a result, it is not surprising that estimates of P^B_s and α^B were greatest in the $FSW_{17:1}$ and $FSW_{3:1}$ samples that had salinities

closest to this range at 27 and 24, respectively. In comparison, the salinity of FSW_{zero} at 9 was furthest from this range and had the lowest estimates of production or photosynthetic efficiency (Table 3.2).

The difference in melt times between the three methods could have contributed to variability in cell survival and productivity, as longer melt times promote gradual changes in environmental conditions that likely limit the shock to cells, but they prolong cellular exposure to melt conditions like darkness. For example, Rintala et al. [2014] found that samples should be melted rapidly at room temperature (<12 h) to minimize the effects of death, predation and pigment degradation that increase over time. However, Mikkelson et al. [2010] concluded the opposite, where they recommend samples be melted slowly (3-5 days) at 4°C for best results. The impact of melt times is beyond the scope of this chapter; however, it is noted that time between sample collection and analysis likely contributed to the differences in chl *a* and production that was observed between melt treatments. In particular, the decrease in α^B with melt time (Table 3.2) could be a result of cellular photoacclimation to darkness by increasing abundance of the chl *a* pigment [Perry et al., 1981; Gosselin et al., 1990]. Although, additional differences in P^B_s between methods suggest that factors independent of photoacclimation and the light reactions of photosynthesis were present.

The average inorganic nutrient content of phosphate (PO_4), nitrate + nitrite (NO_x), and silicate ($Si(OH)_4$) in filtered seawater between 17 May and 5 June was 0.902, 0.943 and 5.421 μmol l^{-1}, respectively, which are comparable to interface concentrations in the region (*see* Chapter Four; Figure 4.5). The concentration of NO_x was also similar to bulk-ice estimates for the bottom 5 cm of ice, which are low for the Canadian Archipelago and

were a limiting factor of algal productivity throughout the spring (*see* Chapter 4; Figure 4.4). As a result, filtered seawater was unlikely to increase productivity of ice samples through enhanced nitrogen supply, as the concentration of NO_x added was minimal.

However, filtered seawater did have an elevated average concentration of dissolved inorganic carbon at 2038.7 μmol l^{-1}, in comparison to $FSW_{8:1}$ (1929.3 μmol l^{-1}), $FSW_{3:1}$ (1752.5 μmol l^{-1}) or FSW_{zero} (769.8 μmol l^{-1}) samples. This illustrates that the addition of filtered seawater could have supplemented sea ice inorganic carbon, which can have an even greater impact on algal production than the addition of inorganic nutrients [Rintala et al., 2014]. Although, the lowest estimates in FSW_{zero} could also represent degassing of samples to reach equilibrium with the atmosphere over the 48 h melt period, versus the < 4 h melt period of $FSW_{8:1}$ and 24 h melt period $FSW_{3:1}$ samples.

This preliminary analysis of melt procedures highlights that at present, there is no perfect approach for analyzing ice samples once removed from the natural environment. Results show that melting ice without filtered seawater exposes cells to salinities that can cause cell death and reduce productivity, while adding filtered seawater can cause an increase in production estimates by either reducing stress or enhancing the supply of inorganic carbon. However, a recent study by Lund-Hansen et al. [2016] has shown that the majority of ice algal cells in the Arctic reside at the very tips of bottom-ice crystals, which suggests that most ice algae are acclimated to environmental conditions characteristic of the ice-ocean interface. Following this rationale it seems that maintaining algal samples at salinity, nutrient and inorganic carbon levels similar to interface water best represents the natural ice algal environment. The $FSW_{8:1}$ melt procedure likely produces conditions most similar to interface water, followed by $FSW_{3:1}$ and FSW_{zero},

respectively. Furthermore, the $FSW_{17:1}$ samples are likely to be the least affected by photoacclimation to prolonged darkness, which can modify estimates of photosynthetic efficiency. Unfortunately the scrape approach ($FSW_{8:1}$) is not well-documented in the literature, except for perhaps measurements with pulse-amplitude-modulated (PAM) fluorometers that require highly concentrated samples for analysis (e.g. McMinn et al., 2005; McMinn et al., 2010). This makes comparisons with other studies on biomass and production difficult. There is also uncertainty associated with precise collection of the bottom 1 cm layer of sea ice, highlighting that inter-comparisons with other methods require standardizing measurements per unit of biomass (i.e. chl *a* or carbon).

3.5 Conclusion

The review of sea ice collection and melt procedures presented in this chapter represents an introduction to the difficulties of sampling sea ice algae and comparing estimates within the literature. Evidence to support the collection of the bottom 5 cm of sea ice before melt in filtered seawater at a ratio of one part ice to three parts filtered seawater has been presented. This includes i) collection of a known section of ice that permits comparisons with the literature, and ii) limiting stress on algal cells that is associated with salinity and processing time. As a result the $FSW_{3:1}$ method of melting ice samples from the bottom 5 cm has been applied in the research of sea ice algae that is outlined in the remainder of this document. For consistency, this approach has also been used in assessments of heterotrophic bacteria.

References

Alou-Font, E., Mundy, C.J., Roy, S., Gosselin, M. and S. Agusti (2013), Snow cover affects ice algal pigment composition in the coastal Arctic Ocean during spring, *Mar. Ecol. Prog. Ser.* 474, 89-104, doi: 10.3354/meps10107.

Arrigo K.R., Mills, M.M., Kropuenske, L.R., van Dijken, G.L., Alderkamp, A.C., and D.H. Robinson (2010), Photophysiology in two major Southern Ocean phytoplankton taxa: photosynthesis and growth of Phaeocystis antarctica and Fragilariopsis cylindrus under different irradiance levels, *Integr. Comp. Biol.* 50, 950–966, doi: 10.1093/icb/icq021.

Arrigo, K.R., and C.W. Sullivan (1992), The influence of salinity and temperature covariation on the photophysiological characteristics of Antarctic sea ice microalgae, *J. Phycol.* 28, 746-756, doi: 10.1111/j.0022-3646.1992.00746.x.

Campbell, K., Mundy, C.J., Barber, D.G., and M. Gosselin (2014), Characterizing the ice algae biomass-snow depth relationship over spring melt using transmitted irradiance, *J. Mar. Syst.* 67(3), 375-387, doi: 10.1016/j.jmarsys.2014.01.008.

Cota, G., and R.E.H. Smith (1991), Ecology of bottom ice algae: II. Dynamics, distributions and productivity, *J. Mar. Syst.* 2, 279-295, doi:10.1016/0924-7963(91)90037-U.

Garrison, L., and K.R. Buck (1986), Organism losses during ice melting: A serious bias in sea ice community studies, *Polar Biol.* 6, 237-239.

Gosselin, M., Legendre, L., Therriault, J.-C., and S. Demers (1990), Light and nutrient limitation of sea-ice microalgae (Hudson Bay, Canadian Arctic), *J. Phycol.* 26, 220-232, doi: 10.1111/j.0022-3646.1990.00220.x.

Horner, R.A. (1985), *Sea Ice Biota*. CRC Press, Inc., Florida, U.S.A.

Lund-Hansen, L.C., Hawes I., Nielsen, M.H., and B.K. Sorrell (2016), Is colonization of sea ice by diatoms facilitated by increased surface roughness in growing ice crystals? *Polar Biol.*, doi:10.1007/s00300-016-1981-3.

McMinn, A., Hirawake, T., Hamoaka, T. Hattori T., and M. Fukuchi (2005), Contribution of benthic microalgae to ice covered coastal ecosystems in northern Hokkaido, Japan, *J. Mar. Biol. Ass.* 85, 283-289, doi: https://doi.org/10.1017/S0025315405011173h.

McMinn, A., Pankowskii, A., Ashworth, C., Bhagooli, R., Ralph, P., and K. Ryan (2010), In situ net primary productivity and photosynthesis of Antarctic sea ice algal, phytoplankton and benthic algal communities, *Mar. Biol.* 157, 1345 – 1356, doi: 10.1007/s00227-010-1414-8.

McMinn, A., Skerratt, J., Trull, T., Ashworth, C. and M. Lizotte (1999), Nutrient stress gradient in the bottom 5 cm of fast ice, McMurdo Sound, Antarctica, Polar Biol. 21, 220-227, doi: 10.1007/s003000050356.

Mikkelson, D.M, and A. Witowski (2010), Melting sea ice for taxonomic analysis: a comparison of four melting procedures, *Polar Res*. 29, 451-454, doi:10.1111/j.1751-8369.2010.00162.x.

Perry, M.J., Talbot, M.C., and R.S. Alberte (1981), Photoadaptation in marine phytoplankton: response of the photosynthetic unit, *Mar. Biol*. 62, 91-101.

Platt, T., Gallegos, C.L., and W.G. Harrison (1980), Photoinhibition of photosynthesis in natural assemblages of marine phytoplankton, *J. Mar. Res*. 38, 687–701.

Rintala, J.-M., Piiparinen, J., Blomster, J., Majaneva, M., Müller, S., Uusikivi, J., and R. Autio (2014), Fast direct melting of brackish sea-ice samples results in biologically more accurate results than slow buffered melting, *Polar Biol*. 37(12), 1811-1822, doi: 10.1007/s00300-014-1563-1.

Rysgaard, S., Kuhl, M., and J.W. Hansen (2001), Biomass, production and horizontal patchiness of sea ice microalgae in a high-Arctic fjord (Young Sound, NE Greenland), *Mar. Ecol. Prog. Ser*. 223, 15-26, doi:10.3354/meps223015.

Smith, R.E.H., and P. Clement (1990), Heterotrophic activity and bacterial productivity in assemblages in microbes from sea ice in the High Arctic, *Polar Biol*. 10, 351-357, doi: 10.1007/BF00237822.

Søgaard, D.H., Hansen, P.J., Rysgaard, S., and R.N. Glud (2011), Growth limitation of three Arctic sea ice algal species: effects of salinity, pH, and inorganic carbon availability, Polar Biol. 34, 1157-1165, doi: 10.1007/s00300-011-0976-3.

CHAPTER FOUR: COMMUNITY DYNAMICS OF BOTTOM-ICE ALGAE IN DEASE STRAIT OF THE CANADIAN ARCTIC

This manuscript has been published in the peer-reviewed journal of *Progress in Oceanography*. The research included in this work was planned, conducted and reported by myself as first author. Note that since the manuscript's publication an erratum pertaining to the magnitude of primary productivity reported has been made. These revisions have been corrected for and are incorporated into this chapter.

Campbell, K., C.J. Mundy, J.C. Landy, A. Delaforge, C. Michel and S. Rysgaard (2016), Community dynamics of bottom-ice algae in Dease Strait of the Canadian Arctic, *Prog. Oceanogr.* 149, 27-39, doi: 10.1016/j.pocean.2016.10.005.

Abstract

Sea ice algae are a characteristic feature in ice-covered seas, contributing a significant fraction of the total primary production in many areas and providing a concentrated food source of high nutritional value to grazers in the spring. Algae respond to physical changes in the sea ice environment by modifying their cellular carbon, nitrogen and pigment content, and by adjusting their photophysiological characteristics. In this study we examined how the ratios of particulate organic carbon (POC) to nitrogen (PON), and POC to chlorophyll *a* (chl *a*), responded to the evolving snow-covered sea ice environment near Cambridge Bay, Nunavut, during spring 2014. We also estimated photosynthesis-irradiance curves using oxygen-optodes and evaluated the resulting time-series of parameters under thin and thick snow-covered sites. There were no significant differences in photosynthesis-irradiance parameters between samples from different overlying snow depths, and only the maximum photosynthetic rates in the absence of

photoinhibition (P^B_s) and photoacclimation (E_s) parameters changed significantly over the spring bloom. Furthermore, we found that both these parameters increased over time in response to increasing percent transmission of photosynthetically active radiation (T_{PAR}) through the ice, indicating that light was a limiting factor of photosynthesis and was an important driver of temporal (over the spring) rather than spatial (between snow depths) variability in photophysiological response. However, we note that spatial variability in primary production was evident. Higher T_{PAR} over the spring and under thin snow affected the composition of algae over both time and space, causing greater POC:chl *a* estimates in late spring and under thin snow cover. Nitrogen limitation was pronounced in this study, likely reducing P^B_s and algal photosynthetic rates, and increasing POC:PON ratios to over six times the Redfield average. Our results highlight the influence of both light and nutrients on ice algal biomass composition and photophysiology, and suggest a limitation by both resources over a diel period.

Keywords: photoadaptation, sea ice, algology, Arctic zone, oxygen, nutrients

4.1 Introduction

Sea ice algae are important contributors to the base of the Arctic marine food web. Their abundance in the bottom of sea ice during the spring bloom provides concentrated nutrition for grazers at a time when resources are otherwise limited [Cota et al., 1989; Legendre et al., 1992]. This food source is particularly significant because diatoms that are prevalent in sea ice algal communities contain large amounts of high-energy poly-unsaturated fatty acids (PUFAs) [Leu et al., 2010]. Ice algal photosynthetic carbon uptake

and oxygen release also significantly affect sea ice carbon dynamics [Brown et al., 2015], thereby influencing air-sea gas exchanges [Else et al., 2012].

For most of the spring the spatial distribution of bottom ice algal biomass [e.g. Campbell et al., 2014a; Rysgaard et al., 2001; Mundy et al., 2007] and production [e.g. Gosselin et al., 1985; Michel et al., 1988; Smith et al., 1988] varies in response to light availability that is largely controlled by snow depth. Ice algal chlorophyll *a* (chl *a*) biomass and production are also influenced by other factors that include nutrient availability [Lavoie et al., 2005], species composition [Gosselin et al., 1997] and stability of the ice matrix [Campbell et al., 2014]. These factors contribute to the range of biomass and production measurements that are reported in the literature, although, the significance of each changes seasonally with the progression of spring melt and between different study regions [Leu et al., 2015].

Ice algae can respond to changing environmental conditions by modifying their cellular carbon and nitrogen composition, as documented by shifts in particulate organic carbon (POC), nitrogen (PON) and chl *a* ratios. On average this results in a ratio of 106 mols carbon to 16 mols nitrogen, or 6.6 mols POC:PON, for marine phytoplankton [Miller & Wheeler, 2016]. Although, recent studies have suggested a broader range for ice algae from 3 to 24 mol:mol [Niemi & Michel, 2015], where values may increase as a result of acclimation to high light intensities or nutrient limitation [Demers et al., 1989; Gosselin et al., 1990]. Particulate carbon to chl *a* ratios typically increase with acclimation to high light and low nutrient conditions [Gosselin et al., 1990; Michel et al., 1996], resulting in a large range of estimates from 5 to 263 mg:mg for ice algae [Nozais et al., 2001].

Ice algae may also adjust the photosynthetic apparatus as seen by changing photosynthesis-irradiance parameters in response to environmental conditions. For example, photosynthesis-irradiance parameters can vary considerably due to inorganic nutrient availability, the activity of photosynthetic enzymes [Michel et al., 1988], as well as light [Cota & Horne, 1989], salinity [Bates & Cota, 1986] and temperature conditions [Michel et al., 1989]. The effects of these often competing or overlapping factors on parameter estimates can make their interpretation complex [Cota & Smith, 1991].

The general flow of surface waters in the Canadian Arctic Archipelago is from west to east; however, water in the Coronation Gulf has been suggested to exit both to the Amundsen Gulf in the west and through Dease Strait to the east [McLaughlin et al., 2004]. These suggested patterns of surface currents in the region of Dease Strait near Cambridge Bay, Nunavut, are largely driven by the high level of riverine input, and indicate that water at the study site may not readily exchange with neighboring water bodies. These factors have the potential to cause low surface-water exchange with surrounding water bodies that could limit the re-supply of new nutrients to the bottom-ice. Furthermore, low nutrient inflow from the Beaufort Sea in the west could also promote nutrient limited conditions in the region of Dease Strait [Tremblay et al., 2015].

The goal of our study is to investigate the influence of inorganic nutrient availability and light intensity on sea ice algal composition and photosynthetic response over the spring bloom in Dease Strait, Nunavut. To meet this goal, we collected field observations in the region during the Ice Covered Ecosystem - CAMbridge bay Process Study (ICE-CAMPS) between April and June, 2014. Measurements of production from optode incubation methods are used to model PI relationships and derive associated

photophysiological parameters for ice algae samples collected under thin and thick snow depths. Coincident measurements of environmental conditions were also recorded to assess potential controls of parameter response.

4.2 Materials and methods

4.2.1 Field site

Samples were collected in the vicinity of an ice camp established in Dease Strait, Nunavut, Canada (69.03°N, 105.33°W), that was about 5 km offshore from the community of Cambridge Bay. The region is in close proximity to mainland Canada, and receives freshwater inputs from the nearby Coppermine, Hood, Burnside and Ellice rivers (Figure 4.1), with historical average flow rates of 255 (above Copper Creek), 75.6, 134 and 83.4 $m^3 s^{-1}$ (Environment Canada). Water depth at the station was 60 m and the landfast first-year sea ice in the region was covered by a drifted snowpack for the duration of sampling. Snow depth was categorized as 'thin' (<10 cm, between snow drifts) or 'thick' (15-25 cm, snow drifts). We sampled on 12 occasions between 21 April and 9 June, at approximately 4-day intervals.

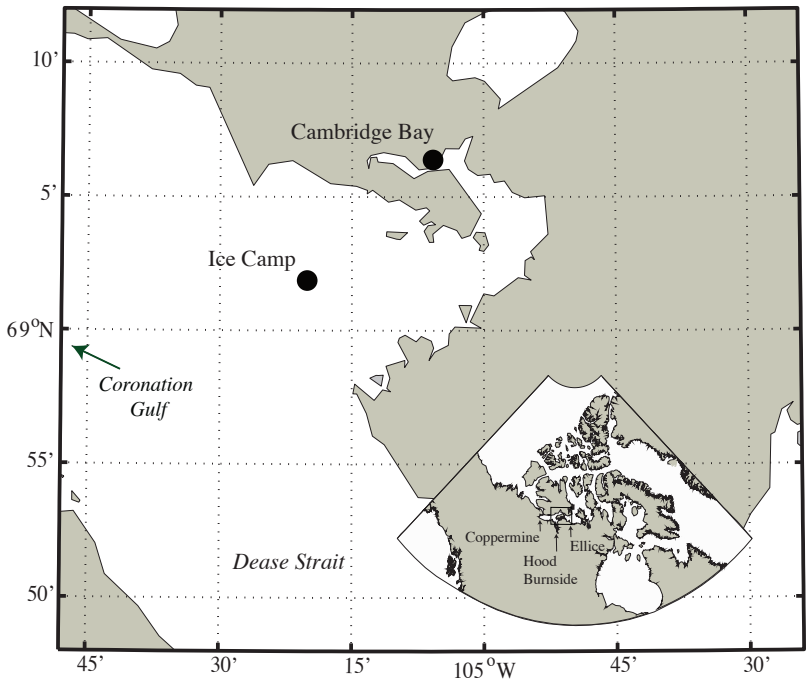

Figure 4.1. Map of study location near Cambridge Bay, Nunavut. Inset includes approximate locations of the main rivers in the area.

4.2.2 Field sampling

Ice cores were collected at newly chosen thin and thick snow sites approximately every four days (one sampling cycle) using a 9 cm *Mark II Kovacs* core barrel. The bottom 0-5 cm of six to eight cores were pooled together for each site, while snow depth and ice thickness for each core were recorded and averaged. A separate core at each snow site was taken for analysis of bulk nutrients.

Three measurements of photosynthetically active radiation (PAR) were taken opportunistically between 9:00 and 12:30 local time throughout the sample period using 2π quantum sensors (*LI-COR*) that were calibrated to air and water, for surface downwelling, surface upwelling, and under-ice downwelling, respectively. The average of the three values was calculated from readings to a *LI-1000* data logger, and albedo was calculated as the ratio of surface upwelling to downwelling [Petrich & Eicken, 2010]. The

under-ice sensor was deployed approximately 30 cm beneath the ice-ocean interface using a mechanical arm and the protocol described in Campbell et al. [2014b]. Transmittance was determined as the percent downwelling PAR transmitted to surface waters under the ice. Due to irregular collection of transmittance data and the need to perform paired statistical analyses (see Section 3.2.5), measurements ± 2 days of core collection were averaged to estimate PAR transmittance at the ice core sampling interval of approximately 4 days. Estimates exceeding this 2-day threshold were not included in averaging, resulting in a total of 10 sampling events that are referred to hereafter as PAR transmittance (T_{PAR}). Finally, daily profiles of conductivity, temperature and depth (CTD) were made of the water column using an RBR XR-620 sensor.

Following transport to laboratory facilities in Cambridge Bay, pooled ice samples were melted in the dark for 24 h in 0.2 μm filtered seawater with a mean ± standard deviation of 28 ± 0.3 salinity, that had been collected and filtered 24 h prior to use, which was added at a ratio of three parts FSW to one part ice. This melted sea ice-filtered seawater solution from the pooled cores was used for all incubations and measurements to follow, except for bulk nutrients that were melted separately in the dark without dilution. To account for filtered seawater dilution when applicable, the volume of each pooled sample were multiplied by the ratio of total volume (filtered seawater + ice melt) to ice melt.

A full core was also taken at the thin snow cover site to measure temperature (*Testo* 720 probe) and salinity (*Orion Star* A212 conductivity meter) for the bottom 0-5 cm, and 10 cm sections above. These values were used to calculate percent brine volume following the equations of Cox & Weeks [1983].

4.2.3 Laboratory analysis

Environmental variables

Two subsamples of chl *a* were measured on the melted cores following filtration on GF/F filters (*Whatmann*) and subsequent pigment extraction in 10 ml of 90% acetone for 24 h. Fluorescence was measured before and after acidification with 5% HCl (*Turner Designs Trilogy* Fluorometer) [Parsons et al., 1984] and chl *a* concentration was determined from these measurements using the equations of Holm-Hansen et al. [1965]. The salinity of all melted ice samples were measured using an *Orion Star* A212 conductivity meter. A sub-sample of the melted ice-filtered seawater solution was also filtered onto pre-combusted GF/F filters for analysis of POC and PON, and a filter blank was also collected for each sampling event. These samples were kept frozen until measurement on a continuous-flow isotope ratio mass spectrometer (*Thermo Scientific*) following Glaz et al. [2014]. Filtrate for nutrient analysis was collected from the undiluted core using sterilized syringe filters and GF/F filters previously combusted at 450°C for 5 h. Samples were frozen for approximately 6 months at -20°C prior to analysis of nitrate (NO_3) and nitrite (NO_2) concentration, together referred to as NO_x, phosphate (PO_4) and silicic acid ($Si(OH)_4$) on an auto analyzer (*Seal Analytical*) [Strickland & Parsons, 1972]. Nutrient analysis was also completed on water of the ice-ocean interface that was collected and processed on days of ice core collection.

Bacteria production using ^{3}H-Leucine

Bacteria production was determined by incubating six 15 ml subsamples of the melted ice-FSW solution of pooled cores, with ^{3}H-leucine following Kirchman [2001].

Subsamples were dispensed into sterile polycarbonate vials and inoculated with ^{3}H-leucine for a final concentration of 10 nM. Immediately after this step, three of the control vials were fixed with 50% trichloroacetic acid (TCA, final concentration 5%), before the samples were vortexed and incubated at -1.5°C in darkness. Following 6 h incubation, the three remaining active subsamples were fixed with TCA (final concentration 5%) before filtration through 0.2 µm cellulose acetate membranes (*Whatmann*). Filters were rinsed with 5% TCA and 80% ethanol before they were dried in 7 ml scintillation vials, and dissolved by adding 0.5 ml ethyl acetate. The activity of the sample was measured on a liquid scintillation counter (*Hidex Triathler*) after an extraction period of 24 to 48 h in 5 ml of Ecolume scintillation cocktail. The specific activity of the ^{3}H-leucine working solution (SA, dpm mol^{-1}) used in incubations was also recalculated for each sampling cycle.

Bacteria production (µmol leucine l^{-1} h^{-1}) was calculated using the equations of Kirchman [1993] that required: the average activity of test and control filters (dpm), SA (dpm mol^{-1}), incubation time (h), filtered volume (l) and a core dilution factor to account for ice melt in the FSW. Values reported as mass (g C l^{-1} h^{-1}) in this study were further multiplied by the theoretical conversion factor of 1.5 kg C mol^{-1} used by Ducklow et al. [2003], which estimates the carbon biomass produced relative to ^{3}H-leucine incorporated into cellular protein.

Optode experimental set-up

Optode incubation chambers were designed similar to a photosynthetron [e.g. Babin, 1994], where black and white-diffuse plexiglass was used to create temperature controlled

and watertight chambers that were attached to an external water circulator (Figure 4.2). Chambers were equipped with four 500 ml *Wheaton* borosilicate glass bottles (size selected to ensure adequate biomass for a robust oxygen signal) that sat on a lip along either side of the false chamber bottom to permit water flow under, as well as above, the incubation bottles. Four holes aligned with the central position of each incubation bottle were also drilled in the incubator lid. Furthermore, chambers were equipped with custom-built stands that housed magnetic stir-plates at each bottle position (Figure 4.2), and were positioned equidistant from a *Hiralite* full spectrum light emitting diode. The use of a light emitting diode was an important aspect of the optode set-up because it's low heat emission minimized incubation temperature fluctuations. However, the limited intensity of this light source, combined with large bottle size and the need for temperature regulation of the chamber, restricted the total number of bottles that could be incubated.

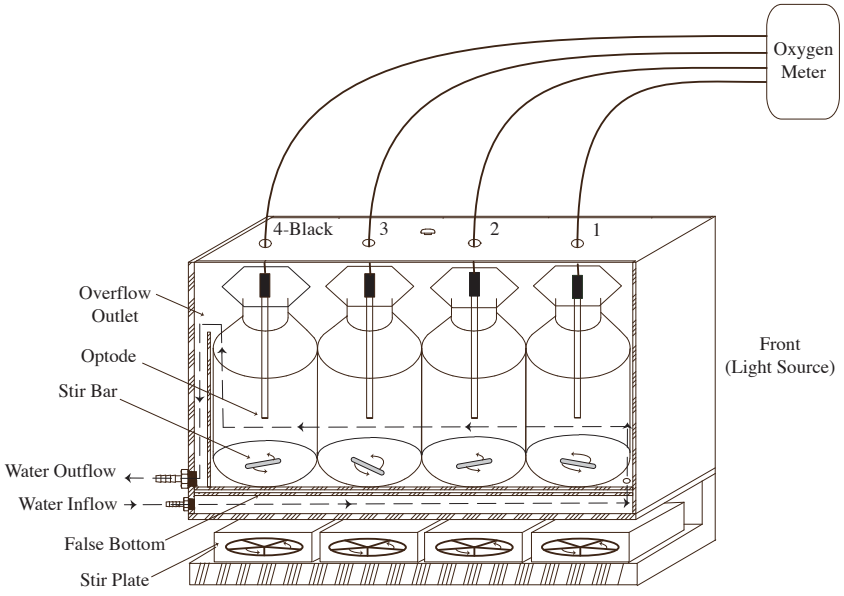

Figure 4.2. Illustration of an optode chamber set-up, showing incubation bottle positions 1 (closest to light) through 4-black (furthest from light) and directionality of water flow (dashed arrows).

Continuous measurements of dissolved oxygen were acquired by fitting each incubation bottle with a 10 mm robust *Firesting* optode (*Pyro Science*) with optical insolation that connected to one of two, four-channel *Firesting* optical oxygen meters. Each meter recorded to a single computer using the *Pyro Oxygen Logger* software version 3.0. We positioned each of the sensors in the middle of the sealed incubation bottles by inserting the probes through holes installed in the chamber lid (Figure 4.2), as well as through holes drilled in the glass bottle stoppers. It is important to note that the diameter of each stopper hole was nearly equivalent to the 3 mm tip diameter of the optode sensors, ensuring negligible exposure of the sample to air.

The clear bottles were arranged consecutively in the chamber from position one (closest to the light) through three (furthest from the light, Figure 4.2), so that samples were incubated at high, medium and low light levels. The average ($n = 3$) intensity of PAR at these positions was measured immediately following incubations by systematically replacing the oxygen sensors and glass stoppers with a scalar PAR probe (*Walz* model US-SQS/L) that read to a data logger (*LI-COR* LI-1000). The incubation bottle at position four (farthest from the light) was darkened to prevent light from entering.

Primary production using optodes

The incubation bottles with magnetic stir bars were filled with the melted ice solution (Section 4.2.2) using a peristaltic pump, to avoid bubbles being trapped, while the bulk sample was periodically re-suspended. Bottles were overfilled with sample to prevent the formation of a headspace during closure of the glass stopper, and placed into darkened

chambers to equilibrate to the set incubation temperature of -1.5°C for approximately 6h, that was representative of *in situ* conditions. Optode sensors were calibrated immediately prior to each incubation using 0% and 100% dissolved oxygen standards of 0.17 M sodium dithionite ($Na_2S_2O_4$) and air saturated water, respectively. This was done to account for any sensor drift or photodegradation that may have occurred with extended use [Bagshaw, 2011].

Samples were incubated for 70 h under continuous illumination and mixing (1 cm magnet at 60 rpm) while the oxygen concentration was recorded for each bottle at approximately one-second time intervals. This length of incubation was chosen to ensure a robust oxygen signal was obtained for all incubations throughout the study period. Daily temperatures within each chamber were manually recorded (*Traceable* digital thermometer) opportunistically (minimum twice per day) and averaged over the duration of incubations. Due to the volume required to circulate through all incubation chambers, actual incubation temperatures, at -0.66 ± 0.25°C, were slightly higher than the desired -1.5°C but remained constant throughout each incubation run.

As a result of minor discrepancies in the initial concentration of oxygen between incubation bottles, hourly averages of oxygen concentration in each bottle were made relative to their respective start (T_0) concentrations. Gross primary production (μmol O_2 l^{-1}) was then calculated for each incubation light intensity as the linear trend of relative oxygen production in illuminated bottles (Figure 4.3a, b) plus absolute (linear) black bottle productivity over the entire duration of the experiment. We note that respiration during light conditions may exceed respiration under dark conditions and therefore our gross primary production estimates represent minimum values. Values were

converted to milligrams of carbon consumption using the photosynthetic quotient (PQ) of 1.2 (Fenchel & Glud, 2000). All samples incubated in our optode set-up exhibited linear trends of oxygen production (positive or negative) with time, whose slopes were consistently highest in bottle position 1 (high light), followed by bottles 2, 3 and 4 (no light) (Figure 4.3). Similar to the trends exhibited in Figure 4.3, samples incubated in the dark (bottle 4, Figure 4.2) displayed net oxygen consumption for all experiments, represented by negative production.

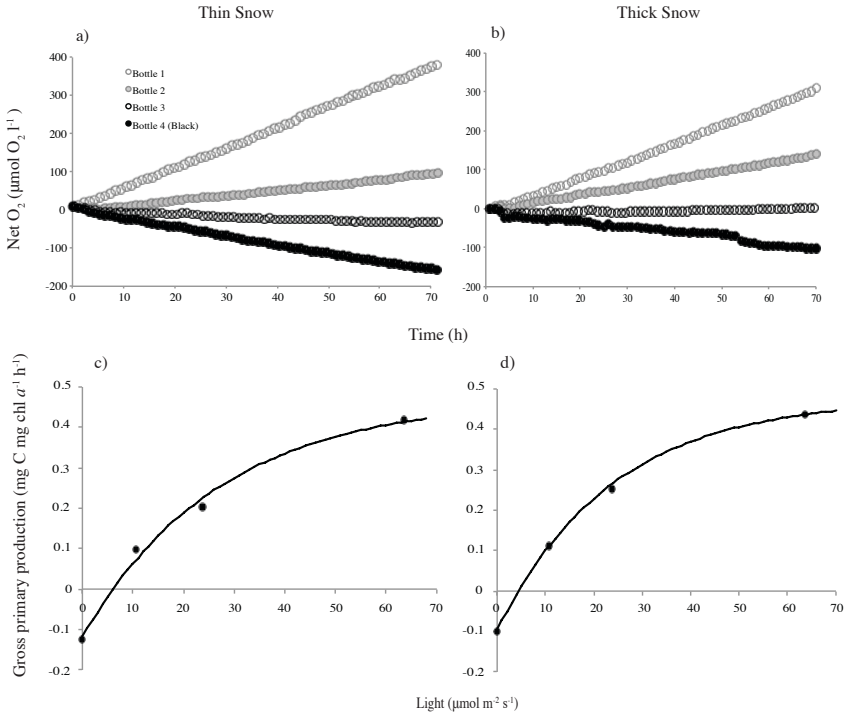

Figure 4.3. Examples of community production estimates for thin (a, c) and thick (b, d) snow covers from 22 May. Net change in oxygen per liter during optode incubations is plotted over the 70 h incubation time period for each bottle (a, b). Optode based gross primary production are also plotted as a function of incubation light intensity, relative to chlorophyll *a*, with their corresponding exponential models (c, d).

4.2.4 Fitting photosynthesis-irradiance relationships

Photosynthesis-Irradiance relationships were obtained from the regression of carbon production versus incubation light intensity for each sample cycle. This included primary production of the clear bottles ($n = 3$), as well carbon consumption (negative production) in the dark bottle (Figure 4.3c, d). Relationships were calculated using the exponential equation of Platt et al. [1980] modified by Arrigo et al. [2010], without the influence of photoinhibition as it was not observed over the range of experimental irradiances. Photosynthetic parameters were calculated relative to chl *a* biomass and included: P^B_s, maximum photosynthetic rate (mg C mg chl a^{-1} h^{-1}), α^B, photosynthetic efficiency (mg C [mg chl a]$^{-1}$ h^{-1} [µmol photons m^2 s^{-1}]$^{-1}$), P_0, production at zero irradiance (mg C mg chl a^{-1} h^{-1}), E_c, irradiance where the rate of photosynthesis is balanced by respiration ($E_c = \frac{P_0^B}{\alpha^B}$) (µmol photons m^2 s^{-1}) and E_s, the photoacclimation parameter ($E_s = \frac{P_s^B}{\alpha^B}$) (µmol photons m^2 s^{-1}) [Cota & Smith, 1991].

4.2.5 Statistical analysis

The analytical software SPSS (*IBM* Version 20) was used to perform all statistical analyses in this research for 95% confidence ($p < 0.05$). Student's paired t-tests were run to test differences between thin and thick snow covers. The test statistic (t_n) is reported following these assessments, where *n* indicates the sample size. Pearson correlation statistics (r) were calculated to evaluate the significance of linear trends over the spring, and between parameters of interest. All statistics were completed on data for the entire sampling period, unless otherwise specified.

4.3 Results

4.3.1 Physical characteristics of the field site

Snow thickness was relatively constant over the spring sampling period, and averaged 7.5 ± 3.5 and 19 ± 5 cm at thin and thick snow cover sites, respectively (Figure 4.4a, b). An exception was the samples collected immediately after a storm on 26 May when snow thickness averaged 18 cm under thin snow and 33 cm under thick snow. These values were not included in the calculated averages of snow depth. Ice thickness (H_I) averaged 1.8 ± 0.10 and 1.7 ± 0.09 m at thin and thick snow cover sites, and increased over the spring from about 1.8 to 2.1 m and 1.75 to 2 m, respectively (Figure 4.4a, b). These differences in snow and ice thickness between sites were significant following a student's paired t-test ($t_{12} = -3.711, p < 0.05$).

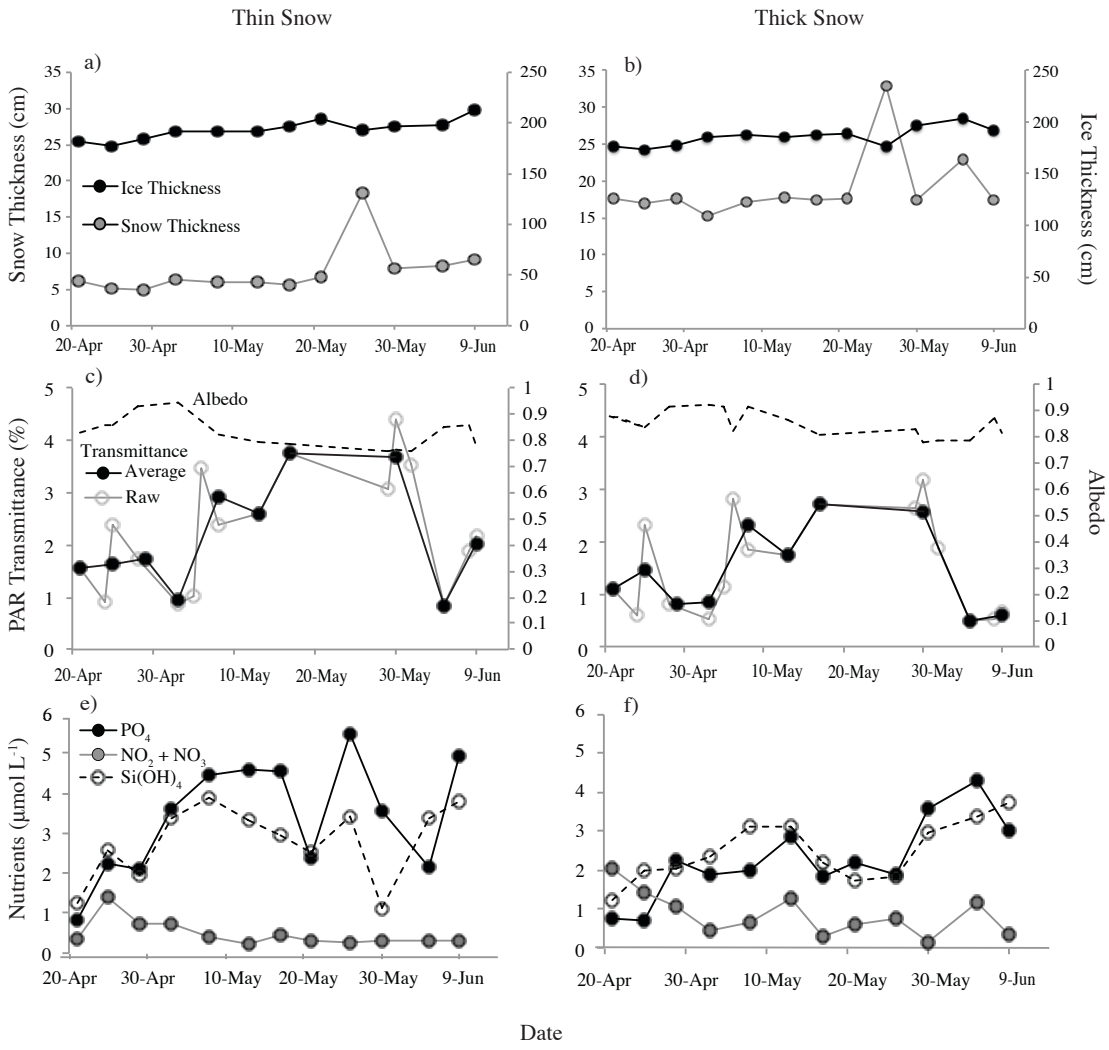

Figure 4.4. Site characteristics over the spring sampling period, including snow and ice thickness (a, b), transmittance of photosynthetically active radiation (PAR) directly measured (Raw) or averaged ± 2 days of core collection (Average) (c, d), and bottom-ice nutrient concentrations (c, d) under thin (a, c, e) and thick (b, d, f) snow covers. Albedo measured over thin (c) and thick (d) snow is also shown.

Snow depth is a dominant control of surface reflectivity prior to melt [Grenfell & Maykut, 1977] and, as a result, the consistency in snow depth for most of the spring corresponds to a largely stable albedo of 0.83 ± 0.06 for thin snow and 0.85 ± 0.05 for thick snow (Figure 4.4c, d). Stable snow depths and albedo indicate the seasonal increase in irregularly sampled and averaged PAR transmittance is due to an increasing angle of

solar elevation, while variability is likely a result of changing weather and cloud conditions.

The percent transmittance of PAR averaged ± 2 days of core collection (T_{PAR}) increased over the spring under thin and thick snow covers from 1.6 and 1.1% on 21 April, to 4.4 and 3.2% on 30 May. A storm on 3 June did not affect the depth of snow sampled as a low site was still found; however, the fresh snow cover and greater depth of snow surrounding the site caused a drop in T_{PAR} on the 5 and 9 June sample dates that represent a period of light conditions in the bottom-ice unique to the rest of the spring. As a result, these outliers on 5 and 9 June that are uncharacteristic of the seasonal trend have been removed for all assessments hereafter that include T_{PAR} (see Table 4.S.1 for additional analyses).

Without the outliers after the 3 June storm, the seasonal increase in T_{PAR} was significant at 0.068% d^{-1} under thin snow ($r^2 = 0.705$, $p < 0.05$) and 0.047% d^{-1} under thick snow ($r^2 = 0.617$, $p < 0.05$). Light availability at the ice-ocean interface was significantly higher under thin snow cover than thick snow cover ($t_8 = -4.926$, $p < 0.05$), with average T_{PAR} from 21 April to 1 June of 2.2 ± 1%. This corresponds to an averaged transmitted PAR irradiance of 27.4 ± 14.6 μmol photons m^2 s^{-1} over the same time period. In comparison, average T_{PAR} under thick snow cover was 1.7 ± 0.8% and average transmitted PAR irradiance was 17.7 ± 10.1 μmol photons m^2 s^{-1} (Figure 4.4c, d).

The bulk concentration of PO_4 and $Si(OH)_4$ in the bottom ice followed similar trends over the spring, but the nature of these relationships differed between snow depths. Under thin snow, PO_4 and $Si(OH)_4$ displayed a sharper increase at the beginning of the sample period (before 8 May), reaching maximum concentrations of 5.5 μmol l^{-1} and 3.8 μmol l^{-1},

respectively (Figure 4.4e). In comparison, PO_4 and $Si(OH)_4$ increased more gradually over the spring under thick snow, to a maximum of approximately 4.3 μmol l^{-1} ($r = 0.799$, $p < 0.05$) and 3.7 μmol l^{-1} ($r = 0.637$, $p < 0.05$), respectively (Figure 4.4f). The concentration of NO_x in sea ice decreased initially in the spring under thin and thick snow covers, before remaining under 1 μmol l^{-1} for most of the study period (Figure 4.4e, f).

Phosphate concentrations were significantly higher under thin than under thick snow cover ($t_{12} = -2.510$, $p < 0.05$), with averages of 3.41 ± 1.44 μmol l^{-1} and 2.27 ± 1.04 μmol l^{-1}, respectively. The concentration of NO_x was significantly greater under thick snow ($t_{12} = 2.212$, $p < 0.05$) with an average of 0.85 ± 0.51 μmol l^{-1} versus 0.48 ± 0.34 μmol l^{-1} under thin snow. However, there was no significant difference in $Si(OH)_4$ concentration between thin (average 2.79 ± 0.93 μmol l^{-1}) and thick (average 2.48 ± 0.77 μmol l^{-1}) snow covers ($t_{12} = -1.288$, $p = 0.224$). Nutrient abundance at the ice-ocean interface did not significantly change over the sampling period (Figure 4.5). The average concentration of PO_4, NO_x, $Si(OH)_4$ were 0.84 ± 0.1 μmol l^{-1}, 1.1 ± 0.2 μmol l^{-1} and 5.6 ± 0.5 μmol l^{-1}, respectively.

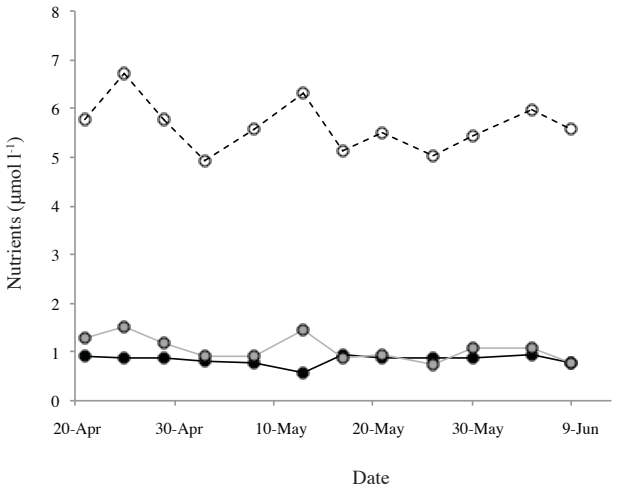

Figure 4.5. Concentration of phosphate (PO_4)(black), nitrate + nitrite ($NO_3 + NO_2$)(grey) and silicate ($Si(OH)_4$)(white) at the ice-ocean interface over the sampling period.

The bottom 5 cm of ice salinity remained fairly constant at 8.3 ± 0.6 and brine volume that averaged 29 ± 6%, did not significantly change ($p = 0.241$) (Figure 4.6a). As a result, the ratio of brine to bulk salinity in the bottom 0-5 cm of sea ice was also stable over the season at 3.1 ± 0.6 ($p = 0.516$). However, seasonal warming drove an increase in brine volume throughout the ice profile over the sampling period (Fig 4.6b).

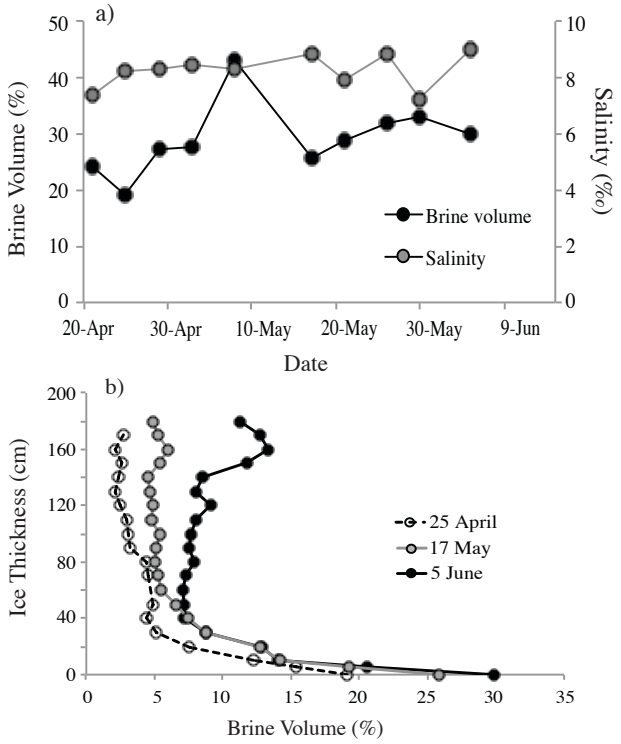

Figure 4.6. Bulk salinity and brine volume over the spring sampling period in the bottom 5 cm of sea ice (a) and brine volume profile from the ocean-ice interface (0 cm) to air-ice interface on 17 May, 25 April and 5 June. Values are from ice under thin snow cover.

4.3.2 Chlorophyll *a*, carbon and nitrogen

Bottom-ice chl *a* increased over the study from 6.1 to 10.5 mg m^{-2} under thin snow ($r = 0.682$, $p < 0.05$), and 4.0 to 11.7 mg m^{-2} under thick snow ($r = 0.451$, $p = 0.141$) (Figure 4.7a). The maximum concentration of bottom-ice chl *a* under thin snow at 10.5 mg m^{-2} occurred on 9 June at end of the time series, while maximum chl *a* under

thick snow occurred prior to this date on 30 May. The concentration of chl *a* in the bottom-ice was not statistically different following a student's t-test ($t_{12} = 1.297$, $p = 0.116$) between thin and thick snow covers, with average values of 6.25 ± 3.1 mg m^{-2} and 5.36 ± 3.5 mg m^{-2}, respectively.

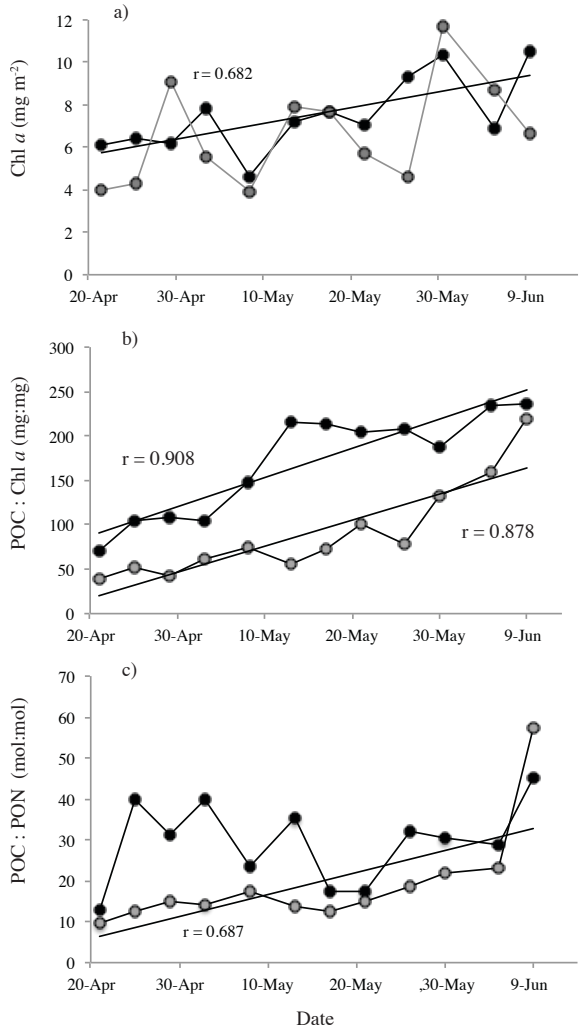

Figure 4.7. Seasonal changes in (a) bottom-ice chlorophyll *a* (chl *a*), (b) ratios of particulate organic carbon (POC) to chl *a*, and (c) POC to particulate organic nitrogen (PON), under thin (black) and thick (grey) snow covers. Significant (solid line) ($p < 0.05$) seasonal trends are also indicated, with associated correlation coefficients.

Particulate organic carbon to chl *a* ratios increased linearly over the study from 70.2 to 235 (average 169 ± 58.6) under thin snow (r = 0.908, p < 0.05) and 29.2 to 218.6 (averaged 90.3 ± 54) under thick snow (r = 0.878, p < 0.05) (Figure 4.6b). Under thin snow these ratios were highly correlated with T_{PAR} following Pearson correlation analysis, followed by NO_x (r = -0.619) and PO_4 (r = 0.589) concentrations in the ice (Table 4.1). The ratio of POC:chl *a* was also highly correlated with T_{PAR} under thick snow (r = 0.716), followed by PO_4 (r = 0.699) and $Si(OH)_4$ (r = 0.697) concentrations in the ice.

Table 4.1. Pearson correlation coefficients (top) and *p*-value (bottom) of particulate organic carbon (POC) to chlorophyll *a* (chl *a*) and POC to particulate organic nitrogen (PON) ratios with environmental variables chl *a*, ice thickness (H_I), snow depth (H_s) and transmittance of photosynthetically active radiation (T_{PAR}), for thin and thick snow cover separately and grouped together. Missing data is excluded pairwise and significance (p < 0.05) is indicated in bold. The number of observations for each parameter is 12, except for T_{PAR} where the outliers from 5 and 9 June are omitted (n = 8).

		Nutrients			Environmental variables			
		PO_4	NO_x	$Si(OH)_4$	Chl *a*	H_I	H_S	T_{PAR}
Thin	POC:chl *a*	**0.589** **0.044**	**-0.619** **0.032**	0.469 0.124	**0.513** **0.088**	**0.796** **0.002**	0.406 0.191	**0.835** **0.01**
	POC: PON	0.374 0.231	0.341 0.279	0.398 0.200	0.448 0.144	0.125 0.698	0.168 0.602	-0.373 0.362
Thick	POC:chl *a*	**0.699** **0.011**	-0.487 0.109	**0.697** **0.012**	0.344 0.274	**0.739** **0.006**	0.090 0.782	**0.716** **0.046**
	POC: PON	0.462 0.130	-0.411 0.184	**0.660** **0.020**	0.158 0.623	0.422 0.172	0.039 0.905	0.474 0.235
Thin & Thick	POC:chl *a*	**0.712** **0**	**-0.612** **0.001**	**0.560** **0.004**	**0.447** **0.029**	**0.809** **0**	0.376 0.070	**0.786** **0**
	POC: PON	**0.510** **0.011**	0.302 0.152	**0.542** **0.006**	0.322 0.124	**0.4017** **0.048**	**0.301** **0**	0.135 0.617

The ratio of POC to PON averaged 29.5 ± 10 under thin snow and did not exhibit any seasonal trend (r = 0.221, p = 0.491). However, POC:PON under thick snow significantly increased (r = 0.687, p < 0.05) over the sample period, averaging 19.3 ± 12.7 (Figure 4.7c).

Both ratios of POC:chl *a* ($t_{12} = -6.093$, $p < 0.05$) and POC:PON ($t_{12} = -3.158$, $p < 0.05$) were significantly higher under thin than thick snow cover. When combining all data from both snow covers there were significant ($p < 0.05$) correlations between POC:chl *a* with T_{PAR} ($r = 0.786$), PO_4 ($r = 0.712$), NO_x ($r = 0.612$), $Si(OH)_4$ ($r = 0.560$) and chl *a* ($r = 0.447$), and between POC:PON and PO_4 ($r = 0.510$), as well as NO_x ($r = 0.342$) (Table 4.1).

4.3.3 Bacterial production

Bacterial production was not significantly different between thin and thick snow ($t_{12} = -0.318$, $p = 0.757$). Estimates were low throughout the spring and averaged approximately $1.7 \times 10^{-7} \pm 1 \times 10^{-7}$ g C l^{-1} h^{-1} over the season for both snow covers (data not shown).

4.3.4 Photosynthesis-irradiance parameter response

Photosynthesis-irradiance parameters calculated over the sampling period for thin and thick snow are shown in Figure 4.8. The estimates of P^B_s and E_s increased linearly over the spring, which were significant ($p < 0.05$) except for P^B_s under thin snow cover ($p = 0.103$). We note that the estimate of P^B_s on 5 June under thin snow was exceptionally high at 1.01 mg C chl a^{-1} h^{-1}, and as a result it, along with the derived E_s (72.6 μmol photons m^{-2} s^{-1}), has not been included in assessments hereafter. The α^B of samples under thin snow appeared to increase until 8 May, after which estimates decreased until the end of sampling on 9 June. This trend was also evident for P_0 under thin and thick snow however, only an exponential decline of α^B under thin snow was significant ($p < 0.05$).

Finally, α^B for samples of thick snow cover and all E_c estimates remained constant over the spring and did not significantly change.

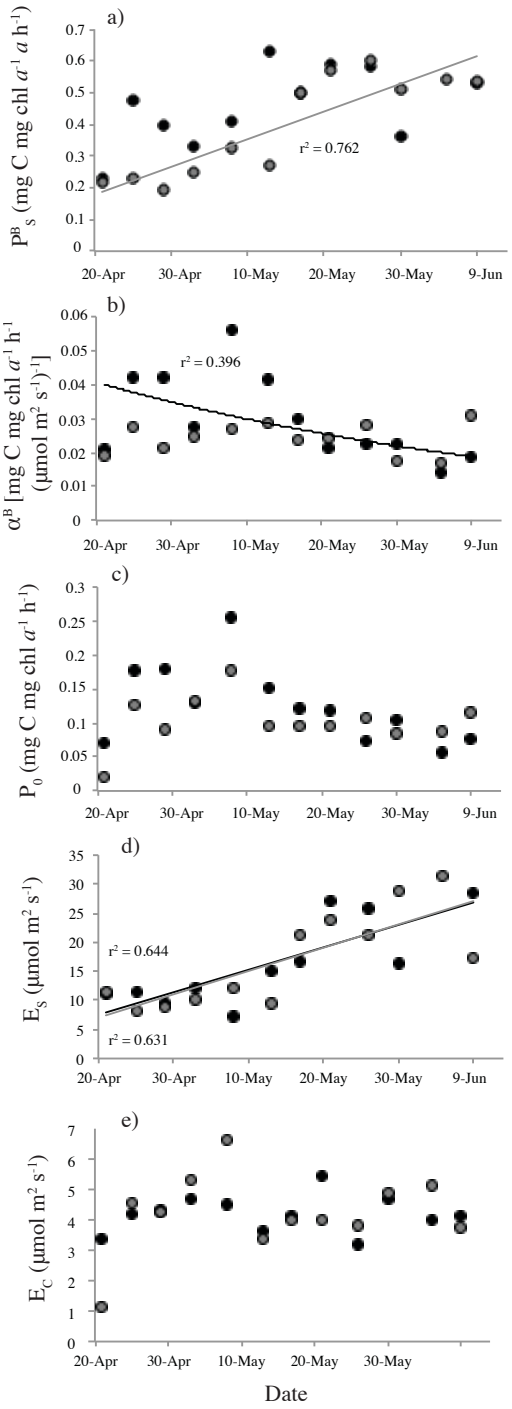

Figure 4.8. Photosynthetic parameters P^B_s (a), α^B (b), P_0 (c), E_s (d) and E_c (e) of ice algae under thin (black) and thick (grey) snow covers (*see* text for definitions). Significant (solid line) ($p < 0.05$) seasonal trends are also indicated, with associated correlation coefficients.

The similarity of photosynthesis-irradiance parameter response between snow cover types in Figure 4.8 is supported by student's paired t-tests, where parameters from thin and thick snow were not found to be significantly different: P^B_s ($t_{11} = -1.701$, $p = 0.120$), α^B ($t_{12} = -1.740$, $p = 0.110$), P_0 ($t_{12} = -1.875$, $p = 0.088$), E_s ($t_{11} = -0.376$, $p = 0.715$), and E_c ($t_{12} = 0.124$, $p = 0.904$). As a result, Photosynthesis-irradiance from thin and thick snow covers have been grouped together for assessments hereafter. Following this grouping of data, only the linear increases in P^B_s ($n = 22$, $r = 0.692$) and E_s ($n = 22$, $r = 0.798$) have significant trends over the sampling period ($p < 0.05$).

The correlations between photosynthesis-irradiance parameters and environmental parameters are summarized in Table 4.2. The negative correlation between E_s and P_0 ($r = -0.415$) was significant, indicating that the rate of carbon production in darkness, decreased when E_s increased. In addition, P_0 demonstrated a significant positive correlation with the α^B ($r = 0.873$) and E_c ($r = 0.514$).

Table 4.2. Pearson correlation coefficients (top) and significance (middle) of photosynthesis-irradiance (see text for definitions) and environmental parameters including chlorophyll *a* (chl *a*), snow depth (H_s) and transmittance of photosynthetically active radiation (T_{PAR}), for samples of thin and thick snow covered ice collectively, except for correlations between I_s and P^B_s or α^B due to co-linearity. Missing data is excluded pairwise and relationships of significance ($p < 0.05$) are highlighted with bold text. The number of observations for each correlation is also indicated (bottom).

		Photosynthesis-Irradiance Parameters					Nutrients			Environmental		
		P^B_s	α^B	P_0	E_s	E_c	PO_4	NO_x	$Si(OH)_4$	Chl *a*	H_S	T_{PAR}
Photosynthesis-Irradiance Parameters	P^B_s		0.1 0.650 23	0.071 0.742 23		0.074 0.736 23	**0.539** **0.008** **23**	**-0.525** **0.01** **23**	0.366 0.085 23	0.270 0.213 23	0.086 0.697 23	**0.661** **0.005** **16**
	α^B			**0.873** **0** **24**		0.042 0.846 24	0.169 0.430 24	-0.004 0.984 24	0.196 0.359 24	-0.382 0.065 24	-0.367 0.078 24	0.232 0.388 16
	P_0				**-0.415** **0.049** **23**	**0.514** **0.010** **24**	0.163 0.447 24	-0.151 0.480 24	0.275 0.193 24	-0.332 0.112 24	-0.359 0.085 24	0.261 0.329 16
	E_s					0.115 0.600 23	**0.439** **0.036** **23**	-0.394 0.063 23	0.236 0.279 23	**0.541** **0.008** **23**	0.307 0.154 23	0.495 0.051 16
	E_c						0.110 0.610	-0.358 0.085	0.259 0.221	0.080 0.709	-0.084 0.696	0.178 0.509

The strongest correlation between P^B_s and environmental parameters was T_{PAR} (Table 4.2), followed by the positive correlation with PO_4 and negative correlation with NO_x concentration. In addition, PO_4 was positively correlated with E_s, which was also correlated with chl *a*.

4.4 Discussion

4.4.1 Seasonality of nutrients in sea ice

The availability of nutrients depends on the location of algae in the bottom-ice and the resulting proximity to brine or interface water, where the largely sedentary cells can only access nutrients in direct contact. The majority of algae in this study were concentrated in the bottommost millimeter of ice (pers. obs., Campbell) and, as a result, there is uncertainty using bulk measurements from the entire 0-5 cm core section to assess nutrient conditions for the algal community. Nevertheless, bulk nutrients provide a proxy of nutrient availability in the ice and are used here to assess potential nutrient limitation.

The concentrations of PO_4 and $Si(OH)_4$ in this study are within the range of 0.26 – 5.5 μmol l^{-1} PO_4 [Riedel et al., 2008] and 0.6 – 3.83 μmol l^{-1} $Si(OH)_4$ [Hsaio et al., 1988; Galindo et al., 2014] that are reported for bottom-ice bulk nutrients in the Canadian Arctic during spring. However, NO_x concentrations were considerably lower than that reported elsewhere in the Canadian Arctic during the ice algal bloom [Hsaio et al., 1988; Galindo et al., 2014] and are more representative of a nitrogen limited ice environment such as that found in some Greenland fjords at < 2.5 μmol l^{-1} [Mikkelsen et al., 2008; Kaartokallio et al., 2013]. Furthermore, the average NO_x concentration at the ice-ocean interface in this study (Figure 4.5) is more representative of nitrate concentrations in the

western Canadian basin's winter surface waters [Tremblay et al., 2015] than elsewhere in the Canadian Arctic [Michel et al. 2006]. In comparison, the average concentrations of PO_4 and $Si(OH)_4$ at the ice interface (Figure 4.5) were within ranges reported for spring in the Canadian Arctic [Riedel et al., 2008; Różańksa et al., 2009].

Bottom ice nutrients often decrease over the ice algal bloom as nutrient demand surpasses supply [e.g. Lee et al., 2008 and Mikkelsen et al., 2008] from the surface waters [Cota et al., 1987]. A decrease in NO_x concentration was observed with increasing chl *a* biomass in this study; however, the concentrations of PO_4 and $Si(OH)_4$ largely increased (Figure 4.4). Positive relationships between nutrient versus chl *a* concentrations have led to the suggestion that ice algae potentially store intracellular nutrients [Cota et al. 1990; Pineault et al. 2013]. Indeed a significant positive relationship was observed between PO_4 and chl *a* in our study ($r = 0.605, p < 0.05$).

4.4.2 Nitrogen limitation in Dease Strait

The limited exchange of surface waters in Dease Strait with neighboring water bodies [McLaughlin et al., 2004] suggests that freshwater from ice melt and surrounding rivers (*see* Figure 4.1) may accumulate in the region. This process would contribute to the low interface salinities that were observed throughout spring, which averaged 28.1 ± 0.2, compared to elsewhere in the Arctic. Low surface water exchange caused by a more stable halocline would limit the re-supply of new nutrients and lead to depletion of regional nutrient inventories overtime. However, nutrient limitation from stratification of low salinity ice melt and runoff water was present in this study only after 27 May, as indicated by a sharp decrease in salinity of the surface waters in CTD profiles (data not

shown). Potential inflow from the Beaufort Sea in the west could also contribute to low salinities and nutrient concentrations observed in the region, as salinities in the surface mixed layer of the Beaufort Sea are relatively fresh at 27-30 [Jackson et al., 2011] and low in nitrogen at 0.1 to 5 μmol l^{-1} [Tremblay et al., 2015].

Turbulence in the upper water column enhances the flux of nutrients into the bottom-ice [Cota et al., 1990]; however, weak current velocities were observed at the ice interface throughout this study at 2.1 ± 1.2 cm s^{-1} (B. Else pers. comm.). Therefore, mixing to alleviate stratification in late spring and enhance nutrient flux throughout the sampling period was limited. Competition for nutrients between ice algae and phytoplankton was not likely a factor in this study, as chl *a* biomass of sub-ice phytoplankton between the interface and 5 m depth was very low at 0.24 ± 0.01 μg l^{-1}. From this assessment we suggest that the nitrogen limitation in the study area was due to the combined influence of: limited replenishment of new nutrients from surrounding water masses, weak sub-ice turbulence and stratification during late spring.

4.4.3 Light versus nutrient limitation

Low estimates of POC:PON and POC:chl *a* are characteristic of algae that are acclimated to very low light intensities [Harrison et al., 1977; Droop et al., 1982; Michel et al., 1996], whereas high ratios of POC:PON and POC:chl *a* in ice algae can indicate the presence of nutrient limitation [Demers et al., 1989; Gosselin et al., 1990]. Indeed, lower POC:PON and POC:chl *a* ratios under thick versus thin snow in our study suggest *a greater* influence of light limitation under the thick*er* snow cover. The lower estimates under thick snow also support an inverse relationship between ice algal POC:chl *a* and

POC:PON ratios with snow thickness that have been documented previously [Arrigo et al., 2013; Niemi & Michel, 2015]. However, seasonal changes in POC:PON were not correlated with light transmittance (Table 4.1) and estimates were high, often exceeding the Redfield average of 6.6 and the range of 3 to 24 that has been reported for sea ice in the spring [Gosselin et al., 1990; Niemi and Michel, 2015]. This indicates that nitrogen limitation was likely of greater significance than light on POC:PON composition ratios. Further supporting the presence of nitrogen limitation are average bottom-ice molar nutrient ratios of NO_x to PO_4 (N:P) and NO_x to $Si(OH)_4$ (N:Si) that were well below the Redfield composition of phytoplankton at 1.07 N:P and 16 N:Si, at 0.20 ± 0.19 and 0.20 ± 0.15 under thin snow, and 0.62 ± 0.83 and 0.42 ± 0.43 under thick snow, respectively.

Particulate carbon to chl *a* ratios reported in this study are within the 5 to 263 mg:mg range reported for sea ice by Nozais et al. [2001]. The significant positive relationship of POC:chl *a* versus light transmittance suggests the ice algae were acclimating to increasing T_{PAR} over time, where the abundance of chl *a* per cell decreases with increasing bottom-ice light intensity [Gosselin et al., 1990]. However, the significant negative relationship between POC:chl *a* and NO_x also suggests an additional influence of nitrogen limitation on the seasonal increase of POC:chl *a* ratios over time, as NO_x limitation should increase with increasing chl *a* biomass and production. These contrasting results support a dual limitation of light and nutrients on ice algal growth. In their ice algal growth model, Lavoie et al. [2005] showed that during night when solar angle is low, light limitation can occur under the snow-covered sea ice, whereas at peak daylight, rapid growth can lead to nutrient limitation due to a finite supply from the water column. Such a condition was

expected to occur in our dataset, which was intensified under thick snow covers due to a longer light-limited period over a diel cycle.

To evaluate this idea we calculated daily estimates of *in situ* production for thin and thick snow covers using daily-integrated estimates of under-ice PAR [Figure 4.9]. Estimates of under-ice PAR for this analysis were obtained by applying the average percent transmittance measured at thin (2.2%) and thick (1.7%) sites over the spring (Section 4.3.1), to hourly averaged downwelling surface PAR recorded at a nearby meteorological tower (μmol photons m^{-2} s^{-1}, *Kipp & Zonen PAR-Lite*) on, or within, ± 3 days of ice core extraction dates (except for 21-April as meteorological measurements did not begin until 26-April). From this assessment the average diurnal production was significantly greater ($t_{11} = 2.389$, $p = 0.038$) under thin snow, which had a higher average production of 1.7 mg C mg chl a^{-1} versus 1.1 mg C mg chl a^{-1} under thick snow (Figure 4.9). This supports studies that have documented inverse relationships between primary production and snow depth as a result of greater light transmission under thin snow cover [Welch and Bergmann 1989; Rysgaard et al., 2001]. The difference in productivity and NO_x concentrations between snow covers also supports our idea that nutrient-limitation of ice algae varies spatially, where higher POC:chl *a*, POC:PON and *in situ* production estimates under thin snow (Figure 4.9) collectively suggest greater NO_x limitation than under thick snow.

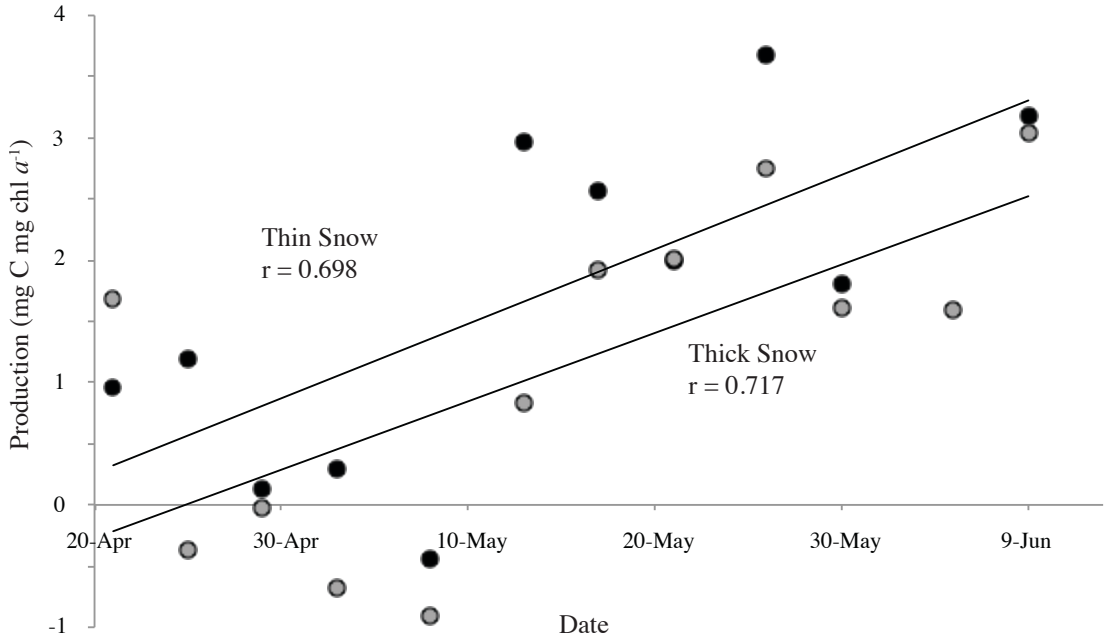

Figure 4.9. Estimates of daily-integrated production of sea ice algae under thin (black) and thick (grey) snow covers. Linear trend lines for production over the sampling period are also indicated.

The bottom-ice algae in this study were predominantly species of diatoms (pers. observ., Campbell) that would have been heavily dependent on silica to form their frustules. The seasonal increase in composition ratios, as a result of changing nitrogen and light conditions, with $Si(OH)_4$ (Table 4.1), are therefore likely due to coincident increases in silica uptake and subsequent leakage into the bottom-ice environment by diatoms. This explanation may also apply to the significant positive relationships between algal composition and PO_4 (Table 4.1), as diatoms are known to accumulate intracellular stores of phosphorus under conditions of nitrogen starvation [Harrison et al., 1977].

4.4.4 Measuring photosynthetic-irradiance response using optodes

Published production and photosynthetic parameters of algae have mainly been calculated from ^{14}C-incubations, but measurements of O_2 exchange have also been used [Geider and

Osborne, 1992]. Both approaches have advantages and limitations, and comparison of ice algal production from these methods has provided variable results [e.g. McMinn and Hegseth 2007; Rysgaard et al., 2001; Glud et al. 2002]. A detailed discussion on the strengths and weaknesses of these methods is beyond the scope of this paper. However, we will briefly assess how differences between our optode setup and traditional ^{14}C methods could have influenced parameter estimates, including: incubation time, the maximum light intensity and the use of four data points in the modeling of PI curves.

All of the incubations in this study showed linear trends of oxygen production or consumption over the 70 h incubation time (Figure 4.3a, b), indicating that factors such as meiofauna consumption of algae and changes in algal physiology that would have produced non-linear responses, were not significant. Low bacterial production in this study (*see* Section 4.3.1) also indicates that error in the calculation of photosynthetic rates from bacterial consumption of oxygen was minimal.

The maximum light intensity in optode incubations of approximately 55 μmol photons m^2 s^{-1} was lower than the maximum intensity typically reached in ^{14}C incubations, which can exceed 100 μmol photons m^2 s^{-1} [Michel et al., 1988]. The result could have been an underestimate of parameters like P^B_s, if the asymptote was actually reached at stronger irradiances. To assess this potential error we compared our estimates of P^B_s with those modeled during five coincident 3h-^{14}C incubations (following methods of Legendre et al., [1983] & Babin, [1994]) that used 10 data points over irradiances up to about 200 μmol photons m^2 s^{-1} (Supplementary Material). We found no significant difference in P^B_s between the methods ($t_9 = -1.032$, $p = 0.332$), indicating that our estimates of maximum photosynthesis were appropriate (Table 4.S.2).

Finally, to investigate the potential dependence of parameters, particularly α^B, on the use of four data points when estimating PI curves, we fit the ^{14}C data (described above) using only the four data points closest to the average optode incubation light intensities of 0, 10, 21 and 55 μmol m^{-2} s^{-1}. We found that P^B_s and α^B parameters calculated from only four data points were significantly correlated with the full 10 data point estimates ($r > 0.9$, $p < 0.05$), and root mean squared errors were low around 0.29 mg C mg chl a^{-1} h^{-1} and 0.03 mg C mg chl a h^{-1} (μmol m^2 s^{-1})$^{-1}$, respectively (Table 4.S.2). This indicates that parameter estimates were not significantly influenced by the number of data points used in our study, because the correlation coefficients would have been much lower if the curves fit from four data points changed considerably. Furthermore, calculation of the standard deviation of optode derived production (i.e., data points on photosynthesis-irradiance curves) was very low, at < 1% of the presented values.

The optode-derived photosynthetic parameters in this study are further supported by comparison with estimates that have previously been reported for the Arctic. Specifically, all calculated parameters (Figure 4.9) are within documented ranges: P^B_s, 0.007 - 9.62 mg C [mg chl a]$^{-1}$ h^{-1}, α^B, 0.0002 - 2.15 mg C [mg chl a]$^{-1}$ h^{-1} [μmol photons m^{-2} s^{-1}]$^{-1}$, E_s, 2 - 222 μmol m^{-2} s^{-1} and E_c, 0.18 - 7.6 μmol m^{-2} s^{-1} [Cota, 1985; Gosselin et al., 1985; Bates and Cota, 1986; Irwin, 1990].

4.4.5 Photosynthesis-irradiance parameters under thin and thick snow cover

There was no statistical difference between the photosynthesis-irradiance of thin and thick snow cover in this study. Therefore, conditions between snow depths were not different enough to cause varied photophysiological responses, particularly given a

difference of only 0.5% T_{PAR} between thin and thick snow (see Section 4.3.1). These results suggest that the photoacclimative state of ice algae did not significantly vary with moderate changes (approximately 10 cm) in snow depth in this study. Although, we acknowledge that the movement of snow drifts and resulting unknown snow depth history of sampling sites adds uncertainty to these insights.

Similar to this study, comparable photosynthesis-irradiance responses of algae simultaneously collected from ice covered by a range of snow depths have been documented [Cota and Horne, 1989]. However, significant differences in the photophysiological state of ice algae following snow removal experiments can occur. For example, higher maximum photosynthetic rates (i.e. P^B_s) and lower α^B for algae have been recorded under snow-cleared ice compared to snow-covered ice [Cota, 1985; Cota and Horne, 1989]. It follows that spatial differences in ice algal photophysiology are likely caused by more extreme changes in snow cover (i.e. light intensity) than observed naturally in our study area.

4.4.6 Seasonal response of photosynthesis-irradiance to local environmental controls

Maximum photosynthetic rate

At saturating light intensities above E_s, the maximum rate of photosynthesis is controlled by the rate of carbon fixation and electron transport in the cell. The P^B_m can therefore be summarized as:

$$P_m^B = \frac{1}{T} \times N^{PSU} \quad (4.1)$$

where T is the time require for electron transfer between water splitting and CO_2 fixation, and N^{PSU} represents the size of the photosynthetic unit, which includes all catalysts and compounds required for the flow of electrons [Geider and Osborne, 1992]. The time of electron transfer increases with light exposure [Barlow et al., 1988] and temperature [Arrigo & Sullivan, 1992], while N^{PSU} increases with the density of photosynthetic reaction centers, electron carriers and pigments [Barlow et al., 1988].

It follows that P^B_m or P^B_s could increase over the spring with light intensity (Figure 4.4) due to increased electron flow, or the resulting increased availability of products formed in the light reactions of photosynthesis that contribute to N^{PSU} [Barlow et al., 1988]. These seasonal responses can explain the increase in P^B_s over the spring that was observed in this study, where the influence of light was particularly important given the significant correlation of P^B_s with T_{PAR} (Table 4.2). The coincident seasonal increases of P^B_s and T_{PAR} indicate that the potential for primary production is greatest late in the spring owing to relatively high light availability and the photoacclimative state of the ice algae. If ice algae were not capable of changing P^B_s over the spring, light saturation would likely occur at lower intensities and the level of primary production achieved would be smaller. For example, if we apply the estimate of P^B_s from 21 April (early spring) to the daily production equation and under-ice downwelling intensities of 9 June (late spring), we find a 50% and 70% decrease in primary production under thin and thick snow covers, respectively.

The activity of photosynthetic enzymes is temperature dependent and can also increase P^B_m and P^B_s [Michel et al., 1988; Arrigo & Sullivan, 1992]. However, the bottom-ice environment remained close to freezing temperatures and thus increases in P^B_s with

bottom-ice temperature were not significant under thin (r = 0.216, p = 0.577) or thick snow (r = 0.173, p = 0.632) in this study. Maximum photosynthetic rates are also affected by nutrient availability, which ensure the elements required to build photosynthetic products are available in the cell [Cota & Horne, 1989]. Although the sea ice environment was affected by nitrogen limitation, the negative correlation between P^B_s and NO_x concentrations indicates that it was not a significant influence (Table 4.2). These results are in contrast to the positive relationship between nutrient supply and P^B_m reported by Cota and Horne [1989], and instead highlight that light availability was the dominant factor controlling seasonal P^B_s in this study.

Photosynthetic efficiency

At sub-saturating light intensities (i.e. below E_s), algal production is controlled by the rate of light absorption and its conversion to chemical energy. In turn the α^B may be described as:

$$\alpha^B = a^* \times \phi_m \quad (4.2)$$

where a^* is the chl a-specific absorption coefficient, also referred to as the cross sectional absorption, and ϕ_m is the maximum photon yield of photosynthesis that is representative of the mols of oxygen produced or CO_2 consumed by a sample per mol of photons that is absorbed [Geider & Osborne, 1992]. From this definition we can see that changes to a^* and, or ϕ_m will affect the photosynthetic efficiency that is measured.

One of the greatest influences on a^* is a pigment packaging effect, where absorption of light by chl a is lower than the absorption potential of chl a in solution (reduced a^*) due to intracellular self-shading. Typically the pigment packaging effect increases with

increasing chl *a* per cell, which is a characteristic acclimation strategy of ice algae to low light intensities [Perry et al., 1981; Gosselin et al., 1990]. The ϕ_m is affected by photoprotective mechanisms like the abundance of photoprotective pigments that decrease the amount of absorbed photons used in photosynthesis (decreasing ϕ_m) [Arrigo et al., 2010], as well as the efficiency of the carboxylation step in photosynthesis (increasing ϕ_m) [Michel et al., 1988; Arrigo & Sullivan, 1992]. As a result of these potentially competing influences, the α^B of algae can increase with *in situ* light intensity [Arrigo et al., 2010], decrease [Perry et al., 1988], or show no association [Michel et al., 1988].

The decrease of α^B under thin snow in this study indicates that ϕ_m could have been reduced from photoprotective mechanisms developed to withstand the greater light intensities of late spring. Although, we note that α^B was not correlated specifically with T_{PAR} ($r = 0.03$, $p = 0.944$), and the melt season that typically brings a large increase in PAR transmission through the ice [Campbell et al., 2015] did not occur. Decreasing NO_x concentrations over the sample period could have also contributed to the decline that was observed (Figure 4.4), as nutrient limitation can reduce estimates of α^B [Cota & Horne, 1989]. However, α^B was also not significantly correlated with ice NO_x concentrations ($r = 0.390$, $p = 0.210$). These findings, in addition to the lack of change in α^B under thick snow, illustrate the complexity of α^B response in sea ice algae and highlight the need for future investigations into the causes of α^B variability.

Parameter of photoacclimation

The photoacclimation parameter (E_s) defines the irradiance at which the dominant limitation on production shifts between the efficiency of light harvesting, and the efficiency of carboxylating steps of photosynthesis. The increase in E_s over the spring that was observed in this study (Figure 4.8) has been documented previously for ice algae, and was a result of increasing light intensity [Gosselin et al., 1985]. The strong correlation between I_s and T_{PAR} that was observed here supports this conclusion (Table 4.2).

Minimum light for photosynthesis and production in darkness

The P_0 and E_c parameters did not significantly change over the study period, indicating that they were largely independent of the environmental factors that were assessed. For example, it is unlikely that algal respiration changed with the photo-physiological state of the algae because an increase in P_0 with T_{PAR} over the spring would have been documented. Furthermore, the minimum light intensity required for photosynthesis (E_c) did not change with light exposure or nutrient concentrations over the spring.

The decline of oxygen concentration in black bottles over the duration of all optode experiments (e.g., Figure 4.3a, b), rather than zero net change, indicates that respiration by a combination of algae and bacteria was significant in all experiments. Bacterial production was low in this study, and was not significantly different between thin and thick snow covers (Section 3.3.3). Also, the average contribution of ^{3}H-leucine derived BP to P_0 was negligible under both thin and thick snow. This contrasts observations that oxygen consumption from bacterial production typically increases with algal activity, as primary production was significantly greater under thin snow (Figure 4.9) [Smith &

Clement, 1990; Ducklow, 2003]. It is beyond the scope of this study to investigate the dependence of bacteria on snow cover, but our results show that photo-stimulus of bacterial production [e.g. Church et al., 2004] that would have occurred under the higher light environment of thin snow, was likely not a factor.

Bacterial respiration would have also contributed to production in the dark bottle, but the influence of bacteria is still likely to be much less than algal respiration. Falkowski and Owens [1978] report a possible range of marine phytoplankton respiration from 10 to 41% of maximum algal photosynthesis, which includes the value of 35% measured by Suzuki et al. [1997] for ice algae in the Canadian Archipelago. Our study's P_0:P^B_s ratios all largely fall within this reported range under thin (average 30.8%) or thick (average 30.3%) snow covers. These ratios also decreased over the spring under thin ($r^2 = 0.369$, $p = 0.047$) and thick snow cover ($r^2 = 0.282$, $p = 0.070$), as a result of relatively constant P_0 but increasing P^B_S (Figure 4.8).

4.5 Conclusions

Oxygen optodes were used in this study to assess changes in the photosynthesis-irradiance response of sea ice algae under thin and thick snow during the spring bloom. Comparison of calculated Photosynthesis-irradiance for algae under thin and thick snow covers showed no statistically significant difference. The strongest changes in PI response documented over the spring were significant increases in P^B_s and E_s parameters, which were largely in response to seasonally increasing percent PAR transmittance. These observations highlight that although differences in PAR values did not appear to be a primary factor in causing spatial differences in Photosynthesis-irradiance from different

snow covers, they were significant in driving seasonal changes in ice algal photophysiology. Seasonally increasing light intensity was also an important influence on algal physiology, as seen in the increasing ratios of POC:chl *a* over the spring.

Nitrogen limitation was also evident in this study from very low NO_x concentrations in sea ice and interface water, low N:P and N:Si ratios and elevated POC:PON ratios throughout the spring. Nitrogen limitation appeared to influence algal Photosynthesis-irradiance, likely resulting in a decrease of P^B_s, α^B and E_s. However, a co-limitation by light was evident over a diurnal period as demonstrated by greater production under thin snow compared to that of thick, which in turn led to greater nutrient stress on the ice algae community.

Acknowledgements

The authors would like to recognize the support from a Northern Scientific Training Program grant and Natural Sciences and Engineering Research Council of Canada (NSERC) Canadian Graduate Scholarship to KC, Canada Foundation for Innovation (CFI) and the Canada Excellence Research Chair grant to SR, an NSERC Discovery and Northern Research Supplement Grants to CJM, and in-kind support from the Canadian High Arctic Research Station (CHARS). They also wish to thank Drs. Michel Gosselin, Brent Else, John Iacozza, as well as Megan Shields and Marjolaine Blais for their support. This work represents a contribution to the research programs of ArcticNet, the Arctic Science Partnership (ASP) and the Canada Excellence Research Chair unit at the Centre for Earth Observation Science (CEOS) at the University of Manitoba.

References

Arrigo, K.R., Brown, Z.W., and M.M. Mills (2013), Sea ice algal biomass and physiology in the Amundsen Sea, Antarctica, *Elementa: Sci. Anth. 2*, doi: 10.12952/journal.elementa.000028.

Arrigo, K.R., Mills, M.M., Kropuenske, L.R., van Dijken, G.L., Alderkamp, A.-C., and D.H. Robinson (2010), Photophysiology in two major southern ocean phytoplankton taxa: Photosynthesis and growth of Phaeocystis Antarctica and Fragilariopsis cylindrus under different irradiance levels, *Integ. Comp. Biol.* 50(6), 950-966, doi: 10.1093/icb/icq021.

Arrigo, K.R., and C.W. Sullivan (1992), The influence of salinity and temperature covariation on the photophysiological characteristics of Antarctic sea ice microalgae, *J. Phycol.* 28, 746-756, doi: 10.1111/j.0022-3646.1992.00746.x.

Babin, M. (1994), An incubator designed for extensive and sensitive measurements of phytoplankton photosynthetic parameters, *Limnol. Oceanogr.* 39(3), 694-702, doi: 10.4319/lo.1994.39.3.0694.

Bagshaw, E.A., Wadham, J.L., Mowlem, M., Tranter, M., Eveness, J., Fountain, A.G., and J. Telling (2011), Determination of dissolved oxygen in the Cryosphere: A comprehensive laboratory and field evaluation of fiber optic sensors, *Environ. Sci. Technol.* 45, 700-705, doi: 10.1021/es102571j.

Barlow, R.G., Gosselin, M., Legendre, L., Therriault, J.-C., Demers, S., Mantoura, R.F.C., and C.A. Llewellyn (1988), Photoadaptive strategies in sea ice microalgae, *Mar. Ecol. Prog. Ser.* 45, 145-152.

Bates, S.S., and G.F. Cota (1986), Fluorescence induction and photosynthetic responses of Arctic ice algae to sample treatment and salinity, *J. Phycol.* 22, 421-429.

Brown, K.A., Miller, L.A., Mundy, C.J., Papakyriakou, T., Francois, R., Gosselin, M., Carnat, C., Swystun, K., and P.D. Tortell (2015), Inorganic carbon system dynamics in landfast Arctic sea ice during the early-melt period, *J. Geophys. Res. Oceans* 120, 3542-3566, doi:10.1002/2014JC010620.

Campbell, K., Mundy, C.J., Barber, D.G., and M. Gosselin (2014), Remote estimates of ice algae biomass and their response to environmental conditions during spring melt, *Arctic* 67, 375-387, doi: 10.14430/arctic4409.

Campbell, K., Mundy, C.J., Barber, D.G., and M. Gosselin (2015), Characterizing the sea ice algae chlorophyll a–snow depth relationship over Arctic spring melt using transmitted irradiance, *J. Mar. Syst.* 147, 76-84, doi: 10.1016/j.jmarsys.2014.01.008.

Church, M.J.H., Ducklow, W., and D.M. Karl (2004), Light dependence of [3H] leucine incorporation in the oligotrophic North Pacific Ocean, *Appl. Environ. Microbiol.* 70,

4079-4087, doi: 10.1128/AEM.70.7.4079-4087.2004.

Cota, G.F. (1985), Photoadaptation of high Arctic ice algae, *Lett. Nature* 315, 219-222.

Cota, G., Anning, J., Harris, L., Harrison, W., and R.E.H. Smith (1990), Impact of ice algae on inorganic nutrients in seawater and sea ice in Barrow Strait, N.W.T, during spring, *Can. J. Aquat. Sci.* 47(7), 1402-1415, doi: 10.1139/f90-159.

Cota, G., and E. Horne (1989), Physical control of arctic ice algal production, Mar. Ecol. Prog. Ser. 52, 111-121.

Cota G.F., Prinsenberg, S.J., Bennett, E.B., Loder, J.W., Lewis, M.R., Anning, J.L., Watson, N.H.F., and L.R. Harris (1987), Nutrient fluxes during extended blooms of Arctic ice algae, *J. Geophys. Res.* 92(C2), 1951-1962.

Cota, G., and R.E.H. Smith (1991), Ecology of bottom ice algae: III, *Compar. Phys. J. Mar. Syst.* 2, 297-315.

Cox, G.F.N., and W.F. Weeks (1983), Equations for determining the gas and brine volumes of in sea-ice samples, *J. Glaciol.* 29, 306-316.

Demers, S., Legendre, L., Maestrini, S.Y., Rochet, M., and R.G. Ingram (1989), Nitrogenous nutrition of sea-ice microalgae, *Polar Biol.* 9, 377-383.

Droop, M.R., Mickelson, M.J., Scott, J.M., and M.F. Turner (1982), Light and nutrient status of algal cells, *J. Mar. Biol. Assoc. U.K.* 62, 403-434.

Ducklow, H.W. (2003), Seasonal production and bacterial utilization of DOC in the Ross Sea, Antarctica, *Biogeochem. Ross Sea*, 143-157, doi: 10.1029/078ARS09.

Else, B.G.T., Papakyriakou, T.N., Galley, R.J., Mucci, A., Gosselin. M., Miller, L.A., Shadwick, E.H., and H. Thomas (2012), Annual cycles of $pCO2_{sw}$ in the southeastern Beaufort Sea: New understandings of air-sea CO2 exchange in arctic polynya regions, *J. Geophys. Res.* 117, G00G13, doi:10.1029/2011JC007346.

Environment Canada. Water Office Historical Hydrometric Data. Web. 21 May, 2016. < http://wateroffice.ec.gc.ca>.

Falkowski, P.G., and T.G. Owens (1978), Effects of Light Intensity on Photosynthesis and Dark Respiration in Six Species of Marine Phytoplankton, *Mar. Biol.* 45, 289-295.

Fenchel, T., and R.N. Glud (2000), Benthic primary production and O_2-CO_2 dynamics in a shallow-water sediment: Spatial and temporal heterogeneity, *Ophel.* 52(2), 159-171, doi: 10.1080/00785236.2000.10409446.

Galindo, V., Levasseur, M., Mundy, C.J., Gosselin, M., Tremblay, J.-E., Scarratt, M., Gratton, Y., Papakiriakou, T., Poulin, M., and L. Lizotte (2014), Biological and physical processes influencing sea ice, under-ice algae and dimethylsulfoniopropionate during spring in the Canadian Arctic Archipelago, *J. Geophys. Res. Oceans* 119, doi:10.1002/2013JC009497.

Geider, R.J., and B.A. Osborne (1992), *Algal photosynthesis: The measurements of algal gas exchange*, Curr. Phycol. 2. Springer Science.

Glaz, P., Sirois, P., Archambault, P., and C. Nozais (2014), Impact of forest harvesting on trophic structure of Eastern Canadian Boreal Shield Lakes, Insights from stable isotope analysis, PLoS ONE 9(4), e96143, doi:10.1371/journal.pone.0096143.

Glud, R.N., Rysgaard, S., and M. Kühl (2002), A laboratory study on O_2 dynamics and photosynthesis in ice algal communities:quantification by microsensors, O_2 exchange rates, ^{14}C incubations and a PAM fluorometer, *Aquat. Microbiol. Ecol.* 27, 301-311.

Gosselin, M., Legendre, L., Therriault, J.-C., and S. Demers (1990), Light and nutrient limitation of sea-ice microalgae (Hudson Bay, Canadian Arctic), *J. Phycol.* 26, 220-232, doi: 10.1111/j.0022-3646.1990.00220.x.

Gosselin, M., Legendre, L., Demers, S., and R.G. Ingram (1985), Responses of sea-ice microalgae to climatic and fortnightly tidal energy inputs (Manitounuk Sound, Judson Bay), *Can. J. Fish. Aquat. Sci.* 42, 999-1006.

Gosselin, M., Levasseur, M., Patricia, A.W., Horner, R.A., and B.C. Booth (1997), New measurements of phytoplankton and ice algal production in the Arctic Ocean, *Deep-Sea Res.* 44(8), 1623-1644, doi: 10.1016/S0967-0645(97)00054-4.

Grenfell, T.C., and G.A. Maykut (1977), The optical properties of ice and snow in the Arctic basin, *J. Glaciology* 18(80), 445-463.

Harrison, P.J., Conway, H.L., Holmes, R.W., and C.O. Davis (1977), Marine diatoms grown in chemostats under silicate or Ammonium limitation III, Cellular chemical composition and morphology of Chaetoceros debilis, Skeletonema costatum and Thalassiosira gravida, *Mar. Biol. Berlin* 43, 19-31.

Holm-Hansen, O., Lorenzen, J., Holmes, R.W., and J.D. Strickland (1965), Fluorometric determination of chlorophyll, *ICES J. Mar. Sci.* 30, 3-15, doi:10.1093/icesjms/30.1.3.

Hsaio, S.I.C. (1988), Spatial and seasonal variations in primary production of sea ice microalgae and phytoplankton in Frobisher Bay, Arctic Canada, *Mar. Ecol. Progr. Ser.* 44, 275-285.

Irwin, B.D. (1990), Primary production of ice algae on a seasonally-ice-covered continental shelf, *Polar Biol.* 10, 247-254, doi: 10.1007/BF00238421.

Jackson, J.M., Allen, S.E., McLaughlin, F.A., Woodgate, R.A., and E.C. Carmack (2011), Changes to the near surface waters in the Canada Basin, Arctic Ocean from 1993–2009: A basin in transition, *J. Geophys. Res.* 116, C10008, doi: 10.1029/2011JC007069.

Kaartokallio, H., Søgaard, D.H., Norman, L., Rysgaard, S., Tison, J.L., Delille, B., and D.N. Thomas (2013), Short-term variability in bacterial abundance, cell properties, and incorporation of leucine and thymidine in subarctic sea ice, *Aquat. Microbiol. Ecol.,* 71, 57-73, doi: 10.3354/ame01667.

Kirchman, D.L. (1993), Chapter 58: Leucine incorporation as a measure of biomass production by heterotrophic bacteria, In: *Handbook of Methods in Aquatic Microbial Ecology*, 509-518.

Kirchmann, D. (2001), Chapter 12: Measuring bacterial biomass production and growth rates from leucine incorporation in natural aquatic environments, In: *Methods in Microbiology* 30, 227-237.

Lavoie, D., Denman, K., and C. Michel (2005), Modeling ice algal growth and decline in a seasonally ice-covered region of the Arctic (Resolute Passage, Canadian Archipelago), *J. Geophys. Res.* 110, C11009, doi: 10.1029/2005JC002922.

Lee, S.H., Whiteledge, T.E., and S.H. Kang (2008), Spring time production of bottom ice algae in the landfast sea ice zone at Barrow Alaska, *J. Exp. Mar. Biol. Ecol.* 367, 204-212, doi: 10.1016/j.jembe.2008.09.018.

Legendre, L., Ackley, S.F., Dieckmann, G.S., Gullicksen, B., Horner, R., Hoshiai, T., Melnikov, I.A., Reeburgh, W.S., Spindler, M., and C.W. Sullivan (1992), Ecology of sea ice biota: Part 2 Global significance, *Polar Biol.* 12, 429–444, doi: 10.1007/BF00243114.

Legendre, L., Demers, S., Yentsch, C.M., and C.S. Yentsch (1983), The 14C method: patterns of dark CO2 fixation and DCMU correction to replace the dark bottle, *Limnol. Oceanogr.* 28, 996-1003.

Leu, E., Mundy, C.J., Assmy, A., Campbell, K., Gabrielsen, T.M., Gosselin, M., Juul-Pedersen, T., and R. Gradinger (2015), Arctic spring awakening – Steering principles behind the phenology of vernal ice algae blooms, *Prog. Oceanogr.* 139, 151-170, doi: 10.1016/j.pocean.2015.07.012.

Leu, E., Wiktor, J., Soreide, J.E., Berge, J., Falk-Peterson, S., and J. Berge (2010), Increased irradiance reduces food quality of ice algae, *Mar. Ecol. Prog. Ser.* 411, 49-60, doi:10.3354/meps08647.

McLaughlin, F.A., Carmack, E.C., Ingram, R.G., Williams, W.J., and C. Michel (2004),

Oceanography of the Northwest Passage, In: Robinson, A.R., Brink, K.H. (eds), *The Sea*, President and Fellows of Harvard College, 1211-1242.

McMinn, A., and E.N. Hegseth (2007), Sea ice primary productivity in the northern Barents Sea, spring 2004, *Polar Biol*. 30, 289-294, doi: 10.1007/s00300-006-0182-x.

Michel, C., Ingram, R.G., and L.R. Harris (2006), Variability in oceanographic and ecological processes in the Canadian Arctic Archipelago, *Prog. Oceanog*. 71, 379-401, doi: 10.1016/j.pocean.2006.09.006.

Michel, C., Legendre, L., Demers, S., and J.-C Therriault (1988), Photoadaptation of sea-ice microalgae in springtime: photosynthesis and carboxylating enzymes, *Mar. Ecol. Progr. Ser*. 50, 177-185.

Michel, C., Legendre, L., Ingram, R.G., Gosselin, M., and M. Levasseur (1996), Carbon budget of sea-ice algae in spring: Evidence of significant transfer to zooplankton grazers, *J. Geophys. Res*. 101(C8), 18345-18360, doi: 10.1029/96JC00045.

Michel, C., Legendre, L., Therriault, J.-C., and S. Demers (1989), Photosynthetic responses of Arctic sea-ice microalgae to short-term temperature acclimation, *Polar Biol*. 9, 437-442.

Mikkelson, D.M., Rysgaard, S., and R.N. Glud (2008), Microalgal composition and primary production in Arctic sea ice: a seasonal study from Kobbefjord (Kangerluarsunnguaq), west Greenland, *Mar. Ecol. Prog. Ser*. 368, 65-74, doi: 10.3354/meps07627.

Miller, C.B., and P.A. Wheeler (2012), *Biological Oceanography*.Wiley Blackwell Publishing, Malaysia.

Mundy, C.J., Barber, D.G., Michel, C., and R.F. Marsden (2007), Linking ice structure and microscale variability of algal biomass in Arctic first-year sea ice using an in situ photographic technique, *Polar Biol*. 30, 1099-1114, doi: 10.1007/s00300-007-0267-1.

Niemi, A., and C. Michel (2015), Temporal and spatial variability in sea-ice carbon:nitrogen ration on Canadian Arctic shelves, *Elementa: Sci. Anthro*. 3(000078), doi:10.12952/journal.elementa.000078.

Nozais, C., Gosselin, M., Michel, C., and G. Tita (2001), Abundance, biomass, composition and grazing impact of the sea-ice meiofauna in the North Water, northern Baffin Bay, *Mar. Ecol. Prog. Ser*. 217, 235-250, doi : 10.3354/meps217235.

Parsons, T.R., Maita, Y., and C.M. Lalli (1984), *Manual of chemical and biological methods for seawater analysis*. Pergamon Press, New York.

Perry, M.J., Talbot, M.C., and R.S. Alberte (1981), Photoadaptation in marine phytoplankton: response of the photosynthetic unit, *Mar. Biol.* 62, 91-101.

Petrich, C., and H. Eiken, H. (2010), Growth, structure and properties of sea ice, In: Thomas D.N., Dieckmann G.S. (eds.), *Sea Ice*, 2nd Ed. Wiley Blackwell Publishing, Malaysia, 22-77.

Pineault, S., Tremblay, J.-E., Gosselin, M., Thomas, H., and E. Shadwick (2013), The isotopic signature of particulate organic C and N in bottom ice: Key influencing factors and applications for tracing the fate of ice-algae in the Arctic Ocean, *J. Geophys. Res. Oceans* 118, 287–300, doi:10.1029/2012JC008331.

Platt, T., Gallegos, C.L., and W.G. Harrison (1980), Photoinhibition of photosynthesis in natural assemblages of marine phytoplankton, *J. Mar. Res.* 38, 687–701.

Riedel, A., Michel, C., Gosselin, G., and B. LeBlanc (2008), Winter-spring dynamics in sea-ice carbon cycling in the coastal, *Arctic. J. Mar. Syst.* 74, 918-932, doi: 10.1016/j.jmarsys.2008.01.003.

Rózanksa, M., Gosselin, M., Poulin, M., Wiktor, J.M., and C. Michel (2009), Influence of environmental factors on the development of bottom ice protist communities during the winter-spring transition, *Mar. Ecol. Progr. Ser.* 386, 43-59, doi: 10.3354/meps08092.

Rysgaard, S., Kuhl, M., and J.W. Hansen (2001), Biomass, production and horizontal patchiness of sea ice microalgae in a high-Arctic fjord (Young Sound, NE Greenland), *Mar. Ecol. Prog. Ser.* 223, 15-26, doi: 10.3354/meps223015.

Smith, R.E.H., and P. Clement (1990), Heterotrophic activity and bacterial productivity in assemblages in microbes from sea ice in the High Arctic, *Polar Biol.* 10, 351-357, doi: 10.1007/BF00237822.

Smith, R.E.H., Anning, J., Clement, P., and G. Cota (1988), Abundance and production of ice algae in Resolute Passage, Canadian Arctic, *Mar. Ecol. Progr. Ser.* 48, 251-263.

Søgaard, D.H., Kristensen, M., Rysgaard, S., Glud, R.N., Hansen, P.J., and K.M. Hilligsoe (2010), Autotrophic and heterotrophic activity in Arctic first-year sea ice: seasonal study from Malene Bight, SW Greenland, *Mar. Ecol. Progr. Ser.* 419, 31-45, doi: 10.3354/meps08845.

Strickland, J.D., and T.R. Parsons (1972), *A practical handbook of seawater analysis*, 2nd edn. Bull. Fish. Res. Bd. Can.

Suzuki, Y., Kudoh, S., and M. Takahashi (1997), Photosynthetic and respiratory characteristics of an Arctic algal community living in low light and temperature conditions, *J. Mar. Syst.* 11, 111-121, doi: 10.1016/S0924-7963(96)00032-2.

Tremblay, J., Anderson, L.G., Matrai, P., Coupel, P., Bélanger, S., Michel, C., and M. Reigstad (2015), Global and regional drivers of nutrient supply, primary production and CO2 drawdown in the changing Arctic Ocean, *Progr. Oceanog.* 139, 171-196, doi: 10.1016/j.pocean.2015.08.009.

Welch, H.E., and M.A. Bergmann (1989), Seasonal development of ice algae and its prediction from environmental factors near Resolute, N.W.T., Canada, *Can. J. Fish. Aquat. Sci.* (46), 1793 – 1804.

Chapter Four Supplementary Material

4.S.1 Tables

Table 4.S.1. Pearson correlation coefficients (top) of T_{PAR} data inclusive of 5 and 9 June, with particulate organic carbon (POC) to chlorophyll *a* (chl *a*) ratios, POC to particulate organic nitrogen (PON) ratios and photosynthesis-irradiance (*see* text for definitions). Correlations are for samples collected under thin, thick or thin and thick snow covers collectively based on their statistical similarity. Significance (middle) and the number of observations for every correlation (bottom) are also indicated.

Parameter	Thin	Thick	Thin & Thick
POC:chl *a*	0.336 0.342 10	-0.260 0.468 10	0.251 0.285 20
POC:PON	-0.334 0.345 10	-0.369 0.294 10	-0.135 0.571 20
P^B_s			0.342 0.152 19
α^B			0.325 0.162 20
P_0			0.338 0.145 20
E_s			0.068 0.783 19
E_c			0.127 0.593 20

Table 4.S.2. Maximum photosynthetic rates (P^B_s) (mg C mg chl a^{-1} h^{-1}) and photosynthetic efficiencies α^B (mg C mg chl a^{-1} h^{-1} (μmol photons m^{-2} $s^{-1})^{-1}$) modeled from 10 or 4 points following incubation of thin or thick snow covered samples with the ^{14}C radioisotope.

	Thin Snow				Thick Snow			
Sampling Date	P^B_S -10	P^B_S - 4	α^B - 10	α^B - 4	P^B_S -10	P^B_S - 4	α^B - 10	α^B - 4
17-May	0.887	1.385	0.023	0.014	0.565	0.570	0.024	0.036
21-May	0.606	0.682	0.018	0.019	0.794	0.794	0.038	0.023
26-May	0.816	0.786	0.026	0.030	5.885	6.321	0.244	0.217
30-May	0.740	0.765	0.030	0.042	0.924	0.877	0.089	0.051
5-June	1.065	1.526	0.014	0.019	0.826	0.822	0.048	0.046

4.S.2 Description of ^{14}C measurement of gross primary production

Measurements of gross primary production using ^{14}C were made by incubating 60 ml of the melted ice-filtered seawater sample in *Corning* polystyrene culture flasks at 10 different light intensities, in addition to two dark bottles that were spiked with 50 µl of 3-3,4-dichlorophenyl-1,1-dimethylurea (DCMU) [Strickland & Parsons, 1972; Legendre et al., 1983]. Samples were incubated with 1 ml of ^{14}C (4 µCi ml^{-1}) in chambers modeled after Babin [1994] for 3h at -1.5°C, that were placed on a shaker table in front of a *Phillips Ceramalux* full spectrum halogen lamp. The average light intensity ($n = 3$) at each bottle position was determined prior to each incubation by measuring integrated PAR (µmol photons m^{-2} s^{-1}) using a scalar PAR probe (*Walz* model US-SQS/L) and data logger (*LI-COR* LI-1000) in a water-filled incubation flask, while keeping surrounding sample-filled flasks in place. Duplicate sub-samples of the melted ice-FSW solution were also collected in 12 ml *Exetainers* at the time of incubations, and were fixed with 20 µl of saturated mercury chloride ($HgCl_2$) solution for later analysis of dissolved inorganic carbon (DIC). The average concentration of DIC was measured within six months of sample collection using an *Apollo Scitech Inc*. infrared CO_2 analyzer.

Samples were filtered onto 25 mm GF/F filters (*Whatmann*) after the incubation period and placed into glass scintillation vials before acidification with 0.5 N HCl and drying. The radioactivity of filters was extracted in 5 ml of scintillation cocktail (*Ecolume*) for 24 to 48 h before measurement on a *Hidex Triathler* liquid scintillation counter. Initial ^{14}C activity was determined from the average of three 50 µl aliquots of spiked sample that had been removed from clear flasks at random prior to the start of incubation. These samples were placed into a solution of 5 ml scintillation cocktail and 50 µl ethanolamine

for extraction prior to counting. Gross primary productivity of ^{14}C incubations was calculated using estimates of DIC concentration, as well as the scintillation counts of samples and initial ^{14}C activity following Søgaard et al. [2010].

CHAPTER FIVE: SEASONAL DYNAMICS OF ALGAL AND BACTERIAL COMMUNITIES IN ARCTIC SEA ICE UNDER VARIABLE SNOW COVER

This manuscript has been submitted to the peer-reviewed journal of *Polar Biology*. The research included in this work was planned, conducted and reported by myself as first author.

Campbell, K., Mundy, C.J., Belzile, C., Delaforge, A. and S. Rysgaard, Seasonal dynamics of algal and bacterial communities in Arctic sea ice under variable snow cover, *Polar Biol*. (in review).

Abstract

Diatoms and heterotrophic bacteria dominate the microbial communities of sea ice in spring. However, their abundance and activity vary with changing environmental conditions and potentially the taxonomic composition of the algal community during this time. In this study we assessed the spring bottom-ice community composition in Dease Strait, Nunavut, and investigated potential controls of biomass and production from early March until early June. We found that using flow cytometry to estimate photosynthetic nanoeukaryotes (2-20 μm) abundance gave results very similar to light microscopy counts, except when pennate diatoms with lengths close to 20 μm, the maximum size detected by flow cytometry, were abundant. Using the average abundance of nanoeukaryotes from the two methods we documented a change in the size of cells comprising the ice algal community over the spring, from largely pico- (<2 μm), to nano- and microeukaryotes (20–200 μm). This shift in algal size corresponded to a bloom in diatoms that drove increases in chlorophyll *a*, particulate organic carbon and primary

productivity. Low salinity and nutrient depleted conditions in the region appeared to support dominance of the centric diatom *Attheya* spp. in particular. Increases in the number and productivity of heterotrophic bacteria in this study were correlated with the number of photosynthetic picoeukaryote cells, potentially due to their supply of dissolved organic carbon substrate, and with brine volume. Our results suggest that low nutrient and high light conditions predicted for the future Arctic may favour an ice algal community dominated by centric diatoms versus the more characteristic pennate diatom-dominated community.

Keywords**:** Arctic, sea ice, diatoms, bacteria, flow cytometry, light microscopy

5.1 Introduction

The brine network of sea ice is a habitat for microbial life, particularly for algae and heterotrophic bacteria that are concentrated in the bottommost centimeters [Smith et al., 1990; Deming, 2010]. The abundance of ice algae and bacteria during spring in the Arctic increases rapidly with favorable growth conditions, namely the availability of light for algal photosynthesis [Gosselin et al., 1985; Campbell et al., 2016] and the abundance of dissolved organic carbon (DOC) for bacterial production [Haecky and Anderson, 1989; Søgaard et al., 2013]. The ice algal bloom is marked by an increase in the quantity of chlorophyll *a* (chl *a*) and particulate organic carbon (POC) in the ice, where the latter provides a concentrated food resource for aquatic grazers [Søreide et al., 2010]. The type of algae comprising biomass in the ice is also an important consideration, as the

nutritional value of different species varies and can impact grazer succession [Li et al., 2009; Leu et al., 2011].

The ice algal bloom in Arctic first-year sea ice is largely comprised of pennate diatoms of the nano- (2-20 μm) and micro- (20-200 μm) size classes [Mendle & Priddle, 1990; Lee et al., 2008]. This includes the typically dominant cryophilic microeukaryote *Nitzschia frigida* [Poulin et al., 2011; Leu et al., 2015], which is high in polyunsaturated fatty acids (PUFAs) that are of nutritional value to grazers [Leu et al., 2011]. Other taxonomic groups including centric diatoms, dinoflagellates, flagellates and ciliates are also present [Mendle & Priddle, 1990; Niemi et al., 2011], although, the relative contribution of each group to the sea ice community varies with environmental conditions [Kirst & Wiencke, 1995]. For example, flagellates can outcompete diatom groups in the ice when photosynthetically active radiation (PAR) is severely restricted [Mikkelsen et al., 2008; Rózańska et al., 2009]. The contribution of small picoeukaryotic cells (<2 μm) in sea ice is not well understood, but recent studies have suggested that auto-, mixo- and heterotrophic picoeukaryotes can be numerous in the ice [Piwosz et al., 2013].

Bacterial and algal production influence carbon fluxes through the ice and contribute to the overall productivity of the marine system, by releasing or consuming CO_2, respectively [Søgaard et al., 2010]. Ice algae account for the majority of production during the spring and typically represent between 3 and 60% of total annual primary production in the Arctic Ocean [Legendre et al., 1992; Gosselin et al., 1997], while bacteria contribute <10% of the total production in sea ice [Deming, 2010]. Autotrophic cyanobacteria also have the potential to influence production; however, they have only

been documented in trace quantities and their contribution to sea ice production is likely to be insignificant as a result [Bowman, 2015; Mundy et al., 2011].

Primary production in sea ice is largely controlled by the intensity of light reaching the bottom-ice [Michel et al., 2002; Campbell et al., 2016], which is inversely related to the thickness of snow cover on the ice surface, and by nutrient supply from the water column [Gosselin et al., 1985; Cota & Horne, 1989]. The photosynthetic state of algae is species-specific, where different taxonomic groups can exhibit varying rates of photoacclimation or respiration in response to changing environmental conditions like growth light intensity [Falkowski & Owens, 1978]. Varied photosynthetic responses of different taxa to environmental conditions suggests that shifts in the taxonomic composition of the bottom-ice algal community that have been observed over the spring [e.g. Hsaio et al., 1992; Mikkelsen et al., 2008; Niemi et al., 2011] are likely to affect primary productivity. The size classification of the algal community may also have a significant effect on production, as smaller cells can be more productive relative to their biomass than larger cells due to their faster turnover rates [Agawin et al., 2000].

Bacteria follow similar distributions to algae over time and space in the sea ice because the majority of DOC required for bacterial production is sourced from the ice algae [e.g. Rysgaard & Glud, 2004; Comeau et al., 2013]. Other factors have also been suggested to affect bacterial abundance and production in sea ice including the number of bacterivores like choanoflagellates [Sime-Ngando et al., 1997; Riedel et al., 2007; Deming, 2010], temperature and cell lysis following viral infection [Maranger et al., 2015]. Quantifying the impact of these controls on bacteria is required to better understand variability in bacterial production that is observed across the Arctic [Bunch &

Harland, 1990; Smith & Clement, 1990; Maranger et al., 1994; Søgaard et al., 2013; Kaartokallio et al., 2013] and the role of sea ice in the microbial food web [Sarmiento & Gruber, 2006].

In this study we document the composition of the microbial community in the bottom centimeters of first-year sea ice over the spring bloom, under comparatively high and low light conditions that are characteristic of thin and thick snow covers, respectively. This includes quantifying the abundance of bacteria and individual size classes (pico-, nano- and micro-) of eukaryotic algae using a combination of flow cytometry and inverted light microscopy, and documenting the taxonomic composition of algal cells. We also compare estimates of nanoeukaryote abundance from these methods in an effort to evaluate the use of flow cytometry in sea ice research. Finally, we discuss how environmental conditions in sea ice may control the community of microorganisms and indirectly affect the biomass and productivity.

5.2 Materials and Methods

5.2.1 Sample collection

Different sample sites of thin (<10 cm) and thick (15-25 cm) snow-covered sea ice were chosen approximately every four days in Dease Strait, Nunavut (Figure 5.1) between 7-15 March and 21 April - 9 June. The bottom 5 cm of six to eight ice cores was collected under both thin and thick snow depths, using a 9 cm *Mark II Kovacs* core barrel. Ice samples from each site were pooled together before melting in 0.2 μm filtered seawater (filtered within 48 hours of collection) that was added at a volumetric ratio of three parts FSW to one part ice melt. The resulting ice-filtered seawater solution of pooled cores was

used for all measurements of pooled cores hereafter. Volume estimates from these samples (abundance, productivity etc.) have been multiplied by the ratio of total volume (filtered seawater + ice melt) to ice melt, to account for core dilution.

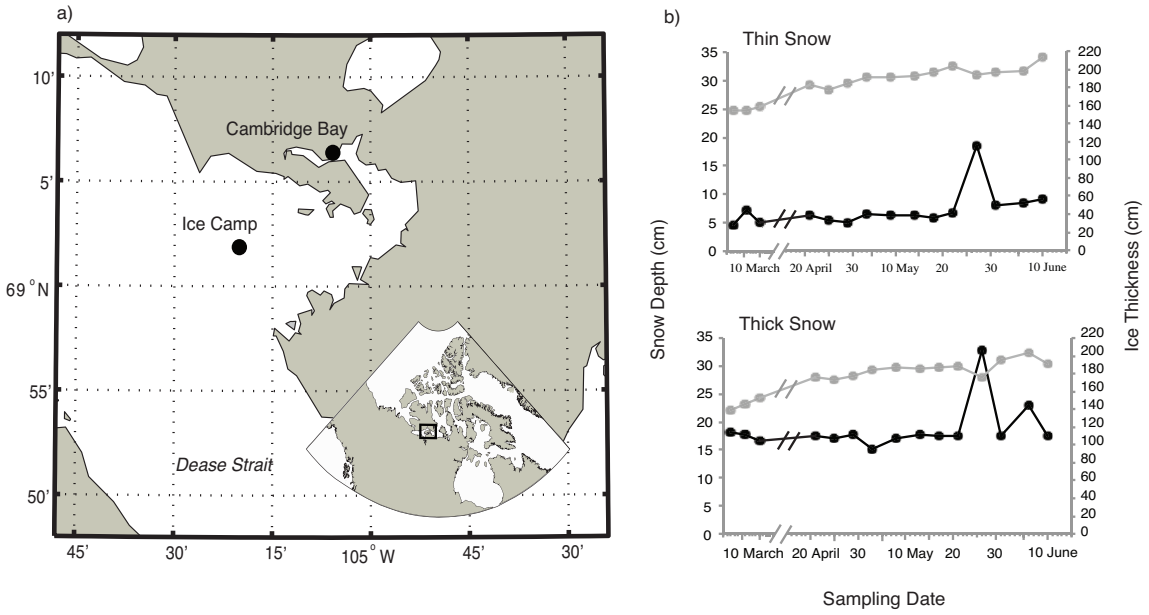

Figure 5.1. (a) Location of sample collection in the Canadian Arctic, with (b) average snow (black) and ice (grey) thickness over the study period shown for sites designated as thin and thick.

5.2.2 Measurements of photosynthetically active radiation and brine volume

The intensity of downwelling PAR at the ocean-ice interface (E_z(PAR)) was measured opportunistically over the sampling period under thin and thick snow covers, and is reported for the respective core collection dates by averaging estimates on, or within, ± 2 days of ice core collection (except for the 21 April sampling event). Measurements were made between 9:00 and 12:30 local time using 2π quantum sensors (LI-COR) and a mechanical arm [Campbell et al., 2016]. Incident downwelling PAR above the snow and ice cover was also recorded at a nearby meteorological tower using a *Kipp & Zonen PAR-Lite* sensor, and is presented as a daily average.

At the thin snow cover site, the bottom 5 cm of an ice core was measured for temperature (*Testo* 720 probe) in the field and salinity (*Orion Star* A212 conductivity meter) after the core bottom was melted with no FSW dilution. These values were used to calculate percent brine volume following the equations of Cox and Weeks [1983].

5.2.3 Biological parameters

Chlorophyll *a* and POC were sampled from the pooled cores by filtration through unburned and pre-combusted GF/F filters (*Whatman*), respectively. Chlorophyll *a* concentration was determined in the field using fluorescence (*Turner Designs Trilogy* Fluorometer; Parsons et al. 1984), while POC filters were frozen until later analysis using a continuous-flow isotope ratio mass spectrometer (*Thermo Scientific*) following Glaz et al. (2014). The concentration of inorganic nitrogen was determined by filtering volume from a separate ice core that was not diluted with FSW through pre-combusted GF/F filters (*Whatman*). Samples were stored at -20°C and later analyzed on an auto analyzer (*Seal Analytical*) for nitrate (NO_3) and nitrite (NO_2), collectively referred to as NO_x, according to Strickland and Parsons [1972]. Measurements of DOC were made on water collected at the ocean-ice interface by filtering pseudo-duplicate 8 ml samples through pre-combusted GF/F filters into glass vials that were previously washed in 10% HCl for 24 h, and burned for 12h at 450°C. Samples were immediately acidified with 100 µl 2N HCl, closed with acid washed caps, and stored at 4°C in darkness until analysis on a high-temperature combustion total organic carbon analyzer (*Shimadzu TOC-*V_{cpn}).

5.2.4 Bacterial and primary production

Bacterial production was calculated from a 6h dark incubation of pooled ice core sample (15 ml) with 10 nM concentration of ^{3}H-leucine, following Kirchman [2001]. Triplicate blanks were fixed with trichloroacetic acid (TCA, 5% final concentration) prior to incubation, and triplicates of active vials were fixed with TCA immediately afterwards. Samples were filtered through 0.2 μm cellulose acetate membranes that were dissolved with 0.5 ml ethyl acetate prior to 24 to 48 hr extraction in Ecolume scintillation cocktail (5 ml) and measurement of activity on a liquid scintillation counter (*Hidex Triathler*). Bacterial production (g C l^{-1} h^{-1}) was calculated using equations outlined in Kirchman [1993] and a carbon conversion factor of 1.5 kg C mol^{-1} [Ducklow et al. 2003].

Estimates of daily primary production were calculated using photosynthetic parameters from Campbell et al. [2016] that were measured on the same pool of ice cores described above (*see* Chapter Four). Therefore, measurements of production were made on all possible size classes of algae present in a given sample. Primary production was only measured from 21 April to 9 June (n = 12). Diurnal estimates of under-ice PAR required for the calculation of production were determined by applying the average PAR transmission under thin (2.2%) and thick (1.7%) snow sites in Campbell et al. [2016] (*see* Chapter Four), to hourly averages of downwelling PAR measured at the meteorological station (E_0(PAR)).

5.2.5 Flow cytometry

Pseudo-duplicate samples of 4.5 ml were taken from the melted pool of ice cores for later assessment of algal and bacterial cell abundance using a flow cytometer. Samples were

fixed with gluteraldehyde for a final concentration of 0.4% immediately after collection, before storage at -80°C for up to six months. They were analyzed using an Epics Altra flow cytometer (*Beckman Coulter*) following the protocols outlined in Tremblay et al. [2009] to determine the abundance of photosynthetic picoeukaryotes (<2 μm), nanoeukaryotes (2-20 μm) and cyanobacteria, and protocols of Belzile et al. [2008] to count heterotrophic bacteria.

5.2.6 Light microscopy

Sub-samples of 100 ml were taken from the pooled ice cores for counts and taxonomic analysis using an inverted light microscope (*Leica DMIL LED*). They were fixed in glass bottles using acidic Lugol's solution with a final concentration of 0.4% [Parsons et al., 1984], and stored at 4°C in the dark for up to one year. Samples were settled in Ütermohl type chambers (*Hydrobios*) for approximately 24 hours before enumeration of visible algae (i.e. >2 μm) using an inverted light microscope. A survey of the chamber bottom was done at 200x and 400x magnification before counting to compile a list of observed species, particularly large diatoms that are more likely to be missed during transect enumeration as a result of their lower abundance, and to ensure even distribution of cells on the slide.

A minimum of 400 cells was counted over at least three transects per sample [Lund et al., 1958] using 400x magnification, and the abundance of cells per milliliter was adjusted to account for core dilution (*see* Section 5.2.1). Ice algae from these counts were also identified to the lowest possible taxonomic rank, mainly using Poulin & Cardinal [1982], Medlin & Priddle [1990] and Tomas [1997] for reference. The abundance of

nanoeukaryotic cells was estimated following this assessment by summing cell counts of taxa that are not known to exceed 20 μm in length, while the abundance of microeukaryotes was calculated by summing cell counts of taxa typically >20 μm (*see* Appendices A, B for specific taxa designations). For consistency between methods the abundance of nano- and microeukaryotes reported from light microscopy is exclusive of choanoflagellates, as these cells do not have chlorophyll fluorescence and are therefore not detected by the flow cytometer. However, reported estimates of total cells that were counted using the light microscope include the abundance of choanoflagellates.

5.2.7 Estimates of relative abundance

The relative abundance of algae within each size class (ie. pico, nano, micro) was determined by calculating the percent of each class relative to the sum total of: picoeukaryotic cells measured with flow cytometry, the average nanoeukaryotic abundance from flow cytometry and light microscopy, and the number of microeukaryotes estimated from light microscopy. The percent composition of taxonomic groups was assessed relative to the total number of classified cells counted with light microscopy. Unidentified cells from light microscopy were not included in estimates of absolute or relative abundance for either size or taxonomic analyses.

5.2.8 Statistical Analysis

Statistical analysis in this research was completed using SPSS software (*IBM* Version 20) and a threshold of 95% confidence ($p < 0.05$). Differences between thin and thick snow covers (e.g. cell abundance) were assessed using paired student's t-tests, where

collectively the test statistic and sample size are reported as t_n. Pearson correlations (r) were performed to investigate the association between parameters. Linear regressions were done to evaluate seasonal trends in data, or where linear models of multiple parameters are reported. We note that there are inherent difficulties in the assessment of time series data using linear correlation and regression, such as autocorrelation between parameters. However, this approach has been used to readily assess biophysical relationships in sea ice research [e.g. Cota & Sullivan, 1990; Mundy et al., 2005; Brown et al., 2011], and as a result, we have adapted this approach throughout the manuscript.

5.3 Results

5.3.1 Study site

The study site was covered by a drifted snowpack for the duration of sampling. Information on the physical characteristics of the field site from April to June are described in detail by Campbell et al. [2016] (*see* Chapter Four). Here we summarize snow and ice conditions inclusive of March sampling. The thickness of snow cover averaged 6.4 ± 1.6 cm under thin sites, and 17.7 ± 2 cm under thick sites (Figure 5.1). These values do not include measurements collected immediately after a snowfall event on 26 May that temporarily increased snow depths to 18 and 33 cm under thin and thick snow sites, respectively. Shortly after the snowfall, wind-driven snow redistribution re-exposed the original drifts. Ice thickness increased between 7 March and 9 June from 156 to 213 cm under thin snow ($r = 0.957$, $p < 0.05$) and 139 to 192 cm under thick snow ($r = 0.953$, $p < 0.05$). Average ice thickness was significantly higher under thin snow sites

following a student's paired t-test on 15 observations ($t_{15} = 4.752, p < 0.05$), averaging 193 ± 10 and 185 ± 9 cm over the spring for thin and thick snow sites, respectively.

5.3.2 Environmental conditions

The E_Z(PAR) increased over the spring with the seasonal increase in E_0(PAR) ($r = 0.890$, $p < 0.05$) (Figure 5.2a). The average intensity of light measured beneath the ice was significantly higher under thin snow ($t_{13} = 5.908$, $p < 0.05$). Low measurements of E_z(PAR) on 5 and 9 June compared to the seasonal increase in light were a result of fresh snow deposits from a storm on 3 June [Campbell et al., 2016] (*see* Chapter Four). Without the measurements from the 5 and 9 June, downwelling PAR under the ice increased from 14.3 to 49.5 μmol m^2 s^{-1} under thin snow ($r = 0.774$, $p < 0.05$) and 3 to 32.9 μmol m^2 s^{-1} under thick snow ($r = 0.860$, $p < 0.05$). Analysis hereafter uses estimates of under-ice PAR downwelling between 7 March and 30 May, designated simply as E_z(PAR), and transmitted PAR data inclusive of June sampling dates are specified as E_z(June) where applicable.

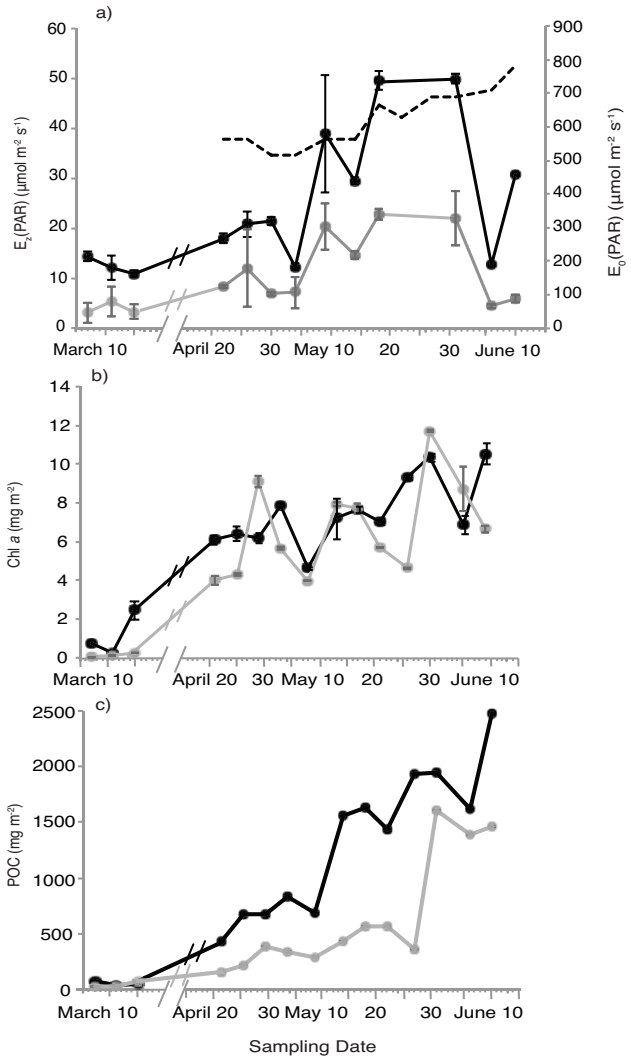

Figure 5.2. Seasonal change in (a) downwelling of photosynthetically active radiation (PAR) averaged daily at the snow-ice surface (E_0(PAR)) (dashed) and measured at the ice-ocean interface (E_z(PAR)) (solid), (b) bottom-ice chlorophyll *a* (chl *a*) with standard deviation (bars) from Campbell et al. [2016] and (c) bottom-ice particulate organic carbon (POC) concentrations. With the exception of downwelling PAR at the surface, estimates were made on ice covered by thin (black) and thick (grey) snow covers.

Temperature and brine volume in the bottom ice from 21 April to 9 June is presented in Campbell et al. [2016] (*see* Chapter Four). Inclusive of March sampling, temperature remained relatively constant at -1.5 ± 0.4°C over the spring (r = 0.542, p = 0.069) and brine volume increased significantly from 14 to 30% (r = 0.728, p < 0.05) with an average of 27 ± 7.8% overall (data not shown).

The concentration of chl *a* in the bottom-ice increased over the spring from 0.8 to 10.5 mg m^{-2} under thin snow ($r = 0.841$, $p < 0.05$) and 0.1 to 12 mg m^{-2} ($r = 0.676$, $p < 0.05$) under thick snow (Figure 5.2b). Chlorophyll *a* was not statistically different between thin and thick snow covers ($t_{15} = 1.662$, $p = 0.119$), averaging 1.2 ± 1.2 mg m^{-2} and 0.1 ± 0.1 mg m^{-2} in March, and 7.5 ± 1.8 and 6.7 ± 2.4 April to June [Campbell et al., 2016] (*see* Chapter Four), under thin and thick snow, respectively. The average concentration of bottom-ice chl *a* for the entire sampling period was 6.3 ± 3.1 mg m^{-2} under thin snow and 5.4 ± 3.5 mg m^{-2} under thick snow.

Particulate organic carbon increased between 7 March and 9 June from 76 to 2480 mg m^{-2} under thin snow ($r = 0.907$, $p < 0.05$) and 26 to 1456 mg m^{-2} ($r = 0.782$, $p < 0.05$) under thick snow, although the maximum concentration of POC under thick snow (1606 mg m^{-2}) was reached on 30 May (Figure 5.2c). Similar to the chl *a* concentrations described above, POC concentrations under thin and thick snow from April to June at 1323 ± 649 mg m^{-2} and 647 ± 520 mg m^{-2}, were greater than concentrations in March at 53 ± 21 mg m^{-2} and 41 ± 25 mg m^{-2}, respectively. Particulate organic carbon was highest under thin snow ($t_{15} = 4.423$, $p < 0.05$), averaging 1069 ± 779 mg m^{-2}, versus 526 ± 525 mg m^{-2} under thick snow. The concentration of DOC in seawater collected from the ocean-ice interface was largely constant over the spring at 1.9 ± 0.3 mg C l^{-1}, with the exception of 7 March where measurements reached 3 mg C l^{-1} (data not shown).

The average concentration of NO_x from 21 April to 9 June was reported in Campbell et al. [2016] as 0.5 ± 0.3 μmol l^{-1} under thin snow, and 0.9 ± 0.6 μmol l^{-1} under thick snow, respectively (*see* Chapter Four). Compared to these mid and late spring estimates, the

concentration of NO_x was slightly higher in March at 1.1 ± 0.5 μmol l^{-1} under thin snow and 0.9 ± 0.3 μmol l^{-1} under thick snow.

5.3.3 Composition of the bottom-ice community

Heterotrophic bacterial abundance and production

The abundance of heterotrophic bacteria in the bottom-ice reached maximum concentrations on 8 May at 10 x 10^6 cells ml^{-1} under thin snow, and 6.5 x 10^6 cells ml^{-1} under thick snow (Figure 5.3a). Cell abundance was fairly constant after this date, at a lower concentration of approximately 2.5 x 10^6 cells ml^{-1}. The number of heterotrophic bacteria was significantly greater under thin snow throughout the spring ($t_{15} = 2.396$, $p < 0.05$), which was reflected by the higher average abundance of cells under thin snow at 2.8 ± 2.8 x 10^6 cells ml^{-1}, than under thick snow at 2.3 ± 1.6 x 10^6 cells ml^{-1}.

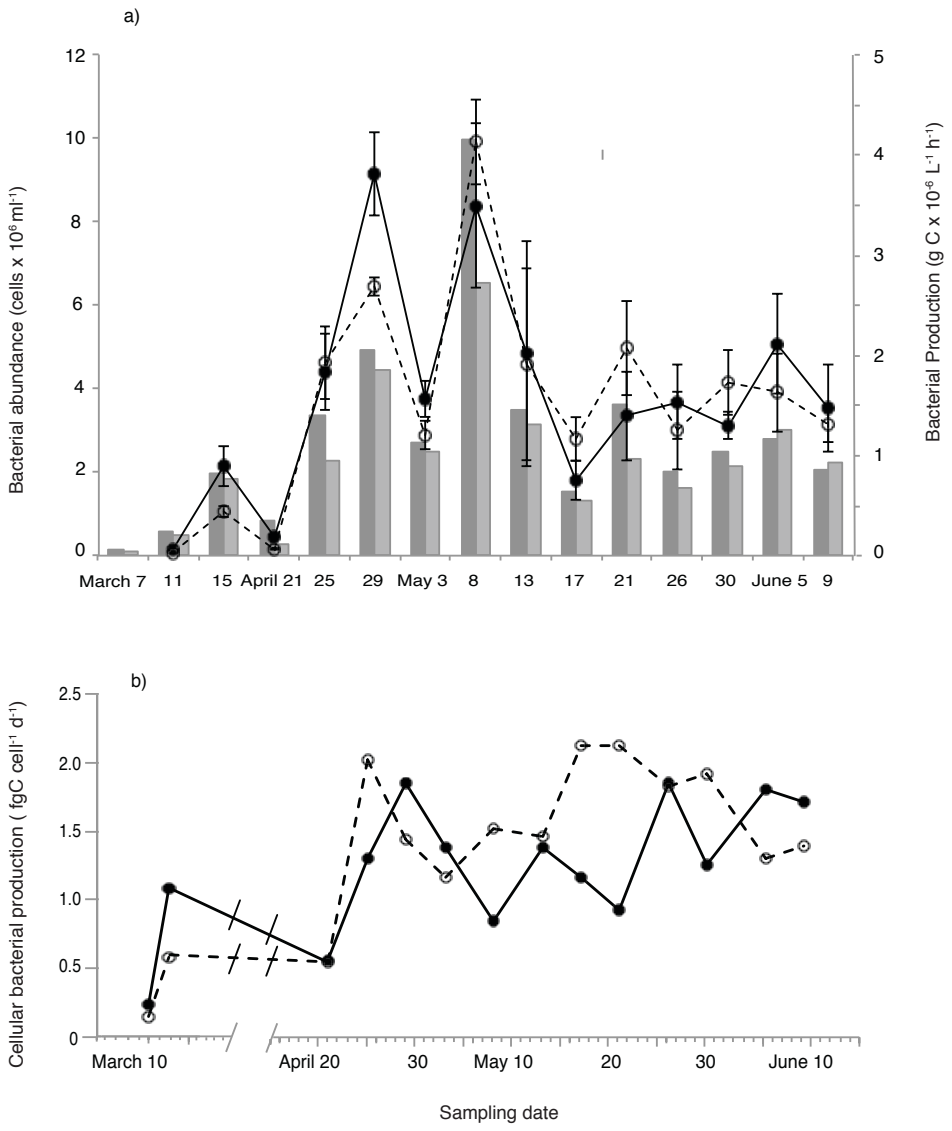

Figure 5.3. (a) Abundance of heterotrophic bacteria (cells x 10^6 ml^{-1}) measured with flow cytometry (bars) under thin (dark grey) and thick (light grey) snow covers. Bacterial production (dots) with the standard deviation between replicates over the sampling period is also shown for cells under thin (solid) and thick (open) snow covers. (b) Daily bacterial production normalized by bacterial abundance in sea ice under thin (solid) and thick (open) snow covers.

Bacterial production and heterotrophic bacterial abundance were strongly correlated under thin ($r = 0.836$, $p < 0.05$) and thick ($r = 0.940$, $p < 0.05$) snow covers, and seasonal trends in production were similar to those described above for cell abundance (Figure 5.3a). Production peaked between 29 April and 8 May at 3.8 x 10^{-7} g C l^{-1} h^{-1} under thin

snow and 4.1 x 10^{-7} g C l^{-1} h^{-1} under thick snow. After 8 May production was relatively constant averaging 1.5 x 10^{-7} g C l^{-1} h^{-1} over the remaining study period. Overall, bacterial production was not statistically different between the snow covers ($t_{14} = 0.480, p = 0.639$), and seasonal averages were similar at 1.6 ± 1.1 x 10^{-7} g C l^{-1} h^{-1}under thin snow and 1.5 ± 1.1 x 10^{-7} g C l^{-1} h^{-1} under thick snow. Daily bacterial production normalized by bacterial abundance was generally < 0.6 fgC $cell^{-1}$ d^{-1} until 25 April (Figure 5.2b). It then increased to values in the range of 0.8-2.1 fgC $cell^{-1}$ d^{-1}, with no defined temporal variation and values that were not significantly different between thin and thick snow sites ($t_{14} = -1.000$, $p = 0.336$). Assuming a carbon content of 10 fgC $cell^{-1}$ d^{-1} [Ducklow, 2000], daily bacterial production was approximately equivalent to 1 bacteria produced every 10 days for each bacteria cell present in the ice.

Abundance of cyanobacteria and eukaryotes in sea ice

The abundance of cyanobacteria was low throughout the spring, and on several occasions cyanobacteria were not documented in the sample volumes analyzed (Figure 5.4). Cyanobacteria counts in the bottom-ice remained below 171 cells ml^{-1} under thin snow, with the exception of a perceived outlier on 8 May where concentrations reached nearly 550 cells ml^{-1}, but did not exceed 138 cells ml^{-1} under thick snow throughout the study. There was no significant difference in the abundance of cyanobacteria between thin and thick snow ($t_{15} = 1.362, p = 0.195$).

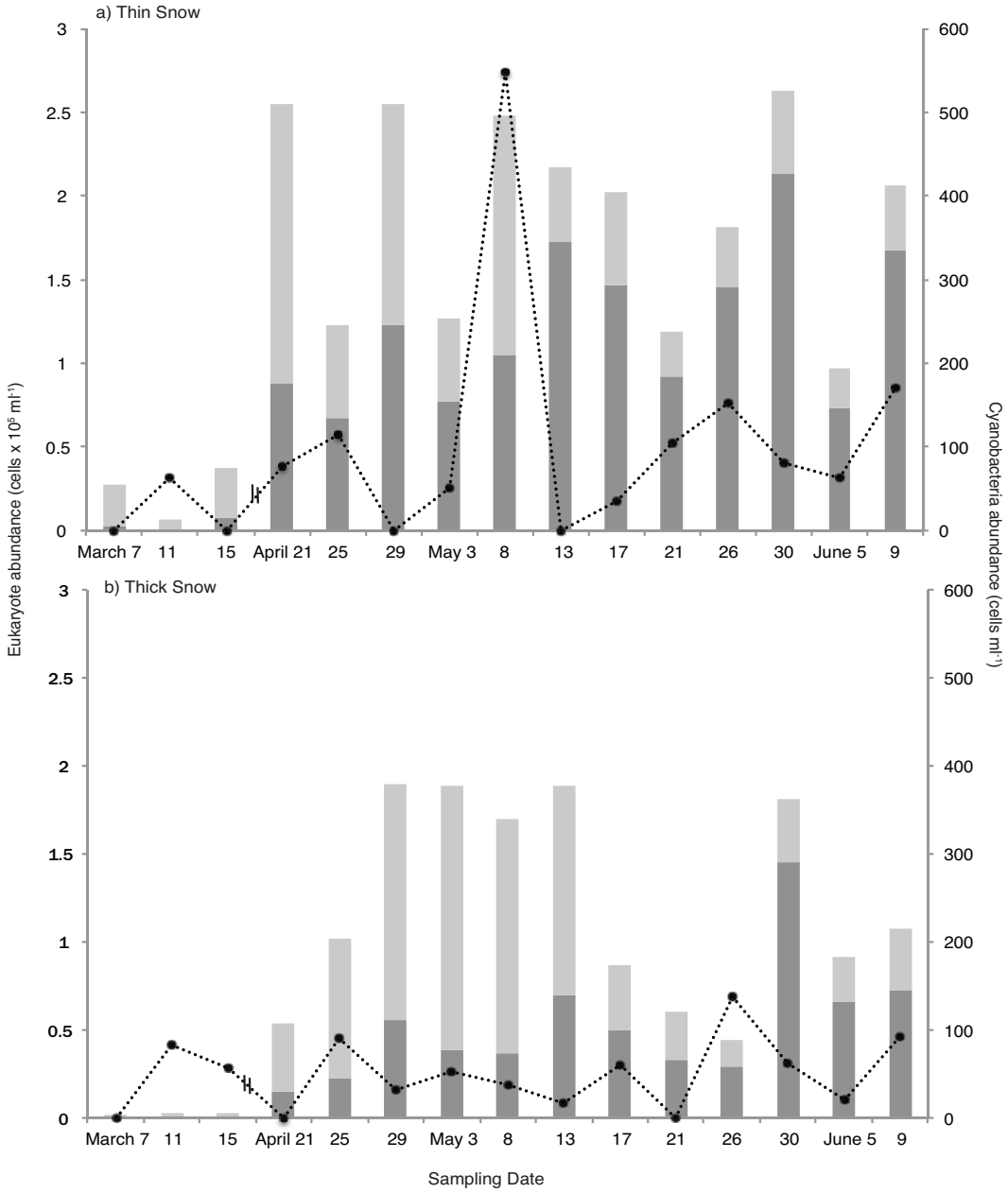

Figure 5.4. Flow cytometry measurements of picoeukaryote (light grey), nanoeukaryote (dark grey) and cyanobacteria (black) abundance under thin (a) and thick (b) snow covers.

Abundance of picoeukaryotes

The abundance of photosynthetic picoeukaryotes over the spring is shown in Figure 5.4, where the concentration of cells in the bottom-ice was lowest in March and highest between 21 April and 30 May. Relative to the total abundance of algae in the ice (*see*

Section 5.2.7), percent abundance of picoeukaryotes decreased under thin snow from 87% (2.5×10^4 cells ml^{-1}) to 11% (3.8×10^4 cells ml^{-1}) over the sampling period ($r = -0.929$, $p < 0.05$) (Figure 5.5). Similarly, the relative abundance of picoeukaryotes under thick snow decreased from 73% (1.1×10^3 cells ml^{-1}) to 19% (3.5×10^4 cells ml^{-1}) over the spring ($r = -0.823$, $p < 0.05$). The numerical abundance of picoeukaryotes was not significantly different between snow depths ($t_{15} = 0.259$, $p = 0.799$) although, the relative abundance of picoeukaryotes was significantly lower under thin than thick snow ($t_{15} = -2.741$, $p = 0.016$), with an average of 35% (5.9×10^4 cells ml^{-1}) versus 43% (5.5×10^4 cells ml^{-1}), respectively (Figure 5.5).

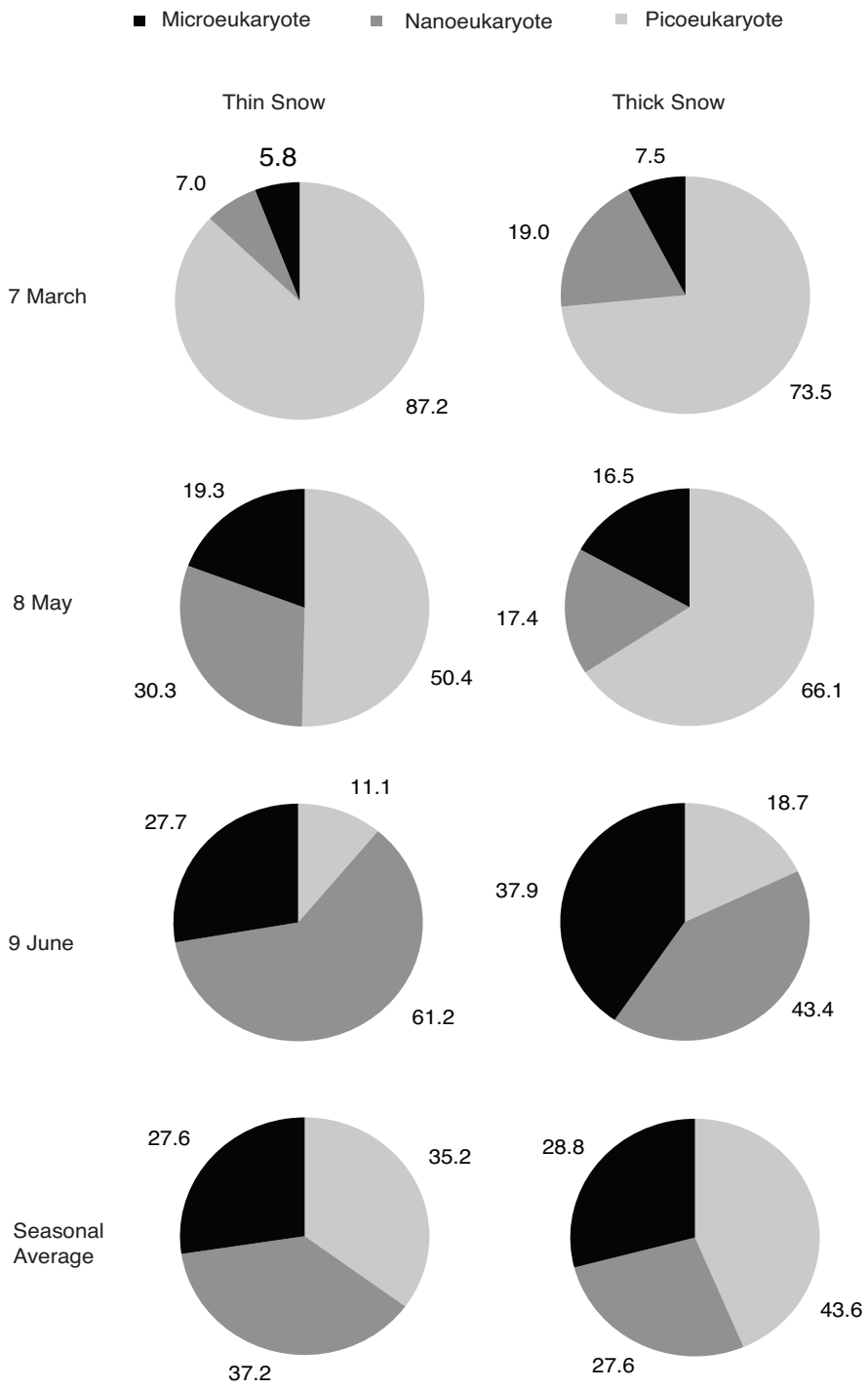

Figure 5.5. Percent abundance of picoeukaryote (< 2 um, light grey), average nanoeukaryote (2-20 um, dark grey) and microeukaryote (21-200 um, black) cells in the bottom-ice at the beginning (7 March), middle (8 May) and end (9 June) of the spring. The average size composition of the sea ice algal community for the entire sampling period is also presented.

Abundance of nanoeukaryotes

Cell abundance of photosynthetic nanoeukaryotes measured with the flow cytometer (Figure 5.4) was significantly higher under thin than that under thick snow covers (t_{15} = 5.629, $p < 0.05$). The seasonal increase in cell abundance was also greater under thin snow, from approximately 2600 to 1.7 x 10^5 cells ml^{-1} ($r = 0.795$, $p < 0.05$), than thick snow cover, from 290 to 7.2 x 10^4 cells ml^{-1} ($r = 0.719$, $p < 0.05$). Similarly, nanoeukaryote abundance estimated from light microscopy showed an increase over time (Figure 5.6) from about 1400 to 2.6 x 10^5 cells ml^{-1} under thin snow ($r = 0.800$, $p < 0.05$) and 300 to 9.0 x 10^5 cells ml^{-1} under thick snow (r = 0.582, $p < 0.05$). The number of estimated nanoeukaryotes was also greatest under thin snow cover (t_{15} = -2.756, $p < 0.05$). Relative cell abundance of all nanoeukaryotes (results from flow cytometry and light microscopy were averaged for each sample), increased over the spring from 7 to 61% under thin snow (r = 0.855, $p < 0.05$) and 19 to 43% under thick snow (r = 0.683, $p <$ 0.05) (Figure 5.5).

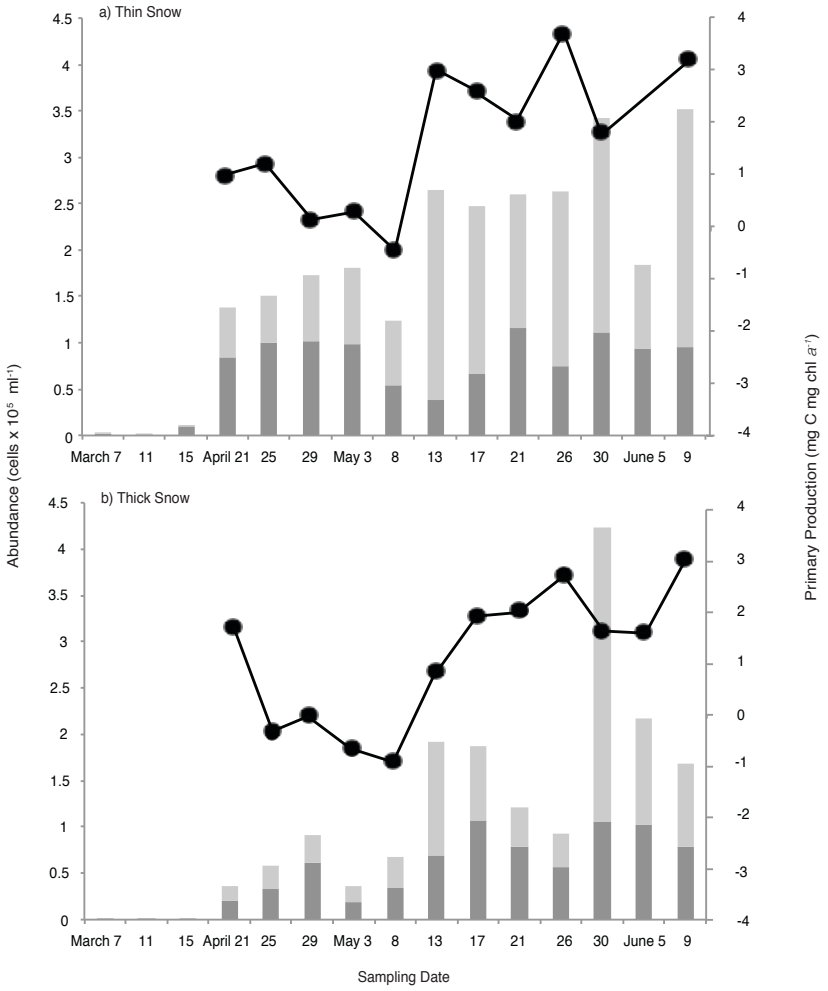

Figure 5.6. Cell abundance time series of nanoeukaryotes (2-20 μm, light grey) and microeukaryotes (21-200 μm, dark grey) under thin (a) and thick (b) snow covers, enumerated over the spring using inverted light microscopy. Seasonal change in estimated daily production from Campbell et al. [2016] is also shown (line).

Abundance of microeukaryotes

The concentration of microeukaryotes ranged from approximately 350 (11 March) to 1.1 x 10^5 cells ml^{-1} (21 May) and 120 (7 March) to 1.0 x 10^5 (17 May) cells ml^{-1} under thin and thick snow covers, respectively (Figure 5.6). Despite these similar ranges, microeukaryotes were significantly more abundant under thin snow cover ($t_{15} = 2.316$, $p < 0.05$), averaging 7 x 10^4 cells ml^{-1} versus 5 x 10^4 cells ml^{-1}. The relative abundance of

microeukaryotes showed a similar trend to nanoeukaryotic cells over the spring, and increased from about 6 to 28% ($r = 0.589$, $p = < 0.05$) under thin snow, and 8 to 38% ($r = 0.743$, $p < 0.05$) under thick snow (Figure 5.5).

Ice algal total cell abundance and production

The total number of ice algal cells counted using the light microscope ranged from about 680 (11 March) to 3.5 x 10^5 cells ml^{-1} (9 June) under thin snow, and from 425 (7 March) to 4.2 x 10^5 cells ml^{-1} (30 May) under thick snow (Figure 5.6). Total abundance of cells measured with light microscopy increased in thin ($r = 0.897$, $p < 0.05$) and thick ($r = 0.718$, $p < 0.05$) snow-covered sea ice, and was significantly higher under thin snow cover ($t_{15} = 3.400$, $p < 0.05$). This was also true for calculated daily averaged production of algae collected from thin ($r = 0.693$, $p < 0.05$) or thick ($r = 0.648$, $p < 0.05$) snow over time, which was significantly greater ($t_{11} = 2.454$, $p < 0.05$) under thin snow at 1.7 ± 1.4 mg C mg chl a^{-1} than under thick snow cover at 1.1 ± 1.4 mg C mg chl a^{-1} (Figure 5.6).

5.3.4 Taxonomic composition of the ice algal community

A total of 63 species were identified and counted in the bottom-ice over our sampling period (Appendix Table 5.1, 5.2). The taxonomic group with the most cells enumerated for thin and thick snow-covered sea ice was large (5-15 μm) and free-living *Attheya* spp., followed by small (5 μm) *Attheya* spp. that were primarily found attached to the third most abundant taxa, *Nitzschia frigida* (Campbell pers. obs.). The small and largely epiphytic fraction of *Attheya* spp. comprised approximately 29.4 ± 11.7% of cells in the genus *Attheya* (inclusive of *Attheya longicornis* and *Attheya septentrionalis*) under thin

snow, and 43.2 ± 14.1% under thick snow. Pennate diatoms *Navicula pelagica* and *Pseudo-nitzschia delicatissima* were also abundant in our study (Appendix Table 5.1, 5.2).

The relative abundance of the main eukaryotic groups collected from sea ice under thin and thick covers is presented in Figure 5.7 (see Appendix Tables 5.1 and 5.2 for detailed taxonomic information and cell counts). Diatoms were the dominant group throughout the spring, consistently accounting for over 60% of the eukaryotes enumerated using light microscopy. However, whether pennate or centric diatoms were most abundant in the bottom-ice was dependent on the sampling date and the depth of snow cover.

The number of both centric ($r = 0.792$, $p < 0.05$) and pennate ($r = 0.800$, $p < 0.05$) diatoms increased over the spring under thin snow, from about 650 to 2.5 x 10^5 cells ml^{-1} and 2 x 10^3 to 9.3 x 10^4 cells ml^{-1}, respectively (Appendix Table 5.1). However, the percent abundance of centric diatoms significantly increased ($r = 0.795$, $p < 0.05$) as the percent abundance of pennate diatoms decreased ($r = -0.738$, $p < 0.05$) (Figure 5.7). The shift in dominance between these taxonomic groups occurred on 8 May, where the abundance of centric diatoms remained largely above 50% and pennate diatoms remained below 50% after this date. Centric diatoms represented 43.5 ± 19.1 % of the bottom-ice community on average, while pennate diatoms accounted for 50.5 ± 17.5%.

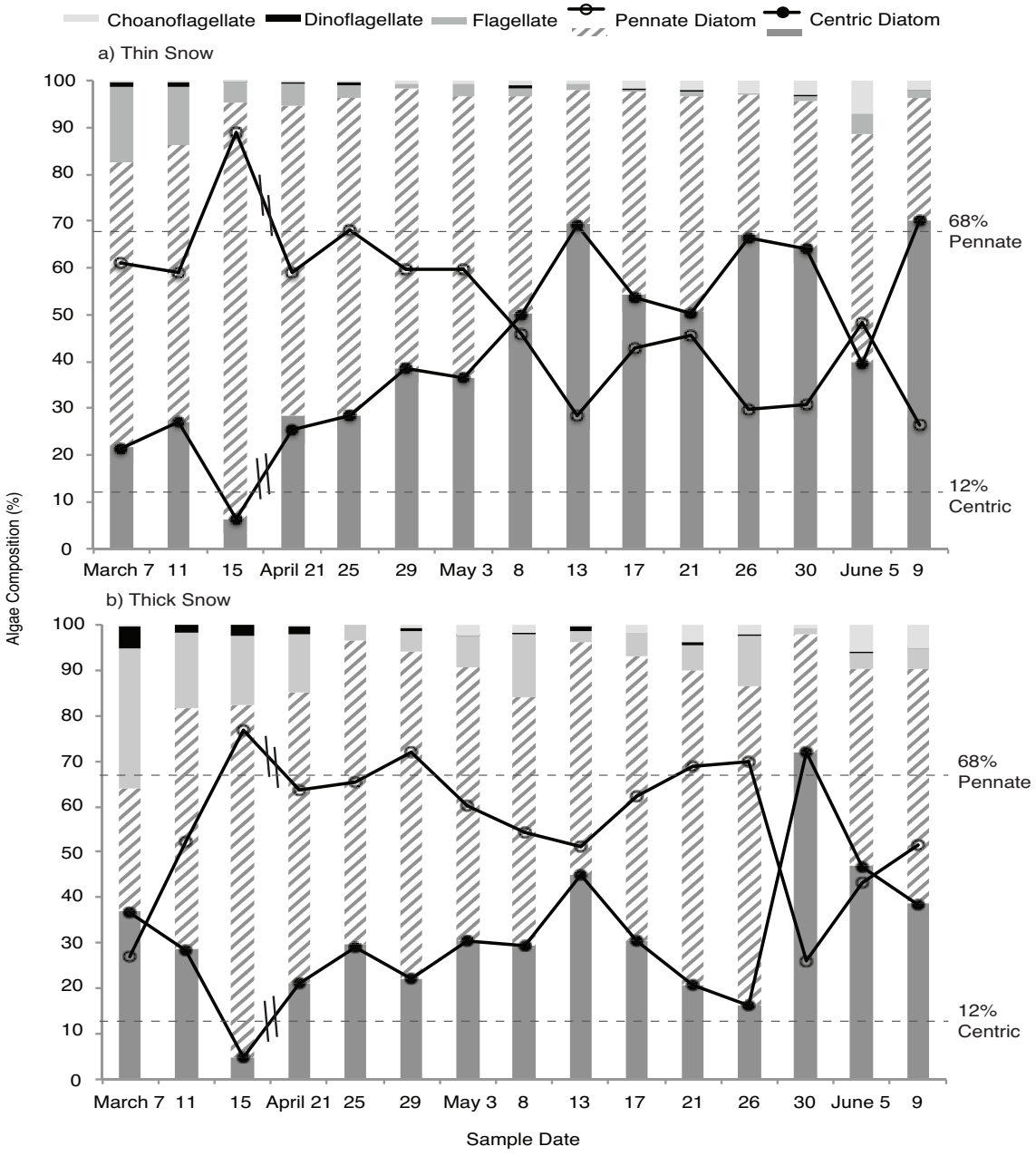

Figure 5.7 Percent composition of the main algal taxonomic groups in the bottom-ice under thin (a) and thick (b) snow covers. Seasonal changes in pennate (open circle) and centric (solid circle) diatom abundance are also highlighted. Dashed lines indicate the average pennate and centric diatom abundance in sea ice of the Canadian Arctic [*see* Poulin et al., 2011].

The number (r = 0.513, p = 0.05) and percent abundance (r = 0.429, p = 0.110) of centric diatoms did not significantly change over the spring under thick snow, with an

average abundance of approximately 5 ± 7.8 x 10^4 cells ml^{-1}. In comparison, a seasonal increase in the number of pennate diatoms (r = 0.849, $p < 0.05$) was observed from approximately 110 to 8.7 x 10^4 cells ml^{-1} (Appendix Table 5.2). However, this increase was not enough to influence a significant trend in relative abundance of pennate diatoms over the spring (r = -0.044, p = 0.877) (Figure 5.6). Pennate diatoms dominated the bottom-ice community under thick snow for the majority of the sampling period, comprising 56.1 ± 15.1% of cells on average, while centric diatoms accounted for 31.5 ± 15.5%. The number of centric and pennate diatoms was greater under thin than thick snow (t_{15} = 2.625, $p < 0.05$) (t_{15} = 2.414, $p < 0.05$), respectively, but centric diatoms accounted for a larger fraction of the bottom-ice community under thin snow cover (t_{15} = 2.575, $p < 0.05$) (Figure 5.7).

After diatoms, flagellates were the next most abundant taxonomic group, ranging between 1.2 (29 April) and 16.3% (7 March) of cells under thin snow, and 1.4 (30 May) and 30.9% (7 March) under thick snow (Appendices Table 5.1, 5.2) (Figure 5.7). The number of flagellates increased over the season from about 500 to 5.5 x 10^3 cells ml^{-1} under thin snow and 130 to 8 x 10^3 cells ml^{-1} under thick snow (Appendix Table 5.1, 5.2), but their overall relative abundance in the bottom-ice community significantly ($p < 0.05$) declined with linear correlation coefficients of -0.730 and -0.797, respectively (Figure 5.7). Flagellate abundance was not significantly different between snow depths (t_{15} = -1.301, p = 0.112), but their percent contribution to the community was greatest under thick snow cover (t_{15} = -4.437, p = < 0.05) (Figure 5.7).

The number of choanoflagellates identified in the ice was under 12.6 x 10^3 cells ml^{-1} (Appendix Table 5.1, 5.2), and accounted for <7% of the ice community under thin snow,

and <6% under thick snow (Figure 5.7). Their abundance increased over the spring under thin ($r = 0.780$, $p < 0.05$) and thick ($r = 0.698$, $p < 0.05$) snow, and was not significantly different between snow depths ($t_{15} = 1.568$, $p = 0.139$). The abundance of dinoflagellates in the bottom-ice was also low at <1.1% (<1.3 x 10^3 cells ml^{-1}) and <5 % (< 1.7 x 10^3 cells ml^{-1}) under thin and thick snow covers, respectively (Appendix Table 5.1, 5.2) (Figure 5.7). Dinoflagellate abundance was not different between snow covers (t_{15} = -0.301, p = 0.768) and did not exhibit any seasonal trends. Ciliates were often not documented in the ice and also showed no significant trends in absolute or relative abundance.

5.3.5 Controls of community composition, biomass and production

Controls of bacterial abundance and production

Pearson correlation coefficients were calculated for heterotrophic bacterial abundance and production versus environmental parameters (chl *a*, DOC, E_z(PAR), temperature, salinity, brine volume) and the abundance of picoeukaryotes, nanoeukaryotes and choanoflagellates (data not shown). Significant correlations ($p < 0.05$) between bacterial abundance or production were only observed for picoeukaryote abundance, after an apparent outlier on 21 April was removed, and for brine volume under thick snow cover. These significant relationships in addition to production versus brine volume under thin snow cover, which was not significant ($r = 0.507$, $p = 0.112$), are plotted in Figure 5.8.

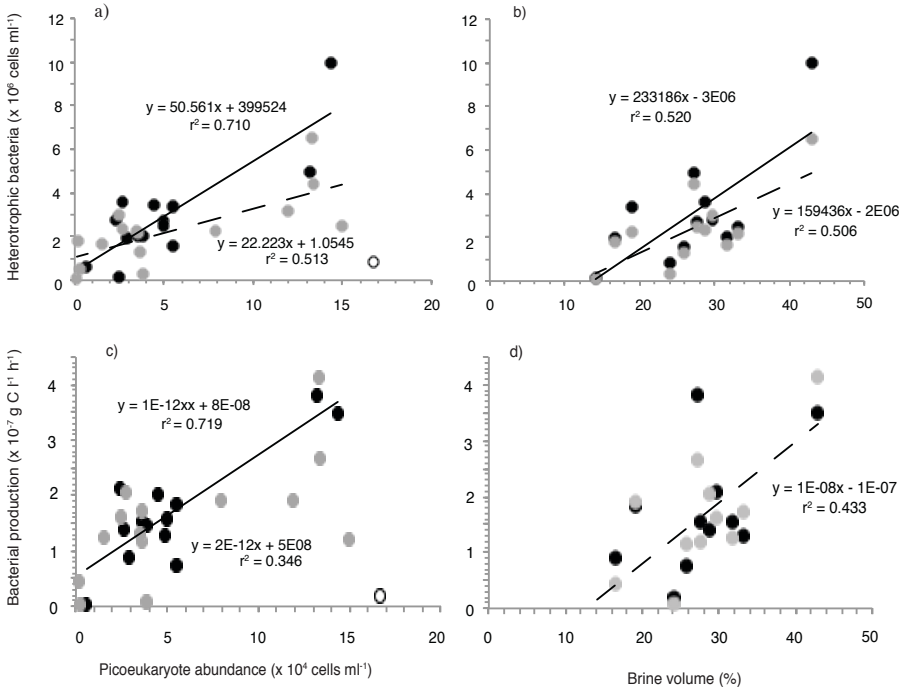

Figure 5.8. Linear regressions between heterotrophic bacterial abundance or bacterial production, with prokaryotic algal cell abundance (a, b) independent of an outlier on 21 April (circle) and brine volume in the bottom 0-5 cm of sea ice (c, d). Samples were collected from under thin (black) or thick (grey) snow covers although, brine volume was calculated for thin snow cover only. Significant ($p < 0.05$) linear models of the data are also shown.

The number of cyanobacteria under thin snow increased with bottom-ice temperature ($r = 0.598$, $p < 0.05$) and brine volume ($r = 0.743$, $p < 0.05$), as well as the abundance of heterotrophic bacteria ($r = 0.766$, $p < 0.05$). However, cyanobacteria were not correlated with any of the parameters listed in Table 5.3 under thick snow cover (data not shown).

Table 5.3. Pearson correlation coefficients (top)—including *p*-values (middle) and sample size (bottom) of correlations—of picoeukaryote and nanoeukaryote abundance measured using flow cytometry ($Pico_{FC}$, $Nano_{FC}$) or estimated from light microscopy ($Pico_{LM}$, $Nano_{LM}$), average nanoeukaryote abundance of measurements from flow cytomtery and light microscopy ($Nano_{AVG}$) and abundance of microeukaryotes estimated from light microscopy ($Micro_{LM}$), with environmental parameters (*see* text for definitions) under thin snow cover. Missing data has been excluded pairwise and correlations of significance ($p<0.05$) are in bold.

	Parameter	Flow Cytometry			Light Microscopy		$Nano_{AVG}$
		$Pico_{FC}$[a]	$Pico_{FC}$	$Nano_{FC}$	$Nano_{LM}$	$Micro_{LM}$	
Independent Environmental Parameters	NO_x	-0.049	-0.128	**-0.655**	**-0.674**	-0.415	**-0.685**
		0.868	0.651	**0.007**	**0.006**	0.124	**0.005**
		14	15	**15**	**15**	15	**15**
	E_z(June)	0.367	0.196	**0.799**	**0.693**	0.413	**0.753**
		0.241	0.521	**0.001**	**0.009**	0.161	**0.003**
		12	13	**13**	**13**	13	**13**
	E_z(PAR)	0.344	0.168	**0.815**	**0.776**	0.453	**0.804**
		0.330	0.622	**0.002**	**0.005**	0.161	**0.003**
		10	11	**11**	**11**	11	**11**
	Temp.	0.467	0.544	0.530	0.422	0.343	0.483
		0.148	0.062	0.077	0.172	0.275	0.112
		11	12	12	12	12	12
	Salinity	0.265	0.107	-0.488	0.455	**0.672**	0.482
		0.431	0.740	0.107	0.137	**0.017**	0.113
		11	12	12	12	**12**	12
	Brine Vol.	0.532	0.348	**0.657**	0.567	0.417	**0.624**
		0.092	0.267	**0.020**	0.054	0.178	**0.030**
		11	12	**12**	12	12	**12**
Dependent Parameters	Chl *a*	0.120	0.087	**0.875**	**0.867**	**0.826**	**0.889**
		0.683	0.757	**0**	**0**	**0**	**0**
		14	15	**15**	**15**	**15**	**15**
	POC	-0.078	-0.200	**0.837**	**0.948**	**0.595**	**0.920**
		0.792	0.475	**0**	**0**	**0.019**	**0**
		14	15	**15**	**15**	**15**	**15**
	PP_{chla}	**-0.764**	**-0.692**	0.567	**0.804**	-0.133	**0.739**
		0.010	**0.018**	0.069	**0.003**	0.696	**0.009**
		10	**11**	11	**11**	11	**11**

[a] Outlier on 21 April was removed

Controls on ice algal community composition

Linear correlations between environmental parameters and size classes of algae are summarized in Tables 5.3 and 5.4 for thin and thick snow covers, respectively. Picoeukaryote abundance was not correlated with any of the environmental parameters

assessed. However, nanoeukaryote abundance measured using the flow cytometer, estimated from light microscopy, or the average from the two methods increased with E_z(PAR) under thin or thick snow-covered sea ice, respectively (Tables 5.3 and 5.4). Nanoeukaryote abundance under thin snow cover also increased with brine volume and decreased with the concentration of NO_x (Table 5.3), while microeukaryote abundance increased with brine salinity under thin snow (Table 5.3) and E_z(PAR) under thick snow (Table 5.4).

Table 5.4. Pearson correlation coefficients (top)—including *p*-values (middle) and sample size (bottom) of correlations—of picoeukaryote and nanoeukaryote abundance measured using flow cytometry ($Pico_{FC}$, $Nano_{FC}$) or estimated from light microscopy ($Pico_{LM}$, $Nano_{LM}$), average nanoeukaryote abundance of measurements from flow cytomtery and light microscopy ($Nano_{AVG}$) and abundance of microeukaryotes estimated from light microscopy ($Micro_{LM}$), with environmental parameters (*see* text for definitions) under thick snow cover. Missing data has been excluded pairwise and correlations of significance ($p<0.05$) are in bold.

	Parameter	Flow Cytometry		Light Microscopy		$Nano_{AVG}$
		$Pico_{FC}$	$Nano_{FC}$	$Nano_{LM}$	$Micro_{LM}$	
Independent Environmental Parameters	NO_x	0.048 0.865 15	-0.412 0.127 15	-0.402 0.137 15	-0.319 0.247 15	-0.411 0.128 15
	E_z(June)	0.327 0.276 13	**0.569** **0.042** **15**	**0.566** **0.044** **13**	**0.619** **0.024** **15**	**0.574** **0.040** **13**
	E_z(PAR)	0.272 0.418 11	**0.708** **0.015** **11**	**0.673** **0.023** **11**	**0.815** **0.002** **11**	**0.693** **0.018** **11**
	Temp.	0.302 0.340 12	0.346 0.270 12	0.244 0.444 12	0.287 0.366 12	0.279 0.381 12
	Salinity	0.415 0.180 12	0.262 0.410 12	0.071 0.826 12	0.549 0.065 12	0.131 0.685 12
	Brine Vol.	0.438 0.154 12	0.518 0.084 12	0.384 0.218 12	0.472 0.121 12	0.430 0.163 12
Dependent Parameters	Chl *a*	0.362 0.185 15	**0.903** **0** **15**	**0.763** **0.001** **15**	**0.892** **0** **15**	**0.818** **0** **15**
	POC	-0.095 0.735 15	**0.856** **0** **15**	**0.824** **0** **15**	**0.739** **0.002** **15**	**0.845** **0** **15**
	PP_{chla}	**-0.874** **0** **12**	0.203 0.527 12	0.290 0.361 12	0.506 0.093 12	0.267 0.402 12

Linear correlations between environmental parameters and the presence of the three dominant taxonomic groups (centric diatoms, pennate diatoms and flagellates), under thin (Table 5.5) and thick snow (Table 5.6) were also investigated. Centric diatom abundance under thin and thick snow covers, and pennate abundance under thick snow significantly increased with E_z(PAR) (Table 5.5, 5.6). However, the type of correlation (positive or

negative) between centric or pennate diatoms and E_z(PAR) was opposite when considering their relative contribution to the bottom-ice community. No other significant correlations were documented for these diatoms under thick snow, but bottom-ice temperature, salinity and brine volume were associated with centric and pennate abundance (absolute or relative) under thin snow (Table 5.5).

Table 5.5. Pearson correlation coefficients (top)—including *p*-values (middle) and sample size (bottom) of correlations—of centric diatom, pennate diatom and flagellate cell counts and their percent abundance of total cells enumerated using light microscopy, with environmental parameters (*see* text for definitions) under thin snow cover. Missing data has been excluded pairwise and correlations of significance ($p<0.05$) are in bold.

	Parameter	Cell Counts			Percent Abundance		
		Centric	Pennate	Flagellate	Centric	Pennate	Flagellate
Independent Environmental Parameters	NO_x	**-0.660** **0.007** **15**	-0.464 0.082 15	**-0.527** **0.044** **15**	**-0.791** **0** **15**	**0.799** **0** **15**	0.422 0.117 15
	E_z(June)	**0.696** **0.008** **13**	0.448 0.125 13	0.166 0.588 13	**0.737** **0.004** **13**	**-0.677** **0.011** **13**	-0.513 0.073 13
	E_z(PAR)	**0.792** **0.004** **11**	0.490 0.126 11	0.392 0.233 11	**0.795** **0.003** **11**	**-0.756** **0.007** **11**	-0.508 0.110 11
	Temp.	0.421 0.173 12	0.334 0.288 12	0.426 0.167 12	**0.601** **0.039** **12**	-0.568 0.054 12	-0.376 0.228 12
	Salinity	0.417 0.177 12	**0.706** **0.010** **12**	0.433 0.159 15	0.557 0.060 12	-0.442 0.150 12	**-0.746** **0.005** **12**
	Brine Vol.	0.564 0.056 12	0.421 0.173 12	0.395 0.203 12	**0.753** **0.005** **12**	**-0.694** **0.012** **12**	-0.558 0.059 12
Dependent Parameters	Chl *a*	**0.859** **0** **15**	**0.849** **0** **15**	**0.670** **0.006** **15**	**0.776** **0.001** **15**	**-0.672** **0.006** **15**	**-0.803** **0** **15**
	POC	**0.944** **0** **15**	**0.638** **0.010** **15**	**0.568** **0.027** **15**	**0.890** **0** **15**	**-0.861** **0** **15**	**-0.616** **0.015** **15**
	PP_{chla}	**0.786** **0.004** **11**	0.037 0.915 11	0.048 0.888 11	**0.731** **0.011** **11**	**-0.729** **0.011** **11**	-0.532 0.092 11

Table 5.6. Pearson correlation coefficients (top)—including *p*-values (middle) and sample size (bottom) of correlations—of centric diatom, pennate diatom and flagellate cell counts and their percent abundance of total cells enumerated using light microscopy, with environmental parameters (*see* text for definitions) under thick snow cover. Missing data has been excluded pairwise and correlations of significance ($p<0.05$) are in bold.

	Parameter	Cell Counts			Percent Abundance		
		Centric	Pennate	Flagellate	Centric	Pennate	Flagellate
Independent Environmental Parameters	NO_x	-0.374 0.169 15	-0.348 0.204 15	-0.293 0.289 15	-0.378 0.165 15	0.350 0.201 15	0.095 0.737 15
	E_z(June)	0.533 0.060 13	**0.616** **0.025** **13**	**0.675** **0.011** **13**	0.441 0.131 13	-0.132 0.667 13	-0.458 0.116 13
	E_z(PAR)	**0.624** **0.040** **11**	**0.823** **0.002** **11**	**0.902** **0** **11**	0.569 0.068 11	-0.209 0.536 11	**-0.599** **0.051** **11**
	Temp.	0.214 0.505 12	0.282 0.375 12	**0.594** **0.042** **12**	0.175 0.587 12	-0.071 0.827 12	-0.228 0.476 12
	Salinity	0.009 0.978 12	0.569 0.054 12	**0.722** **0.008** **12**	-0.027 0.934 12	0.401 0.196 12	**-0.732** **0.007** **12**
	Brine Vol.	0.341 0.279 12	0.475 0.119 12	**0.736** **0.006** **12**	0.290 0.360 12	-0.060 0.854 12	-0.447 0.145 12
Dependent Parameters	Chl *a*	**0.728** **0.002** **15**	**0.877** **0** **15**	**0.543** **0.036** **15**	**0.623** **0.013** **15**	-0.178 0.525 15	**-0.855** **0** **15**
	POC	**0.791** **0** **15**	**0.744** **0.001** **15**	0.474 0.074 15	**0.714** **0.003** **15**	-0.443 0.099 15	**-0.627** **0.012** **15**
	PP_{chla}	0.235 0.463 12	0.562 0.057 12	0.538 0.071 12	0.068 0.833 12	-0.106 0.743 12	-0.128 0.692 12

The abundance of choanoflagellates increased with centric diatom abundance ($r = 0.605$, $p < 0.05$) under thin snow and pennate diatom abundance under thick snow ($r = 0.568$, $p < 0.05$). Their abundance was also positively correlated with the intensity of E_z(PAR) under thin ($r = 0.780$, $p < 0.05$) or thick ($r = 0.853$, $p < 0.05$) snow. The abundance of heterotrophic flagellates significantly decreased with NO_x concentration under thin snow, and showed an increase with all parameters except NO_x under thick

snow (Table 5.6). The percent abundance of flagellates decreased with E_z(PAR) and salinity under thick snow.

Ice algal biomass and production

The potential impact of cell size and taxonomic composition on chl *a* biomass, carbon biomass (POC) and estimated daily primary production were investigated through linear correlation analysis (Tables 5.3 – 5.6). Chlorophyll *a* and carbon biomass increased with nanoeukaryote and microeukaryote abundances, under thin and thick snow, but were not correlated with the concentration of picoeukaryotes (Table 5.3, 5.4). Biomass also significantly increased with the abundance of all taxonomic groups, with the exception of flagellate abundance under thick snow (Table 5.5, 5.6). However, the type of correlation (positive or negative) between biomass and percent abundance of the taxonomic groups indicates that biomass increased with dominance of centric diatoms in the algal community and decreased with the proportion of pennate diatoms and/or flagellate cells.

Primary production decreased with picoeukaryote abundance under both snow covers and was significantly correlated with nanoeukaryote abundance (derived from light microscopy and average abundance) under thin snow, where the relationship was positive (Table 5.3). Production also increased with centric diatoms (abundance or percent composition) and decreased with the relative abundance of pennate diatoms under thin snow (Table 5.5). Primary production was not significantly correlated with any of the taxonomic groups under thick snow cover.

5.4 Discussion

5.4.1 Influences of heterotrophic bacterial abundance and production

The number of heterotrophic bacteria present in the sea ice was within the wide range of estimates that have been reported for spring or summer sea ice in the Arctic, from 5 x 10^5 [Maranger et al., 1994] to 16.4 x 10^{10} cells ml^{-1} [He et al., 2005]. Bacterial production was also representative of literature values for Arctic sea ice, where production over the spring was within the range of 3.6 x 10^{-8} [Maranger et al., 1994] to 3.1 x 10^{-6} g C l^{-1} h^{-1} [Kaartokallio et al., 2013].

Of all environmental factors examined, significant correlations with bacterial production and abundance were only observed with picoeukaryote abundance and brine volume under thick snow [Figure 5.8]. Regression analysis of these parameters indicate that picoeukaryote abundance alone (without the 21 April outlier under thin snow) best explained bacterial production under thin snow ($r^2 = 0.719$, $p < 0.05$), as the regression with brine volume was not significant ($p = 0.112$). Under thick snow, picoeukaryote abundance ($r^2 = 0.397$, $p < 0.05$) along with brine volume ($r^2 = 0.490$, $p < 0.05$) independently explained similar magnitudes of variability. We note that multiple regressions of picoeukaryote abundance and brine volume did not improve the predictability of bacterial production for thin or thick snow covered sea ice (see Table 5.S.3).

Picoeukaryote abundance also explained the majority of variability in multiple regressions of this parameter with bacterial abundance and brine volume under thin ($r^2 = 0.768$, $p < 0.05$) and thick snow ($r^2 = 0.644$, $p < 0.05$). This is represented by higher standardized regression coefficients (β) for picoeukaryote abundance than brine volume

under thin (β_{pico} = 0.641, $p < 0.05$)(β_{brine} = 0.381, p = 0.067) or thick (β_{pico} = 0.501, $p < 0.05$) (β_{brine} = 0.492, $p < 0.05$) snow covers, respectively.

The strong relationships between bacterial abundance and production with the number of picoeukaryotic cells may be due to increased supply of labile dissolved carbon, as diffusive release of DOC is greater from picoeukaryotes than larger cells as a result of a higher surface area to volume ratio [Lopez-Sandoval, 2011]. This supply of organic substrate by ice algae is a well-documented control of bacterial production [e.g. Bunch & Harland, 1990; Mock et al., 1997; Søgaard et al., 2013], but our results suggest that it is the smallest group of algae that could be most important to this relationship. Unfortunately DOC concentrations from the bottom-ice were not available to confirm this hypothesis, and thus further work on the contribution of sea ice picoeukaryotes to bacterial production and the microbial loop is merited.

Over 95% of microbes in sea ice inhabit the liquid brine fraction [Deming, 2010], supporting our observation that cell abundance increased with the volume of brine habitat (Figure 5.8). Increasing brine volume is also associated with greater connectivity of brine inclusions through the ice profile [Golden et al., 1998], which facilitates gravity driven movement of organic carbon and cells previously isolated higher in the ice profile towards the bottom [Deming, 2010]. This in turn could also increase the supply of organic substrate for bacterial production, driving the significant association between bacterial production and brine volume that was observed under thick snow (Figure 5.8). Increasing brine volume in the upper ice was associated with increases in the bottom-ice during this study [Campbell et al., 2016], supporting a drainage mechanism for cell and DOC supply to the bottom-ice (Figure 5.8).

The strong correlations between bacterial abundance and production (Section 5.3.5) indicate that the majority of cells present in the ice were actively respiring. However, the increased bacterial production per cell after 25 April while bacterial abundance showed low seasonal variability (Figure 5.2) indicates that one or a combination of the following were important factors: increasing productivity per cell over the spring, cell loss via grazing, cell death following viral induced lysis, and variable carbon conversion factors in the calculation of bacterial production. Unfortunately we do not have sufficient data to evaluate the specific contribution of each potential factor here.

5.4.2 Using flow cytometry and light microscopy to estimate nanoeukaryote abundance

The abundance of nanoeukaryotes counted with the flow cytometer and enumerated from light microscopy is compared in Figure 5.9. The comparison shows that flow cytometry provided slightly higher estimates of cell counts (i.e. above the 1:1 line) at or below cell concentrations of approximately 0.8 x 10^5 cells ml^{-1}, but lower counts (i.e. below the 1:1 line) above this threshold, relative to light microscopy. Higher flow cytometry based counts of nanoeukaryotes at low cell densities likely represents the effectiveness of the flow cytometer in counting small cells that are easily missed when using a light microscope [Tremblay et al., 2009], while overestimates of cell abundance from light microscopy have been attributed to the lugol staining process that can introduce difficulty in distinguishing cells and separating autotrophic from heterotrophic nanoflagellates [Sherr & Sherr, 1993; Tremblay et al., 2009].

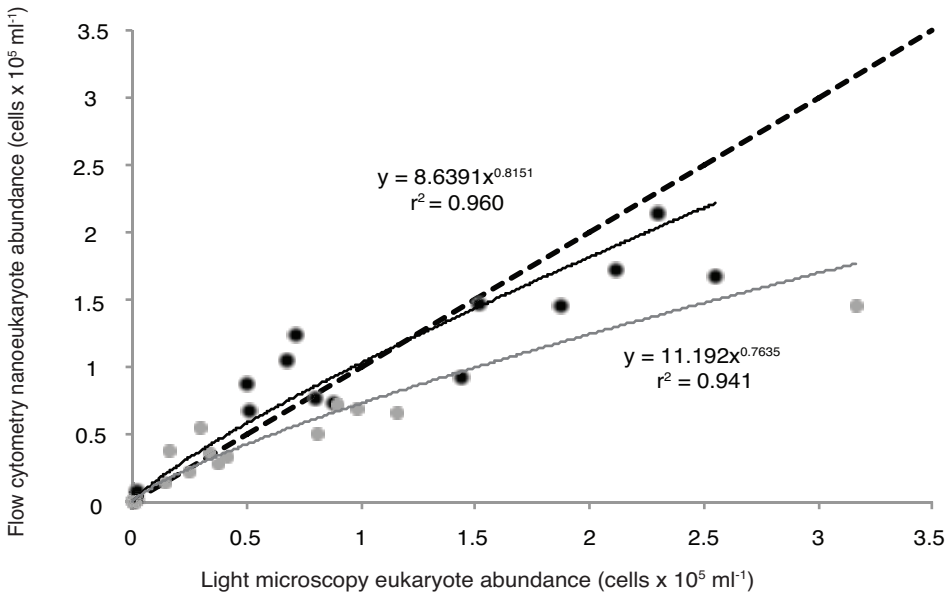

Figure 5.9. Abundance of estimated nanoeukaryotic cells using light microscopy, versus nanoeukaryotic cell counts from flow cytomwtry analysis of samples under thin (black) and thick (grey) snow covers. Power functions (solid) and a 1:1 line (dashed) are also presented.

Data points of light microscope versus flow cytometer based cell counts in Figure 5.9 deviated from the ideal 1:1 relationship to a greater extent under thick snow. This could partially be a result of one data point under thick snow with especially high light microscope counts. However, it may also highlight that the difference in nanoeukaryote abundance between methods was greatest under thick snow cover due to taxonomic differences. Nanoeukaryotic algae under both snow covers were dominated by centric diatoms (Appendix Tables 5.1, 5.2), which comprised 80.7 ± 17.5% of nanoeukaryotes under thin snow and 63.8 ±19.1% under thick snow. However, the relative abundance of pennate diatoms <20 μm was greater under thick snow at 13.2 ± 7.4% in comparison to 8.9 ± 7.1% under thin snow. We suggest that the flow cytometer may not have been able to count pennate diatoms as effectively as centric diatoms because the apical axis of pennates was often estimated to be close to 20 μm diameter, the maximum size detected

by the flow cytometer (Appendix Tables 5.1, 5.2). Our classification of nanoeukaryotes from light microscopy likely compounded this error, as cells deemed <20 μm based on literature size estimates could have been slightly larger. In comparison, centric diatoms which were predominantly of the genus *Attheya* (Appendix Table 5.1, 5.2) had apical and pervalvar axes well within the nanoeukaryotic range (Campbell pers. obs.). Finally, the proportion of *Attheya* spp. that was epiphytic was greater under thick snow (*see Taxonomic composition of the ice algal community*). These cells living largely in association with *Nitzschia frigida* may not have been counted separately by the flow cytometer, which would have contributed to a perceived underestimate of cell abundance relative to estimates from light microscopy.

5.4.3 Seasonal controls of algal community composition, biomass and production

Size classification of the algal community

The concentration of picoeukaryotes in this study was within the range reported for sea ice by Piwosz et al. [2013], except for the peaks in abundance observed between 29 April and 13 May that reached nearly 1.5 x 10^5 cells ml^{-1} (Figure 5.4). These peaks roughly corresponded to the increases observed in the number of heterotrophic bacteria (Figure 5.3), where the presence of picoeukaryotes is thought to have positively affected the number of heterotrophic bacteria and their production in the ice by providing DOC (Section 5.4.1). The high peaks in picoeukaryote abundance could have also been aided by the affinity of picoeukaryotes for nutrient limited environments [Agawin et al., 2000], like the nitrogen depleted conditions documented for sea ice in the study region

[Campbell et al., 2016]. Despite the relatively high abundance of picoeukaryotes in this study, we note that they did not significantly correlate with chl *a* and carbon biomass, or primary productivity (Table 5.3, 5.4). The minimal contribution of picoeukaryotes to chl *a* was also supported through estimates of only 1.2 ± 1.1 % of chl *a* biomass under thin snow and 2 ± 1.2% under thick snow (estimated using the cellular quota of 0.025 pg chl *a* $cell^{-1}$ proposed by Tremblay et al. [2009].

Light availability is a well-documented control of biomass during the accumulation phase of the ice algal bloom [e.g. Gosselin et al., 1985; Mundy et al., 2005; Campbell et al., 2015]. The significant positive correlations between nanoeukaryote algae and E_z(PAR) under both snow covers support these conclusions for algae 2-20 μm in this study. Furthermore, linear regression analyses performed on average nanoeukaryote abundance and all environmental parameters indicate that light was the dominant control (highest r^2, Table 5.S.1), significantly accounting for 65% of variability in nanoeukaryote abundance under thin snow and 48% under thick snow. Light availability likely influenced microeukaryote abundance under thick snow, where correlations between the parameters were significant (Table 5.4) and E_Z(PAR) significantly accounted for 63% of variability in microeukaryote abundance (Table 5.S.2). The absence of a similar relationship under thin snow could potentially highlight that microeukaryotes present experienced less light limitation due to the higher light conditions (Figure 5.2).

Significant correlations between biomass and nanoeukaryotes or micoreukaryotes (Table 5.3, 5.4) suggest that algae >2 μm drove changes in chl *a* and POC (Table 5.3, 5.4). This is perhaps not surprising given that the majority of nanoeukaryotes and microeukaryotes in this study were diatoms (Appendices Table 5.1, 5.2), which can

replicate quickly in response to the favorable light conditions in the Arctic spring [Miller & Wheeler, 2012]. These findings also support previous observations that showed significant correlations between chl *a* and nanoeukaryote abundance in sea ice [Comeau et al., 2013], and cells >5 μm accounting for 50 to 100% of ice algal biomass [Gosselin et al., 1997]. Further calculation of linear regressions indicate that the contribution of microeukaryotes to overall biomass was either insignificant or less important (lower β) than nanoeukaryotes, with the exception of chl *a* under thick snow (see Table 5.S.3).

Picoeukaryote abundance in sea ice can also be controlled by light availability, and has been negatively correlated with snow thickness as a result of its attenuation properties [Piwosz et al., 2013]. Significant relationships between the number of picoeukaryotes and PAR were not specifically documented in this study (Table 5.3, 5.4); however, picoeukaryote abundance was significantly greater under the higher light conditions of thin snow cover (see *Abundance of picoeukaryotes*).

The seasonal shift in the percent composition of the ice algal community from dominance of small to large cells was associated with the percent increase of nanoeukaryotes under thin snow, and similar increases of nanoeukaryotes and microeukaryotes under thick snow (Figure 5.5). Increasing primary production over the spring that was driven by increasing PAR transmission through the ice [Campbell et al., 2016] was mostly influenced by these increases in nano-and microeukaryotes (Figure 5.4, 5.6). The strength of linear regressions further suggests that nanoeukaryotes largely controlled production under thin snow ($r^2 = 0.546$, $p < 0.05$), while microeukaryotes were perhaps slightly more important under thick snow cover ($r^2 = 0.256$, $p = 0.093$) (see Table 5.S.3). These observations support conclusions by Gosselin et al. [1997] that algae >5 μm

account for the majority of production in Arctic sea ice, despite the high potential of picoeukaryotes to contribute to primary production as a result of their high growth rates [Agawin et al., 2000].

Taxonomic composition of the algal community

Diatoms typically dominate the bottom-ice algal assemblage, with pennate diatoms comprising 68% and centric diatoms 12% of average communities in the Canadian Arctic [Poulin et al., 2011]. In comparison to these averages the proportion of pennate diatoms was low and that of centric diatoms was high in our study (Figure 5.7), particularly under thin snow cover where centric species of the genus *Attheya* were abundant (Appendix Table 5.1). Centric diatoms like *Attheya septentrionalis*, in addition to *Melosira arctica* (not documented here), are commonly found in Arctic sea ice [Riedel et al., 2003; vonQuillfedt et al., 2009; Poulin et al., 2011]. However, it is the cryophilic pennate diatom *Nitzschia frigida* that is considered to be the sentinel species of this environment [Poulin et al., 2011; Leu et al., 2015]. We surmise that species of *Attheya* may have been able to outcompete *Nitzschia frigida* in our study area of Dease Strait due to the relatively fresh and nitrogen depleted conditions (Figure 5.2) [Campbell et al., 2016], as centric diatoms likely have a greater affinity for low salinity and nitrogen limited conditions [Melnikov et al., 2002; Monti et al., 1996]. The surface area to volume ratio of the small *Attheya* spp. is also slightly greater than the comparatively large cells of *Nitzschia frigida*. This size difference leads to a greater nutrient uptake potential per growth requirement [Miller & Wheeler, 2012] for *Attheya* spp. that could allow them to outcompete larger diatoms for nutrients.

Seasonal trends in diatom abundance under thin and thick snow covers (Figure 5.7) appear to differ as a result of a rapid increase in *Attheya* spp. under thin snow (Appendix Table 5.1). Although the low salinity and limited nutrients in the region were suggested to have facilitated dominance of the centric diatom *Attheya* spp., the difference in absolute and relative abundance of this genus between thin and thick snow covers indicates that spatial variability across the study area was also important. We suggest that the higher light conditions characteristic of a thin snow cover (Figure 5.2) permitted centric diatoms to outcompete pennate diatoms at thin snow sites and resulted in the strong positive correlations observed between E_Z(PAR) and centric abundance (Table 5.5). This is supported by previous observations that centric diatoms can be more numerous in thin sea ice as a result of greater light availability [Medlin & Priddle, 1990; Melnikov et al., 2002].

The low relative abundance of other remaining taxonomic groups is expected given the dominance of diatoms in this study (Figure 5.6). For example, species of flagellates that typically account for approximately 6% of eukaryotes in sea ice of the Canadian Arctic [Poulin et al., 2011] represented about 4% of the algal population under thin snow and 10% under thick snow. Flagellate species are capable of dominating algal communities under low light conditions [Mikkelsen et al., 2008], and this likely explains the higher proportion of flagellates observed at the beginning of the spring and under thick snow cover (Figure 5.7). Furthermore, limited or nil contributions of choanoflagellates [Poulin et al., 2011], cyanobacteria [Bowman et al., 2015] and ciliates [Riedel et al., 2007] to microbial communities in sea ice during the spring are known to occurr.

The majority of nanoeukaryotes in this study were centric diatoms, while the majority of microeukaryotes were pennate diatoms (Appendix Table 5.1, 5.2). As a result, the significant role of these size classes of algae in driving biomass and potentially primary production discussed previously, also applies to the importance of the taxonomic groups of centric and pennate diatoms. For example, nanoeukaryotes had the greatest correlations with biomass and production under thin snow (Table 5.3), as did centric diatoms (Table 5.5). The significant correlations between the number of flagellates and chl *a* or POC biomass (Table 5.5, 5.6) also shows that despite flagellates representing a small fraction of the sea ice community (Figure 5.7) they may be an important contributor to nanoeukaryotic biomass. We note that negative correlations between NO_x and all three taxonomic groups under thin snow cover highlight the likely presence of nitrogen limitation. This supports observations by Campbell et al. [2016] of a stronger nitrogen limitation influence under thin snow as a result of greater productivity rates, and therefore nutrient demand, at these locations.

5.5 Conclusions

The environmental factors influencing the composition of the microbial community in the bottom of sea ice and its impact on biomass and productivity were investigated in this research. Our time series of measurements showed that the size distribution and taxonomic grouping of algae changed over the spring and differed between depths of snow cover as a result of light intensity. We also found evidence that pre-existing nutrient and salinity conditions of the bottom-ice could influence the prevalence of algal species in a particular region. These changes affect the biomass and potentially the primary

productivity that is achieved, and likely contribute to the spatial variability of these variables. Future studies on species-specific responses to growth conditions would benefit this research, particularly for the species that are most often documented living in the bottom-ice.

The most important algal group driving the spring bloom in this study were diatoms of the nano- and microeukaryotic size classes. The abundance of nanoeukaryotes in particular may be effectively analyzed using either flow cytometry or light microscopy; however, interpretation of flow cytometry measurements are cautioned when cells approach 20 μm in length. Picoeukaryotes were prominent members of the sea ice community during early spring, but they did not appear to influence biomass or production in the ice. Nevertheless, these algae remain an important aspect of the community through their anticipated link to heterotrophic bacteria and the sea ice microbial loop.

A likely fallout of climate warming is the reduction of nutrient inventories in many parts of the Arctic Ocean's surface waters [Tremblay et al., 2016]. Studies have suggested that these changes favor small, picoeukaryotic cells, in the pelagic system [Tremblay et al., 2009; Li et al., 2009] because of their known affinity for low nutrient conditions elsewhere in the global oceans [Legendre et al., 1987; Agawin et al., 2000]. Our results indicate that the response of the sea ice algal community is unique as dominance by diatom taxa are likely to continue, but with a potential for the community to shift away from the typically dominant pennate diatom *Nitzschia frigida* towards centric forms like *Attheya* spp. Such changes are likely to have implications for the nutritional quality of grazer resources because of differences in fat content, and could affect the role sea ice

algae have in sequestering carbon to the deep-ocean if the sinking rates of species is found to differ substantially.

Acknowledgements

Support for this research was provided by a Northern Scientific Training Program grant and Natural Sciences and Engineering Research Council of Canada (NSERC) Canadian Graduate Scholarship to KC, Canada Foundation for Innovation (CFI) and the Canada Excellence Research Chair grant to SR, an NSERC Discovery and Northern Research Supplement Grants to CJM, and in-kind support from the Canadian High Arctic Research Station (CHARS). We also thank Dr. Michel Gosselin and Ms. Sylvie Lessard for their support. This work represents a contribution to the research programs of ArcticNet, MEOPAR, the Arctic Science Partnership (ASP) and the Canada Excellence Research Chair unit at the Centre for Earth Observation Science (CEOS) at the University of Manitoba.

References

Agawin, N.S.R., Duarte, C.M., and S. Agusti (2000), Nutrient and temperature control of the contribution of picoplankton to phytoplankton biomass and production, *Limnol. Oceanog*. 45, 591-600, doi: 10.4319/lo.2000.45.8.1891a.

Belzile, C., Brugel, S., Nozais, C., Gratton, Y., and S. Demers (2008), Variations of the abundance and nucleic acid content of heterotrophic bacteria in Beaufort Shelf waters during winter and spring, *J. Mar. Syst*. 74, 946-956, doi: 10.1016/j.jmarsys.2007.12.010.

Bowman, J.S. (2015), The relationship between sea ice bacterial community structure and biogeochemistry: A synthesis of current knowledge and known unknowns, *Elementa* 3, 1-20, doi:10.12952/journal.elementa.000072.

Brown, T.A., Belt, S.T., Philippe, B., Mundy, C.J., Massé, G., Poulin, M. and M. Gosselin (2011), Temporal and vertical variations of lipid biomarkers during a bottom ice diatom bloom in the Canadian Beufort Sea: further evidence for the use of IP25 biomarker as a proxy for spring Arctic sea ice, *Polar Biol*. 34, 1857-1868. doi: 10.1007/s00300-010-0942-5.

Bunch, J.N., and R.C. Harland (1990), Bacterial production in the bottom surface of sea ice in the Canadian subarctic, *Can. J. Fish. Aquat. Sci*. 43, 1986-1995, doi: 10.1139/f90-223.

Campbell, K., Mundy, C.J., Barber, D.G., and M. Gosselin (2015), Characterizing the sea ice algae chl *a*-snow depth relationship over Arctic spring melt using transmitted irradiance, J. Mar. Syst. 127, 76-84, doi: 10.1016/j.jmarsys.2014.01.008.

Campbell, K., C.J. Mundy, J.C. Landy, A. Delaforge, and S. Rysgaard (2016), Community dynamics of bottom-ice algae in Dease Strait of the Canadian Arctic, *Prog. Oceanogr*. 149, 27-39, doi: 10.1016/j.pocean.2016.10.005.

Comeau, A.M., Philippe, B., Thaler, M., Gosselin, M., Poulin, M., and C. Lovejoy (2013), Protists in Arctic drift and land-fast sea ice, J. Phycol. 49, 229-240, doi: 10.1111/jpy.12026.

Cota, G.F. and C.W. Sullivan (1990), Photoadaptation, growth and production of bottom ice algae in the Antarctic, *J. Phycol*. 26, 399-411.

Caron, D.A., and R.J. Gast (2010), Heterotrophic protists associated with sea ice, In: Thomas DN, Dieckmann GS (eds), *Sea Ice* 2nd Ed, Wiley Blackwell Publishing, Malaysia, pp 327-356.

Cota G, and E. Horne (1989), Physical control of arctic ice algal production, Mar. Ecol. Prog. Ser. 52, 111-121.

Cox, G.F.N., and W.F. Weeks (1983), Equations for determining the gas and brine volumes in sea-ice samples, J. Glaciol. 29(102), 306-316.

Deming, J.W. (2010), Sea ice bacteria and viruses, In: Thomas DN, Dieckmann GS (eds), *Sea Ice* 2nd Ed, Wiley Blackwell Publishing, Malaysia, pp 248-282.

Ducklow, H.W. (2003), Seasonal production and bacterial utilization of DOC in the Ross Sea, Antarctica, *Biogeochem. Ross Sea* 78, 143-158. doi: 10.1029/078ARS09.

Ducklow, H. (2000), Bacterial production and biomass in the oceans, In: Kirchman DL (ed). *Microbial ecology of the oceans*, Wiley-Liss, pp 85-120.

Falkowski, P.G., and T.G. Owens (1978), Effects of light intensity on photosynthesis and dark respiration in six species of marine phytoplankton, Mar. Biol. 45, 289-295.

Glaz, P., Sirois, P., Archambault, P., and C. Nozais (2014), Impact of forest harvesting on trophic structure of eastern Canadian boreal shield lakes: insights from stable isotope analyses, *PLOS ONE* 9(4), doi: 10.1371/journal.pone.0096143.

Golden, K.M., Ackley, S.F., and V.I. Lytle (1998), The percolation phase transition in sea ice, *Science* 282 (5397), 2238-2241, doi: 10.1126/science.282.5397.2238.

Gosselin, M., Legendre, L., Demers, S., and R.G. Ingram (1985), Responses of sea-ice microalgae to climatic and fortnightly tidal energy inputs (Manitounuk Sound, Hudson bay), Can. J. Fish. Aquat. Sci. 42, 999-1006.

Gosselin, M., Levasseur, M., Wheeler, P.A., Horner, R.A., and B.C. Booth (1997), New measurements of phytoplankton and ice algal production in the Arctic Ocean, *Deep-Sea Res. II* 44 (8), 1623-1644, doi: 10.1016/S0967-0645(97)00054-4.

Haecky, P., and A. Anderson (1999), Primary and bacterial production in sea ice in the northern Baltic Sea, Aquat. Microb. Ecol. 20, 107-118, doi:10.3354/ame020107.

He, J., Inghong, C., Iaodong, J.X., Bo, C., and Y. Yong (2005), Characterization of the summer pack ice biotic community of Canada Basin, *Acta Ocean Sinica* 24(6), 80-87.

Hezel, P.J., Zhang, X., Bitz, C.M., Kelly, B.P., and F. Massonnet (2012), Projected decline in spring snow depth on Arctic sea ice caused by progressively later autumn open ocean freeze-up this century, *Geophys. Res. Lett.* 39, L17505, doi: 10.1029/2012GL052794.

Hsaio, S.I.C., (1992), Dynamics of ice algae and phytoplankton in Frobisher Bay, *Polar Biol.* 12, 645-651, doi: 10.1007/BF00236987.

Kana, T.M. (1990), Light-dependent oxygen cycling measured by an oxygen-18 isotope dilution technique, Mar. Ecol. Prog. Ser. 64, 293-300.

Kaartokallio, H., Søgaard, D.H., Norman, L., Rysgaard, S., Tison, J.L.-, Delille, B., and D.N. Thomas (2013), Short-term variability in bacterial abundance, cell properties, and incorporation of leucine and thymidine in subarctic sea ice, Aquat. Microbiol. Ecol. 71, 57-73, doi: 10.3354/ame01667.

Kirchman, D.L. (1993), Chapter 58: Leucine incorporation as a measure of biomass production by heterotrophic bacteria, In: *Handbook of Methods in Aquatic Microbial Ecology*, CRC Press, Florida, USA, pp 509-518.

Kirchmann, D. (2001), Measuring bacterial biomass production and growth rates from leucine incorporation in natural aquatic environments, *Marine Microbiol*. 30, 227-237. doi: 10.1016/S0580-9517(01)30047-8.

Kirst, G.O., and C. Wiencke (1995), Ecophysiology of polar algae, *J. Phycol*. 31, 181-199, doi: 10.1111/j.0022-3646.1995.00181.x.

Leu, E., Søreide, J.E., Hessen, D.O., Falk-Petersen, S., and J. Berge (2011), Consequences of changing sea-ice cover for primary and secondary producers in the European Arctic shelf seas: timing, quantity, and quality, *Prog. Oceanog*. 90, 18-32, doi: 10.1016/j.pocean.2011.02.004.

Lee, S.H., Whiteledge, T.E., and S.-H. Kang (2008), Spring time production of bottom ice algae in the landfast sea ice zone at Barrow Alaska, *J. Exp. Mar. Biol. Ecol*. 367, 204-212, doi: 10.1016/j.jembe.2008.09.018.

Leu, E., Mundy, C.J., Assmy, A., Campbell, K., Gabrielsen, T.M., Gosselin, M., Juul-Pedersen, T., and R. Gradinger (2015), Arctic spring awakening – Steering principles behind the phenology of vernal ice algae blooms, Prog. Oceanog. 139, 151-170, doi: 10.1016/j.pocean.2015.07.012.

Legendre, L., Demers, S., and M. Gosselin (1987), Chlorophyll and photosynthetic efficiency of size-fractionated sea-ice microalgae (Hudson Bay, Canadian Arctic), Mar. Ecol. Prog. Ser. 40, 199-203.

Legendre, L., Ackley, S.F., Dieckmann, G.S., Gullicksen, B., Horner, R., Hoshiai, T., Melnikov, I.A., Reeburgh, W.S., Spindler, M., and C.W. Sullivan (1992), Ecology of sea ice biota: Part 2, Global significance, *Polar Biol*. 12, 429–444.

Li, W.K.W., McLaughlin, F.A,. Lovejoy, C., and E.C. Carmack (2009), Smallest algae thrive as the Arctic Ocean freshens, *Science* 326, 539, doi: 10.1126/science.1179798.

López-Sandoval, D.C., Fernández, A., and E. Marañón (2011), Dissolved and particulate primary production along a longitudinal gradient in the Mediterranean Sea, *Biogeosci*. 8, 815-825, doi: 10.5194/bg-8-815-2011.

Lund, J.W.G., Kipling, C., and E.D. Le Cren (1958), The inverted microscope method of estimating algal number and the statistical basis of estimations by counting, Hydrobiol. 11, 143–170, doi:10.1007/BF00007865.

Maranger, R., Bird, D.F., and S.K. Juniper (1994), Viral and bacterial dynamics in Arctic sea ice during the spring algal bloom near Resolute, NWT, Canada, Mar. Ecol. Prog. Ser. 111, 121–127, doi: 10.3354/meps111121.

Maranger, R., Vaqué, D., Nguyen, D., Hébert, M.-P., and E. Lara (2015), Pan-Arctic patterns of planktonic heterotrophic microbial abundance and processes: Controlling factors and potential impacts of warming, Prog. Oceanog. 139, 221-232, doi:10.1016/j.pocean.2015.07.006.

Melnikov, I.A., Kolosova, E.G., Welch, H.E., and L.S. Zhitina (2002), Sea ice biological communities and nutrient dynamics in the Canada basin of the Arctic Ocean, *Deep-Sea Res. I* 49, 1623-1649, doi: 10.1016/S0967-0637(02)00042-0.

Mendle, L.K., and J. Priddle (1990), *Polar Marine Diatoms*. British Antarctic Survey, Cambridge, UK.

Michel, C., Nielsen, T.G., Nozais, C., and M. Gosselin (2002), Significance of sedimentation and grazing by ice micro- and meiofauna for carbon cycling in annual sea ice (northern Baffin Bay), Aquat. Microbiol. Ecol. 30, 57-68, doi: 10.3354/ame030057.

Mikkelsen, D.M., Rysgaard, S., and R.N. Glud (2008), Microalgal composition and primary production in Arctic sea ice: a seasonal study from Kobbefjord (Kangerluarsunnguaq), west Greenland, Mar. Ecol. Prog. Ser. 368, 65-74, doi: 10.3354/meps07627.

Miller, C.B., and P.A. Wheeler (2012), *Biological Oceanography*. Wiley Blackwell Publishing, Malaysia.

Mock, T., Meiners, K.M., and H.C. Giesenhagen (1997), Bacteria in sea ice and underlying brackish water at 54" 26' 50" N (Baltic Sea, Kiel Bight), *Mar. Ecol. Prog. Ser*. 158, 23-40, doi: 10.3354/meps158023.

Monti, D., Legendre, L., Therriault, J.C. and S. Demers (1996), Horizontal distribution of sea-ice microalgae: environmental control and spatial processes (southeastern Hudson Bay, Canada), Mar. Ecol. Prog. Ser. 133, 229-240.

Mundy, C.J., Barber, D.G., and C. Michel (2005), Variability of snow and ice thermal, physical and optical properties pertinent to sea ice algae biomass during spring, *J. Mar. Syst.* 58, 107-120, doi: 10.1016/j.jmarsys.2005.07.003.

Mundy, C.J., Gosselin, M., Ehn, J.K., Belzile, C., Poulin, M., Alou, E., Roy, S., Hop, H., Lessard, S., Papakyriakou, T.N., Barber, D.G., and J. Stewart (2011), Characteristics of two distinct high-light acclimated algal communities during advanced stages of sea ice melt. *Polar Biol.* 34, 1869-1896, doi: 10.1007/s00300-011-0998-x.

Niemi, A., Michel, C., Hille, K., and M. Poulin (2011), Protist assemblages in winter sea ice: setting the stage for the spring ice algal bloom, *Polar Biol.* 34, 1803-1817, doi: 10.1007/s00300-011-1059-1.

Parsons, T.R., Maita, Y., and C.M. Lalli (1984), *A Manual of Chemical and Biological Methods for Seawater Analysis*, Pergamon, New York.

Piwosz, K., Wiktor, J.M., Niemi, A., Tatarek, A., and C. Michel (2013), Mesoscle distribution and functional diversity of picoeukaryotes in the first-year ice of the Canadian Arctic, *ISME* 7, 1461-1471, doi: 10.1038/ismej.2013.39.

Poulin, M., and A. Cardinal (1982), Sea ice diatoms from Manitounuk Sound, southeastern Hudson Bay (Quebec, Canada). III. Cymbellaceae, Entomoneidaceae, Gomphonemataceae, and Nitzschiaceae, *Can. J. Bot.* 61, 107-118.

Poulin, M., Daugbjerg, N., Gradinger, R., Ilyash, L., Ratkova, T., and C. Quillfeldt (2011), The pan-Arctic biodiversity of marine pelagic and sea-ice unicellular eukaryotes: a first-attempt assessment, *Mar. Biodiv.* 41, 13-28, doi: 10. 1007/s12526-010-0058-8.

Riedel, A., Michel, C., Poulin, M., and S. Lessard (2003), Taxonomy and abundance of microalgae and protists at a first-year sea ice station near Resolute Bay, Nunavut, Spring to Early Summer 2001. *Fisheries and Oceans Canada: Canadian Data Report of Hydrography and Ocean Sciences* 159.

Riedel, A., Michel, C., Gosselin, M., and B. LeBlanc (2007), Grazing of large-sized bacteria by sea-ice heterotrophic protists on the Mackenzie shelf during the winter-spring transition, Aquat. Microb. Ecol. 50, 25-38, doi: 10.3354/ame01155.

Rózańska, M., Gosselin, M., Poulin, M., Wiktor, J.M., and C. Michel (2009), Influence of environmental factors on the development of bottom ice protest communities during the winter-spring transition, Mar. Ecol. Prog. Ser. 386, 43-59, doi: 10.3354/meps08092.

Rysgaard, S., and R.N. Glud (2004), Anaerobic N2 production in Arctic sea ice, *Limnol. Oceanog.* 49, 86-94, doi: 10.4319/lo.2004.49.1.0086.

Sarmiento, J.L., and N. Gruber (2006), *Ocean Biogeochemical Dynamics*, Princeton University Press, Princeton, N.J.

Sherr, E.B., and B.F. Sherr (1993), Preservation and storage of samples for enumeration of heterotrophic protists, In: Kemp, P.F., Sherr, B.F., Sherr, E.B., Cole, J.J. (eds) *Current methods in aquatic microbial ecology*. Lewis Publishers, New York, pp 207–212.

Sime-Ngando, T., Juniper, S.K., and S. Demers (1997), Ice-brine and planktonic microheterotrophs from Saroma-ko Lagoon, Hokkaido (Japan): quantitative importance and trophodynamics, J. Mar. Syst. 11, 149-161, doi: 10.1016/S0924-7963(96)00035-8.

Smith, R.E.H., and P. Clement (1990), Heterotrophic activity and bacterial productivity in assemblages in microbes from sea ice in the High Arctic, *Polar Biol*. 10, 351-357, doi: 10.1007/BF00237822.

Smith, R.E.H, Clement, P., and G.F. Cota (1989), Population dynamics of bacteria in Arctic sea ice, Microb. Ecol. 17, 63-76.

Søgaard, D.H., Kristensen, M., Rysgaard, S., Glud, R.N., Hansen, P.J., and K.M. Hilligsoe (2010), Autotrophic and heterotrophic activity in Arctic first-year sea ice: seasonal study from Malene Bight, SW Greenland, *Mar. Ecol. Progr. Ser*. 419, 31-45, doi: 10.3354/meps08845.

Søgaard, D.H., Thomas, D.N., Rysgaard, S., Glud, R.N., Norman, L., Kaartokallio, H., Juul-Pedersen, T., and N.-X. Gelfius (2013), The relative contributions of biological and abiotic processes to carbon dynamics in subarctic sea ice, *Polar Biol*. 36(12), 1761-1777, doi: 10.1007/s00300-013-1396-3.

Søreide, J., Leu, E., Berge, J., Graeve, M., and S.F. Falk-Petersen (2010), Timing of blooms, algal food quality and Calanus glacialis reproduction and growth in a changing Arctic, Glob. Change Biol. 16(11), doi: 10.1111/j.1365-2486.2010.02175.x.

Strickland, J.D., and T.R. Parsons (1972), *A practical handbook of seawater analysis*, 2nd Ed. Bull. Fish. Res. Bd. Can.

Tomas, C.R. (1997), *Identifirst-year iceng marine phytoplankton*, Academic Press, California, USA.

Tremblay, G., Belzile, C., Gosselin, M., Poulin, M., Roy, S., and J.-E. Tremblay (2009), Late summer phytoplankton distribution along a 3500 km transect in Canadian Arctic waters: strong numerical dominance by picoeukaryotes, Aquat. Microbiol. Ecol. 54, 55-70, doi: 10.3354/ame01257.

Tremblay, J., Anderson, L.G., Matrai, P., Coupel, P., Bélanger, S., Michel, C., and M.

Reigstad (2016), Global and regional drivers of nutrient supply, primary production and CO2 drawdown in the changing Arctic Ocean, *Prog. Oceanog.* 139, 171-196, doi: 10.1016/j.pocean.2015.08.009.

vonQuillfedt, C.H., Hegseth, E.N., Johsen, G., Sakshaug, E., Syvertsen, E.E. (2009), Ice algae, In: Sakshaug E, Johnsen G, Kavacs K (eds) *Ecosystem Barents Sea*, Pair Academic Press, Trondheim, pp 285-302.

Wassmann, P., and M. Reigstad (2011), Future Arctic Ocean seasonal ice zones and implications for pelagic-benthic coupling, *Oceanog.* 24(3), 220–231, doi: 10.5670/oceanog.2011.74.

Webster, M.A., Rigor, I.G., Nghiem, S.V., Kurtz, N.T., Farrell, S.L, Perovich, D.K., and M. Sturm (2014), Interdecadal changes in snow depth on Arctic sea ice, J. Geophys. Res. Oceans 119, 5395– 5406, doi: 10.1002/2014JC009985.

Chapter Five Appendices

Table 5.1 Detailed list of species abundance (cells ml^{-1}) in the bottom 0-5 cm of sea ice under thin snow cover following analysis by light microscopy. Taxonomic orders are highlighted in bold and are underlined, suborders are underlined. Algae included in the estimates of nanoeukaryotes are designated by (n) and microeukaryotes by (m).

	Collection Date	March			April			May							June	
		07	11	15	21	25	29	03	08	13	17	21	26	30	05	09
	Sample Event	1	2	3	4	5	6	7	8	9	10	11	12	13	14	15
	Bacillariophyta	**2558**	**584**	**10989**	**130645**	**145819**	**169851**	**173150**	**118279**	**259023**	**239127**	**248752**	**253055**	**324143**	**161613**	**339436**
	Biddulphiales (Centric Diatoms)	**668**	**188**	**736**	**41348**	**43002**	**67064**	**65562**	**61672**	**183255**	**132896**	**130277**	**174814**	**218629**	**72596**	**246978**
	Coscinodiscineae															
n	*Leptocylindrus* spp. (10-20 μm)	nd	nd	nd	nd	nd	nd	1261	nd	nd	nd	nd	447	nd	nd	nd
n	*Thalassiosira hyperborea* (Grunow) Hasle	nd	nd	9	nd	nd	nd	nd	nd	nd	nd	454	nd	nd	nd	nd
m	*Thalassiosira* spp. (20-50 μm)	nd	nd	nd	nd	323	x	nd	nd	nd	nd	nd	nd	nd	nd	nd
m	*Thalassiosira* spp. (> 50 μm)	nd	nd	nd	nd	nd	nd	nd	nd	nd	nd	nd	nd	nd	nd	nd
	Biddulphiineae															
n	*Attheya longicornis* Crawford & Gardner	19	3	110	9381	10993	10447	10507	3744	6608	19354	12710	29061	25484	4753	23642
n	*A. septentrionalis* (Østrup) Crawford	nd	nd	nd	347	323	337	1261	1542	6608	3871	3631	2683	5365	864	1689
n	*Attheya spp.* (large and distinct)	132	19	258	17721	10993	42800	28998	17841	161229	80856	49024	84054	122504	24631	81059
n	*Attheya* spp. (small with short hairs)	76	4	110	10076	6790	8425	17651	16079	nd	18924	58557	39791	48286	28520	82326
m	*Chaetoceros decipiens* Cleve	nd	nd	nd	nd	nd	nd	nd	nd	nd	nd	nd	x	nd	nd	nd
m	*C. densus* (Cleve) Cleve	nd	nd	nd	nd	nd	nd	nd	nd	nd	nd	nd	nd	nd	nd	nd
n	*C.* c.f. *subtilis* Cleve	nd	nd	nd	nd	nd	nd	nd	nd	nd	nd	454	nd	nd	nd	nd
n	*Chaetoceros* spp. (2-10 μm)	252	115	248	2780	10670	2359	5884	9912	8810	9892	5447	3130	3577	3025	5488
n	*Chaetoceros* spp. (11-20 μm)	nd	nd	nd	nd	323	337	nd	nd	nd	nd	nd	nd	nd	432	nd
m	*Chaetoceros* spp. (21-50 μm)	nd	nd	nd	nd	nd	x	nd	nd	nd	nd	nd	nd	nd	nd	nd
n	*Chaetoceros* / *Attheya* spp. (0-10 μm)	95	40	nd	1042	970	nd	nd	12555	nd	nd	nd	9836	9389	8210	50240
n	*Chaetoceros* / *Attheya* spp. (10-20 μm)	76	6	nd	nd	970	nd	nd	nd	nd	nd	nd	4918	3577	1296	2111
m	*Chaetoceros* / *Attheya* spp. (20-30 μm)	nd	nd	nd	nd	nd	674	nd	nd	nd	nd	nd	nd	nd	nd	nd
n	Centric diatoms spp. (2-10 μm)	13	nd	nd	nd	323	nd	nd	nd	nd	nd	nd	447	447	432	nd
n	Centric diatoms spp. (10-20 um)	6	nd	nd	nd	323	1685	nd	nd	nd	nd	nd	447	nd	432	422
m	Centric diatoms spp. (20-50 μm)	nd	nd	nd	nd	nd	nd	nd	nd	nd	nd	nd	nd	nd	nd	nd
	Bacillariales (Pennate Diatoms)	**1890**	**396**	**10252**	**89297**	**102817**	**102787**	**107588**	**56606**	**75769**	**106231**	**118475**	**78241**	**105514**	**89017**	**92458**
	Fragilariineae															
m	*Fragilariopsis cylindrus* (Grunow) Helmke & Krieger	nd	nd	nd	nd	nd	nd	nd	nd	881	nd	nd	nd	nd	nd	nd
m	*Fragilariopsis* spp. (20-50 μm)	13	nd	267	nd	nd	nd	nd	nd	nd	nd	nd	nd	nd	nd	nd
m	*Fragilariopsis* spp. (> 50 μm)	nd	nd	nd	nd	nd	nd	nd	nd	nd	nd	nd	nd	nd	nd	nd
m	*Synedropsis hyperborea* (Grunow) Hasle, Medlin &	6	nd	46	347	1940	674	841	220	1322	6451	1816	3577	2235	1728	5488

	Syvertsen															
	Bacillarineae															
n	*Pauliella taeniata* (Grunow) Round & Basson	38	nd	nd	nd	nd	nd	nd	x	nd	nd	nd	nd	nd	nd	nd
m	*Ceratoneis closterium* Ehrenberg	76	9	267	x	647	nd	x	661	441	1720	908	894	894	2593	1689
m	***Diploneis litoralis* var. arctica Cleve**	nd	nd	nd	nd	323	nd	nd	nd	nd	nd	nd	nd	nd	nd	nd
m	*D. litoralis* var. *clathrata* (Østrup) Cleve	6	nd	nd	nd	nd	nd	nd	nd	nd	nd	nd	nd	nd	nd	nd
m	*Entomoneis gigantea* (Grunow) Nizamuddin	x	nd	nd	nd	nd	nd	nd	nd	nd	nd	nd	nd	nd	432	nd
m	*E. gigantea* var. *septentrionalis* Grunow	nd	nd	nd	nd	nd	nd	nd	nd	nd	nd	nd	nd	nd	nd	nd
m	*E. kjellmanni* (Cleve) Poulin & Cardinal	nd	nd	nd	nd	nd	337	nd	nd	nd	nd	x	x	nd	x	nd
m	*E. kjellmanni* var. *kariana* (Grunow) Poulin & Cardinal	38	7	28	347	323	x	2101	441	1322	nd	908	x	x	nd	nd
m	*E. paludosa* var. *hyperborea* (Grunow) Poulin & Cardinal	nd	nd	nd	nd	nd	x	x	220	nd	nd	x	nd	nd	nd	nd
m	*E. palludosa* (Smith) Reimer	nd	nd	18	nd	nd	nd	nd	nd	nd	nd	nd	nd	nd	x	nd
m	*Entomoneis* spp.	x	3	37	nd	nd	nd	nd	nd	nd	x	908	x	447	864	nd
m	*Fossula arctica* (Hasle) Syvertsen & von Quillfedlt	nd	nd	nd	nd	nd	nd	nd	nd	nd	860	nd	nd	nd	nd	nd
m	*Gyrosigma concilians* (Cleve) Okolodkov	6	nd	9	nd	nd	nd	420	nd	nd	nd	nd	nd	nd	nd	nd
m	*G. diaphanum* Cleve	x	nd	nd	nd	nd	nd	nd	nd	nd	nd	nd	nd	nd	nd	nd
m	*G. hudsonii* Poulin & Cardinal	6	nd	18	nd	nd	nd	nd	nd	nd	nd	nd	nd	nd	nd	nd
m	*G. tenuissimum* var. *hyperborea* (Grunow) Cleve	x	1	9	nd	nd	nd	nd	nd	nd	nd	nd	nd	nd	nd	x
m	*Gyrosigma* / *Pleurosigma* spp. (> 50 μm)	6	x	18	nd	nd	nd	nd	nd	nd	430	nd	nd	447	nd	422
m	*Haslea crucigeroides* (Hustedt) Simonsen	nd	1	nd	x	647	nd	nd	nd	nd	nd	nd	nd	nd	nd	nd
m	*H.* cf. *crucigeroides* (Hustedt) Simonsen	nd	nd	nd	nd	nd	337	x	nd	nd	1290	nd	nd	nd	nd	nd
m	*H. kjellmanii* (Cleve) Simonsen	nd	nd	nd	nd	323	nd	nd	nd	nd	nd	nd	nd	nd	nd	nd
m	*Haslea vitrea* (Cleve) Simonsen	nd	nd	nd	nd	nd	x	nd	nd	nd	nd	nd	nd	nd	nd	nd
m	*Haslea* spp. (20-100 μm)	6	nd	9	nd	nd	nd	nd	nd	nd	860	nd	nd	nd	nd	nd
m	*Navicula algida* Grunow	nd	nd	nd	nd	nd	nd	nd	nd	nd	nd	nd	nd	nd	nd	nd
m	*N. directa* (Smiths) Ralfs	38	1	37	695	647	x	nd	nd	x	nd	908	nd	nd	nd	nd
m	*N. directa* var. *javanica* Cleve	nd	nd	nd	nd	nd	337	nd	nd	nd	nd	908	447	nd	nd	nd
m	*N. gelida* Grunow	nd	nd	9	nd	nd	nd	nd	nd	nd	nd	nd	nd	nd	nd	nd
m	*N. glacialis* var. *glacialis* (Cleve) Grunow	nd	nd	nd	nd	nd	nd	nd	nd	nd	nd	nd	nd	nd	nd	nd
m	*N. granii* (Jørgensen) Gran	nd	nd	nd	nd	nd	nd	nd	nd	nd	nd	nd	nd	nd	nd	nd
m	*N. kariana* Cleve	13	nd	nd	nd	nd	x	nd	nd	nd	nd	nd	nd	nd	nd	x
m	*N. kariana* var. *detersa* (Grunow) Grunow	nd	nd	18	nd	nd	nd	nd	220	nd	nd	nd	nd	nd	nd	nd
m	*N. pagophila* var. *manitounukensis*	nd	nd	nd	nd	nd	nd	nd	220	nd	nd	nd	nd	nd	nd	nd

	Poulin & Cardinal															
n	*N. pelagica* Cleve (10-20 μm)	19	6	202	695	323	2022	2942	nd	10132	7311	1816	nd	nd	432	nd
m	*N. pelagica* Cleve (20-30 μm)	63	25	773	7992	5173	3370	3362	2863	nd	nd	1362	447	894	1728	2955
m	*N. pelagica* Cleve (>30 μm)	32	12	285	nd	5820	4044	nd	nd	nd	nd	nd	nd	nd	nd	nd
m	*N. pellucidula* Hustedt	nd	x	nd	nd	nd	nd	nd	nd	nd	nd	nd	nd	nd	nd	nd
m	*N. septentrionalis* (Grunow) Gran	69	3	193	3822	970	x	1261	661	x	2581	4993	x	x	1296	422
m	*N. superba* var. *superba* Cleve	nd	nd	nd	nd	nd	nd	nd	nd	nd	nd	nd	nd	nd	nd	nd
m	*N. superba* var. *subacuta* Gran	nd	nd	nd	nd	nd	nd	nd	nd	nd	nd	nd	nd	nd	nd	nd
m	*N. superba* var. *elliptica* Cleve	nd	nd	nd	nd	nd	nd	nd	nd	nd	nd	nd	nd	nd	nd	nd
m	*N. transitans* var. *transitans* Cleve	nd	nd	nd	nd	nd	nd	nd	nd	nd	860	nd	nd	447	nd	nd
m	*N. trigonocephala* var. *trigonocephala* Cleve	nd	nd	nd	nd	nd	nd	nd	nd	nd	nd	nd	nd	nd	nd	nd
m	*N. trigonocephala* var. *depressa* Østrup	nd	nd	nd	nd	nd	nd	nd	nd	nd	nd	nd	nd	nd	nd	nd
m	*N. valida* var. *valida* Cleve & Grunow	nd	nd	18	nd	nd	nd	nd	nd	nd	nd	nd	nd	nd	nd	nd
m	*N. valida* var. *minuia* Cleve	nd	nd	18	nd	nd	nd	nd	nd	nd	nd	nd	nd	nd	nd	nd
m	*N. vanhoeffenii* Gran	50	nd	nd	nd	nd	nd	nd	nd	nd	nd	x	nd	nd	nd	nd
m	*N.* c.f. *vanhoeffenii* Gran	nd	nd	nd	nd	nd	nd	nd	nd	nd	nd	nd	nd	nd	nd	844
n	*Navicula* spp. (10-20 μm)	6	nd	9	nd	323	nd	841	220	3084	1720	nd	nd	nd	1296	nd
m	*Navicula* spp. (20-50 μm)	57	4	276	5559	2263	2022	1261	1762	2203	4301	2270	3130	4471	3457	5911
m	*Navicula* spp. (> 50 μm)	19	1	74	nd	nd	nd	nd	220	nd	nd	nd	nd	nd	432	nd
m	*Nitzschia angularis* Smith	6	nd	9	nd	nd	nd	nd	nd	nd	430	nd	nd	nd	nd	nd
m	*N. arctica* Cleve	44	nd	166	x	nd	nd	841	nd	nd	nd	nd	nd	nd	nd	nd
m	*N. brebissonii* var. *borealis* Cleve	nd	1	9	347	nd	nd	nd	nd	nd	nd	454	nd	nd	432	422
m	*N. distans* var. *erratica* Cleve	nd	nd	nd	nd	nd	nd	nd	nd	nd	nd	nd	nd	nd	nd	nd
m	*N. frigida* Grunow	57	55	1749	17026	28129	38756	45389	14757	20264	30966	47208	16095	33979	11235	20687
m	*N. gelida* Grunow	nd	x	nd	nd	nd	nd	nd	nd	nd	nd	nd	nd	nd	nd	nd
m	*N. gelida* var. *manitounukensis* Poulin & Cardinal	nd	6	18	nd	nd	nd	nd	nd	441	nd	nd	nd	nd	nd	nd
m	*N. hudsonii* Poulin & Cardinal	nd	nd	9	nd	nd	nd	nd	nd	nd	nd	nd	nd	nd	nd	nd
m	*N.* cf. *hudsonii* Poulin & Cardina	nd	6	nd	nd	nd	nd	nd	nd	nd	nd	1362	447	nd	nd	nd
m	*N. laevissima* Grunow	x	3	37	1042	970	337	420	nd	nd	x	x	894	447	nd	nd
m	*N.* c.f. *laevissima* Grunow	nd	nd	nd	nd	nd	nd	nd	nd	nd	nd	nd	894	1341	nd	nd
m	*N. lanceolata* var. *pygmaea* Cleve	nd	1	nd	nd	323	337	nd	nd	nd	nd	nd	nd	nd	nd	nd
m	*N. longissima* Grunow	nd	nd	nd	nd	nd	nd	nd	nd	nd	nd	nd	nd	nd	nd	nd
m	*N. neofrigida* Medlin	nd	nd	46	1042	nd	337	6724	x	2643	860	nd	894	447	nd	422
m	*N. paradoxa* var. *tumidula* Grunow	nd	nd	nd	nd	nd	nd	nd	nd	nd	430	nd	nd	nd	nd	nd
m	*N. promare* Medlin	x	nd	322	3475	nd	1348	2522	nd	2643	nd	nd	2235	2235	6482	844
m	*N. scabra* Cleve	6	nd	9	347	323	337	420	441	nd	nd	454	x	nd	nd	x
m	*Nitzschia* sp.1	nd	nd	nd	x	nd	nd	nd	nd	nd	x	nd	nd	nd	nd	nd
m	*Nitzschia* sp.2	25	nd	55	nd	nd	nd	nd	nd	nd	nd	nd	nd	nd	nd	nd
m	*Nitzschia* spp. (20-50 μm)	nd	1	nd	nd	nd	nd	nd	nd	nd	nd	nd	nd	nd	nd	nd

m	*Nitzschia* spp. (21-50 μm)	6	nd	46	3822	647	337	841	881	14978	28816	nd	1788	447	3025	844
m	*Nitzschia* spp. (51-100 μm)	372	105	2181	30229	21016	25950	20593	20484	nd	nd	28597	20119	37556	28952	32086
m	*Nitzschia* spp. (>100 μm)	25	4	120	nd	nd	337	nd	nd	nd	nd	nd	nd	nd	nd	nd
m	*Pinnularia quadratarea var. bicontracta* (Østrup) Heiden	6	nd	nd	nd	nd	nd	nd	nd	nd	nd	nd	nd	x	nd	nd
m	*P. quadratarea var. constricta* (Østrup) Heiden	6	nd	nd	nd	nd	nd	nd	nd	nd	nd	908	nd	nd	nd	nd
m	*P. quadratarea var. maxima* (Østrup) Boyer	nd	nd	nd	nd	nd	nd	nd	nd	nd	nd	nd	nd	nd	nd	nd
m	*P. semiinflata var. semiinflata* (Østrup) Granow	nd	nd	9	nd	nd	nd	nd	nd	nd	nd	nd	nd	nd	nd	nd
m	*Pinnularia* spp. (20-50 μm)	nd	1	nd	nd	nd	nd	nd	nd	nd	nd	nd	nd	nd	nd	nd
m	*Pleurosigma stuxbergii* Cleve & Grunow	nd	nd	nd	nd	nd	x	nd	nd	nd	nd	nd	x	nd	nd	nd
m	*P. stuxbergii var. rhomboides* (Cleve & Grunow) Cleve	nd	nd	nd	x	nd	nd	nd	nd	nd	nd	nd	nd	nd	nd	nd
m	*Pseudogomphonema arcticum* (Grunow) Medlin / *septentrionale* (Østrup) Medlin	13	3	92	nd	323	674	nd	220	441	nd	908	447	447	864	844
m	*P. groenlandicum* (Østrup) Medlin / *kamtschaticum* (Grunow) Medlin	nd	3	9	nd	nd	nd	nd	nd	nd	nd	454	nd	x	nd	nd
m	*Pseudogomphonema* spp. (20-100 μm)	13	21	64	347	nd	nd	420	nd	nd	430	nd	nd	nd	1296	nd
m	*Pseudo-nitzschia* cf. *delicatissima* Cleve	32	4	175	2432	5497	2022	3362	4625	nd	860	1362	3577	2235	2593	1267
m	*P. seriata* (Cleve) Peragallo	32	nd	92	x	970	2696	1681	nd	nd	1290	nd	x	894	x	nd
m	*P. seriata* f. *obtusa* (Hasle) Hasle	25	nd	92	347	2587	674	x	220	881	1720	1816	1788	nd	nd	nd
m	*Stenoneis inconspicua* var. *baculus* (Cleve) Cleve	13	nd	nd	nd	nd	nd	nd	nd	nd	nd	nd	nd	nd	nd	nd
m	Pennate diatom sp. 1 (20-50 μm)	nd	nd	295	nd	10346	x	nd	nd	nd	860	nd	nd	nd	nd	nd
n	Pennate cells in group (2-10 μm)	nd	nd	nd	nd	nd	nd	nd	nd	nd	nd	nd	nd	nd	nd	nd
n	Pennate cells in group (11-20 μm)	nd	12	18	nd	nd	nd	nd	nd	nd	nd	4993	894	1341	nd	nd
m	Pennate cells in group (21-50 μm)	32	6	313	nd	nd	5392	nd	1322	nd	nd	nd	nd	nd	864	2955
n	Pennate cells solitary (2-10 μm)	32	9	nd	347	323	nd	2101	661	5286	2581	454	6259	nd	nd	nd
n	Pennate cells solitary (11-20 μm)	113	24	285	1737	2910	1011	2942	1322	5727	5161	1362	2235	3130	3889	2955
m	Pennate cells solitary (21-50 μm)	397	46	1160	5212	7436	7751	6304	3524	3084	2581	9532	9389	8495	12964	8444
m	Pennate cells solitary (> 50 μm)	69	9	230	2085	1293	1348	nd	441	nd	860	1816	1788	2683	2161	2955
	Dinophyceae	**32**	**7**	**18**	**347**	**970**	**0**	**0**	**661**	**0**	**1290**	**454**	**0**	**447**	**0**	**844**
n	Gymnodinium / Gyrodinium spp. (2-10 μm)	13	nd	nd	nd	nd	nd	nd	nd	nd	nd	nd	nd	nd	nd	nd
n	Gymnodinium / Gyrodinium spp. (10-20 μm)	19	6	9	347	647	nd	nd	441	nd	860	nd	nd	nd	nd	nd
m	Gymnodinium / Gyrodinium spp. (20-50 μm)	nd	1	nd	nd	323	nd	nd	nd	nd	nd	nd	x	447	nd	844
m	*Peridiniella catenata* (Levander) Balech	nd	nd	nd	nd	nd	nd	nd	nd	nd	nd	nd	nd	nd	nd	nd

n	Dinoflagellates (0-10 μm)	nd	nd	nd	nd	nd	nd	nd	nd	nd	nd	454	nd	nd	nd	nd
n	Dinoflagellates (11-20 μm)	nd	nd	nd	nd	nd	nd	nd	220	nd	nd	nd	nd	nd	nd	nd
m	Dinoflagellates (21-50 μm)	nd	nd	9	nd	nd	nd	nd	nd	nd	430	nd	nd	nd	nd	nd
m	Dinoflagellates (> 50 μm)	nd	nd	nd	nd	nd	nd	nd	nd	nd	nd	nd	nd	nd	nd	nd
Chrysophyceae		**0**	**0**	**0**	**0**	**0**	**0**	**0**	**0**	**0**	**0**	**454**	**0**	**0**	**0**	**0**
m	*Dinobryon faculiferum* (Willén) Willén	nd	nd	nd	nd	nd	nd	nd	nd	nd	nd	454	nd	nd	nd	nd
Prasinophyceae		**6**	**0**	**0**	**0**	**0**	**0**	**0**	**220**	**0**	**0**	**454**	**447**	**1788**	**1728**	**0**
n	*Pyramimonas* cf. *nansenii* Braarud	nd	nd	nd	nd	nd	nd	nd	220	nd	nd	nd	447	nd	432	nd
n	*Pyramimonas* spp. (0-10 μm)	6	nd	nd	nd	nd	nd	nd	nd	nd	nd	454	nd	nd	864	nd
n	*Pyramimonas* spp. (10-20 μm)	nd	nd	nd	nd	nd	nd	nd	nd	nd	nd	nd	nd	1788	432	nd
m	*Pyramimonas* spp. (>20 μm)	nd	nd	nd	nd	nd	nd	nd	nd	nd	nd	nd	nd	nd	nd	nd
Prymnesiophyceae		**0**	**0**	**0**	**0**	**0**	**337**	**1261**	**1101**	**881**	**2150**	**908**	**1788**	**1341**	**0**	**0**
n	*Phaeocystis pouchetii* (Hariot) Lagerheim	nd	nd	nd	nd	nd	337	nd	nd	nd	nd	nd	nd	nd	x	x
n	*P.* c.f. *pouchetii* (Hariot) Lagerheim	nd	nd	nd	nd	nd	nd	nd	nd	nd	nd	nd	894	nd	nd	nd
n	*Prymnesiophyceae* spp. (2-10 μm)	nd	nd	nd	nd	nd	nd	1261	1101	nd	nd	908	894	1341	nd	nd
n	*Prymnesiophyceae* spp. (11-20 μm)	nd	nd	nd	nd	nd	nd	nd	nd	nd	nd	nd	x	nd	nd	nd
m	*Prymnesiophyceae* spp. (> 20 μm)	nd	nd	nd	nd	nd	nd	nd	nd	nd	2150	nd	nd	nd	nd	nd
Flagellates		**498**	**86**	**515**	**6949**	**4203**	**1685**	**4623**	**1982**	**3965**	**860**	**2724**	**894**	**4024**	**8210**	**5488**
n	Family: Geminigeracea (0-10 μm)	6	1	18	695	323	1011	nd	nd	nd	nd	nd	nd	894	864	nd
n	Family: Geminigeracea (11-20 μm)	19	1	nd	1042	323	337	nd	nd	nd	nd	1362	x	1341	1296	844
m	Family: Dinobrycea (>50 μm)	nd	nd	nd	nd	nd	nd	nd	nd	nd	nd	nd	nd	nd	nd	nd
n	Flagellates (2-5 μm)	246	35	258	2085	2263	nd	2522	1101	881	nd	908	nd	447	3025	1689
n	Flagellates (6-10 μm)	183	34	175	1390	970	337	841	441	2643	860	454	447	nd	2593	1689
n	Flagellates (11-20 μm)	44	10	64	695	323	nd	1261	441	441	nd	nd	nd	894	432	1267
m	Flagellates (>20 μm)	nd	3	nd	1042	nd	nd	nd	nd	nd	nd	nd	447	447	nd	nd
Choanoflagellates		**6**	**1**	**18**	**347**	**323**	**1011**	**1261**	**1322**	**1322**	**3871**	**5447**	**6706**	**10283**	**12531**	**6333**
Family: acanthoecideae		6	1	18	347	323	1011	1261	1322	1322	3871	5447	6706	7601	12531	5066
Unidentified choanoflagellates (10-50 μm)		nd	nd	nd	nd	nd	nd	nd	nd	nd	nd	nd	nd	2683	nd	1267
Ciliates		**0**	**0**	**0**	**0**	**0**	**0**	**0**	**0**	**0**	**0**	**0**	**0**	**0**	**0**	**0**
m	*Tintinnopsis* spp. (> 50 μm)	nd	nd	nd	nd	nd	nd	nd	nd	nd	nd	nd	nd	nd	nd	nd
m	Ciliates (20-50 μm)	nd	nd	nd	x	nd	nd	nd	nd	nd	nd	nd	nd	nd	nd	nd
m	Ciliates (> 50 μm)	nd	nd	nd	nd	nd	nd	nd	nd	nd	nd	nd	nd	nd	nd	nd
Unidentified Cells		**718**	**204**	**1104**	**17373**	**35242**	**19883**	**29839**	**20925**	**14978**	**18924**	**22242**	**34426**	**46498**	**59633**	**44329**
Cysts (0-10 μm)		6	nd	9	695	647	0	420	220	nd	nd	908	nd	4918	nd	nd
Cysts (11-20 μm)		44	4	110	347	647	674	1261	1101	2203	nd	908	2683	894	864	nd
Cysts (21-50 μm)		nd	nd	28	347	nd	337	nd	nd	nd	nd	nd	nd	447	nd	nd
Cysts (>50 μm)		nd	nd	nd	nd	nd	nd	nd	nd	nd	nd	nd	nd	nd	nd	nd
Unidentified cells (0-10 μm)		328	130	571	11119	26189	13143	23535	9251	8810	10322	14072	14307	29508	22470	30819
Unidentified cells (11-20 μm)		88	40	230	1737	4850	3033	3782	5066	1762	2581	2724	9389	8942	9075	12666
Unidentified cells (>20 μm)		13	nd	nd	347	323	nd	nd	nd	nd	430	nd	1341	894	432	422
Presence Counts																
Number of Species Counted		**23**	**13**	**29**	**14**	**17**	**15**	**14**	**14**	**12**	**14**	**16**	**12**	**10**	**11**	**10**
Number of Species Observed		**27**	**15**	**29**	**19**	**17**	**22**	**17**	**16**	**14**	**15**	**20**	**19**	**13**	**15**	**14**
Number of Taxa Counted		**36**	**35**	**34**	**23**	**31**	**24**	**20**	**24**	**14**	**22**	**21**	**26**	**28**	**31**	**26**
Number of Taxa Observed		**37**	**36**	**34**	**24**	**31**	**27**	**21**	**24**	**14**	**24**	**21**	**29**	**29**	**31**	**26**

Table 5.2 Detailed list of species abundance (cells ml^{-1}) in the bottom 0-5 cm of sea ice under thick snow cover following analysis by light microscopy. Taxonomic orders are highlighted in bold and are underlined, suborders are underlined. Algae included in the estimates of nanoeukaryotes are designated by (n) and microeukaryotes by (m).

Collection Date		March			April			May							June	
		07	11	15	21	25	29	03	08	13	17	21	26	30	05	09
Sample Event		1	2	3	4	5	6	7	8	9	10	11	12	13	14	15
Bacillariophyta		**270**	**394**	**426**	**29997**	**54492**	**86496**	**32654**	**56721**	**184494**	**174144**	**108104**	**80253**	**414456**	**195318**	**151836**
Biddulphiales (Centric Diatoms)		**155**	**138**	**25**	**7885**	**16719**	**20452**	**11227**	**19852**	**86097**	**57040**	**24988**	**15201**	**304024**	**101548**	**64891**
Coscinodiscineae																
n	*Leptocylindrus* spp. (10-20 μm)	nd	nd	nd	nd	nd	nd	nd	nd	nd	nd	nd	nd	nd	nd	nd
n	*Thalassiosira hyperborea* (Grunow) Hasle	nd	nd	nd	nd	310	nd	nd	nd	nd	nd	789	nd	nd	nd	nd
m	*Thalassiosira* spp. (20-50 μm)	nd	nd	nd	nd	310	nd	nd	nd	nd	nd	nd	nd	nd	nd	x
m	*Thalassiosira* spp. (> 50 μm)	nd	nd	nd	nd	nd	nd	nd	nd	nd	nd	nd	nd	nd	nd	nd
Biddulphiineae																
n	*Attheya longicornis* Crawford & Gardner	nd	nd	1	429	310	1491	1028	834	3393	3025	789	224	10283	3889	848
n	*A. septentrionalis* (Østrup) Crawford	nd	nd	1	nd	nd	nd	nd	nd	424	nd	263	nd	1341	432	nd
n	*Attheya spp.* (large and distinct)	37	17	6	1628	4644	14487	5742	7007	49198	26791	11047	7601	159165	42780	18661
n	*Attheya* spp. (small with short hairs)	57	9	11	2571	2632	4474	3685	10844	15268	19445	6050	4024	124292	50990	39868
m	*Chaetoceros decipiens* Cleve	nd	1	nd	nd	nd	nd	nd	nd	nd	nd	nd	nd	nd	nd	nd
m	*C. densus* (Cleve) Cleve	3	nd	nd	nd	nd	nd	nd	nd	nd	nd	nd	nd	nd	nd	nd
n	*C.* c.f. *subtilis* Cleve	nd	nd	nd	nd	nd	nd	nd	nd	nd	nd	nd	nd	nd	nd	nd
n	*Chaetoceros* spp. (2-10 μm)	9	59	6	857	5573	nd	429	334	17813	1296	2893	671	2683	432	2545
n	*Chaetoceros* spp. (11-20 μm)	nd	nd	nd	nd	155	nd	nd	nd	nd	nd	nd	nd	nd	nd	nd
m	*Chaetoceros* spp. (21-50 μm)	nd	nd	nd	nd	nd	nd	nd	nd	nd	nd	nd	nd	nd	nd	nd
n	*Chaetoceros* / *Attheya* spp. (0-10 μm)	37	15	nd	1886	2167	nd	171	nd	nd	6050	1315	2459	894	2161	2969
n	*Chaetoceros* / *Attheya* spp. (10-20 μm)	nd	nd	nd	171	nd	nd	nd	334	nd	432	1841	224	nd	nd	nd
m	*Chaetoceros* / *Attheya* spp. (20-30 um)	nd	nd	nd	nd	nd	nd	nd	nd	nd	nd	nd	nd	nd	nd	nd
n	Centric diatoms spp. (2-10 μm)	13	37	nd	nd	464	nd	171	500	nd	nd	nd	nd	4024	432	nd
n	Centric diatoms spp. (10-20 μm)	nd	nd	nd	86	155	nd	nd	nd	nd	nd	nd	nd	894	432	nd
m	Centric diatoms spp. (20-50 μm)	nd	nd	nd	257	nd	nd	nd	nd	nd	nd	nd	nd	447	nd	nd
Bacillariales (Pennate Diatoms)		**114**	**255**	**401**	**22112**	**37773**	**65404**	**21426**	**36702**	**98397**	**117105**	**83116**	**65052**	**110432**	**93770**	**86945**
Fragilariineae																
m	*Fragilariopsis cylindrus* (Grunow) Helmke & Krieger	nd	nd	nd	nd	774	nd	857	x	nd	x	789	x	nd	x	2969
m	*Fragilariopsis* spp. (20-50 μm)	nd	5	6	nd	310	426	257	334	nd	864	2104	2012	nd	432	nd
m	*Fragilariopsis* spp. (> 50 μm)	nd	nd	nd	86	nd	1065	nd	2169	nd	nd	nd	447	nd	nd	nd
m	*Synedropsis hyperborea* (Grunow) Hasle, Medlin & Syvertsen	nd	nd	nd	nd	nd	nd	nd	167	424	432	526	671	2235	2593	1272
Bacillarineae																
n	*Pauliella taeniata* (Grunow) Round & Basson	nd	nd	nd	nd	nd	1278	nd	nd	nd	x	nd	nd	nd	nd	nd
m	*Ceratoneis closterium* Ehrenberg	3	1	6	514	x	426	429	167	nd	1728	789	x	nd	864	2545
m	*Diploneis litoralis* var. arctica Cleve	nd	nd	nd	nd	nd	nd	nd	nd	nd	nd	nd	nd	nd	nd	nd

m	*D. litoralis* var. *clathrata* (Østrup) Cleve	nd	nd	nd	nd	nd	nd	nd	nd	nd	nd	nd	nd	nd	nd	nd
m	*Entomoneis gigantea* (Grunow) Nizamuddin	nd	nd	nd	86	155	x	86	nd	424	x	nd	x	x	864	nd
m	*E. gigantea* var. *septentrionalis* Grunow	nd	nd	nd	nd	nd	213	nd	nd	nd	nd	nd	nd	nd	nd	nd
m	*E. kjellmanni* (Cleve) Poulin & Cardinal	nd	3	1	nd	nd	nd	86	nd	nd	nd	x	x	nd	x	nd
m	*E. kjellmanni* var. *kariana* (Grunow) Poulin & Cardinal	5	4	nd	171	155	639	343	667	x	432	1052	x	x	nd	nd
m	*E. paludosa* var. *hyperborea* (Grunow) Poulin & Cardinal	x	x	nd	nd	nd	nd	nd	nd	x	nd	nd	224	nd	nd	nd
m	*E. palludosa* (Smith) Reimer	nd	nd	nd	nd	nd	nd	nd	nd	nd	nd	nd	nd	nd	nd	nd
m	*Entomoneis* spp.	1	nd	1	429	310	x	171	nd	424	1296	263	nd	1341	x	424
m	*Fossula arctica* (Hasle) Syvertsen & von Quillfedlt	nd	nd	nd	nd	nd	nd	nd	nd	nd	nd	nd	nd	nd	nd	nd
m	*Gyrosigma concilians* (Cleve) Okolodkov	nd	nd	nd	nd	nd	nd	nd	167	nd	x	nd	224	447	nd	nd
m	*G. diaphanum* Cleve	nd	nd	nd	nd	nd	nd	nd	nd	nd	nd	nd	nd	nd	nd	nd
m	*G. hudsonii* Poulin & Cardinal	2	x	nd	nd	nd	x	nd	nd	nd	nd	nd	nd	nd	nd	nd
m	*G. tenuissimum* var. *hyperborea* (Grunow) Cleve	nd	nd	nd	86	155	nd	nd	nd	x	nd	nd	nd	nd	nd	nd
m	*Gyrosigma* / *Pleurosigma* spp. (> 50 μm)	nd	nd	2	nd	nd	nd	86	nd	nd	x	nd	nd	nd	nd	nd
m	*Haslea crucigeroides* (Hustedt) Simonsen	nd	nd	1	nd	nd	nd	86	167	x	nd	nd	nd	nd	x	nd
m	*H.* cf. *crucigeroides* (Hustedt) Simonsen	nd	nd	x	nd	nd	nd	nd	nd	nd	nd	nd	nd	nd	nd	nd
m	*H. kjellmanii* (Cleve) Simonsen	nd	nd	nd	nd	nd	nd	nd	nd	nd	nd	nd	nd	nd	nd	nd
m	*Haslea vitrea* (Cleve) Simonsen	nd	x	nd	nd	nd	nd	nd	nd	nd	nd	nd	nd	nd	nd	nd
m	*Haslea* spp. (20-100 μm)	nd	nd	nd	nd	nd	213	nd	167	nd	nd	nd	x	nd	nd	x
m	*Navicula algida* Grunow	nd	x	1	nd	nd	nd	nd	nd	nd	nd	nd	nd	nd	nd	nd
m	*N. directa* (Smiths) Ralfs	1	1	4	257	155	x	171	nd	x	432	nd	224	nd	864	x
m	*N. directa* var. *javanica* Cleve	nd	nd	nd	nd	nd	nd	nd	nd	nd	nd	nd	nd	nd	nd	nd
m	*N. gelida* Grunow	nd	nd	nd	nd	nd	nd	nd	nd	nd	nd	nd	nd	nd	nd	nd
m	*N. glacialis* var. *glacialis* (Cleve) Grunow	1	nd	nd	nd	nd	nd	nd	nd	nd	nd	nd	nd	nd	nd	nd
m	*N. granii* (Jørgensen) Gran	nd	nd	nd	nd	x	nd	nd	nd	nd	nd	nd	nd	nd	nd	nd
m	*N. kariana* Cleve	nd	1	1	nd	nd	nd	nd	nd	nd	nd	nd	nd	nd	nd	x
m	*N. kariana* var. *detersa* (Grunow) Grunow	nd	x	nd	nd	nd	nd	nd	nd	nd	nd	nd	nd	nd	nd	nd
m	*N. pagophila* var. *manitounukensis* Poulin & Cardinal	nd	nd	nd	nd	nd	nd	nd	nd	nd	nd	nd	nd	nd	nd	nd
n	*N. pelagica* Cleve (10-20 μm)	nd	16	nd	514	1858	426	771	1335	3817	2161	263	4024	1341	432	1696
m	*N. pelagica* Cleve (20-30 μm)	3	9	2	3171	3251	6391	1457	3170	17813	17285	2367	4247	7601	1296	8482
m	*N. pelagica* Cleve (>30 μm)	nd	nd	nd	nd	929	2983	600	167	2969	2161	1841	2906	894	nd	2121
m	*N. pellucidula* Hustedt	nd	nd	nd	nd	nd	nd	nd	nd	nd	nd	nd	nd	nd	nd	nd
m	*N. septentrionalis* (Grunow) Gran	nd	29	32	514	x	nd	nd	x	nd	x	1315	1341	nd	4753	nd
m	*N. superba* var. *superba* Cleve	nd	nd	1	nd	nd	nd	nd	nd	nd	nd	nd	nd	nd	nd	nd
m	*N. superba* var. *subacuta* Gran	nd	nd	x	nd	nd	nd	nd	nd	nd	nd	nd	nd	nd	nd	nd
m	*N. superba* var. *elliptica* Cleve	nd	nd	nd	nd	x	nd	nd	nd	nd	nd	nd	nd	nd	nd	nd
m	*N. transitans* var. *transitans* Cleve	nd	nd	nd	nd	nd	nd	86	nd	nd	nd	nd	nd	nd	nd	x
m	*N. trigonocephala* var.	nd	nd	nd	nd	nd	nd	nd	nd	nd	nd	263	nd	nd	nd	nd

	trigonocephala Cleve															
m	*N. trigonocephala* var. *depressa* Østrup	nd	nd	nd	nd	nd	nd	nd	nd	424	nd	nd	nd	nd	nd	nd
m	*N. valida* var. *valida* Cleve & Grunow	nd	nd	nd	nd	nd	nd	nd	nd	nd	nd	nd	nd	nd	nd	nd
m	*N. valida* var. *minuia* Cleve	nd	nd	nd	nd	nd	nd	nd	nd	nd	nd	nd	nd	nd	nd	nd
m	*N. vanhoeffenii* Gran	nd	nd	nd	nd	nd	nd	nd	nd	nd	1728	nd	nd	nd	nd	nd
m	*N.* c.f. *vanhoeffenii* Gran	nd	nd	nd	nd	nd	nd	nd	nd	nd	nd	nd	nd	nd	nd	nd
n	*Navicula* spp. (10-20 μm)	nd	nd	nd	86	619	213	257	167	424	nd	526	224	nd	nd	424
m	*Navicula* spp. (20-50 μm)	nd	4	17	429	2012	1704	771	500	3393	1296	nd	671	3577	2161	2545
m	*Navicula* spp. (> 50 μm)	nd	3	1	171	nd	nd	86	nd	nd	x	nd	nd	nd	nd	nd
m	*Nitzschia angularis* Smith	nd	nd	nd	86	nd	nd	nd	nd	nd	x	nd	nd	nd	nd	nd
m	*N. arctica* Cleve	5	x	8	514	nd	nd	x	167	nd	nd	263	671	nd	2161	nd
m	*N. brebissonii* var. *borealis* Cleve	x	x	nd	86	nd	nd	nd	nd	424	nd	nd	nd	nd	nd	nd
m	*N. distans* var. *erratica* Cleve	nd	nd	nd	nd	nd	nd	nd	nd	nd	nd	nd	nd	nd	nd	nd
m	*N. frigida* Grunow	14	41	79	2571	2632	10013	1200	5172	20782	28088	17886	6706	42027	10803	11875
m	*N. gelida* Grunow	nd	nd	nd	nd	nd	nd	nd	nd	nd	nd	nd	nd		x	nd
m	*N. gelida* var. *manitounukensis* Poulin & Cardinal	nd	nd	1	nd	nd	nd	nd	nd	nd	nd	x	nd	nd	nd	nd
m	*N. hudsonii* Poulin & Cardinal	nd	nd	2	nd	nd	nd	nd	nd	nd	nd	x	nd	nd	x	nd
m	*N.* cf. *hudsonii* Poulin & Cardina	nd	nd	nd	nd	nd	nd	nd	nd	nd	nd	nd	nd	nd	nd	nd
m	*N. laevissima* Grunow	x	3	1	nd	155	nd	nd	nd	nd	1296	nd	224	x	2161	nd
m	*N.* c.f. *laevissima* Grunow	nd	nd	nd	nd	nd	nd	nd	nd	nd	nd	nd	nd	nd	nd	nd
m	*N. lanceolata* var. *pygmaea* Cleve	nd	nd	nd	nd	x	nd	nd	334	848	nd	nd	nd	nd	nd	nd
m	*N. longissima* Grunow	nd	nd	nd	nd	nd	nd	nd	nd	nd	nd	nd	nd	nd	nd	nd
m	*N. neofrigida* Medlin	1	nd	nd	171	x	nd	86	nd	424	x	789	1118	nd	1296	1272
m	*N. paradoxa* var. *tumidula* Grunow	nd	nd	nd	nd	nd	nd	nd	nd	nd	nd	nd	nd	nd	nd	nd
m	*N. promare* Medlin	nd	nd	4	nd	x	426	514	4504	2121	864	7891	2683	nd	6050	848
m	*N. scabra* Cleve	nd	nd	1	86	nd	213	x	nd	nd	nd	x	224	nd	x	nd
m	*Nitzschia* sp.1	nd	nd	nd	nd	3096	nd	nd	nd	nd	6914	x	nd	nd	nd	nd
m	*Nitzschia* sp.2	nd	nd	nd	nd	nd	nd	nd	nd	nd	nd	nd	nd	nd	nd	nd
m	*Nitzschia* spp. (20-50 μm)	nd	nd	nd	nd	nd	426	nd	nd	nd	nd	nd	nd	nd	nd	nd
m	*Nitzschia* spp. (21-50 μm)	nd	nd	13	171	nd	nd	nd	nd	24599	nd	nd	nd	447	nd	424
m	*Nitzschia* spp. (51-100 μm)	26	81	115	3600	7586	18322	6771	6840	nd	15988	11836	6036	29061	30248	21206
m	*Nitzschia* spp. (>100 μm)	nd	1	nd	86	nd	213	nd	nd	424	nd	nd	nd	nd	nd	nd
m	*Pinnularia quadratarea var. bicontracta* (Østrup) Heiden	nd	x	nd	nd	nd	nd	nd	nd	nd	nd	nd	nd	nd	nd	nd
m	*P. quadratarea var. constricta* (Østrup) Heiden	nd	nd	1	86	nd	nd	nd	nd	nd	nd	nd	nd	x	nd	424
m	*P. quadratarea var. maxima* (Østrup) Boyer	nd	nd	nd	nd	nd	nd	nd	nd	nd	432	nd	nd	nd	nd	nd
m	*P. semiinflata var. semiinflata* (Østrup) Granow	nd	x	nd	nd	nd	nd	nd	167	nd	1728	nd	nd	nd	nd	nd
m	*Pinnularia* spp. (20-50 μm)	nd	1	nd	nd	nd	nd	nd	nd	nd	nd	nd	nd	nd	nd	nd
m	*Pleurosigma stuxbergii* Cleve & Grunow	1	nd	1	nd	x	nd	nd	nd	nd	nd	nd	nd	nd	nd	nd
m	*P. stuxbergii var. rhomboides* (Cleve & Grunow) Cleve	nd	nd	1	nd	155	nd	nd	nd	nd	nd	nd	nd	nd	nd	nd
m	*Pseudogomphonema arcticum* (Grunow) Medlin / *septentrionale* (Østrup) Medlin	7	4	5	nd	nd	nd	nd	nd	1272	nd	nd	x	894	nd	nd
m	*P. groenlandicum* (Østrup) Medlin / *kamtschaticum*	nd	nd	nd	nd	nd	nd	nd	nd	nd	nd	nd	nd	nd	nd	nd

	(Grunow) Medlin															
m	*Pseudogomphonema* spp. (20-100 μm)	nd	x	1	nd	619	x	343	nd	424	x	nd	224	nd	432	nd
m	*Pseudo-nitzschia* cf. *delicatissima* Cleve	nd	3	4	600	2477	2130	1114	1835	424	9075	10521	3577	1341	2593	848
m	*P. seriata* (Cleve) Peragallo	nd	nd	1	771	619	639	171	1001	nd	432	1315	1788	nd	1728	x
m	*P. seriata* f. *obtusa* (Hasle) Hasle	nd	nd	10	171	nd	nd	nd	167	nd	nd	nd	x	nd	nd	nd
m	*Stenoneis inconspicua* var. *baculus* (Cleve) Cleve	nd	nd	nd	nd	nd	nd	nd	nd	nd	nd	nd	nd	nd	nd	nd
m	Pennate diatom sp. 1 (20-50 μm)	nd	nd	nd	nd	nd	4900	nd	nd	nd	nd	nd	7824	nd	nd	nd
n	Pennate cells in group (2-10 μm)	nd	nd	nd	nd	nd	nd	943	nd	nd	nd	nd	nd	nd	nd	nd
n	Pennate cells in group (11-20 μm)	nd	nd	nd	nd	nd	nd	nd	1335	nd	nd	nd	nd	nd	864	nd
m	Pennate cells in group (21-50 μm)	8	nd	nd	943	774	nd	686	0	2969	3025	5261	3353	nd	6914	nd
n	Pennate cells solitary (2-10 μm)	2	nd	4	86	619	426	86	167	nd	2161	789	1788	894	nd	424
n	Pennate cells solitary (11-20 μm)	11	11	7	943	1858	2557	686	667	3393	8642	6576	5142	4918	4753	13572
m	Pennate cells solitary (21-50 μm)	20	24	42	4200	5728	8309	2228	4838	8907	7778	7102	6483	9389	7346	12724
m	Pennate cells solitary (> 50 μm)	4	9	20	429	774	852	nd	167	1272	864	789	0	4024	2161	848
Dinophyceae		**21**	**8**	**13**	**600**	**0**	**639**	**86**	**334**	**1696**	**0**	**789**	**447**	**0**	**864**	**424**
n	Gymnodinium / Gyrodinium spp. (2-10 μm)	4	nd	nd	86	nd	nd	nd	167	nd	nd	nd	nd	nd	nd	nd
n	Gymnodinium / Gyrodinium spp. (10-20 μm)	6	4	7	343	nd	213	nd	167	424	nd	789	447	nd	432	nd
m	Gymnodinium / Gyrodinium spp. (20-50 μm)	8	4	5	171	nd	426	86	nd	424	nd	nd	nd	nd	432	nd
m	*Peridiniella catenata* (Levander) Balech	nd	nd	1	nd	nd	nd	nd	nd	nd	nd	nd	nd	nd	nd	x
n	Dinoflagellates (0-10 μm)	nd	nd	nd	nd	nd	nd	nd	nd	nd	nd	nd	nd	nd	nd	nd
n	Dinoflagellates (11-20 μm)	1	nd	nd	nd	nd	nd	nd	nd	nd	nd	nd	nd	nd	nd	424
m	Dinoflagellates (21-50 μm)	1	nd	nd	nd	nd	nd	nd	x	424	nd	nd	nd	nd	nd	nd
m	Dinoflagellates (> 50 μm)	1	nd	nd	nd	nd	nd	nd	nd	424	nd	nd	nd	nd	nd	nd
Chrysophyceae		**0**	**0**	**0**	**0**	**0**	**0**	**0**	**0**	**0**	**0**	**0**	**0**	**0**	**0**	**0**
m	*Dinobryon faculiferum* (Willén) Willén	nd	x	nd	nd	nd	nd	nd	nd	nd	nd	nd	nd	nd	nd	nd
Prasinophyceae		**3**	**5**	**4**	**171**	**1238**	**0**	**0**	**334**	**0**	**864**	**526**	**224**	**0**	**432**	**848**
n	*Pyramimonas* cf. *nansenii* Braarud	nd	nd	nd	nd	nd	nd	nd	nd	nd	nd	nd	nd	nd	nd	x
n	*Pyramimonas* spp. (0-10 μm)	2	5	4	171	1238	nd	nd	167	nd	864	526	nd	nd	nd	424
n	*Pyramimonas* spp. (10-20 μm)	nd	nd	nd	nd	nd	nd	nd	167	nd	nd	nd	nd	nd	432	424
m	*Pyramimonas* spp. (>20 μm)	1	nd	nd	nd	nd	nd	nd	nd	nd	nd	nd	224	nd	nd	nd
Prymnesiophyceae		**0**	**1**	**0**	**0**	**0**	**0**	**0**	**0**	**0**	**0**	**0**	**0**	**0**	**0**	**0**
n	*Phaeocystis pouchetii* (Hariot) Lagerheim	nd	1	nd	nd	nd	nd	nd	nd	nd	nd	nd	nd	nd	nd	nd
n	*P.* c.f. *pouchetii* (Hariot) Lagerheim	nd	nd	nd	nd	nd	nd	nd	nd	nd	nd	nd	nd	nd	nd	nd
n	*Prymnesiophyceae* spp. (2-10 μm)	nd	nd	nd	nd	nd	nd	nd	nd	nd	nd	nd	nd	nd	nd	nd
n	*Prymnesiophyceae* spp. (11-20 μm)	nd	nd	nd	nd	nd	nd	nd	nd	nd	nd	nd	nd	nd	nd	nd
m	*Prymnesiophyceae* spp. (> 20 μm)	nd	nd	nd	nd	nd	nd	nd	nd	nd	nd	nd	nd	nd	nd	nd
Flagellates		**128**	**81**	**78**	**4800**	**2012**	**4048**	**2485**	**9176**	**4665**	**9939**	**6576**	**10283**	**5812**	**7346**	**7210**
n	Family: Geminigeracea (0-10 μm)	2	1	5	nd	nd	nd	257	500	nd	432	263	447	1788	nd	848
n	Family: Geminigeracea (11-20 μm)	3	1	2	86	nd	nd	nd	167	nd	nd	263	nd	x	432	848
m	Family:	nd	nd	nd	nd	nd	nd	nd	nd	424	nd	nd	nd	nd	nd	nd

	Dinobrycea (>50 μm)															
n	Flagellates (2-5 μm)	76	39	30	2743	1238	2130	1286	5672	2545	6914	3419	6036	1341	4321	2545
n	Flagellates (6-10 μm)	34	19	29	1114	774	1704	600	2502	1696	2161	1578	2906	1788	1296	1696
n	Flagellates (11-20 μm)	14	17	6	771	nd	213	343	334	nd	432	1052	894	894	864	1272
m	Flagellates (>20 μm)	nd	4	6	86	nd	nd	nd	nd	nd	nd	nd	nd	nd	432	nd
Choanoflagellates		**1**	**0**	**0**	**171**	**0**	**639**	**857**	**1168**	**848**	**3025**	**4471**	**1788**	**2683**	**12531**	**8482**
Family: acanthoecideae		1	nd	nd	171	nd	639	857	1168	848	3025	4471	1788	2683	12531	8482
Unidentified choanoflagellates (10-50 μm)		nd	nd	nd	nd	nd	nd	nd	nd	nd	nd	nd	nd	nd	nd	nd
Ciliates		**2**	**0**	**1**	**0**	**0**	**0**	**0**	**0**	**0**	**0**	**0**	**0**	**0**	**432**	**0**
m	*Tintinnopsis* spp. (> 50 μm)	nd	nd	nd	nd	nd	nd	nd	nd	nd	nd	nd	nd	nd	432	nd
m	Ciliates (20-50 μm)	2	nd	nd	nd	nd	nd	nd	nd	nd	nd	nd	nd	nd	nd	nd
m	Ciliates (> 50 μm)	nd	x	1	nd	nd	nd	nd	nd	nd	nd	nd	nd	nd	x	nd
Unidentified Cells		**310**	**263**	**100**	**5999**	**13313**	**9161**	**6085**	**16683**	**22479**	**29816**	**25777**	**23025**	**36215**	**23334**	**21630**
Cysts (0-10 μm)		5	1	7	nd	310	213	nd	334	nd	432	nd	671	1788	432	nd
Cysts (11-20 μm)		2	4	11	257	155	213	429	500	424	1296	2104	1341	2235	864	848
Cysts (21-50 μm)		1	3	1	343	nd	nd	171	nd	nd	nd	263	224	nd	nd	nd
Cysts (>50 μm)		nd	nd	nd	nd	nd	nd	nd	nd	nd	nd	nd	224	nd	nd	nd
Unidentified cells (0-10 μm)		227	229	44	4028	7276	7030	3857	12679	11875	15124	16571	13860	20566	15556	15268
Unidentified cells (11-20 μm)		21	24	36	857	4489	426	686	2336	8058	6050	6050	4918	10730	6050	3393
Unidentified cells (>20 μm)		1	nd	nd	nd	nd	nd	nd	834	1696	4753	nd	671	nd	nd	nd
Presence Counts																
Number of Species Counted		**11**	**11**	**23**	**16**	**12**	**10**	**13**	**14**	**11**	**12**	**15**	**13**	**6**	**15**	**8**
Number of Species Observed		**14**	**21**	**24**	**16**	**20**	**13**	**15**	**15**	**16**	**19**	**19**	**19**	**10**	**21**	**14**
Number of Taxa Counted		**28**	**27**	**28**	**33**	**27**	**25**	**28**	**31**	**27**	**25**	**26**	**27**	**26**	**27**	**24**
Number of Taxa Observed		**28**	**28**	**29**	**33**	**27**	**27**	**28**	**32**	**27**	**27**	**27**	**19**	**27**	**28**	**26**

Chapter Five Supplementary Material

Table 5.S.1. Results from linear regression analyses of average nanoeukaryote abundance with environmental parameters (*see* text for definitions) under thin and thick snow covers. The coefficient of determination (r^2) is presented in unstandardized and standardized (brackets) forms, along with the significance of each regression (p) and the associated regression equation when $p < 0.05$.

Snow Cover	Parameter	r^2 (adjusted)	p	Equation
Thin	NO_x	0.469 (0.428)	0.005	171636.301 + NO_x (-112637.72)
	E_z(June)	0.567 (0.528)	0.003	-5652.058 + E_z(June)(4160.687)
	E_z(PAR)	0.647 (0.608)	0.003	-16048.843 + E_z(PAR)(4125.654)
	Temp.	0.233 (0.156)	0.112	-
	Salinity	0.232 (0.155)	0.113	-
	Brine Vol.	0.389 (0.328)	0.030	-40569.711 + Brine Vol. (5048.007)
Thick	NO_x	0.169 (0.105)	0.128	-
	E_z(June)	0.330 (0.269)	0.040	4983.863 + E_z(June)(3206.471)
	E_z(PAR)	0.480 (0.422)	0.018	-17331.702 + E_z(PAR)(3940.891)
	Temp.	0.078 (-0.015)	0.381	-
	Salinity	0.017 (-0.081)	0.685	-
	Brine Vol.	0.185 (0.103)	0.163	-

Table 5.S.2. Results from linear regression analyses of average microeukaryote abundance with environmental parameters (*see* text for definitions) under thin and thick snow covers. The coefficient of determination (r^2) is presented in unstandardized and standardized (brackets) forms, along with the significance of each regression (p) and the associated regression equation when $p < 0.05$.

Snow Cover	Parameter	r^2 (adjusted)	p	Equation
Thin	NO_x	0.172 (0.109)	0.124	-
	E_z(June)	0.170 (0.095)	0.161	-
	E_z(PAR)	0.206 (0.117)	0.161	-
	Temp.	0.118 (0.029)	0.275	-
	Salinity	0.452 (0.397)	0.017	6.46 + Salinity(1.906E-05)
	Brine Vol.	0.174 (0.091)	0.178	-
Thick	NO_x	0.102 (0.032)	0.247	-
	E_z(June)	0.383 (0.327)	0.024	14404.735 + E_z(June)(2232.005)
	E_z(PAR)	0.664 (0.627)	0.002	-4929.905 + E_z(PAR)(2871.580)
	Temp.	0.082 (-0.009)	0.366	-
	Salinity	0.301 (0.231)	0.065	-
	Brine Vol.	0.223 (0.145)	0.121	-

Table 5.S.3. Results from linear regression analyses of chlorophyll *a* (chl *a*), particulate organic carbon (POC) or primary production relative to chlorophyll *a* (PP_{chla}) with average nanoeukaryote ($Nano_{AVG}$) and/or microeukaryote ($Micro_{LM}$) abundance under thin and thick snow covers. The standardized coefficient for multiple regressions (β), the coefficient of determination (r^2) in unstandardized and standardized (brackets) forms and the associated regression equation when $p < 0.05$ are shown. The significance (p) of each standardized coefficient and regression equation are also presented.

Snow Cover	Parameters		Standardized Coefficient		Model		
	Dependent	Independent(s)	β	*p*	r^2 (adjusted)	*p*	Equation
Thin	Chl *a*	$Nano_{AVG}$ $Micro_{LM}$	0.615 0.461	0 0	0.927 (0.915)	0	0.595 + ($Nano_{AVG}$)2.6003E-05 + ($Micro_{LM}$)3.741E-05
	POC	$Nano_{AVG}$ $Micro_{LM}$	0.875 0.076	0 0.596	0.849 (0.824)	0	6.134 + ($Nano_{AVG}$)0.009 + ($Micro_{LM}$)0.002
		$Nano_{AVG}$	-	-	0.846 (0.834)	0	65.629 + ($Nano_{AVG}$)0.010
		$Micro_{LM}$	-	-	0.353 (0.304)	0.019	217.186 + ($Micro_{LM}$)0.012la
	PP_{chla}	$Nano_{AVG}$ $Micro_{LM}$	0.736 -0.015	0.016 0.952	0.546 (0.432)	0.043	-0.474 + ($Nano_{AVG}$) 1.69E-5 + ($Micro_{LM}$) -0.000001
		$Nano_{AVG}$	-	-	0.546 (0.495)	0.009	-0..572 + ($Nano_{AVG}$) 1.696E-5
		$Micro_{LM}$	-	-	0.018 (-0.091)	0.696	-
Thick	Chl *a*	$Nano_{AVG}$ $Micro_{LM}$	0.330 0.640	0.09 0.004	0.840 (0.814)	0	1.418 + ($Nano_{AVG}$)1.959E-06 + ($Micro_{LM}$)5.817E-05
		$Nano_{AVG}$	-	-	0.670 (0.644)	0	2.868 + NanoAVG(4.86E-05)
		$Micro_{LM}$	-	-	0.795 (0.779)	0	1.264 + ($Micro_{LM}$)8.109E-05
	POC	$Nano_{AVG}$ $Micro_{LM}$	0.673 0.225	0.013 0.348	0.735 (0.691)	0	58.269 + ($Nano_{AVG}$)0.006 + ($Micro_{LM}$)0.003
		$Nano_{AVG}$	-	-	0.714 (0.692)	0	135.817 + ($Micro_{LM}$)0.008
		$Micro_{LM}$	-	-	0.546 (0.511)	0.002	10.452 + ($Micro_{LM}$)0.01
	PP_{chla}	$Nano_{AVG}$ $Micro_{LM}$	-0.170 0.626	0.679 0.150	0.271 (0.109)	0.241	-
		$Nano_{AVG}$	-	-	0.071 (-0.022)	0.402	-
		$Micro_{LM}$	-	-	0.256 (0.182)	0.093	-

CHAPTER SIX: NET COMMUNITY PRODUCTION IN THE BOTTOM OF ARCTIC SEA ICE OVER THE SPRING BLOOM

This manuscript has been submitted to the peer-reviewed journal of *Geophysical Research Letters*. The research included in this work was planned, conducted and reported by myself as first author.

Campbell, K., Mundy, C.J., Gosselin M., Landy, J.C., Delaforge, A. and S. Rysgaard, Net community production in the bottom of Arctic sea ice over the spring bloom, *Geophys. Res. Lett.* (in review).

Abstract

The balance of photosynthesis and respiration by organisms like algae and bacteria determines whether the sea ice is net heterotrophic or autotrophic. In turn this describes the influence of microbes on ocean-ice gas fluxes, and their contribution to the trophic system. In this study we define two phases of the spring bloom based on net community production and algal growth in the bottom ice. Phase I was characterized by low productivity, which at times resulted in net heterotrophy, and limited algal accumulation that was likely supported by pelagic carbon. Greater productivity in Phase II drove rapid algal accumulation that consistently produced net autotrophic conditions. The different phases were caused by seasonal shifts in light availability and species dominance in the algal community. The results of this study demonstrate the importance of community respiration in assessments of spring productivity, as rates of respiration can maintain a heterotrophic state independent of algal growth.

Key Points

- Sea ice can be net heterotrophic during the Arctic spring, despite sufficient light being available for photosynthesis
- A rapid (within 1 week) switch from heterotrophy to autotrophy coincided with a transition in the algal community from pennate to centric diatoms

Index Terms: Cryobiology, sea ice, photosynthesis, respiration

Keywords: algae, oxygen, heterotrophy, autotrophy, centric and pennate diatoms

6.1 Introduction

Autotrophic protists and bacteria dominate the microbial communities of sea ice, inhabiting brine inclusions and the surfaces of ice crystals, principally at the ice growth interface [Legendre et al., 1992; Deming, 2010]. In addition to brine and meltwater dynamics [Glud et al., 2002], the photosynthetic and respiratory activities of these organisms regulate the concentration of O_2 in sea ice [Søgaard et al., 2010]. The overall difference between photosynthesis and respiration represents net community production, and describes whether sea ice may be considered as a net autotrophic (O_2 gain) or heterotrophic (O_2 loss) system [Codispoti et al., 2013]. The productive state of the biological community affects gas fluxes between the ice and ocean [Brown et al., 2015], as well as carbon cycling within the Arctic marine system [Matrai and Apollonio, 2013; Michel et al., 2015].

Absent or limited availability of light through the Arctic winter and early spring prevents or restricts photosynthesis and instead favors bacteria and protist heterotrophy [Riedel et al., 2007, 2008]. However, a seasonal increase in downwelling irradiance during spring instigates a bloom that is typically characterized by the rapid growth and

production of autotrophic protists (algae) in the bottom portion of the sea ice [Leu et al., 2015]. The temporal shift in microbial composition and productivity affects the balance of O_2 losses and gains, which can result in the bottom ice environment transitioning from overall state of net equilibrium or heterotrophy prior to the ice algal bloom, to a state of autotrophy once the bloom commences [Søgaard et al., 2010]. Heterotrophic processes may once again dominate the bottom ice with the bloom's decline and following its termination [Kaartokallio et al., 2004]. Other factors potentially affecting respiration and photosynthesis include temperature [Arrigo and Sullivan, 1992; Kirchmann, 2008], nutrient availability [Gosselin et al., 1990; Kaartokallio et al., 2013] and algal species composition [Campbell et al., subm.]. However, estimates of sea ice net community production are relatively sparse [e.g. Rysgaard et al., 2008; Nguyen and Maranger, 2011; Glud et al., 2014] and it is not well understood how changing environmental conditions influence net community production throughout the spring algal bloom. It will be important to understand the mechanisms controlling net community production for predicting the response of sea ice communities to climate induced changes, such as greater light availability under a potentially thinner future snow cover [Webster et al., 2014].

As part of the 2014 Ice Covered Ecosystem - CAMbridge bay Process Study (ICE-CAMPS) we assessed the potential for net heterotrophy during the ice algal bloom by recording net community production of bottom first-year sea ice for approximately seven weeks in the spring. We define the productive state of the bottom ice environment based on these measurements and evaluate its seasonal evolution.

6.2 Data collection and processing

Samples were collected on 12 occasions between 21 April and 9 June 2014 from the landfast first-year sea ice in Dease Strait (69°1'N, 105°19'W), near Cambridge Bay, Nunavut. Sites with <10 cm snow cover (relatively high light availability) were sampled approximately every four days over the spring. During each sampling event the bottom 5 cm of ice cores were collected and melted in filtered seawater to determine the concentration of chlorophyll *a* (chl *a*), particulate organic carbon (POC) [Campbell et al., 2016] (s*ee* Chapter Four), and taxonomic composition of the algal community [Campbell et al., subm.] (*see* Chapter Five; 6.S.1). All reported measurements of abundance and productivity (described below) have been corrected for the filtered seawater dilution.

Net community production was calculated as the change in oxygen over time (μmol O_2 l^{-1} h^{-1}). It was determined by incubating aliquots of the melted ice sample in bottles equipped with oxygen optodes according to Campbell et al. [2016] (*see* Chapter Four), under conditions of darkness and at light intensities of approximately 10, 21 and 55 μmol m^{-2} s^{-1} (6.S.2). Net community production at the different incubation light intensities was modeled using the exponential equation of Platt et al. [1980] modified by Arrigo et al. [2010] that excludes photoinhibition, as this was not observed at our incubation light intensities. The exponential model was used to estimate the light intensity (μmol m^{-2} s^{-1}) at which net community production was equivalent to zero, which we define as the light compensation point of the bottom ice community (C_{EC}). We differentiate this from the light compensation point (E_c) that is typically defined in modeling of photosynthesis-irradiance curves, as E_c represents the light intensity when gross primary production rather than net community production is zero.

Hourly estimates of scalar irradiance averaged for the bottom ice algal layer ($\bar{E}_0$) were calculated according to Ehn and Mundy [2013], which assumes constant exponential attenuation across a 2.5 cm algal layer. This calculation used estimates of downwelling photosynthetically active radiation (PAR) transmitted through the ice and bottom-ice chl *a* (6.S.3). Hourly estimates of scalar light intensity for the ice algal layer volume ($\hat{E}_0$), derived from the principle of energy conversion (Gershun's equation) assuming a 2.5 cm bottom ice algal layer [Ehn and Mundy, 2013], were also calculated to provide an upper theoretical limit of light absorbed by algal cells. It is noted that $\hat{E}_0$ is always greater than $\bar{E}_0$ in sea ice due to multiple scattering [Ehn and Mundy, 2013].

Hourly variations of *in situ* net community production were estimated for days of ice core collection by solving the exponential model described above at *in situ* scalar irradiances. Hourly estimates of net community production from $\bar{E}_0$ or $\hat{E}_0$ were then integrated over the 24 h diurnal period, giving net community production over the full diurnal cycle.

6.3 The ice algal community

Ice algae were present in the region prior to the start of the study, with chl *a* and POC concentrations between 7 and 15 March averaging 1.2 and 53.4 mg m^{-2}, respectively. These estimates are considerably lower than concentrations in Figure 6.1, indicating positive accumulation, with daily net production rates and standard errors on the order of 0.12 ± 0.02 mg chl *a* m^{-2} d^{-1} and 8.89 ± 1.43 mg C m^{-2} d^{-1} during early spring (8 March to 21 April). Chlorophyll *a* and POC accumulated in the bottom ice from April to June, following a seasonal increase in light availability [Campbell et al., 2016] (*see* Chapter

Four). However, the rates of accumulation were not constant and the study period can be divided into two phases, particularly surrounding a jump in POC between 8 and 13 May (Figure 6.1).

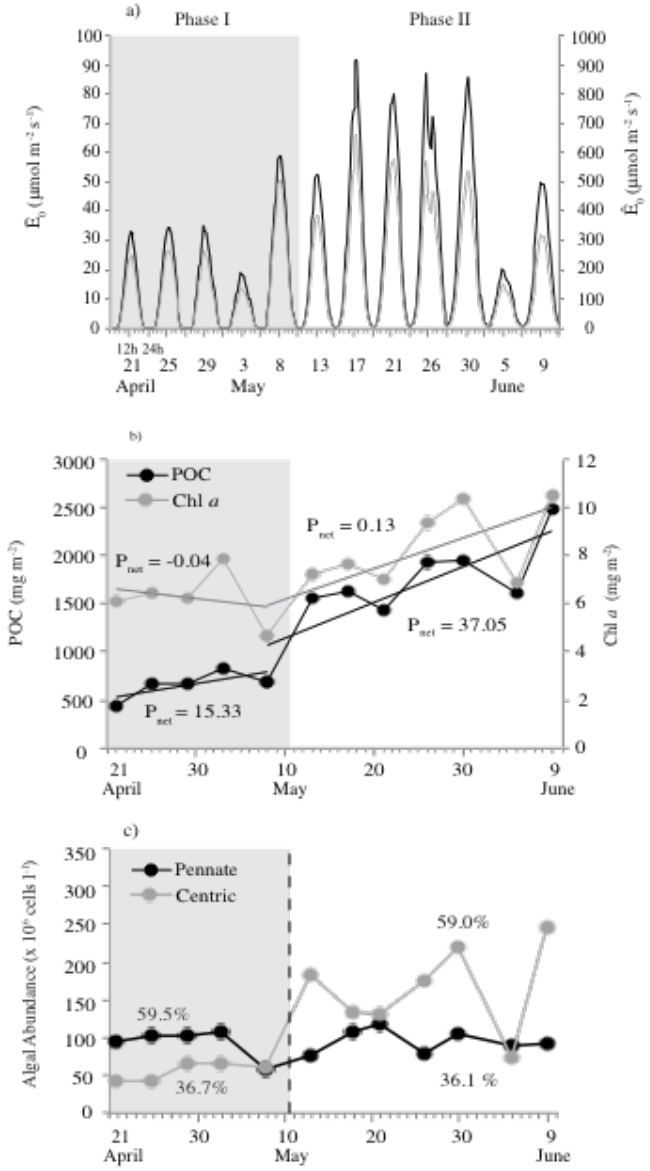

Figure 6.1. (a) ($\bar{E}_0$) (grey) and $\hat{E}_0$ (black) for days of ice core collection, (b) seasonal concentration of bottom ice particulate organic carbon (POC) and chlorophyll *a* (chl *a*) with linear trend lines and daily net production rates (P_{net}) (mg m^{-2} d^{-1}) before and after 8 May, and (c) abundance of pennate and centric diatoms in the ice algal community over the spring during Phases I (grey) and II (white). The dashed line on (c) highlights the approximate division between pennate and centric diatom dominance in the bottom ice community, where the specific percent abundance of each taxonomic group relative to the entire bottom ice community is reported for each phase.

The seasonal daily net production rates for this study period (21 April to 9 June) was 0.07 ± 0.03 mg m^{-2} d^{-1} for chl *a* and 37.14 ± 4.76 mg m^{-2} d^{-1} for POC. However, in Phase I from April 21 to 8 May, chl *a* accumulation was nearly zero (-0.04 ± 0.10 mg m^{-2} d^{-1}) and POC accumulation was approximately 2.5 times lower (15.33 ± 8.80 mg m^{-2} d^{-1}) than the overall trend (Figure 6.1). Phase II from 8 May to 5 June was characterized by significantly greater chl *a* ($p < 0.05$) and POC ($p < 0.05$) (Table 6.S.1). This resulted in 85% higher daily net production rates for chl *a* (0.13 ± 0.05 mg m^{-2} d^{-1}) and nearly equivalent daily net production rates for POC (37.05 ± 11.04 mg m^{-2} d^{-1}; s = 326.58), relative to seasonal trends. Excluding estimates between 8 and 13 May from this comparison of Phase II daily net production rates, seasonal trends of chl *a* (0.09 ± 0.06 mg m^{-2} d^{-1}) and POC (25.17 ± 11.5 mg m^{-2} d^{-1}) are still greater than in Phase I.

Daily averaged $\bar{E}_0$ ($\bar{E}_{0(daily)}$) and $\hat{E}_0$ ($\hat{E}_{0(daily)}$) were also greater in Phase II ($p < 0.10$). We note that the difference in scalar irradiance between phases had greater significance ($p < 0.05$) when outliers from 5 and 9 June sample dates were excluded from analysis. A late-season snowstorm on 3 June caused a large drop in PAR transmittance that resulted in unseasonably low $\bar{E}_0$ and $\hat{E}_0$ estimates for subsequent measurements.

Diatoms dominated the algal community during both growth phases, particularly the pennate diatom *Nitzschia frigida* and centric diatoms of the genus *Attheya*. However, an increasing abundance of centric forms over the spring shifted the composition of the ice algal community from dominant pennates to dominant centrics after 8 May (i.e. between Phases I and II) (Figure 6.1c). The transition to a significantly greater ($p < 0.05$) abundance of centric diatoms in Phase II (Table 6.S.1) primarily drove the seasonal trends in chl *a* and POC (Figure 1b). It was likely a result of centric diatoms outcompeting

pennate forms in the low nitrogen and low salinity conditions of the study region (Table 6.S.1), once light intensities were less limiting [Campbell et al., subm.] (*see* Chapter Five).

6.4 Optode-derived measurements of net community production

The net community production of samples incubated under the various light intensities and in darkness are shown in Figure 6.2. Illuminated estimates were far below maximum rates of sea ice net community production reported by Suzuki et al. [1997], that were on the order of 50-190 μmol O_2 l^{-1} h^{-1}, but are comparable to incubation estimates with similar light conditions once differences in biomass have been accounted for [Rysgaard et al., 2008; Søgaard et al., 2010]. Although estimates of net community production in darkness can vary considerably, the average estimate in this study at 2.2 ± 0.6 μmol O_2 l^{-1} h^{-1} was also within the range documented in Arctic sea ice of 0.04-93.8 μmol O_2 l^{-1} h^{-1} [Suzuki et al., 1997; Nyugen and Maranger, 2011]. Furthermore, dark respiration contributed 30% of gross primary production [Campbell et al., 2016] (*see* Chapter Four), which is similar to previous estimates of between 10 and 41% [Falkowski and Owens, 1978; Suzuki et al., 1997].

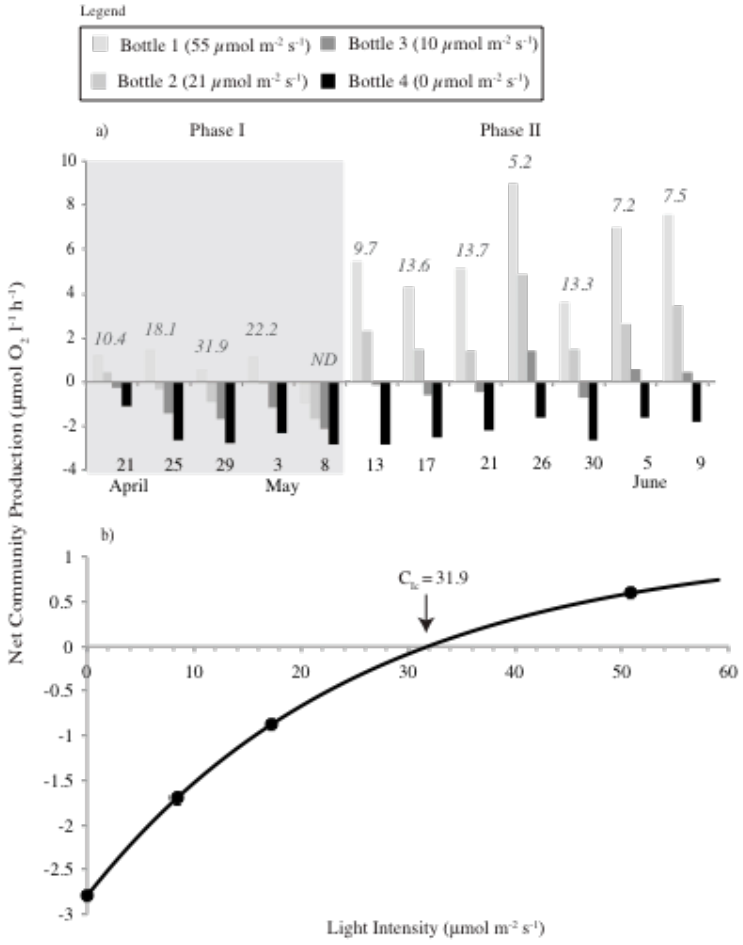

Figure 6.2. (a) Net community production of bottom-ice samples (5 cm) incubated at light intensities of approximately 0, 10, 21 and 55 μmol m^{-2} s^{-1} during Phases I (grey) and II (white) and (b) an exponential model of net community production on 29 April to highlight the community light compensation point (C_{EC}) parameter. In (a), values of C_{EC} (μmol m^{-2} s^{-1}) calculated for all incubations are listed above the respective production estimates, expect for 13 May where it was not defined (ND).

In all incubations the production of oxygen increased or consumption was reduced with light intensity, due to the contribution of algal photosynthesis exceeding that of community respiration. However, during Phase I hourly net community production was considerably lower than during Phase II (Table S1). This corresponded to significantly higher C_{EC} estimates (Table S1) in Phase I, meaning that on average 100% higher light intensity was required to create positive net production in the bottom ice community at

this time. Photoacclimation cannot account for the observed difference in C_{EC} between phases, as the compensation light intensity (E_C) of individual cells did not significantly change over the spring [Campbell et al., 2016] (*see* Chapter Four).

6.5 Seasonal changes in net community production

There is uncertainty associated with estimating light available to algae living in the bottom ice due to measurement error, as well as the effects of multiple scattering and self-shading within the algal layer [Ehn and Mundy, 2013]. As a result, our estimates of daily net community production represent approximations of the productive state in bottom sea ice. In an effort to characterize the potential range of daily net community production, we present estimates calculated from both $\bar{E}_0$ and $\hat{E}_0$ (Figure 6.3), as the average intensity of $\hat{E}_0$ was around six times greater than $\bar{E}_0$. It follows that net community production calculated from $\bar{E}_0$ approximates a lower limit while those calculated from $\hat{E}_0$ represent the upper theoretical limit.

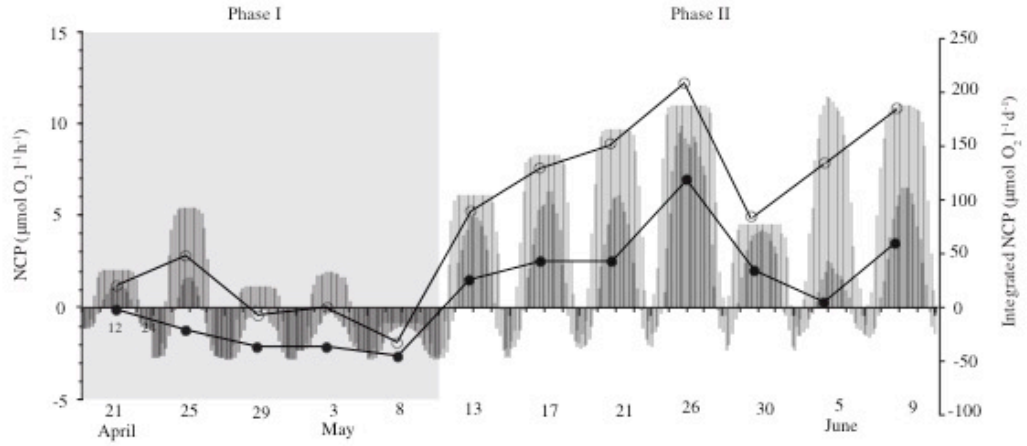

Figure 6.3. Net community production in the bottom-ice samples (5 cm) modeled over 24 hours on core collection days, using $\bar{E}_0$ (dark grey) or $\hat{E}_0$ (light grey) during Phases I (grey) and II (white). Circles indicate daily-integrated estimates of net community production modeled from $\bar{E}_0$ (black) and $\hat{E}_0$ (hollow), respectively.

There is a clear difference in daily-integrated net community production between Phases I and II (Figure 6.3). Between 21 April and 8 May net community production calculated from $\bar{E}_0$ was negative (oxygen was consumed in the sea ice) and average production over 24 h was -27.87 μmol O_2 l^{-1} h^{-1} (-1394 μmol O_2 m^{-2} h^{-1}). In comparison, net community production calculated from $\bar{E}_0$ after 8 May was consistently positive (oxygen was produced in the sea ice more than it was consumed) and average production over 24 h at 47.28 μmol O_2 l^{-1} h^{-1} (2364 μmol O_2 m^{-2} h^{-1}) was significantly greater (Table 6.S.1). It follows that based on $\bar{E}_0$ and the influence of biology alone (i.e. excluding contributions from brine or meltwater drainage) the bottom ice can be classified as net heterotrophic during growth Phase I (21 April – 8 May), before transitioning into a net autotrophic system in Phase II (13 May – 9 June). Although, we note that hourly net community production based on $\bar{E}_0$ remained heterotrophic for a portion of the nighttime

throughout the spring, with net oxygen consumption occurring for 19 ± 5 h in Phase I and 9 ± 2 h in Phase II.

Our findings support previous observations by Rysgaard & Glud [2004] and Rysgaard et al. [2008] that net heterotrophy can occur in the presence of primary production in sea ice. However, to our knowledge we report the first observations of a strong shift in the productive state of sea ice over the bloom period. The potential for heterotrophic conditions during the ice algal bloom indicates that algal photosynthesis does not necessarily always create a sink for CO_2 (e.g. Delille et al., 2007). Instead, the role of sea ice in the biological pump is likely more complex and depends on the seasonally-evolving balance between community photosynthesis and respiration.

Estimates for the higher light intensity ($\hat{E}_0$) net community production were also significantly greater during Phase II than Phase I (Table 6.S.1), and they highlight a transition from low to high productive states between 8 and 13 May. However, the average daily productivity based on $\hat{E}_0$ was nearly 300% greater than estimations from $\bar{E}_0$, which resulted in heterotrophic (negative) estimates for only two of five sampling days during Phase I (Figure 6.3). Nevertheless, these observations support the potential for net heterotrophy to occur during periods of moderate carbon biomass accumulation in the bottom ice, in spite of relatively high PAR availability (Figure 6.1). We note that the potential for heterotrophic conditions is likely to decrease with carbon accumulation, as net community production calculated from either $\bar{E}_0$ ($r = 0.80$) or $\hat{E}_0$ ($r = 0.86$) is significantly ($p < 0.05$) and positively correlated with POC over the study period.

The seasonal increase in net community production and associated higher net community production during Phase II (Table 6.S.1) are in part driven by increasing

scalar irradiance throughout the spring (Figure 6.1a). However, the rapid shift in net community production between 8 and 13 May did not directly correspond to a rapid change in light intensity (Figure 6.1a) or a reduction in the contribution of community respiration (Figure 6.2a). Instead, it parallels the equally rapid shift in community composition from a majority of pennate to centric diatoms (Figure 6.1c). The influence of diatom abundance is further supported by significant ($p < 0.05$) linear correlations of numerical centric abundance with net community production based on $\bar{E}_0$ ($r = 0.74$) and $\hat{E}_0$ ($r = 0.67$), respectively. We note that temperature and the concentration of dissolved inorganic nitrogen (nitrate + nitrite) in the bottom ice did not directly affect net community production variability, as these variables were not significantly different between phases (Table 6.S.1) and were not correlated with $\bar{E}_0$ or $\hat{E}_0$ based production over the spring (data not shown). However, we note that low nitrogen conditions in the region indirectly affected net community production by facilitating growth of centric diatoms in the ice, which ultimately resulted in the observed shift in species dominance (*see* Campbell et al., 2016; Chapter Four).

6.6 Early spring biomass accumulation under net heterotrophic conditions

It is notable that POC increased slowly during Phase I, even though the bottom ice community was principally net heterotrophic (Figures 6.1b, 6.3). Accumulation of POC could have been possible during this period i) if non-algal respiration exceeded photosynthetic production of oxygen, ii) under conditions of facultative heterotrophy and/or iii) if there was an exogenic supply of biomass to the ice.

Bacteria are generally accepted as one of the most abundant heterotrophic organisms in sea ice with the greatest influence on community respiration [Deming, 2010; Nguyen and Maranger, 2011]. In systems of low primary productivity the contribution of bacterial respiration can even exceed that of phytoplankton production [Cota et al., 1996; del Giorgio et al., 1997]. In this study, dark bacterial production from ^{3}H-Leucine incubations on the bottom 5 cm of sea ice ranged from about 0.02-0.38 μg C l^{-1} h^{-1} during this study period (*see* Campbell et al., subm.; Chapter Five). Based on these estimates of bacterial production and a bacterial growth efficiency of 0.186 [Nguyen et al., 2012], we estimate that the combined influence of bacterial production and respiration accounted for < 7.5% of oxygen consumption in the dark incubation bottles. This emphasizes that bacteria, which typically dominate the heterotrophic signal of bottom ice communities, were not responsible for the productive state in Phase I. Moreover, bacterial production and net community production in the dark were not significantly different between Phases I and II (Table 6.S.1), indicating that variability in algal or bacterial respiration were not the causes of the seasonal shift in productive state. However, the contribution of other community members to respiration cannot be assessed here.

We note the potential for bacterial biomass to contribute to POC in the bottom ice, particularly following the possible stimulation of bacterial production with supply of dissolved organic carbon (DOC) substrate from the water column (Thomas et al., 2001). However, the impact is likely to be minimal given the low estimates of bacterial production, and lack of association between interface DOC that averaged 1.8 ± 0.06 mg C l^{-1} (data not shown) and bacterial production during the study period [Campbell et al., subm.] (*see* Chapter Five).

To survive winter, it has been suggested that sea ice diatoms use a combination of facultative heterotrophy, a reduced metabolic state, and utilization of intracellular energy stores as well as exoploymeric substances (EPS) previously released (Palmisano and Sullivan 1982; Zhang et al. 1998; Niemi et al. 2011). Although such strategies have not been directly observed in nature, the potential for sea ice diatoms to deploy them represents a potential mechanism of POC increase during heterotrophic conditions.

Passive incorporation of algae into sea ice by effectively scavenging and sieving cells from the water column is an accepted means of colonization during initial ice formation [Syvertsen, 1991; Spindler, 1994; Rózanska et al., 2008]. Further active attachment of pelagic cells may also occur during lamellar ice growth [Spindler, 1994; Lund-Hansen et al., 2016], a process that is aided by the production of EPS from algae > 4 μm [Rózanska et al., 2008; Krembs et al., 2011]. We speculate that these active mechanisms of cell colonization at the growth interface contributed to the moderate increase in POC documented in Phase I (Figure 6.1), where cells were slowly concentrated from the sparsely populated water column that had average chl *a* concentrations of only 0.24 μg l^{-1} at 5 m depth over the spring.

The mechanisms of exogenic biomass supply could be particularly evident given that the sea ice continued to grow over the entire sampling period [Campbell et al., subm.] (*see* Chapter Five) and that the dominant ice species of *Nitzschia frigida* and *Attheya* spp. (both > 4 μm) were regularly documented in the water column. These species averaged approximately 900 cells l^{-1} and 2300 cells l^{-1} in Phase I, respectively (A. Delaforge pers. observ.). Such insights support previous hypotheses that biomass accumulation via pelagic colonization of sea ice may exceed *in situ* growth [Krembs et al. 2000, 2002], if

algal productivity is low. We note that bottom ice POC could have partially originated from the upper horizon of the sea ice by the mechanisms of brine drainage [Lund-Hansen et al., 2014] and cellular migration [Aumack and Krembs, 2014]. Although, concentrations of POC and chl *a* from 5-10 cm in the ice remained constant or even increased during Phase I, which suggests that the downward movement of particulate carbon was likely not significant (data not shown).

6.7 Conclusions

This study shows the potential for net heterotrophic conditions in the bottom of sea ice during the Arctic spring, despite sufficient light being available for photosynthesis and the moderate accumulation of carbon biomass. These findings highlight the importance of i) species composition on productive state, ii) community respiration on net oxygen fluxes between the ice and ocean, and iii) the potential influences of facultative heterotrophy or sustained ice colonization by pelagic cells throughout the bloom. The occurrence of a net heterotrophic state at a time when algae dominate the ice community also challenges the common assumption that photosynthesis during the spring bloom will always result in positive net production (autotrophy) [e.g. Kaarokallio, 2004]. Such assumptions are especially problematic if measurements of gross primary production are used to assess the contribution of sea ice algae to carbon cycling, as heterotrophy (negative production) cannot be quantified by the commonly used ^{14}C incubation method [Williams, 1993]. Instead, future studies should consider the influence of respiration in sea ice throughout the ice algal bloom to ensure accurate representations of productive state, for example, by using an oxygen optode system like the present study or under water eddy covariance techniques [Glud et al., 2014]. Carbon cycling in sea ice

communities may be more complex than previously anticipated. Given the observed rapid reductions in sea ice cover it becomes important to take a closer look of their function in Arctic ecosystems.

Acknowledgements

Research support was given by a Northern Scientific Training Program (NSTP) grant and Natural Sciences and Engineering Research Council of Canada (NSERC) Canadian Graduate Scholarship to KC, Canada Foundation for Innovation (CFI) and the Canada Excellence Research Chair grant to SR, an NSERC Discovery and Northern Research Supplement Grants to CJM, and in-kind support from the Canadian High Arctic Research Station (CHARS). This work represents a contribution to the research programs of ArcticNet, MEOPAR, the Arctic Science Partnership (ASP) and the Canada Excellence Research Chair unit at the Centre for Earth Observation Science (CEOS) at the University of Manitoba. The authors also wish to thank Dr. Tim Papakyriakou for his contribution of data associated with the meteorological station.

References

Aumack, C.F., A.R. Juhl, and C. Krembs (2014), Diatom vertical migration within land-fast Arctic sea ice, *J. Mar. Syst.*, *139*, 496–504, doi: 10.1016/j.jmarsys.2014.08.013.

Arrigo, K.R., and C.W. Sullivan (1992), The influence of salinity and temperature covariation on the photophysiological characteristics of Antarctic sea ice microalgae, *J. Phycol.*, *28*, 746–756, doi: 10.1111/j.0022-3646.1992.00746.x.

Brown, K.A., L.A. Miller, C.J. Mundy, T. Papakyriakou, R. Francois, M.Gosselin, C. Carnat, K. Swystun, and P.D. Tortell (2015), Inorganic carbon system dynamics in landfast Arctic sea ice during the early-melt period, *J. Geophys. Res. Oceans*, *120*, 3542–3566, doi:10.1002/2014JC010620.

Campbell, K., C.J. Mundy, C. Belzile, A. Delaforge, and S. Rysgaard (in review), Seasonal dynamics of algal and bacterial communities in Arctic sea ice under variable snow cover, *Polar Biol.*, Submitted October 4, 2016.

Campbell, K., C.J. Mundy, J.C. Landy, A. Delaforge, and S. Rysgaard (2016), Community dynamics of bottom-ice algae in Dease Strait of the Canadian Arctic, *Prog. Oceanogr.* 149, 27-39, doi: 10.1016/j.pocean.2016.10.005.

Codispoti, L.A., C.N. Flagg, and J.H. Swift (2013), Hydrographic conditions during the 2004 SBI process experiments, *Deep-Sea Res.*, *56*, 1144–1163, doi: 10.1016/j.dsr2.2008.10.013.

Cota, G.F., L.R. Pomeroy, W.G. Harrison, E.P. Jones, F. Peters, W.M. Sheldon Jr., and T.R. Weingartner (1996), Nutrients, primary production and microbial heterotrophy in the southeastern Chukchi Sea: Arctic summer nutrient depletion and heterotrophy, *Mar. Ecol. Prog. Ser.*, *135*, 247–258.

del Giorgio, P.A., J.J. Cole, and A. Cimbleris (1997), Respiration rates in bacteria exceed phytoplankton production in unproductive aquatic systems, *Nature, 385*, 148–151.

Delille, B., Jourdain, B., Borges, A.V., Tison, J.-L., and D. Delille (2007), Biogas (CO_2, O_2, dimethylsulfide) dynamics in spring Antarctic fast ice, *Limnol. Oceanogr.*, *52*, 1367-1379, doi: 10.4319/lo.2007.52.4.1367.

Deming, J.W. (2010), Sea ice bacteria and viruses In: Thomas DN, Dieckmann GS (eds), Sea Ice 2nd Ed, Wiley Blackwell Publishing, Malaysia, pp. 248-282.

Ehn, J.K., and C.J. Mundy (2013), Assessment of light absorption within highly scattering bottom sea ice from under-ice light measurements: Implications for Arctic ice algae primary production, *Limnol. Oceanogr.*, *58*(3), 893-902, doi: 10.4319/lo.2013.58.3.0893.

Falkowski, P.G., and T.G. Owens (1978), Effects of light Intensity on Photosynthesis and

Dark Respiration in Six Species of Marine Phytoplankton, *Mar. Biol.* 45, 289-295.

Galindo, V., M. Levasseur, C.J. Mundy, M. Gosselin,, J.-É. Tremblay, M. Scarratt, Y. Gratton, T. Papakiriakou, M. Poulin, and M. Lizotte (2014), Biological and physical processes influencing sea ice, under-ice algae, and dimethylsulfoniopropionate during spring the Canadian Arctic Archipelago, *J. Geophys. Res. Oceans*, 119, 3746–3766, doi:10.1002/2013JC009497.

Glud, R.N., S. Rysgaard, and M. Kühl (2002), A laboratory study on O_2 dynamics and photosynthesis in ice algal communities: quantification by microsensors, O_2 exchange rates, ^{14}C incubations and a PAM fluorometer, *Aquat. Microb. Ecol.*, 27(3), 301–311 doi: 10.3354/ame027301.

Glud, R.N., S. Rysgaard, G. Turner, D.F. McGinnis, and R.J.G Leaky (2014), Biological and physical induced oxygen dynamics in melting sea ice of the Fram Strait, *Limnol. Oceanogr.*, *59*(4), 1097–1111, doi: 10.4319/lo.2014.59.4.1097.

Gosselin, M., L. Legendre, J.-C. Therriault, and S. Demers (1990), Light and nutrient limitation of sea-ice microalgae (Hudson Bay, Canadian Arctic), *J. Phycol.*, *26*, 220–232.

Horner, R.A. (1985), Sea Ice Biota, CRC Press Inc., Florida, U.S.A.

Kaarokallio, H. (2004), Food web components, and physical and chemical properties of Baltic Sea ice, *Mar. Ecol. Prog. Ser.* 273, 49-63, doi: 10.3354/meps273049.

Kaartokallio, H., D.H. Søgaard, L. Norman, S. Rysgaard, J.-L. Tison, B. Delille, and D.N. Thomas (2013), Short-term variability in bacterial abundance, cell properties, and incorporation of leucine and thymidine in subarctic sea ice. *Aquat. Microb. Ecol., 71*, 57–73, doi:10.3354/ame01667.

Kirchmann, D.L. (2008), Microbial Ecology of the Oceans, 2nd Ed. John Wiley and Sons Inc., N.J., U.S.A.

Krembs, C., Gradinger, R., and M. Spindler (2000), Implications of brine channel geometry and surface area for the interaction of sympagic organisms in Arctic sea ice, *J. Exp. Mar. Biol. Ecol.* 243, 55–80, doi: 10.1016/S0022-0981(99)00111-2.

Krembs, C., Tuschling, K., and K. Juterzenka (2002), The topography of the ice–water interface—its influence on the colonization of the sea ice by algae. *Polar Biol.* 25, 106–117.

Krembs, C., Eicken, H., and J.W. Deming (2011), Exopolymer alternation of physical properties of sea ice and implications for ice habitability and biogeochemistry in a warmer Arctic, *PNAS* 108(9), 3653-3658, doi: 10.1073/pnas.1100701108.

Legendre, L., Ackley, S.F., Dieckmann, G.S., Gullicksen, B., Horner, R., Hoshiai, T., Melnikov, I.A., Reeburgh, W.S., Spindler, M., and C.W. Sullivan (1992), Ecology of sea ice biota: Part 2. Global significance, *Polar Biol*. 12: 429–444.

Leu E., Mundy C.J., Assmy, A., Campbell, K., Gabrielsen, T.M., Gosselin, M., Juul-Pedersen, T., and R. Gradinger (2015), Arctic spring awakening – Steering principles behind the phenology of vernal ice algae blooms. *Prog. Oceanogr*. 139, 151-170, doi:org/10.1016/j.pocean.2015.07.012.

Lund-Hansen, L.C., Hawes, I., Sorrell, B.K., and M.H. Nielsen (2014), Removal of snow cover inhibits spring growth of Arctic ice algae through physiological and behavioral effects, *Polar Biol*. 37(4), 471-481, doi: 10.1007/s00300-013-1444-z.

Lund-Hansen, L.C., Hawes I., Nielsen, M.H., and B.K. Sorrell (2016), Is colonization of sea ice by diatoms facilitated by increased surface roughness in growing ice crystals? *Polar Biol*., doi:10.1007/s00300-016-1981-3.

Matrai, P., and S. Apollonio (2013), New estimates of microalgae production based upon nitrate reductions under sea ice in Canadian shelf seas and the Canada Basin of the Arctic Ocean, *Mar. Biol., 160*, 1297–1309. doi: 10.1007/s00227-013-2181-0.

Michel, C., Hamilton, J., Hansen, E., Barber, D., Reigstad, M., Iacozza, J., Seuthe, L., and A. Niemi (2015), Arctic Ocean outflow shelves in the changing Arctic: A review and perspectives, *Prog. Oceanogr*. 139, 66-88, doi: 10.1016/j.pocean.2015.08.007.

Mundy, C.J., Barber, D.G, and C. Michel (2005), Variability of snow and ice thermal, physical and optical properties pertinent to sea ice algae biomass during spring, *J. Mar. Syst*. 58(3-4), 107 – 120, doi: 10.1016/j.jmarsys.2005.07.003.

Niemi, A., Michel, C., Hille, K., and M. Poulin (2011), Protist assemblages in winter sea ice: setting the stage for the spring ice algal bloom, Polar Biol. 34, 1803-1807, doi: 10.1007/s00300-011-1059-1.

Nguyen, D., and R. Maranger (2011), Respiration and bacterial carbon dynamics in Arctic sea ice, *Polar Biol*. 34, 1843-1855, doi: 10.1007/s00300-011-1040-z.

Nyugen, D., Maranger, R., Tremblay, J.-É., and M. Gosselin (2012), Respiration and bacterial carbon dynamics in the Amundsen Gulf, western Canadian Arctic. *J. Geophys. Res*. 117, C00G16, doi: 10.1029/2011JC007343.

Palmisano, A.C., and C.W. Sullivan (1982), Physiology of sea ice diatoms I, Response of three polar diatoms to a simulated summer-winter transition, J. Phycol. 18, 489–498, doi: 10.1111/j.1529-8817.1982.tb03215.x.

Platt, T., Gallegos, C.L., and W.G. Harrison (1980), Photoinhibition of photosynthesis in natural assemblages of marine phytoplankton, *J. Mar. Res*. 38, 687–701.

Riedel, A., Michel, C., Gosselin, M., and B. LeBlanc (2007), Enrichment of nutrients, exopolymeric substances and microorganisms in newly formed sea ice on the Mackenzie shelf, *Mar. Ecol. Prog. Ser.* 342, 55-67, doi: 10.3354/meps342055.

Riedel, A., C. Michel, M. Gosselin, and B. LeBlanc (2008), Winter-spring dynamics in sea-ice carbon cycling in the coastal Arctic Ocean, *J. Mar. Syst.*, *74*, 918–932, doi:10.1016/j.jmarsys.2008.01.003.

Rysgaard, S., Glud, R.N., Sejr, M.K., Blicher, M.E., and H.J. Stahl (2008), Denitrification activity and oxygen dynamics in Arctic sea ice, *Polar Biol.* 31, 527–537, doi:10.1007/s00300-007-0384-x.

Rysgaard S., and R.N. Glud (2004), Anaerobic N_2 production in Arctic sea ice. *Limnol. Oceanogr.* 49, 86-94, doi: 10.4319/lo.2004.49.1.0086.

Søgaard, D.H., Kristensen, M., Rysgaard, S., Glud, R.N., Hansen, P.J., and K.M. Hilligsoe (2010), Autotrophic and heterotrophic activity in Arctic first-year sea ice: seasonal study from Malene Bight, SW Greenland. *Mar. Ecol. Prog. Ser.* 419, 31-45, doi:10.3354/meps08845.

Spindler, M. (1994), Notes on the biology of sea ice in the Arctic and Antarctic, *Polar Biol.* 14, 319-324. doi: 10.1007/BF00238447.

Suzuki, Y., S. Kudoh, and M. Takahashi (1997), Photosynthetic and respiratory characteristics of an Arctic algal community living in low light and temperature conditions. *J. Mar. Syst.* 11(1-2), 111-121, doi:10.1016/S0924-7963(96)00032-2.

Syvertsen, E.E. (1991), Ice algae in the Barents Sea: types of assemblages, origin, fate and role in the ice-edge phytoplankton bloom, Pp. 277-287 in Sakshaug, E., Hopkins, C. C. E. & Oritsland, N. A. (eds.): Proceedings of the Pro Mare Symposium on Polar Marine Ecology, Trondheim, 12-16 May 1990. *Polar Res.* l0(1), 1751-8369.

Thomas, D.N., Kattner, G., Engbrodt, R., Giannelli, V., Kennedy, H., Haas, C., and G.S. Dieckmann (2001), Dissolved organic matter in Antarctic sea ice, Annals Glaciol. Soc. 33, 297-303, doi: 10.3189/172756401781818338.

Thomas, D.N., Lara, R.J., Eicken, H., Kattner, G., and A. Skoog (1995), Dissolved organic matter in Arctic multiyear sea ice during winter: major components and relationship to ice characteristics, *Polar Biol.* 15(7), 477-483, doi: 10.1007/BF00237461.

Webster, M.A., Rigor, I.G., Nghiem, S.V., Kurtz, N.T., Farrell, S.L., Perovich, D.K., and M. Sturm (2014), Interdecadal changes in snow depth on Arctic sea ice. *J. Geophys. Res. Oceans* 119, 5395– 5406, doi: 10.1002/2014JC009985.

Williams, P.J. leB. (1993), Chemical and tracer methods of measuring plankton production, *ICES Mar. Sci. Symp.*, *197*, 20–36.

Worster, M.G., and D.W.R. Jones (2015), Sea-ice thermodynamics and brine drainage, *Phil. Trans. R. Soc.* 373, 20140166, doi:10.1098/rsta.2014.0166.

Zhang, Q., Gradinger, R., and M. Spindler (1998), Dark survival of marine microalgae in the high Arctic (Greenland Sea), *Polarforsch* 65, 111–116.

Chapter Six Supplementary Material

This section contains additional text outlining i) details on the collection and processing of ice samples ii) the set-up and procedure of calculating net community production from oxygen optodes and iii) methods for determining variables associated with light intensity. Also included is a table that summarizes biological and environmental variables in Phases I and II of this study.

6.S.1 Ice core collection and processing

The bottom 5 cm of six to eight ice cores were collected using a 9 cm *Mark II Kovacs* core barrel, as the majority of chlorophyll *a* (chl *a*) is typically located in the bottom 3 to 5 cm [Horner, 1985; Mundy et al., 2005; Galindo et al., 2014]. Core segments were pooled together, transported to laboratory facilities and diluted with 0.2 μm filtered seawater at a ratio of about three parts FSW to one part ice, before melting in darkness for 24 hours. The resulting solution of melted sea ice and filtered seawater was subsampled for all biological parameters.

6.S.2 Oxygen optode incubations

Melted ice samples were incubated at approximately -1.5°C for 70 hours in 4-500 ml *Wheaton* borosilicate glass bottles equipped with routinely calibrated 10 mm robust *Firesting* oxygen optodes. One bottle was incubated in darkness, while the other three were exposed in sequence to a *Hiralite* full spectrum light emitting diode that created incubation light intensities of approximately 10, 55 and 21 μmol m^{-2} s^{-1}, respectively. These light intensities were specifically measured for every incubation using a scalar

PAR probe (*Walz* model US-SQS/L). Throughout the incubations customized stir plates mixed samples and oxygen concentration was recorded every second by the optodes. These measurements were later averaged on an hourly basis before net community production was calculated as the change in oxygen over time relative to initial concentrations (T_0) (μmol O_2 l^{-1} h^{-1}) [Campbell et al., 2016].

6.S.3 Measurements of light intensity

The percent transmittance of photosynthetically active radiation (T_{PAR}) was estimated from opportunistic measurements of average downwelling irradiance between 9 and 12:30 h local time, that were made above the snow cover and approximately 30 cm below the ice subsurface using 2π quantum sensors (*LI-COR*). Transmittance on dates of ice core collection was estimated from these sampled T_{PAR} measurements by averaging data typically within ± 2 days. Hourly averages of downwelling PAR incident to the snow surface were also recorded over a diurnal period at a nearby meteorological station (μmol m^{-2} s^{-1}, *Kipp & Zonen PAR-Lite*). Estimates of downwelling PAR transmitted through the ice were obtained by applying T_{PAR} to surface downwelling PAR. To produce estimates comparable to scalar incubation light intensities, the estimates of under ice PAR were used with corresponding chl *a* concentrations to calculate hourly average scalar irradiance for the ice algal layer ($\bar{E}_0$) or the volume averaged scalar irradiance ($\hat{E}_0$) according to Ehn and Mundy [2013]. Downwelling PAR measurements on, or within ± 3 days of ice core collection were used in calculations of $\bar{E}_0$ and $\hat{E}_0$. This is with the exception of 21 April where the first possible recording by the station on 26 April was used. Daily averages of scalar irradiance were determined by averaging $\bar{E}_0$ or $\hat{E}_0$ over the 24 h diurnal period, and are reported as $\bar{E}_{0(daily)}$ or $\hat{E}_{0(daily)}$, respectively.

Table 6.S.1. Test statistic (*t*) and significance (*p*) of student independent *t*-tests (df = 10) performed on variables including: daily average $\bar{E}_0$ ($\bar{E}_{0(daily)}$) and $\hat{E}_0$ ($\hat{E}_{0(daily)}$), the community compensation point (C_{IC}), chlorophyll *a* (chl *a*), particulate organic carbon (POC), numerical abundance of centric (C_N) and pennate (P_N) diatoms, and percent abundance of centric (C_P) and pennate (P_P) diatoms, salinity of the ice-ocean interface, nitrate + nitrite (NO_x) in the bottom ice, bottom-ice temperature, hourly net community production in darkness (NCP_{dark}), at 10 µmol m^2 s^{-1} (NCP_{10}), 21 µmol m^{-2} s^{-1} (NCP_{21}) and 55 µmol m^{-2} s^{-1} (NCP_{55}), daily integrated net community production calculated from $\bar{E}_{0(daily)}$ ($NCP_{\bar{E}0}$) and $\hat{E}_{0(daily)}$ ($NCP_{\hat{E}0}$), and bacterial production (BP). Data were grouped based on collection date (≤ 8 May, >8 May), where the mean and standard deviation (brackets) for each time period are presented. Bolded values indicate $p > 0.05$.

	Variable	Mean (SD)		*t*	*p*
		≤ 8 May	> 8 May		
Light	$\bar{E}_{0(daily)}$ (µmol m^{-2} s^{-1})	13.84 (5.92)	27.65 (10.61)	-2.61	0.026
	$\hat{E}_{0(daily)}$ (µmol m^{-2} s^{-1})	109.49 (55.50)	188.47 (70.06)	-2.08	**0.063**
	$\bar{E}_{0(daily)}$ (µmol m^{-2} s^{-1}) *	13.84 (5.92)	32.47 (6.57)	-3.67	0.006
	$\hat{E}_{0(daily)}$ (µmol m^{-2} s^{-1}) *	109.49 (55.50)	222.09 (40.34)	-4.71	0.002
	C_{IC} (µmol m^{-2} s^{-1}) **	20.65 (8.93)	10.33 (3.32)	2.83	0.020
Biomass	Chl *a* (mg m^{-2})	6.26 (1.15)	8.43 (1.59)	-2.60	0.027
	POC (mg m^{-2})	658.62 (143.68)	1797.59 (355.83)	-6.70	0
Community composition	C_N (× 10^6 cells l^{-1})	55.6 (12.4)	165.6 (58.9)	-4.80	0.002
	P_N (× 10^6 cells l^{-1})	93.1 (20.8)	9.51 (15.7)	-0.19	0.851
	C_P (%)	36.68 (8.57)	59.02 (11.50)	-3.66	0.004
	P_P (%)	59.49 (8.43)	36.07 (9.23)	4.49	0.001
Environmental variables	Salinity (psu)	28.02 (0.19)	28.14 (0.13)	-1.25	**0.256**
	NO_x (µmol l^{-1})	0.74 (0.41)	0.31 (0.07)	2.31	**0.080**
	Temperature (°C)	-1.45 (0.44)	-1.44 (0.15)	-0.02	**0.985**
Hourly production	NCP_{dark} (µmol O_2 l^{-1} h^{-1})	-2.34 (0.72)	-2.17 (0.50)	-0.49	**0.635**
	NCP_{10} (µmol O_2 l^{-1} h^{-1})	-1.33 (0.68)	0.07 (0.76)	-3.285	0.008
	NCP_{21} (µmol O_2 l^{-1} h^{-1})	-0.52 (0.80)	2.52 (1.28)	-4.65	0.001
	NCP_{55} (µmol O_2 l^{-1} h^{-1})	0.70 (0.10)	5.98 (1.92)	-5.56	0.000
Daily production	$NCP_{\bar{E}0}$ (µmol O_2 l^{-1} d^{-1})	-27.87 (16.99)	47.28 (35.53)	-4.34	0.001
	$NCP_{\hat{E}0}$ (µmol O_2 l^{-1} d^{-1})	6.28 (30.08)	141.40 (45.61)	-5.75	0
Bacterial production	BP (μg C l^{-1} h^{-1})	0.22 (0.15)	0.15 (0.05)	0.98	**0.379**

* Measurements on 5 and 9 June excluded

** C_{IC} on 8 May not defined, df = 9

CHAPTER SEVEN: SUMMARY AND CONCLUSIONS

7.1 Summary of major contributions

7.1.1 Contribution 1

An alternative method to radioisotope-based measurements of sea ice gross primary production and photosynthesis-irradiance parameters, which can also be used to characterize sea ice net community production

An alternative approach to assessing productivity that does not require radioisotope use was developed and is described in Chapter Four. It consists of equipping 4-500 ml glass bottles with continuously recording *Firesting* oxygen optodes, and incubating samples for 70 h at zero, 10, 21 and 55 μmol m^{-2} s^{-1} light intensities under constant temperature. Following a comparison of melt procedures in Chapter Three, the buffered melt of ice cores in filtered seawater was shown to be an effective method of obtaining liquid incubation samples for a standardized ice thickness section sample. This is in part due to filtered seawater i) buffering changes in salinity that reduce the percentage of cell deaths by over half in comparison to melt without the addition of seawater, and ii) creating conditions (nutrient, carbon, salinity) similar to the ice-ocean interface water that bottom-ice communities are likely accustomed to.

The linear change in oxygen over time that is recorded by these optode incubations can be used to calculate gross primary production or net community production at experimental light intensities. From these measurements photosynthesis-irradiance parameters may then be calculated. This application of the oxygen optode method to calculate gross primary production was done in Chapter Four, and findings indicate that resulting photosynthesis-irradiance parameters of maximum photosynthetic rate and photosynthetic efficiency are comparable to ^{14}C-derived estimates. Photosynthesis-

irradiance parameters may also be used to estimate daily gross primary production assuming minimal bacterial activity is present and provided *in situ* light intensities can be approximated, an application of the method that is used in Chapters Four and Five. Based on these results, we suggest that our oxygen optode method is an effective means of measuring the photoacclimative state and gross primary productivity of sea ice algae without the use of radioisotopes. In fact, the only chemicals required are a strong reductant to calibrate the zero percent oxygen standard (e.g. sodium dithionite) and antifreeze (e.g. ethylene glycol) to maintain the temperature-regulating water bath at *in situ* temperatures.

In Chapter Six, the oxygen optode method was also used to estimate net community production at experimental light intensities, model the resulting photosynthesis-irradiance parameters and calculate daily net community production. The results highlight the potential importance of heterotrophy in the sea ice community, which cannot be assessed using ^{14}C incubation methods [Williams, 1993].

7.1.2 Contribution 2

First known production and community composition measurements in the Dease Strait region of the Arctic

The study of ice algal and bacterial production in the Canadian Arctic has largely taken place in the most productive regions, like Barrow Strait (Section 2.2.2). Data presented in Chapters Four, Five and Six are the first production related measurements in the previously undocumented region of Dease Strait, near Cambridge Bay, Nunavut (Figure 2.6, 2.7). Therefore, our estimates represent a baseline that future changes associated with climate warming can be compared against.

In Chapter Four, photosynthesis-irradiance parameters and daily gross primary production are presented. These estimates are at the lower end of measurements that have been reported for Arctic sea ice. For example, average assimilation rates for the study were approximately 0.06 mg C mg chl a^{-1} h^{-1}, which represents the lowest category on Figure 2.7. Chapter Four also summarizes regional environmental conditions that are unique to the Canadian Archipelago, namely low nitrogen and low salinity surface waters created by limited exchanges with neighboring water bodies (low nutrient replenishment) and significant riverine input. Resulting nitrogen limitation (supported by algal physiological response) contributed to the low assimilation rates and reduced photosynthesis-irradiance parameters that were documented, like the maximum photosynthetic rate (P^B_s), photosynthetic efficiency (α^B) and the photoacclimation parameter (E_s).

In Chapter Five low bacterial production was also documented in the region, and would be represented on Figures 2.6, 2.7 as the lowest category. The taxonomic composition of the later spring ice algal community is atypical of others typically found in Arctic sea ice [Poulin et al., 2011], where the presence of centric diatoms was uniquely significant.

In Chapter Six the measurements of net community production contribute to a relatively sparse database of sea ice net community production estimates [e.g. Rysgaard et al., 2008; Nguyen and Maranger, 2011; Glud et al., 2014]. Daily estimates of net community production at *in situ* light intensities indicate that the bottom of sea ice in the region may, at times, be net heterotrophic despite the accumulation of particulate carbon biomass.

7.1.3 Contribution 3

Improved understanding of the factors controlling algal and bacterial production in sea ice

The availability of light and nutrients are the most commonly reported controls of ice algal productivity due to their roles in photosynthesis and biomass production (Section 2.2.2). Our assessment in Chapter Four supports the co-limitation of light and nitrogen on ice algal photosynthesis-irradiance parameters and gross primary productivity in Dease Strait. However, results also highlight the complexity of their influence over the course of our extensive time series and between depths of snow cover. For example, light availability drove seasonal and spatial responses of gross primary production, but was only responsible for seasonal trends in photoacclimation (photosynthesis-irradiance parameters) that were observed.

In Chapter Five, we also document the potentially indirect influence of light and nutrient conditions on gross primary production through species selection. Our results suggest that the nitrogen depleted conditions in Dease Strait, in combination with low salinity surface waters (Chapter Four), facilitated the development of a centric diatom population that enhanced gross primary production and biomass accumulation in the ice. Furthermore, an apparent affinity of centric diatoms for higher light conditions likely contributed to greater gross primary production and biomass under thin snow, as well as later in the spring. This study is the first to detail a seasonal shift of significant magnitude from the typically dominant pennate diatoms to centric forms in sea ice, and the first to highlight the potential consequences of such a shift on gross primary production and biomass.

In Chapter Six, we show that light availability and changes in algal taxonomic composition collectively affect net community production and determine whether the bottom ice may be considered net heterotrophic or autotrophic. Although, the productive state of the ice (heterotrophic or autotrophic) is highly dependent on assumptions of light accessibility in the bottom-ice. We also note that unlike the paralleled responses of gross primary production and biomass documented in Chapter Four, trends of net community production and biomass may differ.

Increases in the abundance and productivity of heterotrophic bacteria in sea ice are often associated with development of the ice algal bloom due to increased supply of dissolved organic matter (Section 2.2.3). The results of Chapter Five support this general association, but also specify that the smallest algae, picoeukaryotes, likely have the most important role in supplying dissolved organic matter to the sea ice microbial loop. Bacterial abundance and productivity in the bottom ice may also benefit from the movement of cells and dissolved organic matter downwards as the ice warms, and brine channels connect (represented by increases in brine volume). The consumption of bacteria by aquatic grazers has documented as a control of bacterial production in some regions of the Arctic (Table 2.4). However, despite the consistent presence of bacteria consuming choanoflagellates in this study, the influence on bacterial abundance and production was inconclusive.

7.2 Future recommendations

This thesis has outlined an alternative approach to measuring gross primary production and net community production, and has summarized the factors driving its variability in Dease Strait. However, the methods were not perfect. Therefore, the following describes

and recommends aspects of the incubation method that can be improved and highlights important questions that require additional research.

7.2.1 Modifications to the oxygen optode incubation method

The incubation method developed in this research was described in detail in Chapter Four. Advantages and disadvantages of this incubation method are summarized briefly in Table 7.1, while additional descriptions of (1) modifications to the set-up and (2) changes to incubation time period are detailed below.

Table 7.1. Summary of advantages and disadvantages of the oxygen optode method developed in this research, as well as recommendations for its future application.

Advantages	Disadvantages	
	Concern	**Recommendation**
Results are highly representative of traditional ^{14}C incubations Estimates of P^B_s (T_9 = 1.44) and α^B (T_{10} = 1.542) are not significantly different (p>0.05) from coincident ^{14}C-based estimates using a paired student t-test (Chapter Four) This supports other studies that have successfully modeled photosynthesis-irradiance parameters in sea ice using four or less points [e.g. Lee et al. 2008, Søgaard et al. 2010]	**Photosynthesis-irradiance modeling of four data points may increase model error** This reduces confidence in P^B_s estimates (although they compared well with ^{14}C-derived estimates here, Chapter Four), and does not permit measurement of photoinhibition	The chamber should be modified to include more (smaller bottles) over a greater range of light intensities Potential light source: Cojtech IP54 Llight emitting diode with intensities up to 400 umol m^{-2} s^{-1} (Fernendez-Mendez pers. comm.)
Provides a number of applications for a given incubation The optode method can be used to quantify gross primary production, photosynthesis-irradiance parameters (Chapter Four), net community production, community respiration in darkness (Chapter Six)	**70 h incubation time increases the likelihood of bottle effects** •Grazing: Samples were not pre-filtered to remove aquatic grazers prior to incubation. Their presence (shown to be low, Chapter Five) could enhance the O_2 consumption signal •Photoacclimation: Cells could have modified their physiology over the incubation. This has been shown to cause overestimates of P^B_s and underestimates of α^B [Lewis & Smith 1983] •Population growth: Cells could have grown a number of generations during the 70h. Although, non-linear responses in this research suggest this impact was not significant (Chapter Four)	Samples should be pre-filtered using zooplankton mesh to remove potential heterotrophic grazers in solution Incubation times should be reduced based on the concentration of sample to limit the extent of bottle effects (Figure 7.1) Measurements of chlorophyll *a* and/ or cell abundance should be done prior to **and after** the incubation to account for potential changes in the algal and bacterial population. Measurements of nutrients would also permit assessment of nutrient limitation during incubations. Future experiments should be done to assess the distribution of microbes in sample bottles, and the influence of probe positioning relative to them
Does not require use of radioisotopes, and chemicals required are limited to the reductant used for 0% probe calibration (sodium dithionite)		

This makes it easier and safer to use than the conventional ^{14}C method	•Bottle artifacts: Growing cells for a prolonged period in the incubation bottles may promote attachment to surfaces (limit their signal on probe central in the bottle) and nutrient limitation	
Optode technology provides reliable estimates of O_2 change over time (continuous) Optodes are useful for long term incubations (required for of low chl *a*) because of their sensitivity, resistance to degradation, and they do not consume O_2 (unlike electrodes)	**Destructive sampling is required** •The incubation setup requires melting of ice samples, which likely subjects cells to salinity, nutrient and light stress • Destructive Sampling does not permit a true time series of measurements, as different samples are collected for each incubation	Future adaptations of the method could consider incubating the bottom of ice cores following McMinn et al. [1999], although, this would limit estimates of production to cells largely at the growth interface A combination of in situ measurements [e.g. Else et al. 2015] and laboratory-based incubations (as presented) would best characterize production in the sea ice environment
Measurement of all parameters (production, chl *a*, abundance, taxonomy etc.) are done on the same sample This may improve accuracy of assimilation estimates [McMinn & Hegseth 2007]		
Incubations are low maintenance following set-up This is perhaps with the exception of temperature monitoring	**Temperature control** must be strictly maintained for the duration of incubations This could create difficulties in using the incubation setup in field camp settings	Modifications to the setup could include: •Insolating the chambers •Using water pumped directly from the ocean-ice interface to maintain chamber temperature (instead of a water bath) •Automated temperature recordings so temperature fluctuations can be accounted for in post-processing

1. In Chapter Four we discussed how differences in setup between our oxygen optode incubations and traditional ^{14}C incubations could have affected the similarity of photosynthesis-irradiance parameters. Of particular interest was the shorter range of light intensities used during oxygen optode incubations, and the use of four (O_2) versus ten (^{14}C) incubation bottles. Statistical analyses demonstrated that the maximum photosynthetic rate (P^B_s) and photosynthetic efficiency (α^B) were not significantly affected by these differences. However, increasing the range of incubation light intensities to reach upwards of 100 $\mu mol\ m^2\ s^{-1}$ could permit measurements of photoinhibition (see Section 2.2.1), and increasing the number of bottles is likely to reduce the already low root mean squared error between incubation methods. Using a stronger, full spectrum light emitting diode would increase the irradiance range of photosynthesis-irradiance curves. We caution that any alternative light sources should

have limited heat emissions to avoid influencing the temperature sensitive oxygen incubations. Reducing the size of individual bottles while increasing the number in each incubation chamber is also advised, to ensure appropriate temperature regulation of samples (i.e. water baths may have difficulty regulating temperatures in increasingly larger chambers).

2. The linear trends of oxygen production observed during optode incubations remained constant over time (e.g. Figs. 4.3a, b), which suggests that the length of incubation could be reduced without changing the result. This is beneficial, as it could potentially permit a greater frequency of incubations during individual research studies. To assess the optimum length of optode incubation, the linear slope of gross primary production for every incubation was iteratively recalculated, while sequentially removing hourly measurements (ie. production from 70, 69, 68 hours, etc.). The minimum required length for incubation was identified as the hour at which the recalculated gross primary production deviated by more than 30% from the original (i.e. full 70-hour incubation) gross primary production value. Comparing the calculated minimum required length for incubation with the chl *a* concentration in each bottle (ie. not dilution corrected) demonstrates that the minimum required length for incubation decreases as a non-linear function ($r = 0.81$) of algal biomass (Fig. 7.1). From this analysis three distinct groups of points are evident: (1) samples of chl $a < 5$ μg l^{-1}, (2) samples from 20 to 40 μg l^{-1} and (3) samples greater than 45 μg l^{-1}. From this observation, the following incubation times based on incubation biomass are recommended: (1) 70 hours when algae biomass is less than 5 μg l^{-1} chl *a*, (2) 35 hours when the biomass is between 20 and 40 μg l^{-1}, and (3) 10 hours when the biomass is 45 μg l^{-1} chl *a* or greater. Assuming a 5 cm bottom-ice algal

layer and 3:1 FSW dilution, this corresponds to approximate *in situ* areal concentrations below 1 mg m^{-2}, from 4 to 8 mg m^{-2} and greater than 9 mg m^{-2}, respectively.

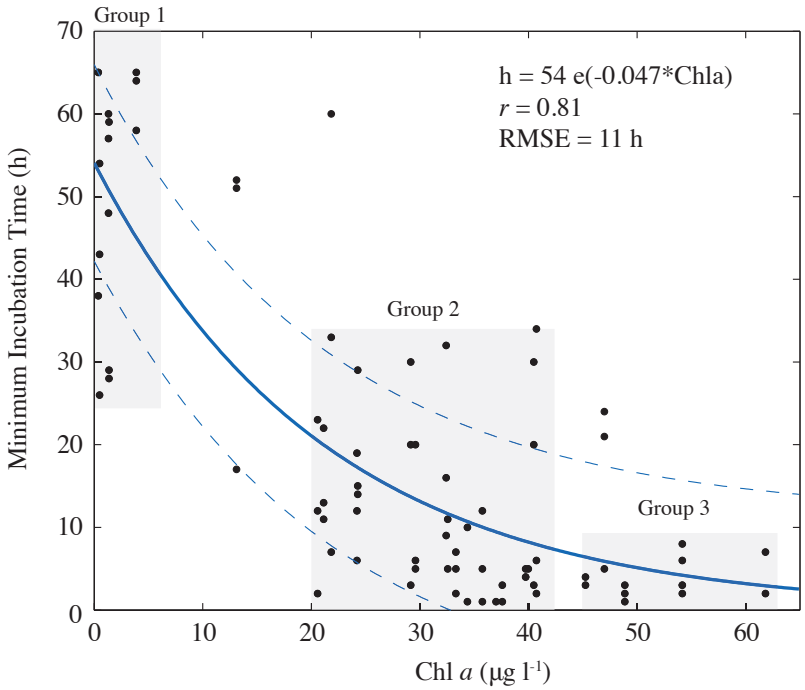

Figure 7.1. Minimum incubation time required for optode incubations based on 30% deviation of gross primary production from the original 70 h incubation, versus chlorophyll *a* (chl *a*) concentration (uncorrected for dilution). Samples include gross primary production for all illuminated bottles over all sample cycles, collected from thin and thick snow covers. Exponential relationship (RMSE = 12 h) with ±1 SD, and grouping of data points 1-3 discussed in the text are highlighted for reference.

7.2.2 Standardized approaches for processing sea ice biological samples

In Chapter Three, differences in chl *a* and gross primary productivity between ice melt treatments demonstrate the potential contribution of scientific protocols to variability of estimates that are reported across the Arctic (Figure 2.6, 2.7). That is, estimates of sea ice pigments and productivity may be artificially enhanced or reduced in individual studies depending on how the samples are melted (i.e. time, volume of filtered seawater, temperature). Evidence to support different, and sometimes contrasting, approaches exists

in the literature [e.g. Mikkelsen & Witkowski, 2010; Rintala et al., 2014]. However, additional experiments are still required to build a consensus within the scientific community on best practice melt procedures that can be universally adopted. This is not a trivial task, but promising strides have been made in other scientific areas like marine trace elements through GEOTRACES and their standardized reports on sampling and sample handling [Cutter et al., 2010].

7.2.3 Laboratory studies for assessing the controls of algal and bacterial production

1. Over 1000 algal taxa have been reported in Arctic sea ice [Poulin et al., 2011]. In Chapter Five we provide evidence that such differences in taxonomic composition may occur because of nutrient, salinity, and/or light conditions, and that these differences could influence gross primary production. However, additional culture-based experiments are required to further elucidate this relationship. Furthermore, we show that the taxonomic composition can vary at the local scale (e.g. between different snow depths), which adds complexity to accurately characterizing the productivity of study locations. In Chapter Six additional evidence shows that seasonal changes in species composition affect net community production, and potentially the productive state of the ice. Future dedicated laboratory studies are required to build off of these observations in order to better assess i) species affinity for different environmental conditions and ii) how the most commonly documented ice algal species (e.g. *Nitzschia frigida*) may respond to them (e.g. change their productivity). Such studies have been performed on various species of phytoplankton, and have showed species-specific nitrogen requirements and storage that likely impact cellular productivity [e.g. Pederson & Borum, 1996].

Experiments tailored to assess species response to anticipated future conditions with climate warming (e.g. lower nutrients) would be especially beneficial.

2. Conclusions from Chapter Five highlight the potentially important role of picoeukarytic algae and brine drainage in supplying dissolved organic carbon to heterotrophic bacteria that inhabit the bottom of sea ice. Additional studies investigating these mechanisms of carbon supply are required. For example, conducting experiments to monitor the magnitude of dissolved organic carbon release by different size fractions of ice algae.

7.2.4 Documenting *in situ* light conditions

Estimates of net community production are presented in Chapter Six. A range of values is provided due to uncertainty associated with the intensity of light actually available to algae for photosynthesis. That is, a lower estimate of light for photosynthesis is given as scalar photosynthetically active radiation at the bottom-ice algal layer, and an upper estimate is given by applying an additional scaling factor to account for the possible effects of multiple scattering [Ehn & Mundy, 2013]. The difference in these light intensities causes an average discrepancy in daily net community production of nearly 300%. It follows that in order to achieve more accurate estimates of production in sea ice, a better understanding of light absorbed by ice algae *in situ* is required.

7.2.5 Statistical assessments of time series data

Changes in algal composition (carbon, nitrogen, chl *a*) (Chapter Four), algal community composition (Chapter Five) and production in sea ice (Chapters Four, Five & Six) were

summarized over a sampling period of approximately two to three months in this research. In the majority of assessments, linear correlation or regression analyses were performed to determine the potential causes of observed variability. However, there is error associated with correlating parameters over time, and with evaluating multidimensional responses with these statistical tests. As a result, analysis of a similar dataset could benefit from applying additional approaches of data reduction or cluster analyses. Furthermore, it is best to report regressions of parameter response over time, rather than correlations.

7.3 Closing Comments

This research has documented sea ice algal and bacterial production in Dease Strait of the lowermost Northwest Passage, and has investigated the factors influencing its production. From this assessment it is apparent that Dease Strait is a unique region of the Arctic marine system, with low salinity and nutrient depleted surface waters that reduce production and facilitate atypical communities of sea ice algae. These characteristics may limit the applicability of results to the broader Arctic at present; however, they do offer valuable insight into sea ice microbial response to a potentially fresher, low nutrient Arctic Ocean in the future [Holland et al., 2007; Tremblay et al., 2016].

The development of models is also a useful tool in understanding the potential effects of climate warming on sea ice ecosystems (e.g. Lavoie et al., 2005). Furthermore, they permit large-scale predictions of sea ice algal and bacterial production contributions to CO_2 fluxes and the trophic system (e.g. Arrigo et al., 1998; Deal et al., 2011). However, the power of such models is dependent on the accuracy of input parameters that are

derived from small-scale observations (i.e. microbial response to environmental conditions), and results in this thesis have highlighted their complexity. For example, Chapter Four showed that variable light conditions affected maximum photosynthetic rates and photosynthetic efficiencies of algae over the spring, but not between thin (high light) and thick (low light) snow covers. Moreover, Chapter Five showed that the taxonomic composition of the algal community has the potential to affect gross primary production, although further laboratory studies are required to investigate this potential relationship. Finally, Chapter Six showed how taxonomic composition and community respiration may influence the net community production of sea ice. It follows that cellular and community level parameters, like photoacclimation, species abundance and community respiration, have the potential to affect production estimates and should be accounted for in modeled assessments of sea ice productivity.

Finally, the conclusions presented in this thesis were possible because of the multidisciplinary nature of the research, where physical, biological and chemical processes were collectively analyzed to create a comprehensive summary of sea ice productivity in the region. These system approaches are required to understand responses of sea ice communities to their dynamic environments, particularly in the face of ongoing climate forced changes.

References

Arrigo, K., Worthen, D.L., Dixon, P., and M.P. Lizotte (1998), Primary productivity of near surface communities within Antarctic pack ice, Lizotte M.P. and K. R. Arrigo (Eds.), *Antarctic Sea Ice: Biological processes, interactions, and variability*. Antarctic Res. Ser. 73, 23–43.

Ehn, J.K., and C.J. Mundy (2013), Assessment of light absorption within highly scattering bottom sea ice from under-ice light measurements: Implications for Arctic ice algae primary production, *Limnol. Oceanogr.*, *58*(3), 893-902, doi: 10.4319/lo.2013.58.3.0893.

Else, B.G.T., Rysgaard, S., Attard, K., Campbell, K., Crabeck, O., Galley, R.J., Geilfus, N.-X., Lemes, M., Lueck, R., Papakyriakou, T., and F. Wang (2015), Under-ice eddy covariance flux measurements of heat, salt, momentum, and dissolved oxygen in an artificial sea ice pool, *Cold Reg. Sci. Technol.* 119, 158-169, doi: 10.1016/j.coldregions.2015.06.018.

Cutter, G. , Andersson, P. , Codispoti, L. , Croot, P. , François, R. , Lohan, M. C. , Obata, H. and M.R.v.d. Loeff (2010), Sampling and Sample-handling Protocols for GEOTRACES Cruises , [Miscellaneous], http://www.geotraces.org/libraries/documents/Intercalibration/Cookbook.pdf (Accessed January 2017).

Deal, C., Jin, M., Elliot, S., Hunke, E., Maltrud, M., and N. Jeffery (2011), Large-scale modeling of primary production and ice algal biomass within arctic sea ice in 1992, J. Geophys. Res. 116, C07004, doi:10.1029/2010JC006409.

Glud, R.N., Rysgaard, S., Turner, G., McGinnis, D.F., and R.J.G. Leakey (2014), Biological- and physical induced oxygen dynamics in melting sea ice of Fram Strait, *Limnol. Oceanogr.* 59(4), 1097-1111, doi: 10.4319/lo.2014.59.4.1097.

Holland, M.M., Finnis, J., Barrett, A.P., and M.C. Serreze (2007), Projected changes in Arctic Ocean freshwater budgets, *J. Geophys. Res.* 112, G04S55, doi: 10.1029/2006JG000354.

Lavoie, D., Denman, K., and C. Michel (2005), Modeling ice algal growth and decline in a seasonally ice-covered region of the Arctic (Resolute Passage, Canadian Archipelago), *J. Geophys. Res.* 110, C11009, doi: 10.1029/2005JC002922.

Lee, S.H., Whitledge, T.E. and S. Kang (2008), Carbon uptake rates of sea ice algae and phytoplankton under different light intensitites in a landfast sea ice zone, Barrow, Alaska, *Arctic* 61(3).

Lewis, M. and J.C. Smith (1983), A small volume, short-incubation-time method for measurement of photosynthesis as a function of incident irradiance, *Mar. Ecol. Prog. Ser.* 13, 99-102.

McMinn, A., Skerratt, J., Trull, T., Ashworth, C. and M. Lizotte (1999), Nutrient stress gradient in the bottom 5 cm of fast ice, McMurdo Sound, Antarctica, *Polar Biol.* 21, 220-227, doi: 10.1007/s003000050356.

McMinn, A., and E.N. Hegseth (2007), Sea ice primary productivity in the northern Barents Sea, spring 2004, *Polar Biol.* 30, 289-294, doi: 10.1007/s00300-006-0182-x.

Mikkelson, D.M, and A. Witowski (2010), Melting sea ice for taxonomic analysis: a comparison of four melting procedures, *Polar Res.* 29, 451-454, doi:10.1111/j.1751-8369.2010.00162.x.

Nguyen, D., and R. Maranger (2011), Respiration and bacterial carbon dynamics in Arctic sea ice, *Polar Biol.* 34, 1843-1855, doi: 10.1007/s00300-011-1040-z.

Pederson, M.F., and J. Borum (1996), Nutrient control of algal growth in estuarine waters. Nutrient limitation and the importance of nitrogen requirements and nitrogen storage among phytoplankton and species of macroalgae, Mar. Ecol. Prog. Ser. 142, 261-272, doi:10.3354/meps142261.

Poulin, M., Daugbjerg, N., Gradinger, R., Ilyash, L., Ratkova, T., and C. Quillfeldt (2011), The pan-Arctic biodiversity of marine pelagic and sea-ice unicellular eukaryotes: a first-attempt assessment, *Mar. Biodiv.* 41, 13-28, doi: 10. 1007/s12526-010-0058-8.

Rintala, J.-M., Piiparinen, J., Blomster, J., Majaneva, M., Müller, S., Uusikivi, J., and R. Autio (2014), Fast direct melting of brackish sea-ice samples results in biologically more accurate results than slow buffered melting, *Polar Biol.* 37(12), 1811-1822, doi: 10.1007/s00300-014-1563-1.

Rysgaard, S., Glud, R.N., Sejr, M.K., Blicher, M.E., and H.J. Stahl (2008), Denitrification activity andoxygen dynamics in Arctic sea ice, *Polar Biol.* 31, 527–537, doi: 10.1007/s00300-007-0384-x.

Søgaard, D.H., Kristensen, M., Rysgaard, S., Glud, R.N., Hansen, P.J., and K.M. Hilligsoe (2010), Autotrophic and heterotrophic activity in Arctic first-year sea ice: seasonal study from Malene Bight, SW Greenland, *Mar. Ecol. Progr. Ser.* 419, 31-45, doi: 10.3354/meps08845.

Tremblay, J., Anderson, L.G., Matrai, P., Coupel, P., Bélanger, S., Michel, C., and M. Reigstad (2016), Global and regional drivers of nutrient supply, primary production and CO2 drawdown in the changing Arctic Ocean, *Prog. Oceanog.*,

doi:10.1016/j.pocean.2015.08.009.

Williams, P.J. leB. (1993), Chemical and tracer methods of measuring plankton production, –*ICES Mar. Sci. Symp*. 197, 20-36.

APPENDIX A: CONTRIBUTIONS OF COLLABORATING AUTHORS

This thesis represents a compilation of original research that was lead by myself. I was the primary designer and organizer of the scientific studies, I collected and processed the large majority of data, and I synthesized the resulting findings (text and figures) into the chapters of this document. Other colleagues also supported this work, and their specific contributions towards chapters three to seven (this chapter) are outlined below.

Chapter Three

Drs. Søren Rysgaard and C.J. Mundy helped develop the idea for a methods comparison. Aurelie Delaforge assisted in the collection of field data and measurement of scintillation counts and fluorescence. Dr. Jack Landy wrote the Matlab code for photosynthesis-irradiance modeling. These contributions of Aurelie Delaforge and Dr. Jack Landy also apply to chapters Four, Five and Six.

Chapter Four

Samples of particulate organic carbon (POC) were collected and packaged by myself for analysis via mass spectroscopy, which was completed by Mathieu Babin at the Université de Québec à Rimouski. Pascal Rioux analyzed samples I collected for assessment of inorganic nutrient concentrations at the Université de Québec à Rimouski. Dr. Jack Landy wrote a Matlab code to average hourly estimates of optode derived oxygen concentration from smaller time intervals. Drs. Søren Rysgaard, C.J. Mundy and Christine Michel

provided logistical and, or, financial support. All co-authors mentioned here also helped design and review the manuscript.

Chapter Five

I collected and prepared samples for liquid scintillation counting before Dr. Claude Belzile analyzed them at the Université de Québec à Rimouski. Dr. Belzile also contributed the discussion related to Figure 5.3b and edited the manuscript. Drs. Søren Rysgaard and C.J. Mundy provided logistical and financial support, and reviewed the manuscript.

Chapter Six

Dr. C.J. Mundy provided the insight to use a range of light estimates in the calculation of daily net community production. Drs. Søren Rysgaard, C.J. Mundy, Michel Gosselin and Jack Landy also helped design and review the manuscript. Drs. Søren Rysgaard and C.J. Mundy provided logistical and financial support.

Chapter Seven

Using Matlab Dr. Jack Landy created Figure 7.1 that illustrates how incubation time can vary with chl *a*.

APPENDIX B: ADDITIONAL CONTRIBUTIONS TO THE PEER-REVIEWED LITERATURE

In addition to the three peer-reviewed manuscripts that make up this thesis, I co-authored nine peer-reviewed manuscripts that are currently published and four manuscripts in preparation or review. I also contributed to the synthesis of a report for the Inuit Circumpolar Council and an electronic book related to the Centre for Earth Observation Science's Bay Systems (BaySys) project. These contributions are outlined below.

Published manuscripts

Pogorzelec N., Mundy C., Findlay C., **Campbell K**., Diaz A., Ehn J., Rysgaard S., and K. Gough (2017), FTIR imaging analysis of cell content in sea-ice diatom taxa during a spring bloom in the lower Northwest Passage of the Canadian Arctic, *Mar. Ecol. Prog. Ser.* 569, 77-88, doi: 10.3354/meps12088.

I helped supervise field sample collection for this manuscript and provided environmental data collected during the 2014 ICE-CAMPS. I contributed to review of this manuscript prior to acceptance.

Gelfius, N.X., Galley, R., Else, B.G.T., **Campbell, K**., Papakyriakou, T., Crabeck, O., Lemes, M., Delille, and S. Rysgaard (2016), Estimates of ikaite export from sea ice to the underlying seawater in a sea ice-seawater mesocosm, *The Cryosph.* 10, 2173-2189, doi: 10.5194/tc-10-2173-2016.

In this manuscript I measured the concentration of chlorophyll *a* (chl *a*) and bacterial production (^{3}H leucine incubations) in ice at the Sea-Ice Environmental Research Facility (SERF) during winter 2014. I provided a summary of the protocols in the methods section and estimates in the discussion section of the manuscript.

Elliot A., Mundy, C.J., Gosselin, M., Poulin, M., **Campbell**, **K**., and F. Wang (2015), Production of mycosporine-like amino acids in sea ice covered Arctic waters, *Mar. Ecol. Prog. Ser.* 541, 91-104, doi: 10.3354/meps11540.

In this manuscript I helped collect and pre-process ice samples during the 2011 Arctic-Ice-Covered-Ecosystem (Arctic-ICE) field campaign (Allen Bay, Nunavut), which were later analyzed for mycosporine-like amino acid content. I also measured the irradiance data presented within the manuscript. I edited drafts of the manuscript before and during the review process.

Else, B.G.T., Rysgaard, S., Attard, K., **Campbell, K**., Crabeck, O., Galley, R.J., Geilfus, N.-X., Lemes, M., Lueck, R., Papakyriakou, T., and F. Wang (2015), Under-ice eddy covariance flux measurements of heat, salt, momentum, and dissolved oxygen in an artificial sea ice pool, *Cold Reg. Sci. Technol.* 119, 158-169, doi: 10.1016/j.coldregions.2015.06.018.

In this manuscript I measured bacterial production (^{3}H leucine incubations) in ice at the SERF during winter 2014, and helped maintain the facility during experiments. I provided production estimates and reviewed the manuscript.

Leu, E., Mundy, C.J., Assmy, P., **Campbell, K.,** Gabrielsen, T.M., Gosselin, M., Juul-Pedersen, T., and R. Gradinger (2015), Arctic spring awakening - steering principles behind the phenology of vernal ice algae blooms, *Prog. Oceanog.* 139, 151-170, doi: 10.1016/j.pocean.2015.07.012.

In this manuscript I collected and analyzed estimates of sea ice chl *a* concentration from the 2011 Arctic-ICE field campaign (Allen Bay, Nunavut). I participated in reviews of the manuscript prior to publication.

Rysgaard, S., Wang, F., Galley, R.J., Grimm, R., Notz, D., Lemes, M., Geilfus, N.X., Chaulk, A., A. Hare, A.A., Crabeck, O., Else, B.G.T., **Campbell, K.,** Sørensen, L.L., Sievers, J., and T. Papakyriakou (2014), Temporal dynamics of ikaite in experimental sea ice, *Cryosph.* 8(4),1469-1478, doi: 10.5194/tc-8-1469-2014.

In this manuscript I measured bacterial production (^{3}H leucine incubations) in ice at the Sea-Ice Environmental Research Facility (SERF) during winter 2014, and helped maintain the SERF facility during experiments. I provided production estimates and reviewed the manuscript.

MacDonald, S. Koulis, T., Ehn, J. **Campbell, K**., Gosselin, M., and C.J. Mundy (2014), A functional regression model for predicting optical depth and estimating attenuation coefficients in sea ice covers near Resolute Passage, Canada, *Anals Glaciol*. 56(69), 147-154, doi: 10.3189/2015AoG69A004.

In this manuscript I collected seasonal estimates of chl *a* and under-ice photosynthetically active radiation during the 2011 Arctic-ICE field campaign (Allen Bay, Nunavut) that were the basis of analyses in this manuscript. I worked with Shaun MacDonald to develop the manuscript, and participated in reviews prior to publication.

S. Rysgaard, Wang, F., Galley, R.J., Grimm, R., Lemes, M., Geilfus, N.X., Chaulk, A., Hare, A.A., Crabeck, O., Else, B.G.T., **Campbell, K**., Papakyriakou, T., Sørensen, L.L., Sievers, J., and D. Notz (2013), Dynamic ikaite production and dissolution in sea ice - control by temperature, salinity and pCO2 conditions, *Cryosph*. 7, 6075-6099, doi: 10.5194/tcd-7-6075-2013.

Similar to Rysgaard et al. [2014] above, I measured bacterial production (^{3}H leucine incubations) in ice at the SERF, and helped maintain the facility during experiments in winter 2014. I provided production estimates and reviewed the manuscript.

Mundy, C.J., Gosselin, M., Gratton, Y., Galindo, V., Brown, K., **Campbell,** K., Levasseur, M., Barber, D.G., Papakriakou, T., and L. Miller (2014), Role of environmental factors on phytoplankton bloom initiation under landfast sea ice in Resolute Passage, Canada, *Mar. Ecol. Prog. Ser.* (497), 39-49, doi: 10.3354/meps10587.

I assisted in the collection of biological and optical data used in this manuscript during the 2011 and 2012 Arctic-ICE field campaigns (Allen Bay, Nunavut). I was involved in editing the manuscript drafts.

Manuscripts in preparation or review

Dalman, L., Else, B., Williams, W.J., Carmack, E., **Campbell, K.,** Barber, D., and C.J. Mundy (in prep.), Enhanced ice algal biomass along a tidal strait in the lower NW Passage of the Canadian Arctic, *Arctic*.

I have assisted Laura Dalman in the planning and preparation of her 2016 field campaign in Cambridge Bay, Nunavut. I have been regularly consulted on the preparation of this manuscript to date.

Delaforge, A., Belzile, C., **Campbell, K**., Gosselin, M., Rysgaard, S., and C.J. Mundy (in prep.), Spring-summer progression of phytoplankton and heterotrophic bacteria in Dease Strait, Canadian Arctic Archipelago, *Polar Biol*.

I collected data for this manuscript during the 2014 Ice Covered Ecosystem - CAMbridge bay Process Study (ICE-CAMPS) and have contributed discussion on preliminary results.

Galindo, V., Gosselin, M., Mundy, C.J., Ferland, J., Delaforge, A., **Campbell, K.**, Raimbaud, P., and S. Rysgaard (in prep.), Differences in production regime in two simulated under-ice blooms during the Arctic spring, *Deep Sea Res. II*.

I analyzed the taxonomy data for this manuscript and have contributed discussion on results.

Diaz, A., Ehn, J.K., Landy, J.C., Else, B., **Campbell, K**., Luque, S., and T., Papakyriakou (in prep), The energetics of extensive meltwater flooding of level first-year sea ice, *J. Geophys. Res*.

I collected the temperature-salinity data used in this manuscript during the 2014 ICE-CAMPS, and have reviewed the manuscript.

Other Contributions

Campbell, K. (in prep.), Chapter 5: Building Blocks of the Bay, Hinam, H., Barber, L. and D. Barber (Eds.), *Expedition Churchill: Gateway to Arctic Research 1st Ed*.

In support of the Centre for Earth Observation Science's Bay Systems (BaySys) project that comprehensively explores the biological, chemical and physical charactaristics of Hudson Bay, educational outreach material in the form of an electronic book is in preparation. I wrote this chapter on carbon cycling in Hudson Bay, which required translation of complex scientific concepts to text for a general audience.

Campbell, K. (in prep.), Chapter 6: The Heart of the Bay, Hinam, H., Barber, L. and D. Barber (Eds.), *Expedition Churchill*: *Gateway to Arctic Research 1st Ed*.

I wrote this chapter of the BaySys electronic book (described above), where I detail the presence of algal blooms in Hudson Bay, summarize their dominant controls, and highlight the importance of algal blooms for carbon cycling and the trophic system.

Campbell, K. (in press), Chapter 7, Section E: Lower Trophic Levels In: Inuit Circumpolar Council, *Pikialasorsuaq Commission: The North Water Polynya*. Ottawa Canada.

In this report I completed a literature review of microbiological activity and controls on the North Water Polynya, and summarized this information into a chapter.